Cracking of Plastic Concrete in Slab-Like Elements

by
Riaan Combrinck

Dissertation presented for the degree of
Doctor of Philosophy in Engineering
in the Faculty of Engineering
at Stellenbosch University

Supervisor: Prof William Peter Boshoff

March 2016

Declaration

By submitting this dissertation electronically, I declare that the entirety of the work contained therein is my own, original work, that I am the sole author thereof (save to the extent explicitly otherwise stated), that reproduction and publication thereof by Stellenbosch University will not infringe any third party rights and that I have not previously in its entirety or in part submitted it for obtaining any qualification.

March 2016

Summary

The cracking of plastic concrete involves two cracking types namely: plastic settlement cracking which is caused by differential settlement of the concrete and plastic shrinkage cracking which is caused by evaporation of free concrete pore water. These cracks are mainly a problem for slab-like elements exposed to conditions with high evaporation rates and typically occur within the first few hours after the concrete has been cast. The early occurrence of these cracks greatly reduces the durability and service life of a concrete structure. These cracks remain a problem in the construction industry even though there are several effective, but mostly neglected, precautionary measures. The reasons these cracks remain a problem are due to the complex nature of the cracking as well as the lack of a unified theory or model that can account for all the complexities involved.

With this in mind, this study aims to fundamentally understand both plastic settlement and plastic shrinkage cracking in slab-like elements individually and combined as well as to determine the tensile material properties of plastic concrete. Once the cracking is fundamentally understood the final objective is to develop a model that can simulate the cracking of plastic concrete using a finite element method approach.

The fundamental understanding of these cracks was obtained by conducting various tests on different mixes at various climates and in various moulds. The tests showed that both crack types can occur separately, where plastic settlement cracking occurs first in the form of multiple cracks at the surface as well as shear induced cracks beneath the surface, followed by plastic shrinkage cracking in the form of a singular, well defined crack. In addition, a significant deviation from the individual cracking behaviour was observed when combining these cracks, highlighting the shortfall of most available literature where these cracks are seldom researched in tandem. From all the tests, six different cracking behaviours were identified depending on the potential severity for each cracking type. The test also showed worryingly that both these cracks can be present internally without being visible at the concrete surface where they act as weak spots for future crack growth.

The practically challenging tensile testing of plastic concrete was conducted with a newly built direct tensile test setup, which provided stress-strain curves that were used to determine the tensile material properties of plastic concrete such as: Young's modulus, tensile strength, strain capacity and fracture energy. This included tests at different temperatures as well as cyclic tests. The results showed that the tensile material properties develop significantly faster, the greater the ambient temperature surrounding the concrete as well as the resilient nature of a still plastic concrete which

proved to be capable of withstanding cyclic loading without failure, while a solid but still weak concrete could not.

The tensile material properties together with the measured strains of plastic concrete were combined to provide both an analytical and numerical estimation of the cracking behaviour of plastic concrete. The analytical estimation was more simplistic and required a few crude assumptions, while the numerical estimation used finite element methods to create a model that accounted for the major complexities involved such as time-dependency of material properties and anisotropic volume change of plastic concrete. Both the analytical and finite element model gives adequate representation of the cracking behaviour for extreme climates but not for normal climates, with the size discrepancy between the interior and surface cracks during experiments as well as the relaxation of stresses in plastic concrete being provided as the main reasons for the poor correlation.

The finite element model was further used to conduct a parameter study, where the settlement and shrinkage strains were shown to govern the size of the final crack, while the material properties only influence the time of crack onset and rate of crack widening. Finally, the finite element model was successfully applied to a large scale example of a concrete slab, indicating that the model can be a helpful tool to simulate the cracking of plastic concrete without the need to perform timely experiments.

Opsomming

Die kraak van plastiese beton betrek twee kraak tipes naamlik: plastiese versakkings krake wat deur differensiële versakking veroorsaak word en plastiese krimp krake wat veroorsaak word deur die verdamping van vry porie water in beton. Die krake is hoofsaaklik ’n probleem vir vloer-tipe elemente wat blootgestel word aan kondisies met hoë verdampings tempo’s en gebeur tipies binne die eerste paar ure nadat die beton gegiet is. Die vroeë voorkoms van die krake verlaag die duursaamheid en dienslewe van ’n beton struktuur drasties. Die krake bly ’n probleem in die konstruksiebedryf al is daar verskeie effektiewe, maar meestal geminagte, voorsorgmaatreëls. Die rede hoekom die krake ’n probleem bly is weens die komplekse natuur van die krake sowel as ’n gebrek aan ’n algehele aanvaarde teorie of model wat al die kompleksiteite in ag neem.

Na aanleiding van bogenoemde beoog die studie om fundamentele kennis te ontwikkel van beide plastiese versakkings en plastiese krimp krake in vloer-tipe elemente individueel en gekombineer sowel as om die trek materiaal eienskappe van plastiese beton te bepaal. Sodra die krake fundamenteel verstaan word, is die finale doel om ’n model te ontwikkel wat die kraak van plastiese beton kan simuleer deur gebruik te maak van ’n eindige element metode benadering.

Die fundamentele kennis van die krake was verkry deur verskeie toetse te doen op verskillende mengsels by verskeie klimate in verskillende vorms. Die toetse het gewys dat beide kraak tipes afsonderlik kan plaasvind, met plastiese krimp krake wat eerste plaasvind as meervoudige krake op die oppervlakte sowel as skuif geïnduseerde krake onder die oppervlakte, gevolg deur plastiese krimp krake as goed gedefinieerde enkel kraak. Verder is ’n drastiese verskil in individuele kraak gedrag opgemerk wanneer die krake gekombineer word. Dit beklemtoon die tekortkoming van meeste beskikbare literatuur waar beide kraak tipes selde in tandem ondersoek word. Uit al die toetse is ses verskillende tipes kraak gedrag geïdentifiseer afhanklik van die omvang van elke kraak tipe. Die toetse het ook kommerwekkend gewys dat beide kraak tipes intern teenwoordig kan wees sonder dat dit op die oppervlakte van die beton sigbaar is en dus kan dien as swakplek vir verdere kraking.

Die praktiese uitdagende trek toetsing van plastiese beton was uitgevoer met ’n nuut geboude direkte trektoetsopstelling, wat spanning-vervormings kurwes gelewer het vir die bepaling van die trek materiaal eienskappe van plastiese beton soos: Young’s modulus, trek sterkte, vervormings kapasitiet en fraktuur energie. Dit sluit in toetse by verskillende temperature sowel as sikliese toetse. Die resultate het gewys dat die trek materiaal eienskappe merkwaardig vinniger ontwikkel by hoër

temperature sowel as die veerkragtige natuur van plastiese beton wat gesien kan word as 'n materiaal wat sikliese belasting kan hanteer sonder faling, in vergelyking met 'n meer soliede beton wat faling ondergaan.

Verder is die trek materiaal eienskappe saam met die gemete vervormings van plastiese beton gekombineer om beide 'n analitiese en numeriese voorstelling van kraak gedrag in plastiese beton te gee. Die analitiese voorstelling is meer simplisties en benodig 'n paar gru aannames terwyl die numeriese voorstelling van eindige element metodes gebruik gemaak het om 'n model te skep wat al die belangrike kompleksiteite in ag neem soos die tyd afhanklikheid van materiaal eienskappe en anisotropiese volume verandering. Beide die analitiese en eindige element model gee voldoende voorstelling van die kraak gedrag vir uiterste klimate, maar nie vir normale klimate nie. Die kraak grootte verskil tussen die interne krake en oppervlak krake tydens toetse sowel as die ontspanning van spannings in plastiese beton is gegee as redes vir die swak korrelasie.

Die eindige element model is verder gebruik vir 'n parameter studie wat gewys het dat die versakking en krimp vervormings die finale grootte van die krake bepaal, terwyl die materiaal eienskappe slegs die tyd van eerste kraakvorming en die tempo van kraakopening beïnvloed. Laastens is die eindige element model suksesvol aangewend om 'n grootskaalse voorbeeld van 'n betonvloer te analiseer, wat aantoon dat die model 'n handige instrument kan wees vir die simulasie van krake in plastiese beton sonder die nodigheid om tydsame eksperimente uit te voer.

Acknowledgements

I would like to thank the following people for their assistance and support during this study:

- My promoter, Prof Billy Boshoff, for his continued support and guidance.
- The National Research Foundation (NRF) as well as the Wilhelm Frank Trust for their financial support.
- The staff in the laboratory and workshop at the Civil Engineering Department of Stellenbosch University, for their assistance and time during the experimental work.
- The administration staff of Civil Engineering Department of Stellenbosch University, for their assistance and time during this study.
- My parents for their unconditional support.
- My wife, Maretha, for her support, love, friendship, exercise and much needed distraction during this time.
- My baby daughter, Mia, for her smile in the morning and sleep during the night.
- My two dogs, Jaba and Wuzi, for always being happy to see me.
- Finally, my Creator, for giving me the opportunity and ability to conduct this study.

Contents

List of figures

List of tables

List of symbols

ASTM	American Standard Testing Methods
CNC	Computer numerical controlled
COV	Coefficient of variation
E	Young's modulus
EN	European Standard
ER	Evaporation rate
FEA	Finite element analysis
FCM	Fictitious crack model
FPZ	Fracture process zone
F_t	Tensile strength
G_F	Fracture energy
G_f	Initial fracture energy
L	Linear
LVDT	Linear variable displacement transducer
P	Pressure build-up
MPa	Megapascal
N	Non-linear
PPC	Pretoria Portland Cement
PVC	Polyvinyl chloride
r	Relative humidity
R	Radius of water meniscus
SANS	South African National Standards
SCM	Supplementary cementitious materials
T_a	Air temperature
T_c	Concrete temperature
V	Wind velocity
w	Crack band width
$\Delta_{max}G_f$	Maximum displacement to initial fracture energy
ε_{cap}	Strain capacity
ε_{res}	restrained strain
σ	normal stress

σ_t	Surface tension

Chapter 1. Introduction

Concrete in basic form consists of cement, sand, stone and water which, once mixed, give a chemical reaction between cement and water. This reaction, called hydration, binds all the constituents together to form a strong and hard material called concrete. Over the past 150 years concrete has been one of the most consumed materials in the world, especially in terms of engineering materials, highlighting the significance and influence of concrete not only on the development of infrastructure but also on modern society in general (Domone & Illstone, 2010).

One of the key aspects to concretes success is its ability to be moulded into almost any shape. This is only possible due to the liquid or plastic behaviour of concrete after mixing which allows the concrete to fill almost any mould. Once the concrete has filled a mould it remains plastic for a brief period of around 4 to 8 hours depending on the type of mix as well as the environmental conditions. Within this period the concrete stiffens and solidifies to change from a plastic material to a solid material (Mehta & Monteiro, 2006). The exact transition point where the concrete changes from a plastic to a solid material is not known and is believed to be in the vicinity of final setting time of concrete (ACI 231R, 2010 and Sant et al., 2009). During this initial plastic period the concrete does not possess any significant strength or stiffness, especially when compared to hardened concrete.

It is further necessary to distinguish between plastic concrete and early age concrete. Although plastic concrete can be thought of as early age concrete, the term early age concrete normally refers to the period from after the final setting time to a concrete age of around 7 days (ACI 231R, 2010). During both the plastic and early age periods, concrete is subjected to volume change. If the concrete is restrained against the volume change, stresses develop within the concrete which typically leads to cracking.

The plastic period is dominated by two types of volume change namely plastic settlement and plastic shrinkage. Plastic settlement is a vertical volume reduction caused by the settlement of solid particles in the fresh concrete mixture, while plastic shrinkage is mainly a horizontal volume reduction, although there is also a vertical component, caused by a pressure build-up in the capillary pores of the plastic concrete. This capillary pressure is due to the evaporation of free pore water from the exposed concrete surface.

The larger the exposed surface of the concrete the greater the risk for plastic shrinkage and therefore cracking. For this reason elements with large exposed surfaces such as slabs on ground, suspended slabs in buildings, concrete pavements and bridge decks are mostly prone to plastic shrinkage cracking, especially in conditions with high evaporation rates which results in a higher capillary pressure build-up. These slab-like elements are also prone to plastic settlement cracks, especially if the slab contains embedded reinforcing steel, which hinders the settlement of the concrete above it causing differential settlement. It is this differential settlement that results in tensile stresses above the steel and also possible plastic settlement cracks.

After the plastic period, there are also several types of volume change that occur within the early age period. These include volume change due to temperature variations, cement hydration and drying. All these types of volume change in both the plastic and early age periods can result in cracking if restrained. Cracking in turn is one of the most unwanted defects associated with concrete structures, since cracks not only degrade the aesthetical appearance of any concrete structure but also accelerate the degradation of the concrete itself as well as any reinforcing steel imbedded within the concrete (Qi, 2003 and Deif et al., 2009).

It can be argued that the earlier cracking occurs in a structure the greater the possible negative influence on the durability and service life of a structure. According to this reasoning, plastic settlement and plastic shrinkage cracking give the largest potential for the reduction of the durability and service life of a structure. The necessity of preventing these cracks is evident and emphasised even further by the insignificant duration of the plastic period in which these cracks occur if compared to the typical 50-year design life of normal concrete structures. For these reasons it was decided to investigate the cracking of concrete in this plastic period which is further on referred to in this study as the cracking of plastic concrete. Furthermore, this study only considers slab-like elements as this is where both plastic settlement and plastic shrinkage cracking are most likely to occur.

Over the past 60 years, the cracking of plastic concrete has been well documented in literature (Lerch, 1957; Ravina & Shalon, 1968; Wittmann, 1976; Shaeles & Hover, 1988; Kronlöf, 1995 and Slowik et al., 2008). However, although the causing mechanisms and basic phenomological behaviour of both cracking types are known, cracking during the plastic period remains a problem in the construction industry even though there are several effective but mostly neglected precautionary measures that can be taken to minimise the cracking.

One of the main reasons for this is that most research conducted on this topic either focuses on plastic settlement cracking or plastic shrinkage cracking individually and not combined. Another reason why these cracks remain a problem is because there is no prediction model that accounts for all the complexities involved which range from the time dependency of material properties and volume change to different restraining and environmental conditions to different casting conditions and mix designs. This means that there are no tools available to engineers or contractors for designing a concrete element with the least possible potential for plastic cracking before it is constructed.

1.1. Objectives

This study sets out to achieve the following main objectives:

- Isolate and fundamentally understand the plastic settlement cracking of concrete in slab-like elements.
- Isolate and fundamentally understand the plastic shrinkage cracking of concrete in slab-like elements.
- Shed light on the combined cracking behaviour if both plastic settlement and plastic shrinkage cracking occur simultaneously.
- Experimentally determine the tensile material properties of plastic concrete.
- Develop a model that can simulate the cracking of plastic concrete in slab-like elements using a finite element method approach.

1.2. Methodology

The methodology adopted to achieve the objectives of this study is as follows:

- Conduct an in depth literature study on the cracking behaviour of plastic settlement and plastic shrinkage cracking individually as well as combined. The literature study should also include the tensile material properties of plastic concrete as well as the modelling of the cracking of plastic concrete.
- Conduct experiments on the cracking of plastic concrete, starting with tests where both plastic settlement and plastic shrinkage cracking are isolated and investigated individually, followed with tests where the two cracking types are combined. During the majority of these tests, important aspects and influencing factors such as: crack evolution, evaporation, bleeding, settlement, shrinkage, capillary pressure and setting times should be continuously monitored.

- Conduct experiments to determine the tensile material properties of plastic concrete. This requires a newly constructed test setup for conducting the tensile tests on plastic concrete.
- Develop a finite element model that uses the tensile material properties of plastic concrete together with the measured settlement and shrinkage of the concrete to simulate the cracking behaviour of plastic concrete. Furthermore, validate the model by using the results of the conducted experiments on the cracking of plastic concrete.

1.3. Research significance

The importance of preventing cracks in hardened concrete is well known due to possible decrease in durability and service life of a structure. However, the importance of cracking in the plastic period is often overlooked or neglected even though these cracks can occur within the first day of the concretes life resulting in severe premature durability and maintenance issues. This study highlights the complexity involved with these plastic cracks as well as the importance of preventing these cracks.

The study also provides the fundamental knowledge to understand and distinguish plastic settlement and plastic shrinkage cracking separately and combined. This knowledge is important to correctly identify and assess the observed cracks in a structure. Furthermore, the tensile material properties of plastic concrete, as determined in this study, assist in the understanding of the cracking behaviour by using familiar engineering concept such as stresses and strains which are practically very challenging to obtain for plastic concrete.

The study also provides a model that accounts for both plastic settlement and shrinkage cracking which can be used as a possible tool for determining the potential and severity of cracking in plastic concrete for any climate, mix and boundary conditions. Currently no such tool or model exists that can be used by engineers and contractors to prevent the cracking of plastic concrete.

Finally, all the knowledge and tools gained from this study greatly assist in ultimately preventing these rather complex cracks. The prevention of these cracks will not only improve the overall durability and performance of a structure but also reduce maintenance cost. This supports the global drive towards the building of sustainable, economical, aesthetical, useable, safe and longer lasting infrastructure.

1.4. Report outline

Chapter 1 provides an introduction as well as the objectives, methodology and research significance of this study.

Chapter 2 provides the background needed to firstly understand the cracking of plastic concrete and secondly to serve as basis for experiments and modelling as conducted further in the study. This includes background on the hydration and volume change of concrete at early ages as well as plastic settlement and plastic shrinkage cracking individually and combined. Furthermore, background is also given on the tensile properties of plastic concrete as well as the modelling of cracking in plastic concrete.

Chapter 3 describes the experimental framework of this study for both the tests on the cracking of plastic concrete as well as the tensile testing of plastic concrete. This includes descriptions of the test setups, moulds, mixes, conditions, testing procedures and test program.

Chapter 4 provides and discusses the results of tests on the cracking of plastic concrete. This includes tests on setting times, bleeding versus settlement as well as plastic settlement and plastic shrinkage cracking separately and combined.

Chapter 5 provides and discusses the results of tensile tests on plastic concrete using a new test setup. This includes discussions regarding the performance of the test setup as well as the tensile material properties achieved. Furthermore, links between the tensile tests and the tests on the cracking of plastic concrete are also considered.

Chapter 6 describes a finite element model used to simulate the cracking of plastic concrete. This includes the results achieved as well as the verification thereof. Furthermore, a parameter study and application of the model are also given.

Chapters 7 and 8 give the final conclusions that can be drawn from this study as well as recommendations for future studies.

Chapter 2. Background study

This chapter provides background on the cracking of plastic concrete in slab-like elements, starting with the definition of this term, followed by discussions regarding the hydration and volume change of concrete at early ages. Next, the durability issues related to cracking are discussed, followed by sections on the two earliest types of cracking in concrete namely, plastic settlement and plastic shrinkage cracking. Finally, the tensile material properties of plastic concrete are discussed as well as the principals of crack formation and approaches followed to model the cracking of plastic concrete.

2.1. Cracking of plastic concrete in slab-like elements

The *cracking of plastic concrete in slab-like elements* can be related to several different research areas. It is therefore appropriate to first describe the meaning of the term as used in this study. The term can be split into four parts, each describing an important aspect related to the overall meaning of the term. The four parts are: *cracking*, *plastic*, *concrete and slab-like elements*.

Cracking refers to the formation of cracks in a material. A crack is furthermore defined by the Oxford dictionary as: “a line on the surface of something along which it has split without breaking apart” or “a narrow space between two surfaces which have broken apart or been moved apart” or “a vulnerable point or flaw”. The ACI 201.1R (2008) defines a crack as: “a complete or incomplete separation of either concrete or masonry into two or more parts produced by breaking or fracturing”. From these definitions it can be concluded that cracking is the formation of line-like openings in a body of material which acts as weak points or flaws.

Plastic gives an indication to the state of matter or phase of the concrete while the cracking occurs. Concrete that is able to be shaped or moulded is said to be plastic (Powers, 1968). The concrete therefore behaves similar to a liquid. Concrete is only plastic for a limited time after mixing with water before it hardens to form a solid. The exact point in time where concrete changes from a plastic material to form a solid material is still unclear but is believed to be somewhere within the setting stage which end at the final setting time of concrete (ACI 231R, 2010 and Sant et al., 2009). Since the exact point where concrete is no longer plastic is not known, this study considers all

cracking that occurs up to the end of the setting stage, identified by the final setting time, as possible cracks in plastic concrete. In general, the plastic period only lasts around 3 to 8 hours after casting the concrete, although this time can fall outside of the mentioned range, depending on the type of mix used and temperatures conditions. It is further necessary to clarify the meaning of the following two terminologies that are used throughout this study: plastic concrete or concrete in the plastic period refers to concrete from being placed up to the final setting time and early age concrete or concrete in the early age period refers to concrete from the final setting time up to only a few days old (ACI 231R, 2010).

Concrete is defined as a mixture of cement, water, fine aggregate (sand) and coarse aggregate (gravel or crushed rock) in which the cement and water have hardened through a chemical reaction called hydration that binds the nearly inert aggregate (Domone & Illston, 2010). This definition covers traditional concrete, however modern day concrete also contain several admixtures and additions. Admixtures, normally in fluid form, are added to the concrete mostly to improve the fresh properties of the concrete such as workability, while additions or supplementary cementitious materials (SCM) are fined powders added to replace part of the cement. These additions can be inert such as grounded limestone or actively take part in the hydration reaction such as fly ash or slag. These additions together with the cement are referred to as the binder content of a mix.

Slab-like elements refers to the type of concrete element where these cracks, also referred to as plastic cracks, are most likely to occur. Slabs-like elements are generally thin flat elements with a large surface that is exposed to the environment. The thicknesses of these elements are normally less than 300 mm. This includes most slabs on ground such as pavements and warehouse floors as well as various types of suspended slabs such as bridge decks and flat- or coffer slabs in multi-storey buildings.

The term, *cracking of plastic concrete in slab-like elements,* therefore refers to all cracks that occur in slab-like concrete elements while the concrete is in a plastic state. Since these cracks occur so early in the life of a structure, they are greatly influenced by the hydration processes as well as the volume change that occur within young concrete as discussed in the next section.

2.2. Hydration and volume change of young concrete

In this study, young concrete refers to concrete from being cast up to only a few days old and includes concrete in the plastic period and early age period. The hydration, setting times, scheduling

of construction operations and volume change related to young concrete as well as the significance of these aspects on the cracking of plastic concrete are discussed in the following sections.

2.2.1. Stages of hydration

The hydration process of concrete can be divided into stages of *stiffening*, *setting* and *hardening* as shown in Figure 2.1. The figure also shows the type of volume change that occur, the states of matter of the concrete, rate of heat liberated from hydration reactions as well as the relative amount of change in the permeability, porosity and strength of the concrete (Powers, 1968; Mehta & Monteiro, 2006; Sant et al., 2009 and Domone & Illston, 2010).

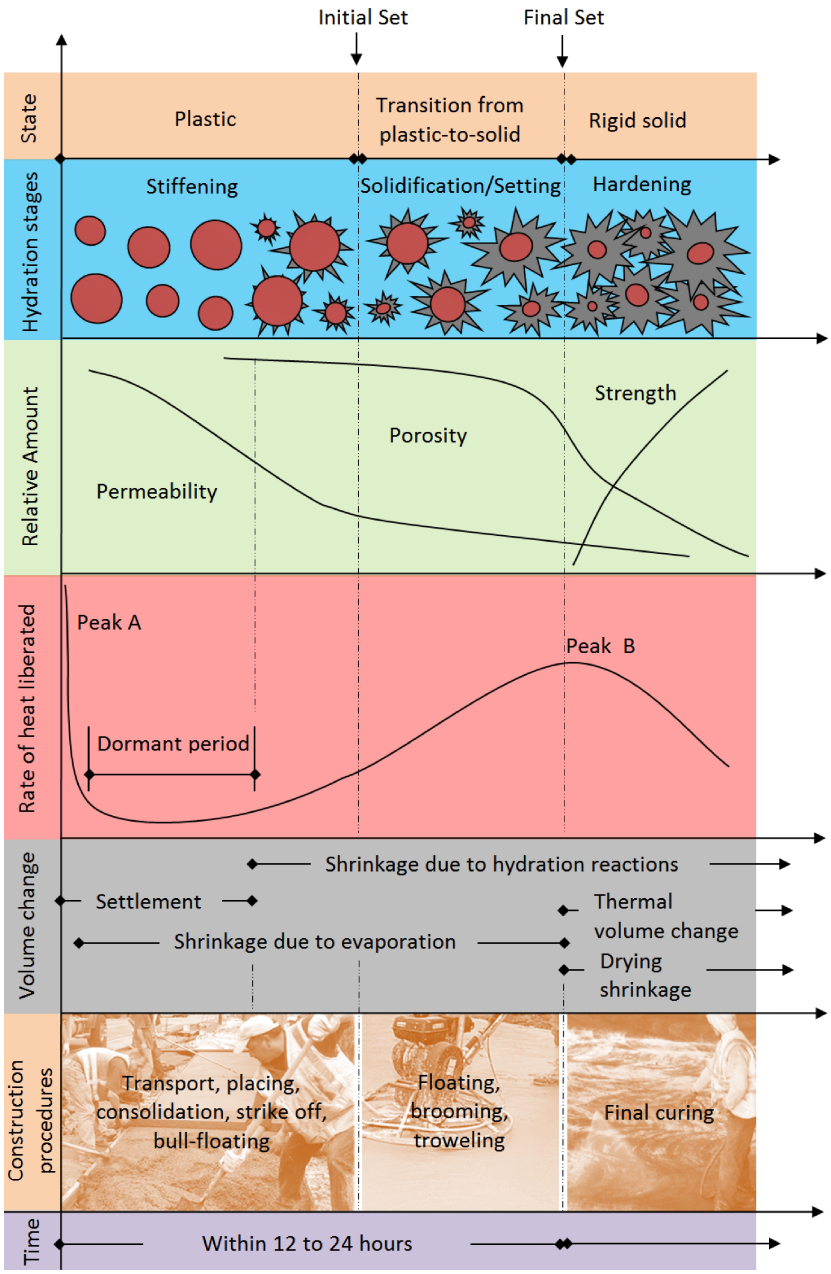

Figure 2.1. Illustration of the different stage in the hydration process (Adapted from Powers, 1968; ACI 308R, 2001; Mehta & Monteiro, 2006; Sant et al., 2009 and Domone & Illston, 2010).

The first stage, called the *stiffening stage*, starts once the concrete has been cast. During this stage the concrete is in a plastic state. The plastic nature of the concrete is due to the free water between the solid particles. This free water is gradually lost resulting in a reduction in plasticity or in other words the stiffening of the concrete, hence the stiffening stage. The water can be lost due to evaporation, absorption by unsaturated aggregates, formwork or subgrade as well as the formation of hydration products (Mehta & Monteiro, 2006). The hydration reaction is not immediate and only starts in the latter halve of the stiffening stage. The period before hydration starts is called the dormant period (Powers, 1968).

The hydration reaction is exothermic which allows the evolution of the hydration reaction to be identified by measuring the rate of heat liberated as shown in Figure 2.1. The initial intense Peak A as shown in the figure is due to the reaction between gypsum and aluminates in the cement. The gypsum is added to prevent the more intense reaction between the aluminates and water which causes immediate stiffening of the concrete, which would have made the placement of concrete problematic. After this short peak there is a dormant period where little to no heat is liberated meaning no hydration reactions. Without this dormant period concrete would not have been workable long enough to be cast and finished. Hydration of the silicates in the cement signifies the end of the dormant period and can be identified by the start of the ascending portion up to Peak B of the rate of heat liberated curve shown in Figure 2.1. This reaction can continue for many years and is the main contributor to the strength of concrete (Domone & Illston, 2010).

The second stage is called the *setting* or *solidification stage* where the concrete is in transition from a plastic material to a solid material, hence the solidification stage. The concrete does not solidify suddenly and requires a couple of hours to become fully rigid. The solidification is mainly due to the formation of hydration products corresponding with the large rate of heat liberated during this stage ending close to Peak B as indicated in Figure 2.1 (Mehta & Monteiro, 2006). The exact point in time where concrete changes from a plastic to a solid material is still unclear but is believed to be in the latter halve of this stage (Sant et al., 2009). At the end of the setting stage the concrete has solidified and is no longer plastic.

The final stage is called the *hardening stage* where the concrete starts to harden as well as gain significant strength. At the start of the hardening stage the concrete is still a weak solid with the hydration products only just filling the major voids in the concrete to create a solid skeleton. As the stage continues the hydration products start to overlap and intertwine to give a significant gain in

strength and stiffness. This process can be seen by the significant reduction in porosity of the concrete as shown in Figure 2.1 (Mehta & Monteiro, 2006). Although the hardening and strengthening of concrete can continue for many years the rate at which this occurs is most significant within the first few weeks after the concrete has been placed (Domone & Illston, 2010).

2.2.2. Setting times and scheduling of construction operations

Identifying the start and end of the stages of hydration is crucial for the scheduling of construction operations such as placement, compaction, finishing and curing of concrete. The initial and final setting times are used to distinguish between these stages. The end of the stiffening stage and start of the setting stage is at the initial setting time which is defined as the point in time when the concrete becomes unworkable and accordingly the placement, consolidation and bull-floating of concrete should be completed before the initial setting time as shown in Figure 2.1 (ACI 308R, 2001).

The end of the setting stage and beginning of the hardening stage is at the final setting time which marks the point in time for the start of hardening and significant strength gain of the concrete (Mehta & Monteiro, 2006). The setting stage is also called the window of finishability and accordingly all final finishing operations such as power floating and trowelling as well as brooming should be completed before the final setting time (ACI 308R, 2001). Final curing measures should be applied as soon as finishing is complete, which is normally around the final setting time.

The measurement of the initial and final setting times involves the measurement of penetration depths or resistance of needles or plungers into a setting paste. The methods used to measure these times do not signify a specific or sudden change in physical or chemical nature of the cement paste and merely provides a time when a paste reaches a certain degree of firmness or resistance to a penetrating object (Mehta & Monteiro, 2006 and Domone & Illston, 2010). However, although the measurement of these times is not precisely linked to a specific physical or chemical occurrence, the times have proven useful in distinguishing between the different stages of hydration as well as to provide an indication of the state of matter of the concrete.

2.2.3. Types of volume change

There are several types of volume change that can occur in young concrete. These types of volume change are normally driven by certain processes which can be dependent on time as well as the state of matter of the concrete. The volume change that occurs first is called settlement which is caused by the vertical settlement of the solid particles in the fresh concrete leaving a concrete body with a reduced vertical dimension. The settlement of the solid particles is also responsible for the

displacement of water to the concrete surface, called bleeding. Settlement starts once the concrete has been placed and ends at the end of the dormant period (Powers, 1968). Settlement causes a purely vertical reduction in volume and cannot be called a shrinkage or swelling type of volume change as this requires a process that brings about a volume change in all three directions. A more detailed discussion of settlement is given in Section 2.4.

The second volume change is a shrinkage caused by the evaporation of concrete pore water which causes a capillary suction within the pore water system of the concrete paste bringing about volume change in both the vertical and horizontal directions. This shrinkage starts once all the bleed water on the concrete surface has evaporated and ends once the concrete is no longer plastic i.e. at the end of the setting stage (Powers, 1968). This shrinkage is generally called plastic shrinkage and is discussed in more detail in Section 2.5.

The third volume change is the shrinkage due to hydration reactions and can be divided into two types of shrinkages namely chemical and autogenous shrinkage. When water reacts with cement (hydration reaction), the calcium silicate crystals that form have a smaller volume than the original water and cement. This volume reduction is called chemical shrinkage and it should be emphasised that this is the internal reduction in the absolute volume of solids and liquids in a concrete paste (ACI 231R, 2010). Chemical shrinkage starts once hydration starts at the end of the dormant period and continues as long as hydration continues (Sant et al., 2009).

Chemical shrinkage also drives autogenous shrinkage which occurs once the concrete paste solidifies and forms a porous structure. As hydration (chemical shrinkage) continues water is drawn from the vapour-filled pores creating internal capillary stresses that result in a visible dimensional change in the concrete sample which is often also referred to a self-desiccation. This reduction in external volume due to self-desiccation is called autogenous shrinkage (Sant et al., 2009).

In plastic concrete the chemical shrinkage is equal to the autogenous shrinkage. This is since the plastic nature of the system does not allow for the creation of empty pores and therefore the system collapses freely due to continuing chemical shrinkage resulting in the overall dimensional reduction of the concrete sample. After solidification the system cannot collapse freely anymore and forms a porous structure which is susceptible to autogenous shrinkage. Chemical and autogenous shrinkage are only considered to be significant for mixes with water-to-cement ratios of less than 0.4 (Sant et al., 2009 and CCIP-048, 2010).

Other sources of volume change such as, thermal effects and drying shrinkage only become significant once the concrete starts to harden and therefore do not have a noteworthy contribution to the volume change of plastic concrete (CCIP-048, 2010; ACI 231R, 2010 and Neville, 2011).

2.2.4. Importance to the cracking of plastic concrete

The discussions in Sections 2.2.1 to 2.2.3 hold the following importance or applicability in terms of the cracking of plastic concrete:

- The end of the setting or solidification stage can be conservatively assumed to be a point in time where concrete is definitely no longer plastic and any crack that occurs before this time should be considered as a possible plastic type crack. This assumption is in line with the Concrete Society's Technical Report No.22 (CCIP-048, 2010) which refers to cracks as plastic cracks if they form before the concrete starts to harden at the end of the setting stage.

- Cracks in concrete are principally formed by tensile stresses which develop in a concrete body when strains due to volume change are restrained. The volume change in plastic concrete can be attributed to three main sources. The first is a vertical volume reduction called settlement. The second is called plastic shrinkage and the third source is shrinkage (chemical and autogenous) due to hydration, with the latter only being significant for mixes with a water-to-cement ratio of lower that 0.4 (Sant et al., 2009 and CCIP-048, 2010). Mixes with such a low water-to-cement ratio does not form part of this study.

In conclusion, with regard to the scope of this study it is assumed that plastic settlement and plastic shrinkage together with the mentioned restraints are responsible for the cracking of plastic concrete in slab-like elements. Therefore the only two cracking types that need to be investigated are plastic settlement cracking and plastic shrinkage cracking. A more detailed discussion of both these cracking types follows in Sections 2.4 and 2.5 respectively.

2.3. Durability issues related to cracking

Cracking is a major concern for all concrete structures. Cracks are firstly unsightly and lower the aesthetical appeal and value of a structure. Secondly, cracks lower the stiffness of a structure, leading to increased deflections which can bring the serviceability and even safety of the structure into question. Finally, cracks create and accelerate durability issues in a concrete structure which

either leads to expensive reparation costs or a reduced service life or both (Qi, 2003 and Deif et al., 2009).

One of the main causes of durability issues in concrete structures is the corrosion of reinforcing steel embedded in the concrete. The corrosion process is started once the protective passivation layer around the reinforcing steel is destroyed. This protective layer forms due to the high alkalinity of the concrete and is destroyed by chloride ions or if the pH of the concrete is lowered through for example, carbonation. The movement of chloride ions and the carbonation front into the concrete is a timely process, naturally providing the steel protection against corrosion for a considerable time. The length of this time depends on factors such as the quality of the concrete in terms of permeability and the amount of concrete cover (Owens, 2009).

In the presence of cracks this entire corrosion process is significantly accelerated even if the concrete has the highest possible quality (Owens, 2009). Cracks acts as a type of highway whereby corroding agents such as water, oxygen, chloride ions and carbon dioxide can enter the concrete. This not only results in the deeper and faster penetration of these agents but in several cases directly exposes the reinforcing steel to the environment (Otieno et al., 2010). It is therefore important to prevent the formation of cracking in concrete for as long as possible to ensure that the expected service life of a structure can be reached without expensive repair costs. It can also be concluded that the earlier a concrete structures cracks the shorter its expected service life would be.

With this in mind, it can be argued that cracks formed in plastic concrete has the largest potential of all cracking types to result in premature durability issues and a corresponding reduction in service life. This is due to the early occurrence of these cracks in the life of a structure where they act as immediate penetration points for corrosion agents as well as weak points for further crack growth due to later volume change such as thermal-, chemical- and drying shrinkage (Weyers et al., 1982; Holt & Leivo, 2004; Slowik et al., 2009a and Kwak et al., 2010).

Another reason, for the reduced durability due to plastic cracking, is since these cracks are typically located directly above the horizontal reinforcing steel. This is illustrated in Figure 2.2 a) which shows a typical example of a plastic type crack pattern that coincides with the spacing of the reinforcing steel within a concrete slab. Figure 2.2 b) also shows a core that was drilled from the slab illustrating the penetration of the crack to the exact depth and location of the reinforcing steel. This highlights

the importance of preventing cracking in plastic concrete since, if present, these cracks promote and accelerate the start of durability issues within the first day after casting the concrete.

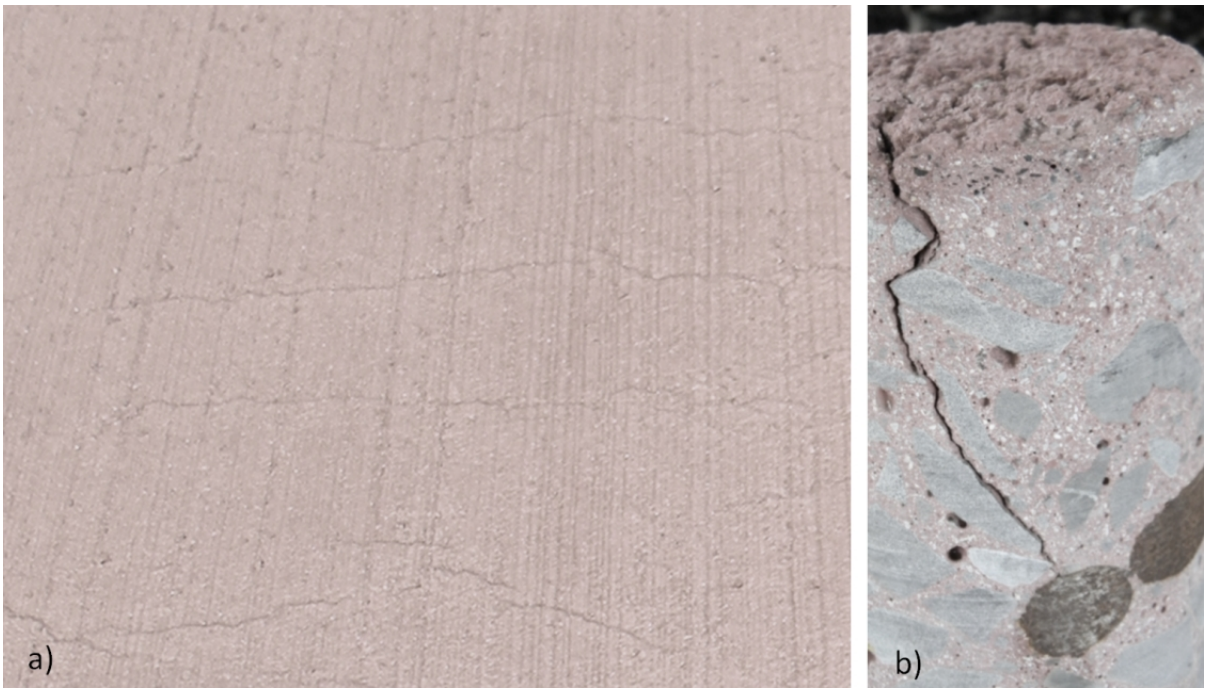

Figure 2.2. a) Typical plastic type crack pattern in a concrete slab clearly showing the reinforcing steel layout. b) Drilled core of slab showing the penetration of the crack to the depth and location of the reinforcing steel.

2.4. Plastic settlement cracking

Freshly mixed concrete is a mixture of solid particles and water. The solid particles range from sizes in micrometres in the form of cement particles to sizes in millimetres in the form of sand and stone particles. All these solid particles are denser than water with relative densities between 2.5 and 3.2. This means the solid particles tends to settle vertically in a freshly mixed concrete due to gravitation. As the solid particles settle, they displace water to the surface of the concrete. As this water flows past the particles it results in an upward force due to the viscous drag caused by the flowing water (Powers, 1968).

Figure 2.3 shows the major forces acting on a settling solid particle in a fresh concrete mix. The displaced water collects on the surface of the concrete and is called bleeding. This bleed water is removed, normally through evaporation, leaving a concrete body with reduced vertical dimension, called settlement (Powers, 1968). As mentioned in Section 2.2.3, settlement is a one-dimensional volume change driven by gravitation and cannot be defined as a shrinkage or three-dimensional volume change.

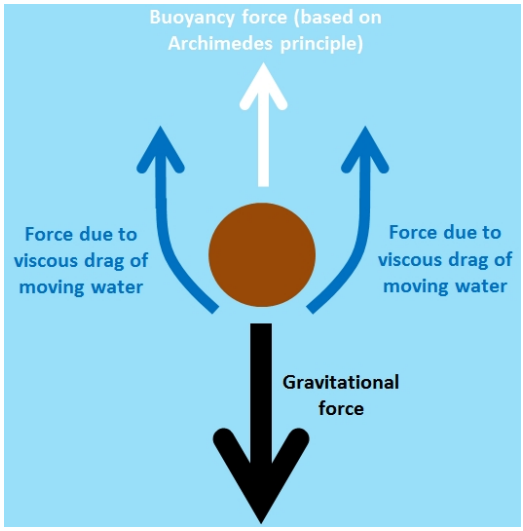

Figure 2.3. Major forces acting on settling solid particle in a fresh concrete mix.

The potential for plastic settlement cracking is only present if the process of settlement is active. The time when settlement ceases is generally at the end of the dormant period when hydration starts as discussed in Section 2.2.1. At this time the hydration products form bridges between the narrowest of interparticle gaps which hinders settlement. Settlement can also be ceased mechanically before the end of the dormant period if the solid particles physically come in contact with one another hindering further settlement (Powers, 1968). If the settlement of the concrete is restrained, cracks are likely to develop near the cause of the restraint, called plastic settlement cracks. The mechanism, influencing factors and preventative measures of plastic settlement cracking are discussed in the following sections.

2.4.1. Mechanism

Settlement can be seen as the driving force behind plastic settlement cracking. However, settlement alone will only result in a reduced vertical dimension with no cracks. Cracking can only occur if the uniform settlement of the concrete is disrupted creating a situation of differential settlement within a concrete specimen i.e. the concrete settles at different rates and amounts in different parts of the concrete body. Differential settlement occurs if a concrete body such as a slab has a non-uniform thickness which is caused by rigid inclusions in the slab such as reinforcing steel bars or a change in sectional height as with T-beams or coffer slabs (CCIP-048, 2010).

Figure 2.4 a) shows different zones of settlement caused by the inclusion of reinforcing steel bars. The concrete directly above the steel bars cannot settle as freely as the concrete between the steel bars. This causes a tensile stress to form above the steel bars which ultimately leads to cracking as shown in Figure 2.4 c). This also explains why crack patterns observed for plastic settlement cracking are linked to the spacing of the reinforcing steel bars as shown in Figure 2.2. Figure 2.4 c) also shows

the void that forms beneath a steel bar, which greatly reduces the bond between the concrete and steel. Similarly Figure 2.4 b) and d) show the differential settlement and cracks observed due to a change in sectional height in a T-beam. Differential settlement can therefore be seen as the cause or mechanism of plastic settlement cracking (Weyers et al., 1982 and Kwak et al., 2010). Practically, the bigger the difference in settlement between two opposite settlement zones, the greater the potential for cracking.

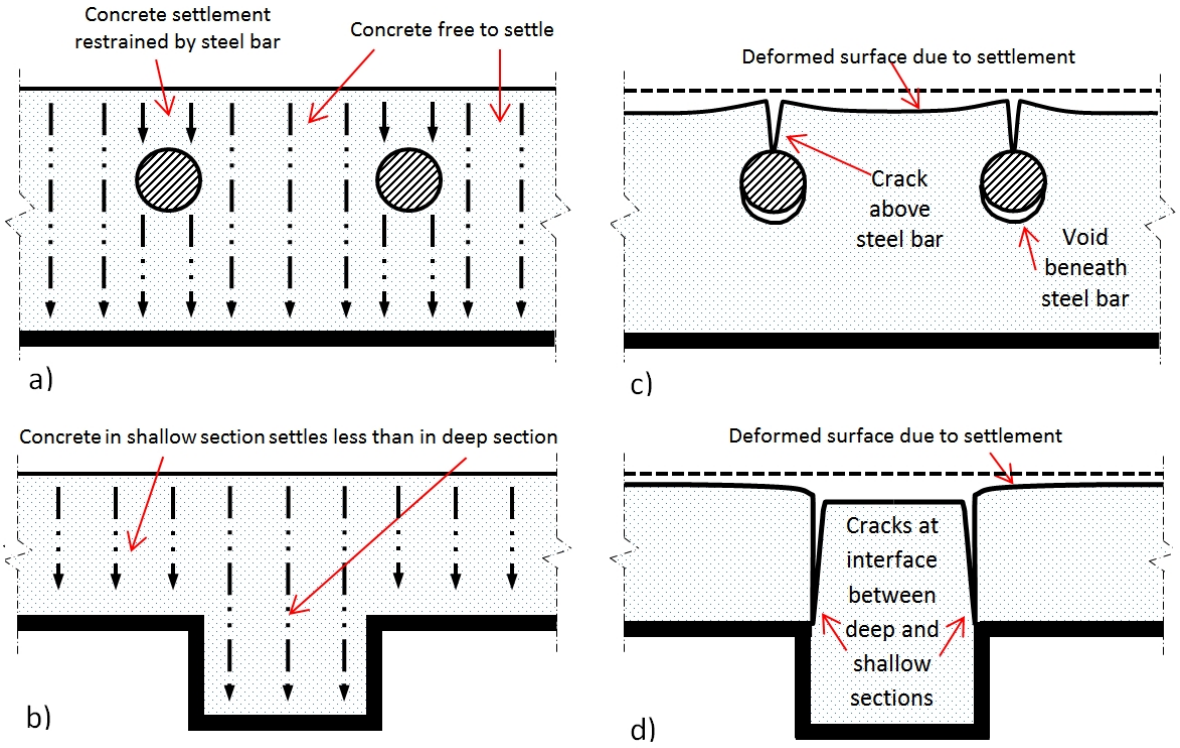

Figure 2.4. a-b) Slab just after placement showing differential settlement of concrete due to steel bars and a T-beam respectively. c) Slab showing the deformed surface due to differential settlement as well the plastic settlement crack above a steel bar and void beneath steel bar. d) Slab with change in depth for T-beam showing the deformed surface due to differential settlement as well as the plastic settlement crack at the interface between the deep and shallow sections.

2.4.2. Influencing factors

There are numerous factors that influence the plastic settlement cracking of concrete, however most of these factors are linked to two aspects namely: the amount and rate of settlement as well as the degree of differential settlement. The higher the amount and rate of settlement as well as the degree of differential settlement, the greater the potential for cracking. The main factors influencing the amount and rate of settlement are: setting times, concrete depth, water content, aggregate dispersion, fine content, wall effect and capillary pressure, while the main factors influencing the degree of differential settlement are: formwork geometry, concrete cover, as well as all the mentioned factors influencing the rate and amount of settlement. A discussion regarding each of these factors is given in the following sections.

Setting times

The rate of hydration (i.e. setting times of the concrete) influences the length of the dormant period in which settlement occurs. Settlement ceases once hydration starts at the end of the dormant period and therefore the faster the cement starts to hydrate (i.e. fast setting times) the shorter the period of settlement and the less potential for cracking. Water-to-cement ratio, cement type, temperature and admixtures mainly influences the setting times of concrete. In general, the more reactive the cement, the lower the water-to-cement ratio and the higher the ambient temperature the faster the setting times. Admixtures can also increase (retarders and certain plasticisers) or decrease (accelerators) setting times (Domone & Illston, 2010).

Concrete depth

The deeper a concrete slab, the more room and therefore potential for settlement to occur (Kwak & Ha, 2006).

Water content

The more water added to a concrete mix the more room and therefore potential for settlement to occur (Kwak & Ha, 2006).

Aggregate dispersion

The amount of settlement that can occur is governed by the dispersion of the aggregates. If the aggregates are dispersed evenly with large spaces between them, settlement can occur uniformly giving the aggregates space to settle unhindered by other aggregates. If however, the aggregates are spaced unevenly or to close together, the amount of settlement is reduced as the aggregates do not have enough space to settle unhindered by other aggregates (Powers, 1968). It is especially the dispersion and quantity of the large aggregates (stone) in a mix that determines the amount of settlement. A mix with a lot of stone does not provide ample room for the stone to settle before coming into contact with one another and vice versa, a mix with little stone provides plenty of room and therefore potential for unhindered settlement (Kwak & Ha, 2006).

Fine content

The amount, size and shape of the fines influence the amount of settlement and generally the more fines the lower the settlement. However, the size of the fines referred to is important and includes all particles smaller than 300 µm (Owens, 2009). Furthermore, the smaller the particles the less the settlement and it is especially the ultra-fine particles (smaller than 75 µm) that results in the greatest reduction in settlement. This includes the dust content of the fine aggregate (sand) as well as all cement and SCM particles. The shape of the particles also influences the settlement and the more angular the particles or in order words the less spherical, the less the settlement. The essential reasons why fines reduce the settlement are as follow (Powers, 1968):

- Fines decrease the permeability of the concrete which slows the bleeding/settlement rate by decreasing the movement rate of displaced water to the surface.
- The smaller the particle the larger the upward force due to the viscous drag as shown in Figure 2.3 which results in a lower overall downward force and therefore less settlement.

Wall effect

The rate and amount of settlement is less at the wall or side of a mould than in the centre of the mould. This is because the wall influences the symmetry of the flow pattern of water around a particle as illustrated in Figure 2.3. The particles near the wall experience a greater upward viscous drag and therefore settle at a slower rate. The viscous drag on these wall particles are higher partly since the wall is generally smooth and vertical facilitating more effective water movement, but mainly since the wall is stationary and does not move downward with the particles. This lower settlement near the side of the mould can even lower the amount of settlement in the middle of the mould if the mould is to narrow. To avoid such effects the diameter of the mould should be at least greater than the depth of the mould (Powers, 1968). Other research suggests that the range within which the settlement is influenced by the wall effect is 24 % of the mould depth (Kwak et al, 2010). This is an important aspect to keep in mind when selecting the geometry of the moulds for settlement measurements.

Capillary pressure

Capillary pressure can develop in the pore system of the concrete due to the evaporation of pore water from the surface. This only occurs once all the bleed water has evaporated, which is normally only the case in conditions with high evaporation rates. This capillary pressure has a vertical and horizontal component, where the vertical component forces the particles downward resulting in additional settlement. Capillary pressure can also increase the rate and amount of settlement as well as extend the time period in which settlement occurs (Powers, 1968). Capillary pressure is also the main mechanism responsible for the plastic shrinkage cracking of concrete and a detailed discussion is given in Section 2.5.1.

Formwork geometry

The geometry of the formwork influences the depth of the concrete slab. If the slab has any changes in depth such as with a T-beam or coffer slab, differential settlement can occur. The greater the difference in depth the higher the potential for cracks (Weyers et al., 1982).

Concrete cover

Concrete cover is the smallest distance between the outer surface of embedded reinforcing steel and the concrete's outer surface. With regards to plastic settlement cracking in slabs it is the distance

from the top most point of the top steel bars to the top surface of the slab. The smaller the cover, the greater the difference in settlement between the concrete above the steel bars and the concrete adjacent to the steel bars resulting in the development of larger tensile stresses above steel bars. This means that the smaller the cover the greater the potential for cracks (Weyers et al., 1982).

Settlement rate and amount

The higher the rate and amount of settlement the greater the difference in settlement would be between different settlement zones. The means that all the factors that influence the rate and amount of settlement as discussed earlier also influences the degree of differential settlement. For example, if the water content of the mix is increased, the amount of settlement would also increase resulting in a bigger difference in settlement of the concrete above and adjacent to a steel bar, thereby increasing the potential for cracking.

2.4.3. Preventative measures

There are three methods of dealing or preventing plastic settlement cracking. The first two aim to reduce the amount and rate of settlement as well as the degree of differential settlement while the other method entails the re-vibration of the concrete. A discussion of each of these methods follows:

- Any reduction in settlement can reduce the potential for cracking as discussed in the Section 2.4.2. Settlement can be reduced by increasing the ultra-fine content of the sand. The addition of the fine fraction of a crusher sand is especially effective in reducing the settlement. The settlement can also be reduced by the addition of synthetic micro fibres (± 0.9 kg/m³ of concrete) or through the addition of an air-entrainer. It should be noted that the addition of an air-entrainer will reduce the strength of the concrete (CCIP-048, 2010).
- The degree of differential settlement can be reduced by increasing the cover to reinforcing steel by as much as possible and in general the cover should be a least twice the maximum aggregate size (CCIP-048, 2010). In addition, avoiding any sudden change in sectional depth will reduce the potential for cracking. Another method of reducing the degree of differential settlement is through the sequential casting of the concrete. This means that the concrete slab is placed in different layers or sections. For example, if the deep parts of a T-beam as shown in Figure 2.4 b) is placed first and allowed to settle before the rest of the concrete is added, the degree of differential settlement is greatly reduced (Powers, 1968 and Kwak et al., 2008).
- Re-vibrating the plastic concrete just after settlement has ceased will close all cracks as well as any voids formed below reinforcing steel bars. However, the timing of the re-vibration is important. If it is applied to soon, settlement can still occur and lead to possible cracks and if it is applied to late it can negatively affect the strength of the concrete (CCIP-048, 2010).

2.5. Plastic shrinkage cracking

Concrete in a plastic state of matter can be seen as a mixture of solid particles and water. These particles settle, as discussed in Section 2.4, and displace water to the surface called bleeding. If the concrete surface is exposed to the environment, this bleed water evaporates. Once all the bleed water on the surface has evaporated, the free water within the concrete pore system is drawn out by the continuing evaporation. The evaporation of the pore water results in a shrinkage of the concrete, called plastic shrinkage. Plastic shrinkage is most severe if concrete elements with large exposed surfaces such as bridge decks, pavements, slabs on ground and suspended slabs are exposed to conditions with high evaporation rates.

The potential for plastic shrinkage is only present if pore water is evaporated out of plastic concrete. Once the concrete solidifies it forms a solid skeleton able of resisting the shrinkage stresses caused by the evaporation of pore water (Wittmann, 1976). The end of the setting stage can be taken as a point in time where the concrete is definitely no longer a plastic material but a solid as discussed in Section 2.2. The final setting time gives an adequate approximation of the end of the setting stage and can therefore be used as indication of when plastic shrinkage is no longer significant.

If the plastic shrinkage of the concrete is restrained, cracks are likely to form and are called plastic shrinkage cracks. The position and pattern of cracks depends on the type of restraint. If the element has a uniform thickness, cracking is mostly random and is referred to as a “crazed” crack pattern as shown in Figure 2.5 a). If the slab has a non-uniform thickness as a result of a varying depth or rigid inclusions such as reinforcing steel, cracks are normally linked to the positions of these slab non-uniformities as shown in Figure 2.5 b). However, it should be noted that these cracks may include crack growth due to both plastic shrinkage cracking and plastic settlement cracking as discussed further in Sections 2.6. The mechanism, phenomological behaviour, influencing factors and preventative measures of plastic shrinkage cracking are discussed in the following sections.

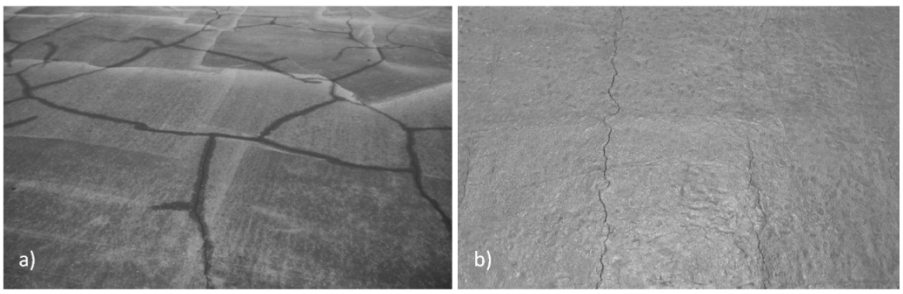

Figure 2.5. Plastic shrinkage cracking patterns: a) Crazed crack pattern (Slowik et al., 2008). b) Crack pattern linked to steel reinforcement layout.

2.5.1. Mechanism

Evaporation can be seen as the driving force behind plastic shrinkage cracking, while the actual mechanism responsible for the cracking is the capillary pressure build-up within the pore water system of the concrete (Wittmann, 1976, Cohen et al., 1990 and Slowik et al., 2008). Figure 2.6 illustrates the important stages (A, C and E) and points (B and D) during the capillary pressure build-up process within the pore system of plastic concrete.

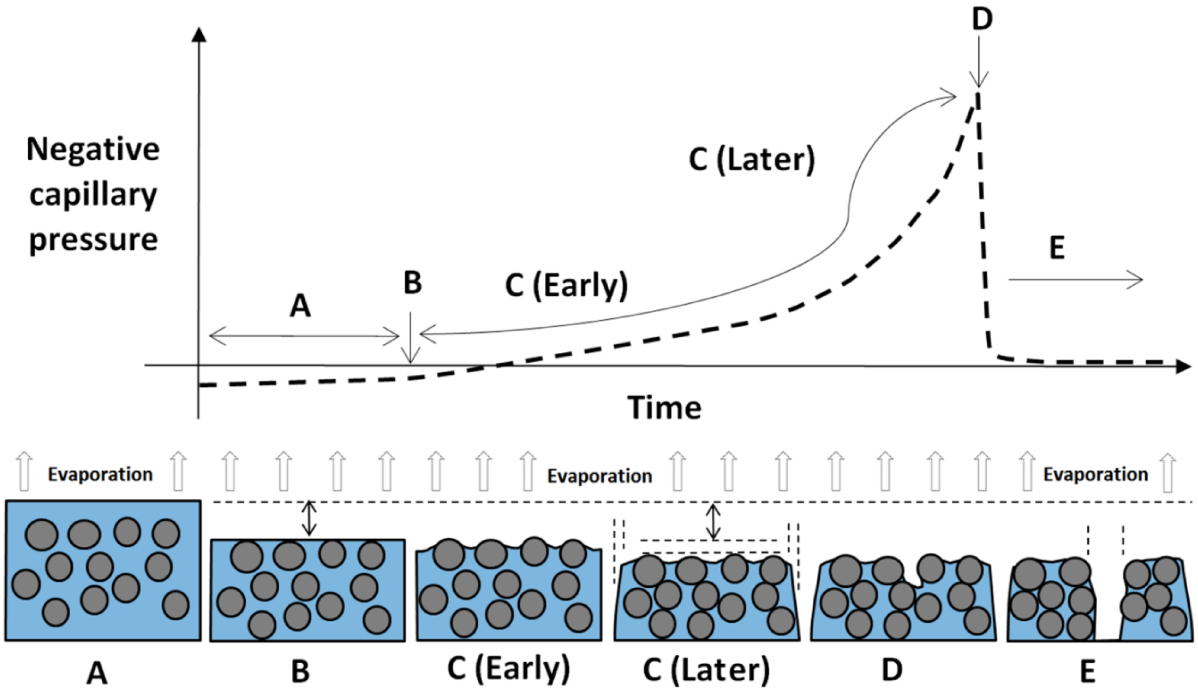

Figure 2.6. Important stages and points during the capillary pressure build-up process within the pore system of plastic concrete (Adapted from Slowik et al., 2008).

Stage A occurs directly after the concrete has been placed and represents the stage where the amount of bleed water on the surface is more that the amount of water that has evaporated from the surface. In the beginning of this stage the bleeding rate is more than the evaporation rate, while in the latter part of this stage the evaporation rate exceeds the bleeding rate. No capillary pressure can develop during this stage, since the surface of the concrete is continuously covered with a layer of bleed water. This stage ends at Point B where all the bleed water on the surface of the concrete has evaporated and this point is called the drying time.

From the drying time onwards the evaporation rate exceeds the bleeding rate resulting in the evaporation of pore water from within the concrete. This marks the start of the capillary pressure build-up as represented by Stage C. Once the pore water evaporates the water surface curve downward through adhesive forces and surface tension creating concave water surfaces between the solid particles called water menisci (Slowik et al., 2009b). These water menisci results in

contraction forces that tend to pull the particles together in both the vertical and horizontal directions as shown in Figure 2.7.

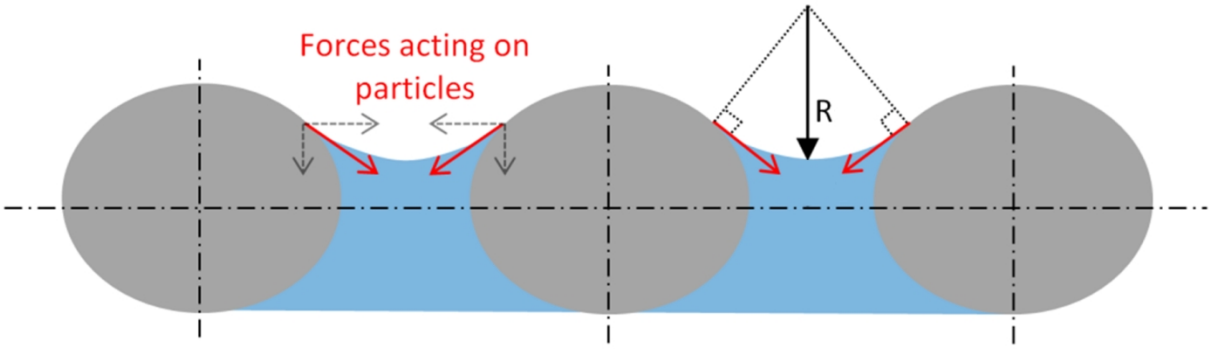

Figure 2.7. Forces caused by menisci forming in capillary pores.

As the particles move closer to one another they also compress the pore water resulting in a negative capillary pressure build-up. The vertical forces are responsible for an additional source of settlement that can aggravate the plastic settlement cracking as discussed in Section 2.4.2. This settlement due to capillary pressure also displaces additional bleed water to the surface, which can slightly relieve the capillary pressure build-up (Powers, 1968). This effect is however not noticeable in the later halve of Stage C due to the high rate of evaporation compared to the near zero bleeding rate. The pressure build-up P is inversely proportional to the radius R (shown in Figure 2.7) of the water meniscus as well as the surface tension σ_t of the water (Wittmann, 1976). This is called the Gauss-Laplace equation which reveals that the more concave the water menisci become the larger the capillary pressure.

$$P = -\frac{2\sigma_t}{R} \qquad (Eq.\ 2.1)$$

with:

P = pressure build-up [N/m^2]

σ_t = surface tension [Pa]

R = radius of water meniscus [m]

Point D marks the end of Stage C and is called the time of air-entry. This is the time where the radii of the menisci become too small to bridge the gap between particles resulting in the entrance of air into the pore system as well as a relocation of pore water. Air-entry occurs locally, often starting at the largest pores, and naturally forms weak spots for possible cracks if evaporation continues. However, although air-entry does not necessarily result in a crack, a crack cannot form at a location before air-entry has not occurred (Slowik et al., 2008).

It should be noted that the occurrence of air-entry does not mean the end of capillary pressure build-up in the plastic concrete as the graph in Figure 2.6 suggests. The graph merely indicates that the capillary pressure at the location of air-entry cannot be measured since the tip of the measuring device used is no longer be in contact to the pore water system. In other words, the capillary pressure continues to build-up in the concrete next to the air-entered locations as long as evaporation continues. Furthermore, the time of air-entry also coincides with the point of maximum settlement indicating that the horizontal component of the capillary pressure now plays the dominate role (Slowik et al., 2008).

Stage E is the cracking stage where the capillary pressure continues to build-up in the concrete adjacent to the air-entered location. This build-up of capillary pressure is relieved by the horizontal contraction of the concrete which now dominates the volume change. If this horizontal contraction is restrained, a weak spot formed by air-entry widens to form a plastic shrinkage crack.

2.5.2. Phenomological behaviour

The typical phenomenological behaviour for plastic shrinkage cracks can be summarised as shown in Figure 2.8 (Combrinck, 2011; Maritz, 2011 and Boshoff & Combrinck, 2013). This figure was compiled through the observation and measurements made during numerous tests on a wide variety of ordinary concrete mixes and environmental conditions.

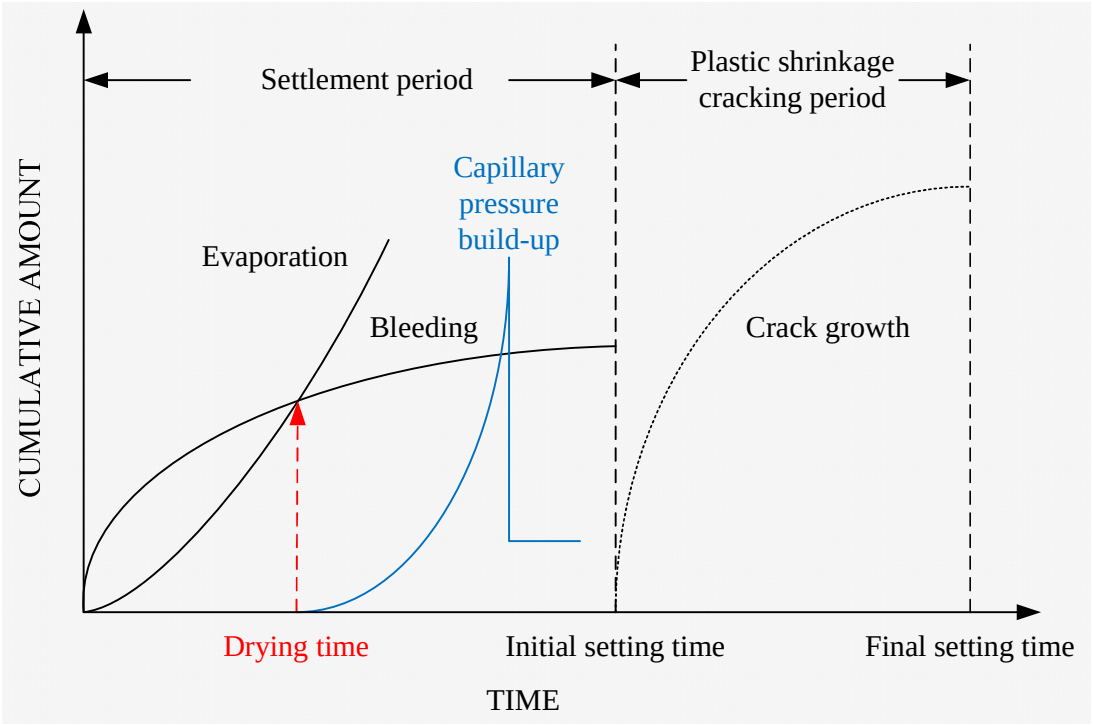

Figure 2.8. Typical phenomenological behaviour of plastic shrinkage cracks (Combrinck, 2011; Maritz, 2011 and Boshoff & Combrinck, 2013).

Figure 2.8 shows two time periods, starting with the settlement period and followed by the plastic shrinkage cracking period. The settlement period is directly after the concrete has been placed and includes the start of capillary pressure build-up once all the bleed water on the surface has evaporated, called the drying time. The capillary pressure, which was measured at the crack location, reduces suddenly and is known as the time of air-entry. These locations of air-entry form weak spots for future crack growth.

Air-entry occurs around the initial setting time which also marks the end of the settlement period. The majority of plastic shrinkage crack growth starts around the initial setting time and stabilises around the final setting time. This is called the plastic shrinkage cracking period and corresponds to the setting or solidification period as discussed in Section 2.2.1. Cracks may continue to widen after this period, but at a significantly lower rate and may include cracking due to thermal and/or drying shrinkage.

2.5.3. Influencing factors

There are numerous factors that influence the plastic shrinkage cracking of concrete. These factors typically vary with time and are also interdependent i.e. that the influence of these factors not only change with time but also affects the influence that other factors have on plastic shrinkage cracking. In addition, the material properties of the concrete during the first few hours after placement change rapidly as hydration transforms the concrete from a plastic material to a rock-like solid.

The complexity involved with the plastic shrinkage cracking of concrete should be kept in mind when considering its influencing factors. Cracking often only occurs when numerous factors combine in a certain and sometimes unpredictable manner. This makes predicting whether a specific factor will increase or decrease the risk for cracking difficult as a change in a specific factor also influences several other factors (CCIP-048, 2010). Some of the main influencing factors are evaporation, bleeding, material constituents, mix proportions, setting and restraint. A discussion of each is given in the following sections.

Evaporation

Evaporation is the process whereby a liquid such as water is converted into a vapour or gas. The water molecules can only escape the liquid as a vapour if the molecules absorb heat or if the vapour pressure above the liquid surface is less than in the liquid (Uno, 1998). The higher the rate of water evaporation the greater the risk for plastic shrinkage cracking. The main factors that influence the evaporation rate of free water are: wind speed, relative humidity, air temperature, concrete temperature, difference between air and concrete temperature as well as solar radiation

(Uno, 1998). In general, the higher the wind speed, concrete temperature, solar radiation and the lower the relative humidity the higher the evaporation rate. A large difference between the concrete and air temperature (i.e. a higher concrete temperature than air temperature) also results in a high evaporation rate.

However, conditions with high air temperatures are also often associated high evaporation rates, since higher air temperatures gradually heats up the concrete and more importantly lowers the relative humidity (ACI 308R, 2001). Relative humidity gives an indication of the water vapour saturation level of air at a certain temperature. A 100 % relative humidity means that the air at that specific temperature is fully saturated with water vapour and therefore there is no potential for water evaporation. If the air temperature increases, the relative humidity decreases allowing more space in the air for water to evaporate. The lower the relative humidity the more potential for water evaporation.

Theoretically, conditions giving the highest possible difference between concrete and air temperatures (i.e. concrete temperature should be much higher than air temperature) together with the highest possible wind speed and lowest possible relative humidity result in the highest evaporation rate. In arid and warm countries, such as South Africa, conditions with high air temperatures are more commonly associated with a high potential for plastic shrinkage cracking. This is because a high air temperature is normally associated with a high concrete temperature, low relative humidity and intense solar radiation which all increase the evaporation rate.

Uno (1998) developed an equation that can be used to estimate the evaporation rate. This equation accounts for most of the above mentioned factors and can be expressed as follows:

$$ER = 5 \times 10^{-6} (V + 4)[(T_c + 18)^{2.5} - r\,(T_a + 18)^{2.5}] \qquad (Eq.\ 2.2)$$

with:

ER = evaporation rate [kg/m^2/h]

V = wind velocity [km/h]

T_c = concrete temperature [°C]

r = relative humidity [%]

T_a = air temperature [°C]

Bleeding

Bleeding is the thin layer of water that can be observed on the surface of the concrete shortly after it has been placed. Bleeding is caused by the settlement of solid particles in the fresh concrete mix

which displaces water upwards as discussed in Section 2.4. Bleeding normally has two phases: first a phase where bleeding occurs at a constant rate, followed by a phase where the bleeding gradually diminishes to zero (Powers, 1968). The bleed water delays the capillary pressure build-up as long as the bleed water on the surface is more than the evaporated water. Once all the bleed water at the concrete surface has evaporated it gives a point in time from where capillary pressure can start developing and therefore also plastic shrinkage cracking.

In general, the more bleeding the less potential for plastic shrinkage cracking. However, increasing the bleeding of a concrete mix as a method to reduce plastic shrinkage cracking is not advisable (CCIP-048, 2010) as this will not only increase the risk for plastic settlement cracking but can also result in concrete quality issues such as surface laitance. Surface laitance refers to a poor quality concrete surface that occurs due to a higher water-to-cement ratio at the surface of concrete mixes with a high amount of bleeding. The factors influencing the amount and rate of bleeding are similar to the factors influencing the amount and rate of settlement as discussed in Section 2.4.2. These factors are setting times, fine content, aggregate dispersion, concrete depth and water content.

Material constituents and mix proportions

The material constituents and proportions of the concrete mix can influence the potential for plastic shrinkage cracking of concrete on both a chemical and physical level. On a chemical level the type of cement and admixture as well as the water-to-cement ratio influences the rate of hydration, which influences the setting and bleeding of the concrete. On a physical level the amount, shape and size of fines as well as the distribution of aggregates influences the bleeding and the capillary pressure build-up.

In general, the more fines in a concrete mix, the more potential for plastic shrinkage cracking (Uno, 1998). This is because smaller particles (fines) increases the amount of menisci and reduces the radii of menisci that form during the capillary pressure build-up as discussed in Section 2.5.1. This, together with the lower bleeding rate due to the fines, increases the magnitude of the capillary pressure build-up. Finer particles also has a higher mobility due to smaller resultant forces acting on them (see Figure 2.3) and are therefore more likely to result in large deformations if subjected to capillary pressure (Slowik et al., 2008). All of the above increases the potential for plastic shrinkage cracking in mixes with a high fine content. Fines include all fine aggregate, cement and SCM.

Setting

The setting of concrete is the process where freshly placed concrete gradually transforms from a plastic material to a solid through the hydration of cement as discussed in Section 2.2.1. In general,

the longer a concrete takes to set, the longer the plastic concrete is exposed to the environment increasing the potential for plastic shrinkage cracking. Factors that influence the setting are discussed in Section 2.4.2.

Restraint

As mentioned in Section 2.5, cracking can only occur if the shrinkage due to capillary pressure is restrained. The more the shrinkage is restrained the more potential for cracking. Restraint can be due to the uneven drying of the concrete, where the upper part of the concrete is restrained by the lower part of the concrete. The lower part shrinks less than the drying upper part and can also be restrained by the surface roughness of the underlying formwork or sub-grade. Restraint is also caused by changes in sectional height of a slab as well as ridgid inclusions such as reinforcing steel (CCIP-048, 2010).

2.5.4. Preventative measures

Despite the complex nature of plastic shrinkage cracking in concrete, it can be prevented if care is taken during the construction process. The short time period in which the cracking occurs as well as only one primary cause which is the loss of water through evaporation, emphasise that plastic shrinkage cracks can easily be prevented. However, negligence and the lack of knowledge during the construction process often result in cracking. In general, the correct construction procedures can in most cases prevent cracking. Most of these procedures or precautionary measures are aimed at reducing the water loss of the concrete and include the following (Uno, 1998; ACI308R, 2001 and CCIP-048, 2010):

- Protecting the concrete from wind by erecting temporary wind breaks. Although this is practically difficult on most sites, it remains an effective method of reducing the evaporation rate if constructed correctly.
- Casting the concrete early in the morning, late in the afternoon or even at night as well as using sunshades can greatly reduce the evaporation rate.
- Lowering the temperature of the aggregates used for mixing (by storing in shaded cool areas) or adding ice to the mixing water, reduces the concrete temperature and therefore evaporation rates.
- Initial curing procedures, for example: spraying a fine water mist above the concrete surface called fogging, covering the concrete with hessian or plastic sheeting, spraying curing compound or evaporative retarders all minimises the evaporation rate. The timing and correct application of these curing procedures are crucial to their success. Curing can only be effective if applied before

the cracking has occurred and cannot close cracks once formed. To prevent plastic shrinkage cracks these curing measures should be applied once all the bleed water on the surface has evaporated especially if this occurs before the finishing operations begin as discussed in Section 2.2.2.

In addition, changes in the mix design of the concrete can also be considered as an internal method of reducing the potential for plastic shrinkage cracking and include the following (Uno, 1998; Wontanakitcharoen, 2005 and CCIP-048, 2010):

- Reducing any excessive fines in the concrete mix decreases the cracking potential by increasing the bleeding and lowering the capillary pressure build-up.
- The addition of a low volume (± 0.9 kg/m³ of concrete) of synthetic polymer fibres to concrete lowers and controls plastic shrinkage cracking.

2.6. Plastic settlement and shrinkage cracking combined

Both plastic settlement and plastic shrinkage cracking are caused by different mechanisms and can occur separately in concrete elements without interaction. However, in the majority of slab-like elements this is seldom the case, especially elements containing reinforcing steel. Despite this, most literature either considers plastic settlement cracking or plastic shrinkage cracking individually, with only a few making reference to the interaction between these cracks.

Lura et al. (2007) investigated the influence of shrinkage-reducing admixtures on plastic shrinkage cracks and identified differential settlement as one of four driving forces for cracking. Ghoddousi et al. (2011) investigated the effect of reinforcement on plastic shrinkage and settlement of self-consolidating concrete as repair material and mentioned that plastic settlement cracking dominates plastic shrinkage cracking when the steel bars are placed near the surface of the concrete. Finally, Kwak et al. (2010) conducted experimental and numerical investigations on plastic settlement and briefly mentioned that plastic shrinkage cracks can be caused by plastic settlement and further stated that a study based on Korean conditions estimated that 40 % of plastic shrinkage cracking are caused by plastic settlement.

The apparent interaction between plastic settlement and plastic shrinkage cracking under certain conditions is evident and even obvious, since both cracks occur in quick succession of each other in a short time period and since both cracks share several important influencing factors such as bleeding,

capillary pressure and sources of restraint. This together with the short time period within which these cracks occur increases the difficulty of clearly distinguishing between the cracks. In general, plastic settlement cracking occurs first followed by plastic shrinkage cracking. However, the exact interaction between these two cracking types remains complex and to a large extent unknown.

2.7. Tensile material properties of plastic concrete

If the volume reductions due to both plastic settlement and plastic shrinkage are restrained, tensile stresses develop in the plastic concrete and cracks are likely to occur if the plastic concrete cannot withstand these stresses. Alternatively, cracks form once the tensile strain developed in the plastic concrete due to volume change exceeds the tensile strain capacity of the concrete. A more detailed discussion regarding the principles of crack formation is given in Section 2.9. In either case, both approaches to crack formation highlight the importance of determining and characterising the tensile material properties of plastic concrete. However, the liquid nature of plastic concrete significantly complicates the tensile test setup needed to determine these properties.

The tensile material properties of concrete can be tested directly or indirectly. Indirect tests, such as wedge spitting test and flexural testing of beams, are generally easier to conduct whereas direct tensile test provide more consistent results (Swaddiwudhipong et al., 2003). In terms of applicability to the cracking in plastic concrete the direct tensile tests provides a better representation of the actual cracking behaviour than indirect tests. In addition, the practical implementation of indirect tensile testing methods on plastic concrete will lead to incoherent and unreliable results (Ostergaard et al., 2004). Direct tensile test are therefore considered to be the appropriate choice for the tensile testing of plastic concrete. A discussion of the type of direct tensile testing setup needed as well as the typical tensile behaviour of plastic concrete is given in the following sections.

2.7.1. Test setups for tensile testing of plastic concrete

Plastic concrete, as mentioned, is a challenging material to test and it requires a rather special testing apparatus capable of handling and testing the still weak and mouldable concrete. Concrete displays a near liquid behaviour during mixing and placement, but once placed it starts stiffening, solidifying and hardening to form a rigid solid. The concrete therefore changes rapidly within a few hours from a plastic to a solid material as discussed in Section 2.2.1. Furthermore, the hydration products that form are still fragile during this period and can be disturbed by shock or movement (Hannant et al., 1999). Any test apparatus needs to account for both the changes that concrete undergoes during the first few hours after mixing as well as the sensitivity of the concrete to disturbance. The plastic

nature of the concrete further increases the difficulty of applying a tensile load to a concrete sample as well as complicates the measurement of strains and stresses that develop (Hannant et al., 1999).

The attempts made to measure the tensile material properties of plastic concrete generally used steel mould halves that are uniaxially pulled apart in a horizontal direction (Abel & Hover, 1998; Hannant et al., 1999 and Dao et al., 2009). At such a young age this is considered to be the most viable method of conducting direct tensile test as the plastic concrete is not yet able to support its own weight which rules out any vertical or mould-less type tests. The key issues that need to be overcome by the test apparatus are as follows:

- A method of gripping is needed to apply the tensile load to the plastic concrete specimen. Ideally this method should not induce any significant stress concentrations in the concrete sample, since this can lead to the localisation of cracks outside of the gauge area. The gauge area is a section of a test sample, normally in the middle, where the strain of the sample due to an applied stress is measured. This section should have a constant cross-sectional area.
- The vertical support of the mould halves should allow near frictionless horizontal movement. This is because even a small amount of friction could significantly influence the results due to the low strength of the plastic concrete.
- The measurement of the mould displacement is not adequate for the determination of the tensile material properties of plastic concrete due to the possible movement between the plastic concrete and the mould halves. The measurement of the actual deformation of the plastic concrete is therefore needed. This is problematic since the concrete is still wet and plastic which complicates the connection of traditional measuring devices such as linear variable displacement transducers (LVDTs) or strain gauges. Other non-contact methods such as digital image correlation are also complicated due to the still wet and non-constant appearance of the plastic concrete surface.
- The boundary conditions used at both the fixed and moving ends of the mould halves also influences the results obtained (Van Mier, 1997). The boundary conditions can be fixed or freely rotating (pinned) as shown in Figure 2.9 as well as a combination of the two. Fixed boundary conditions can lead to eccentric loading which causes an additional bending moment on the test specimen. This influences the appearance of mainly the post-peak stress-crack opening diagram, which shows a bump as shown in Figure 2.9. Pinned boundary conditions prevent additional bending moments, but can result in significant lateral deflection due to the heterogenic nature of concrete which generally causes the crack to start from one side of the specimen. In addition,

significant compression stresses can develop on the side of the specimen where the crack did not start if significant rotation occurs. It is still under debate which of these boundary conditions are best for uniaxial tensile tests on hardened concrete (Van Mier, 1997), and therefore even more so for plastic concrete where only a limited amount of these type of tests have been performed. For hardened concrete it has been found that the material properties such as tensile strength, Young's modulus and fracture energy are much lower for pinned tests than for fixed test and that the scatter of data for pinned tests are significantly larger than for fixed tests (Van Mier, 1997).

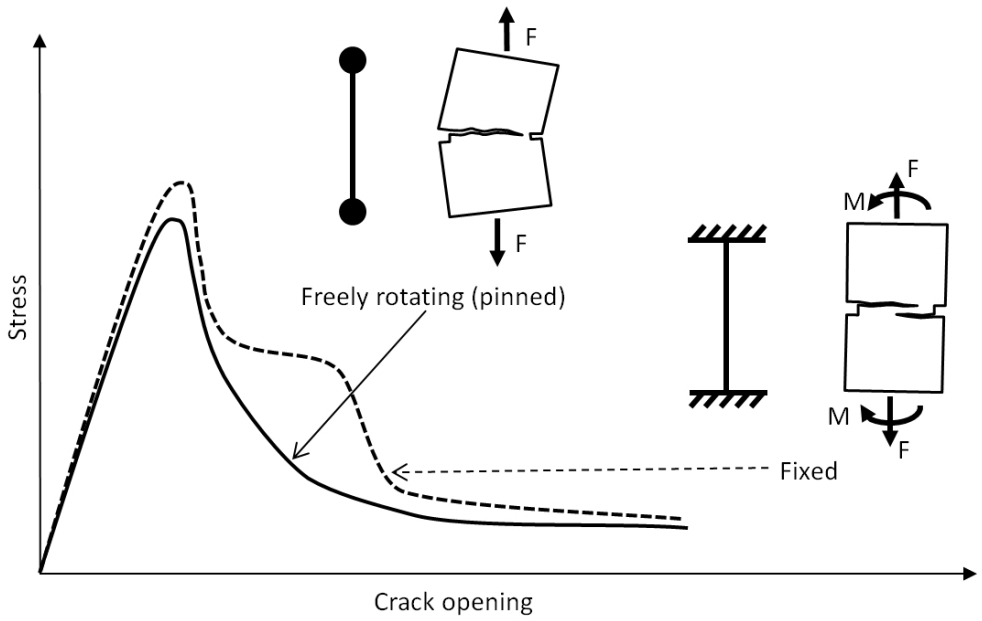

Figure 2.9. Typical uniaxial tensile stress-crack opening diagram showing the difference between freely rotating and fixed boundary conditions (Adopted from Van Mier, 1997).

The substantial practical difficulties associated with the determination of the tensile material properties of plastic concrete has resulted in limited research being conducted on this topic. However, a few notable contributions have been made in this field.

Abel and Hover (1998) conducted tensile tests on plastic concrete by pulling apart two cubed shaped mould halves containing shear keys to help grip the concrete. The mould halves were supported on ball-bearing slides to minimise the friction during horizontal movement. No displacements were measured on the concrete during these tests and no clear indication of the boundary conditions was given. Hannant et al. (1999) and Branch et al. (2002) also used a setup consisting of two cube shaped mould halves but with several significant improvements. The moulds included shear keys on the side to help grip the concrete as well as a curved neck section to force the crack in the gauge area. The strain on the concrete was measured by a LVDT that was attached to tapered sockets that were cast directly into the concrete. The boundary conditions were fixed on the stationary mould halve side to

prevent lateral movement while the moving mould halve was free to rotate through the use of universal joints. Finally, the moulds were floated on an air bearing which allowed virtually frictionless horizontal movement. Figure 2.10 shows the test setup used by Hannant et al. (1999) and Branch et al. (2002).

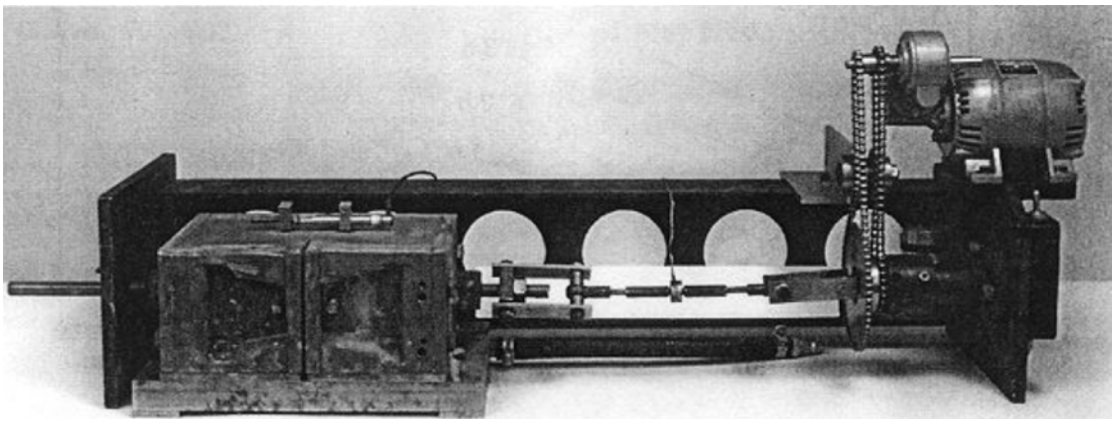

Figure 2.10. Tensile test apparatus used by Hannant et al. (1999) and Branch et al. (2002).

Dao et al. (2009) made further progress in the field of the tensile testing of plastic concrete, especially by improving the mould design of the concrete specimens. A split dog-bone shape mould was used as shown in Figure 2.11. The curved transitions effectively transmitted the tensile load to the concrete and also promoted failure to the middle section of the specimen by eliminating significant stress concentrations that could cause unwanted cracking outside of the middle section. The mould halves were also floated on an air bearing to reduce friction. No strain measurements were taken on the concrete itself, instead only the relative displacement of the mould halves was measured.

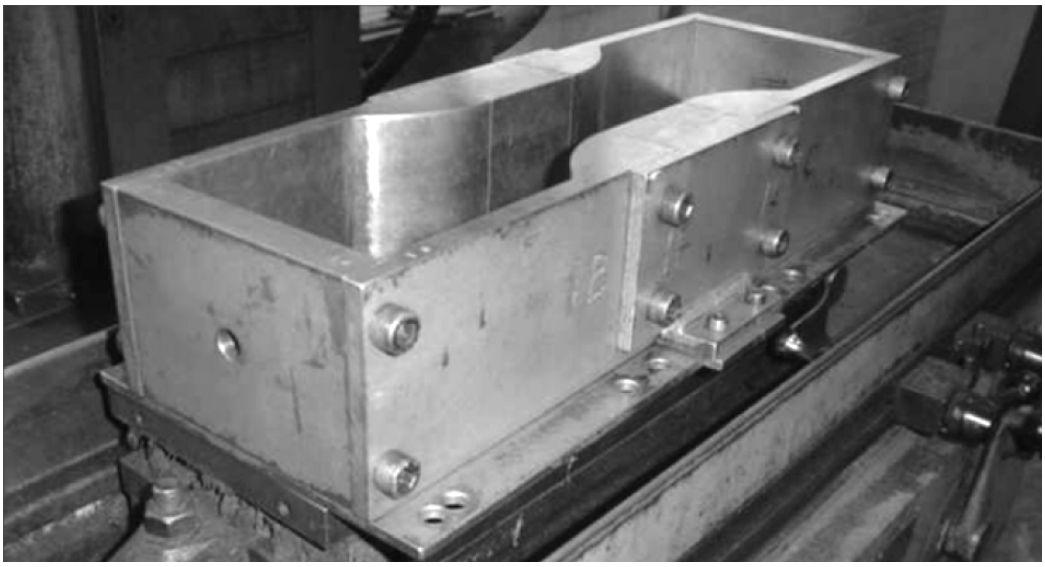

Figure 2.11. Steel dog-bone shaped mould used for tensile testing of plastic concrete by Dao et al. (2009).

To obtain the strain of the concrete, Dao et al. (2009) conducted a finite element analysis which determined that before peak stress is reached, the strain in the concrete within the gauge area (70 mm middle section) is 50 % of the measured mould displacement, while after peak stress it is 90 % of the measured mould displacement. This assumption was used to determine the tensile material properties of the plastic concrete. However, the correctness of this assumption remains questionable. Finally, in terms of boundary conditions, the stationary halve of the mould was pinned connected and although not specifically stated it is assumed that the moving mould halve was also pinned connected since the air bearing box had four adjustable steel lugs to prevent sideways movement of the mould during testing.

Form the above discussion of different test setups it can be concluded that a test setup with the following characteristics is sought after:

- A dog-bone shaped mould with curved transition to reduce stress concentrations.
- An air bearing vertical support structure beneath the mould to provide frictionless horizontal motion.
- Strain measurement on the concrete is needed to determine the material properties of the concrete.
- The boundary conditions needed it still unclear, although it seems that a compromise between fully fixed and freely rotating is needed.

2.7.2. Tensile behaviour of plastic concrete

Characterising the tensile material properties of plastic concrete is rather complex and still in its infancy with only limited research available on the topic and even less research capable of showing the complete stress-strain curve of plastic concrete (Hannant et al., 1999 and Dao et al., 2009). This is due to the rapid change that concrete undergoes as it transforms from a plastic material to a solid in just a few hours as well as the difficulties associated with conducting tensile tests on such a material. Furthermore, the application of the principles used to describe the mechanics of solid materials on a still plastic material is also questionable, but it is believed to be a necessary step towards gaining a better understanding of the cracking of plastic concrete.

Figure 2.12 shows a typical stress-strain relationship of a quasi-brittle material obtained from a uniaxial tensile test. The important tensile material properties that can be determined from such a graph can be spilt into two sections namely the pre- and post-peak properties. The pre-peak or ascending properties are the *tensile strength* (Ft), *Young's modulus* (E) and *strain capacity* (ε_{cap}),

while the post-peak or softening properties are related to *fracture energies* (G_F and G_f). These properties are defined as:

- The *tensile strength* (F_t) is the maximum stress that the specimen can withstand before failure and is also called the peak stress.
- The *Young's modulus* (E) is the gradient of a straight line fitted to the ascending section of the stress-strain curve and is the property indicating the stiffness of a material.
- *The strain capacity* (ε_{cap}) is the strain at maximum strength (F_t) or peak stress and gives an indication of the brittleness or ductility of the material. Materials that can undergo large strains or deformations before failure are called ductile materials and materials that fail at small strains are called brittle materials. The term ductile and brittle, in the strict sense of the word, relates to the mode of failure or fracture that occurs. Brittle failure is therefore sudden and unexpected due to the lack of large deformations, while ductile failures are more timely and accompanied by large deformations.
- *Fracture energy* is the amount of external energy needed to create and fully separate a unit crack surface area. The *total fracture energy* (G_F) is the shaded grey area under the stress-strain curve as shown in Figure 2.12. The *initial fracture energy* (G_f) is the dotted area under the stress-strain curve and follows the initial gradient of the softening curve as shown in Figure 2.12. The unshaded region in the figure represents irreversible strains outside of the fracture process zone (Dao et al., 2009).

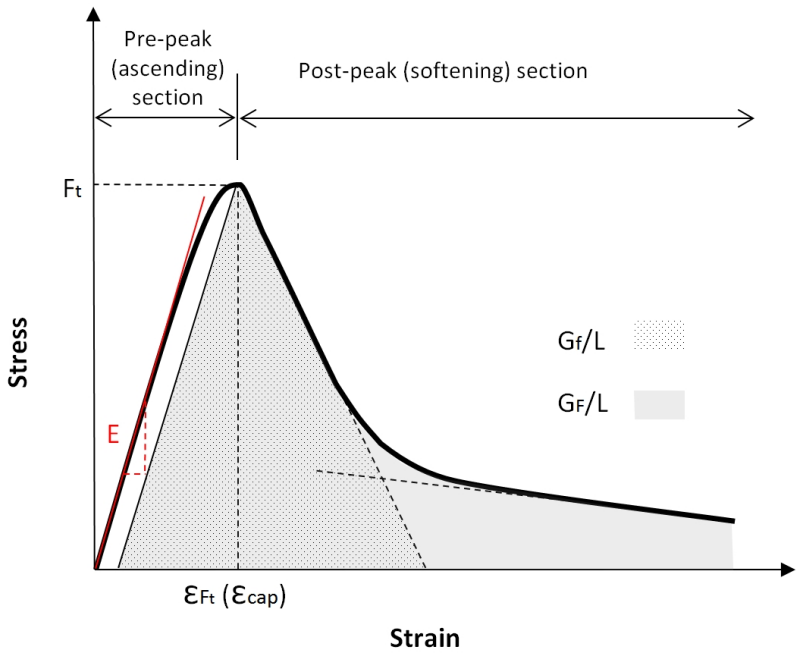

Figure 2.12. Typical stress-strain curve from uniaxial tension test showing definitions of important tensile material properties.

The study conducted by Hannant et al. (1999) was one of the first to publish the complete stress-strain curves for both a so-called retarded high strength concrete as well a normal concrete as shown in Figures 2.13 and 2.14 respectively. The figures clearly show the significant variation in tensile behaviour of plastic concrete as time progresses in 1 hour intervals up to an age of 5 hours. The 1 and 2 hour tests for both concrete mix types reveals a material with a very low stiffness and strength that behaves in a ductile manner. This means the concrete at such an early age is capable of large deformations before it fails (ductile failure).

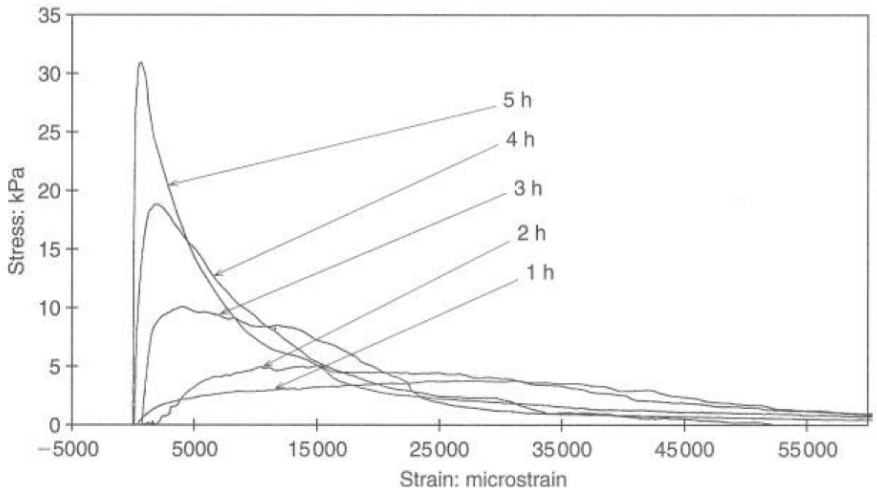

Figure 2.13. Tensile stress-strain curves obtained for a so-called retarded high strength concrete mix by Hannant et al. (1999).

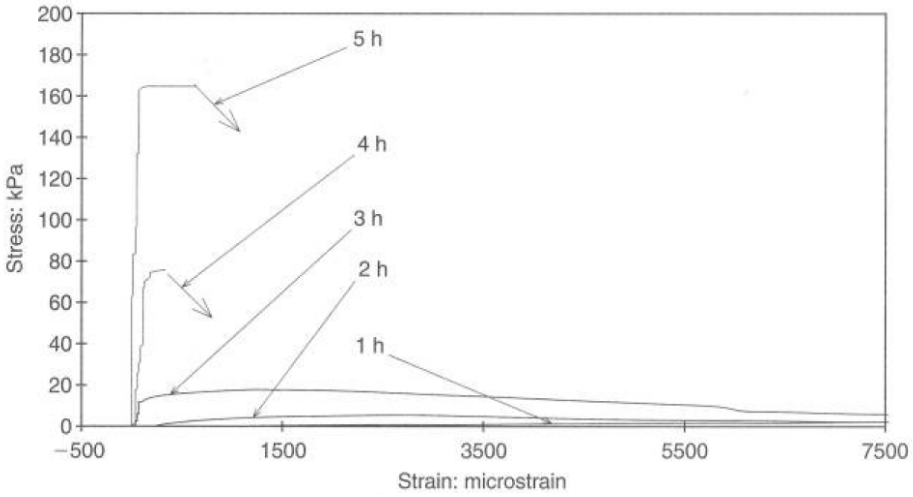

Figure 2.14. Tensile stress-strain curves obtained for a normal concrete mix by Hannant et al. (1999).

The 3, 4 and 5 hour tests for both concrete mixes show a significant increase in strength and stiffness, but failure occurred at a much lower strains (brittle failure) which is especially noticeable for the 4 and 5 hour tests. The failure mode of the concrete therefore changed suddenly from a ductile to a brittle or quasi-brittle type failure. In fact, the data recording system used by Hannant et

al. (1999) could not follow the post-peak behaviour of the normal concrete mix for the 3 hour test and onwards due to the sudden (brittle) nature of the failure as shown in Figure 2.14.

The tensile strength is the property of plastic concrete that has been studied the best in the available literature and although these studies used different mixes they all showed a similar trend, where the tensile strength initially developed slowly, after which it increased exponentially at around 3 to 5 hours after mixing (Abel & Hover, 1998; Hannant et al., 1999; Branch et al., 2002 and Dao et al., 2009). This is illustrated in Figure 2.15 which shows the results of tensile strength as a function of time for three different concrete mixes as achieved by Dao et al. (2009). The mixes were named according to their strength and slump value for example: Mix 32-25 means the concrete had a 32 MPa 28-day strength and 25 mm slump.

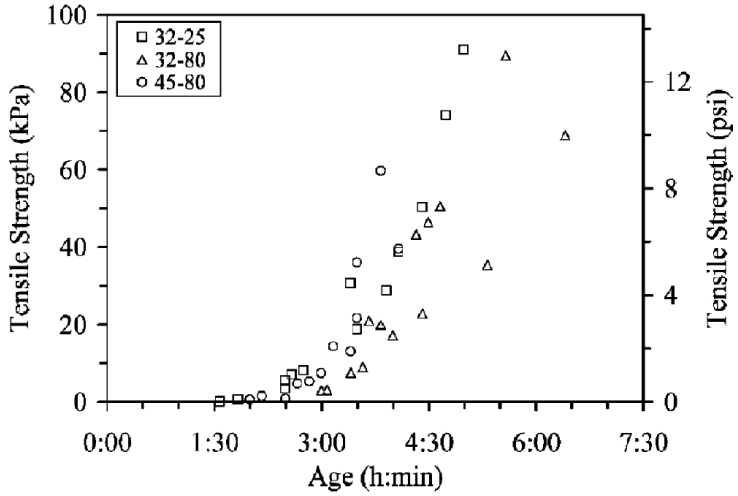

Figure 2.15. Results of tensile strength versus age of concrete as achieved by Dao et al. (2009) for three different concrete mixes.

The strain capacity of plastic concrete has been defined in this section as the strain at peak stress, but it can also be described as the maximum tensile strain a material can undergo before it fails or cracks. This makes the strain capacity a very important property for not only plastic concrete but also hardened concrete as discussed further in Section 2.9 regarding the principles of crack formation. Boshoff and Combrinck (2013) composed a graph of strain capacity as a function of time using the results of several different studies as shown in Figure 2.16. The figure shows that the strain capacity of plastic concrete is initially very high, in fact several orders of magnitude larger than hardened concrete. However, as the plastic concrete stiffens and solidifies the strain capacity drops significantly to its lowest value which is believed to be somewhere within the setting time of concrete. As the concrete hardens the strain capacity increases again but never to the same levels as obtained for plastic concrete.

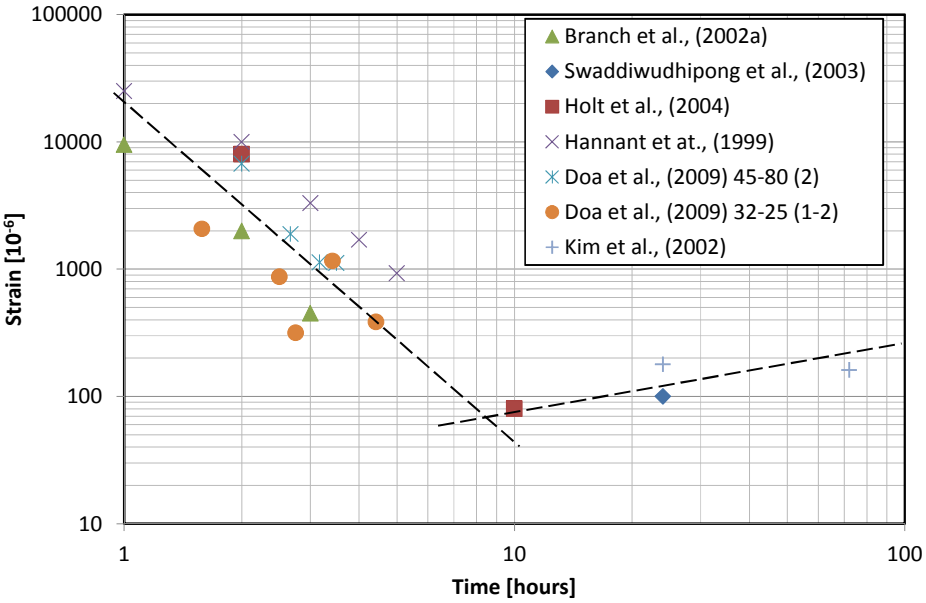

Figure 2.16. Tensile strain capacity of concrete versus time as composed by Boshoff and Combrinck (2013).

The determination of Young's modulus and total fracture energy of normal plastic concrete has not received significant attention in literature and the work of Dao et al. (2009) was the only study that could be found that determined these materials properties. Dao et al. (2009) showed that the Young's modulus and the total fracture energy of the plastic concrete follow a similar trend as the tensile strength. In fact, Dao et al. (2009) suggested a near linear relationship between the tensile strength and both the stiffness and total fracture energy respectively. Figures 2.17 and 2.18 respectively show the exponential increase in stiffness and total fracture energy of plastic concrete at around 3 hours after the initial slow development as measured for the three concrete mixes tested by Dao et al. (2009).

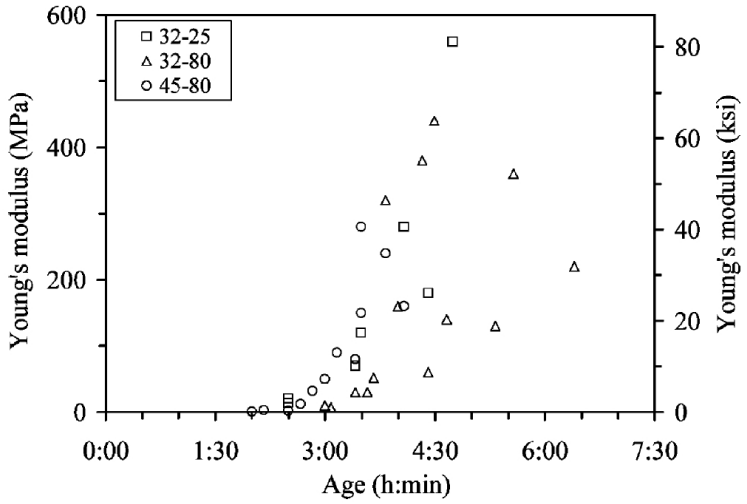

Figure 2.17. Results of Young's modulus versus age of concrete as achieved by Dao et al. (2009) for three different concrete mixes.

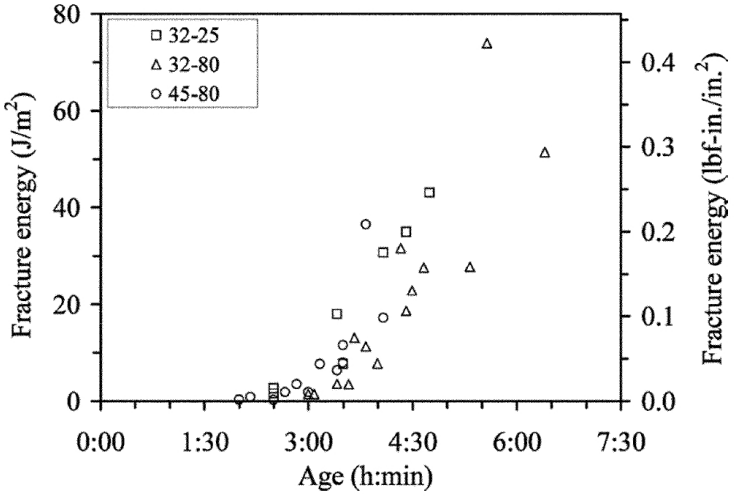

Figure 2.18. Results of total fracture energy versus age of concrete as achieved by Dao et al. (2009) for three different concrete mixes.

Figure 2.19 shows results obtained by Branch et al. (2002) comparing the peak stress and strain capacity of a normal concrete mix (control) with a high-strength concrete (ms). Branch et al. (2002) conducted at least four tests per hour per mix to obtain more statistically valid results. The 95 % confidence intervals for the test results as shown in Figure 2.19 reveal the great variability and scatter that occur when conducting tensile test on plastic concrete. In fact, Branch et al. (2002) stated that tests on plastic concrete probably show greater variability than test on hardened concrete. Furthermore, the results obtained by Dao et al. (2009) suggest that the results of Young's modulus and fracture energy are even more scattered than for the tensile strength and strain capacity. The possible large scatter that can be expected when conducting tensile test on plastic concrete should be kept in mind if the results are to be used for comparison between different mixes. In such a case, more than one test needs to be performed to achieve statistically valid results.

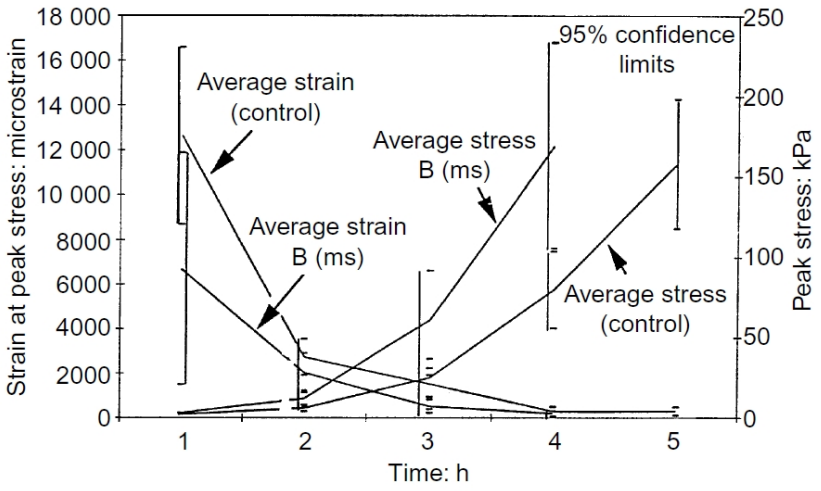

Figure 2.19. Indication in the significant variability and scatter in results obtained by Branch et al., (2002) comparing the peak stress and strain capacity of two different concrete mixes.

2.8. Fracture mechanics

Fracture mechanics is the study of the growth of cracks in materials, where the basic criteria is that cracks can only grow if the energy required to create a crack surface is provided. This field of study was probably first initiated by Griffith in 1920, who studied the fracture of brittle materials such as glass. Since then, there has been considerable development where fracture mechanics has been successfully applied to ductile materials such as metals as well as quasi-brittle materials such as concrete. However, the application of fracture mechanics to plastic concrete is not well-established (Dao et al., 2009) and it is therefore more appropriate to discuss the successful application of fracture mechanics to the fracture of mature concrete. This serves as background and starting point for the possible application of fracture mechanics to the fracture of plastic concrete. Discussions regarding the fracture process zone as well as concrete fracture models as applied to mature concrete are given in the following sections.

2.8.1. Fracture process zone

The concept of a fracture process zone (FPZ) was first applied to concrete by Hillerborg et al. in 1976 although being developed earlier for materials with plastic and softening behaviour such as metals. Both concrete and metal structures of normal size exhibit non-linear fracture mechanics with the development of a large non-linear zone at the fracture front as shown in Figure 2.20 (Bazant, 2002). This non-linear (N) zone can also be explained as the transition zone from a fully open crack to undamaged or uncracked material that still exhibits linear (L) behaviour. The tip of this non-linear zone, i.e. the tip of the crack, is called the FPZ. The FPZ is where the material undergoes softening damage such as tearing while in the non-linear zone that surrounds the FPZ there is hardening plasticity or perfect yielding (Bazant, 2002).

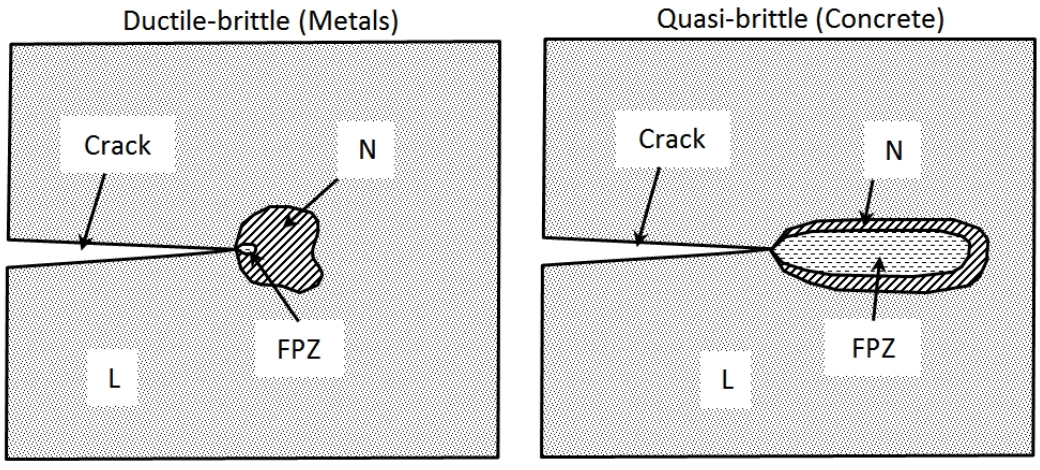

Figure 2.20. Fracture process zone (FPZ), non-linear hardening zone (N) and linear zone (L) in ductile-brittle materials (metals) and quasi-brittle materials (concrete) (Bazant & Oh, 1983).

There are considerable differences between the size of the FPZ and non-linear zones for ductile-brittle materials (metals) compared to quasi-brittle materials (concrete) as shown in Figure 2.20. For metals the FPZ is small, while the non-linear zone, where plastic flow typically occurs, is large. However, for concrete the non-linear zone is almost completely filled by a large FPZ (Bazant, 2002). The FPZ of concrete can further be divided into a bridging and microcracking zone as shown in Figure 2.21 (Shi, 2009). The bridging zone is where the aggregates in the concrete bridge the crack although the bond at the interface between the cement paste and aggregates has significantly reduced in this zone while the microcracking zone shows multiple ultra-fine cracks indicating only the start of the debonding at the interface between the cement paste and aggregate.

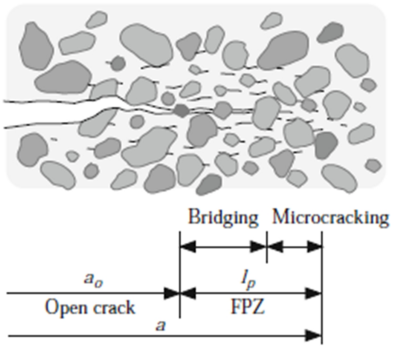

Figure 2.21. Typical fracture process zone (FPZ) for concrete in front of the crack opening (Shi, 2009).

2.8.2. Concrete fracture models

The study of the fracture of concrete requires a model that defines the FPZ that develops in front of the crack tip in concrete. The two most notable and widely used models are the fictitious crack model (FCM) as proposed by Hillerborg et al. (1976) as well as crack band model as proposed by Bazant and Oh (1983).

The FCM describes the FPZ as a fictitious line crack that can transfer a normal stress (σ) which is a function of the opening of the crack (w) as shown in Figure 2.22 a) and b). At the start of the FPZ, corresponding to the maximum crack opening, the normal stress is zero, while at the end of the FPZ where the crack opening is zero the normal stress is at its maximum, corresponding to the maximum tensile strength of the concrete. The area under the normal stress-strain curve from the start to end of the FPZ (i.e. the softening stress-crack opening curve) represents the energy dissipated per unit surface crack area and therefore also the external energy required to fully open a unit surface crack area. This energy is more commonly referred to as fracture energy. Before the start of the FPZ the crack is assumed to be fully open and therefore no stresses are transferred over the crack once it has fully opened (Hillerborg et al., 1976).

The crack band model is based on similar concepts as used for the FCM, except the FPZ is described within a certain finite bandwidth as shown in Figure 2.21 c) instead of a line crack as with the FCM. The strain induced by crack opening is then uniformly distributed over this bandwidth. Furthermore, the behaviour after cracking is described by a stress-strain relationship (Figure 2.21.d) and not a stress-crack opening relationship as with the FCM (Bazant & Oh, 1983).

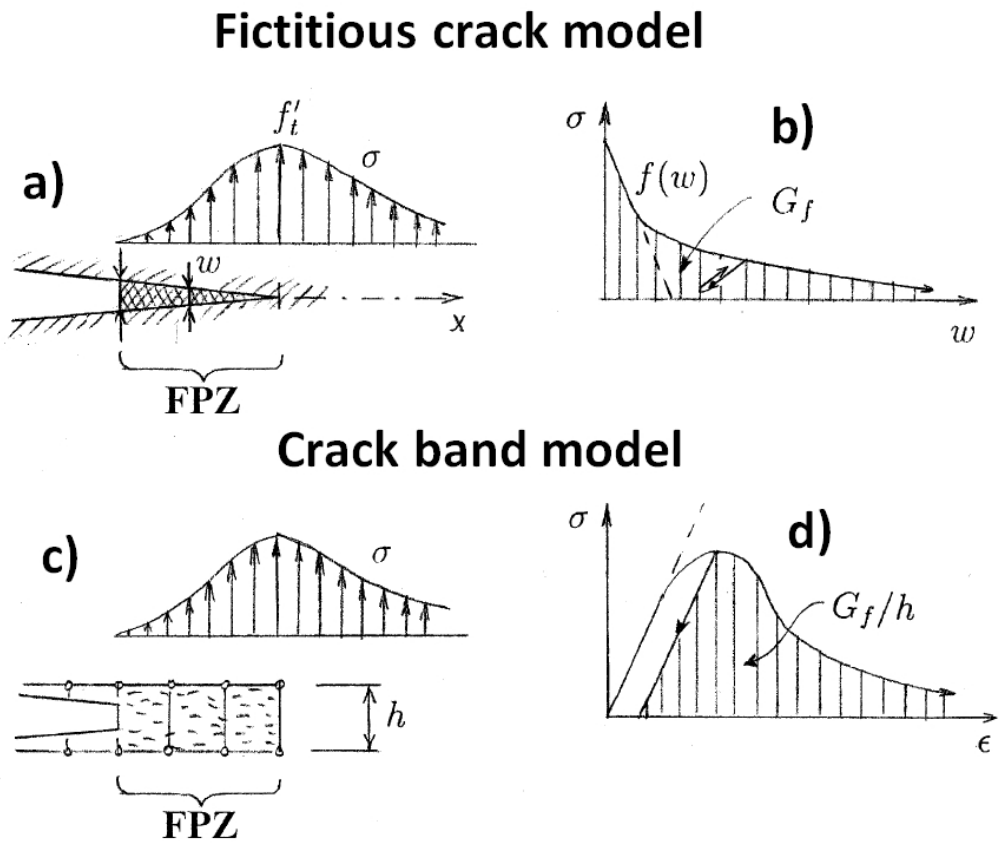

Figure 2.22. a-b) Stress distribution and softening curves for the fictitious crack model (FCM). c-d) Stress distribution and softening curves for the crack band model (Bazant, 2002).

2.9. Principles of crack formation

The formation of cracks in concrete is complex and even more so when the concrete is still plastic. This is mainly due to the time-dependency of influencing factors such as material properties, loads, environmental conditions etc. There are two principles or philosophies of when cracks occur or start in concrete (CCIP-048, 2010), each of which can be applied to both plastic and hardened concrete. The first principle is concerned with the tensile strength of the concrete and states that cracks can only occur if the tensile stress that develops in a concrete body is higher than the tensile strength of concrete. The second principle is concerned with the tensile strain capacity of the concrete and states that cracks can only occur if the tensile strain that develops in a concrete body is higher than

the tensile strain capacity of the concrete. A hypothetical example of when cracks occur in a plastic concrete due to plastic shrinkage using both crack principles is given in Figures 2.23 to 2.25. The values used in the example in terms of material properties are based on the results of Dao et al. (2009), while the values of shrinkage strains are based on the results of Slowik et al. (2008).

Figure 2.23 shows the development of Young's modulus of a plastic concrete with time as well as a high and a low plastic shrinkage strain that develops due to a capillary pressure build-up. In a worst case scenario where all the shrinkage is restrained, a tensile stress develops in the concrete body depending on the stiffness (Young's modulus) of the concrete. This tensile stress can be determined by multiplying the shrinkage strain with the Young's modulus of the plastic concrete and the results of this for both the high and low plastic shrinkage are shown in Figure 2.24.

From Figure 2.24 it can be seen that significant stress only starts to develop at around 120 minutes even though the shrinkage already started at around 80 minutes. This shows that stress can only develop in a body with a certain amount of stiffness. Figure 2.24 also shows the development with time of the tensile strength of the concrete. The figure shows that the stress that develops in the concrete body due to the high plastic shrinkage strain exceeds the tensile strength of the concrete at around 150 min and according to the first principle of crack formation a crack forms as indicated in the figure. In addition, the influence of the amount of plastic shrinkage is clearly shown by the stress build-up due to the lower plastic shrinkage which does not exceed the tensile strength of the concrete at any time resulting in no cracks according to the first principle of crack formation.

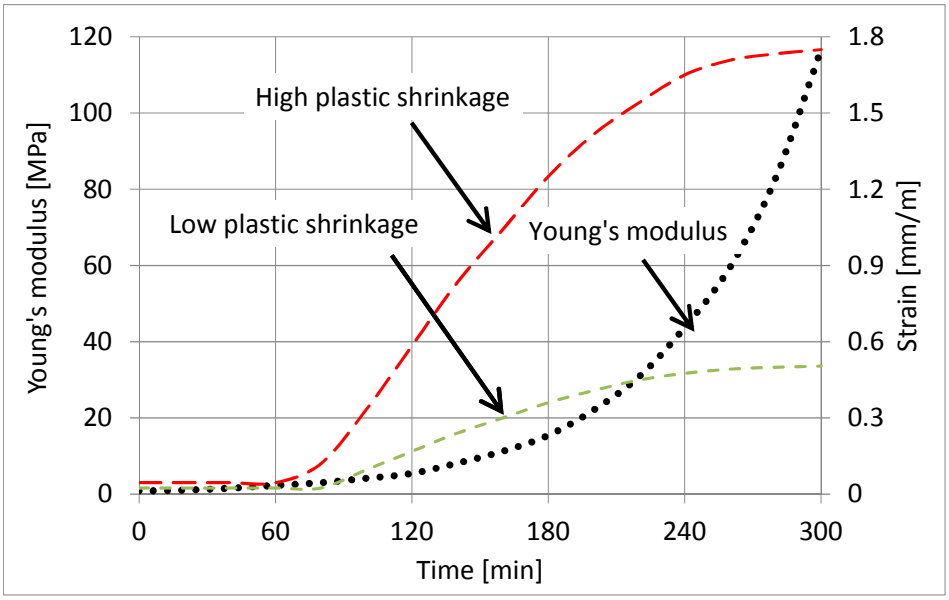

Figure 2.23. Development of Young's modulus as well as both a low and high plastic shrinkage strain in a plastic concrete.

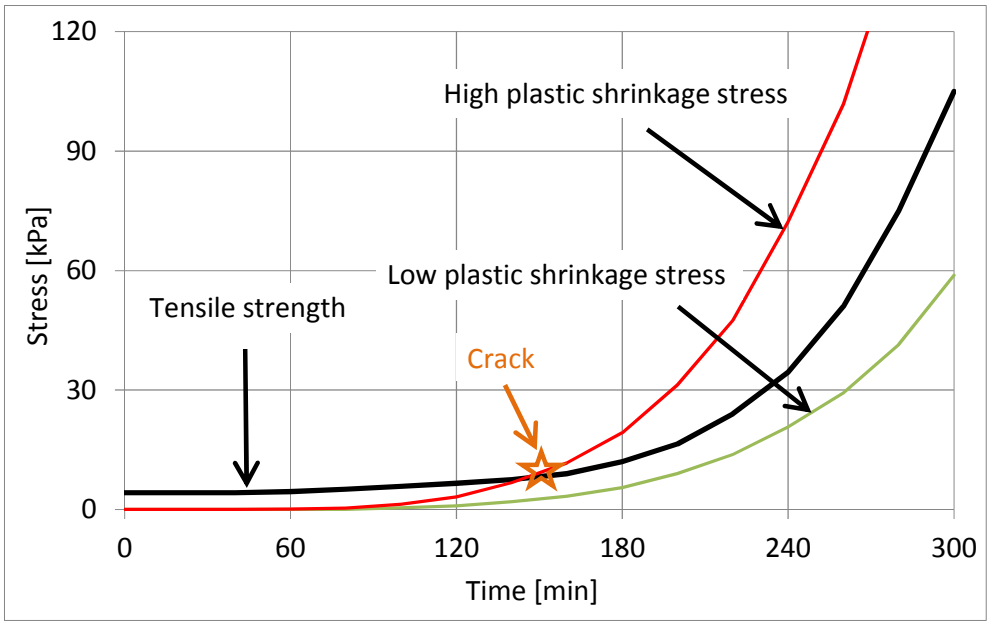

Figure 2.24. Cracking due to the first principle of crack formation.

Figure 2.25 shows the development of tensile strain due to both a low and high plastic shrinkage in a concrete body. The figure also shows the strain capacity of the plastic concrete which can be defined as the maximum strain the concrete can undergo before it cracks. At around 180 minutes the tensile strain in the concrete body due to the high plastic shrinkage exceeds the strain capacity of the concrete and according to the second principle of crack formation a crack forms as indicated. No crack is formed for the low plastic shrinkage as the strain capacity of the concrete is higher than the tensile strain due to the low plastic shrinkage, which once again shows the influence of the magnitude of the shrinkage.

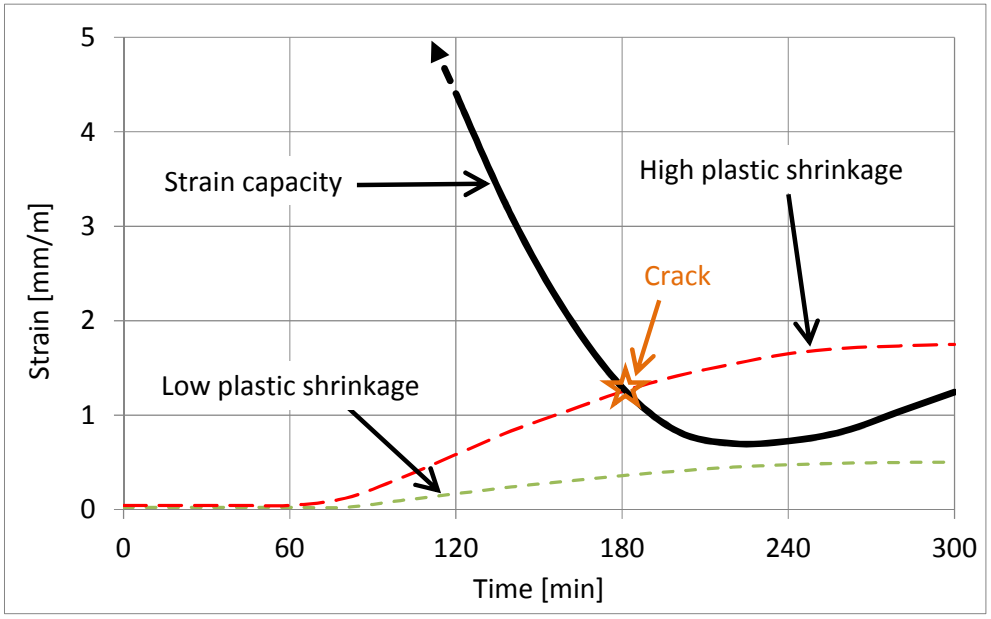

Figure 2.25. Cracking due to the second principle of crack formation.

It should be highlighted that these examples illustrate the two principles of crack formation in a simplified manner and do not account for specific boundary conditions or the other factors which can influence the cracking behaviour. In addition, the examples only account for plastic shrinkage and do not include plastic settlement which can significantly influence the cracking behaviour as discussed in Section 2.6.

2.10. Approaches to modelling the cracking of plastic concrete

A model, according to the Oxford dictionary, is "a simplified description, especially a mathematical one, of a system or process to assist calculations and predictions". A model is therefore at best only a simplified version of reality that only accounts for the aspects the model maker believed to be important. The true complexity of most real world problems are nearly impossible to describe in their entirety with a model and this is certainly also the case for the cracking of plastic concrete. However, models do serve an important purpose, by acting as helpful vehicles for understanding and describing otherwise overly difficult problems. Models are also often used for predictions or calculations that could save time and money. It should also be kept in mind that since models are per definition simplifications of reality generally developed for a specific purpose, they should not be judged unnecessarily strict against inappropriate criteria (Dolado et al., 2011). The modelling of cracking in plastic concrete can and has been approached on three different levels namely the *micro-, meso- and macro level*.

Micro level modelling considers all the constituents of the concrete such as all the different solid particles and water individually as well as the physical and chemical processes or forces influencing them (Dolado et al., 2011). An example of such a micro model was developed by Slowik et al. (2009b), whom conducted a numerical simulation of the capillary pressure development in a drying suspension consisting of inert solid particles surrounded by water. The model simulated the loss of water due to evaporation by incrementally increasing the absolute capillary pressure value and accordingly calculating the water front in the drying suspension by assuming a constant curvature of the water surface. Furthermore, each individual solid particle was subjected to gravitational and capillary pressure forces as well as interparticle forces such as electrostatic and van-der-Waals forces.

The model was numerically solved using an iterative process that searched for a state of force and distance equilibrium between the particles for each increment of capillary pressure. Although the model did not consider the change of particle size due to cement hydration, it was able to simulate

the volume change of a drying suspension due to capillary pressure, including localised crack initiation and growth. Figure 2.26 shows the visual results obtained with this model. Finally, Slowik et al. (2009b) used the knowledge gained from this model to develop a closed-loop concrete curing technique aimed at preventing plastic shrinkage cracking. The technique involves the continuous monitoring of the capillary pressure within a concrete slab with electronic pressure sensors and once a certain threshold pressure is reached, the slab is moistened with a fog spray. This regular relief in capillary pressure greatly reduces the risk for plastic shrinkage cracking.

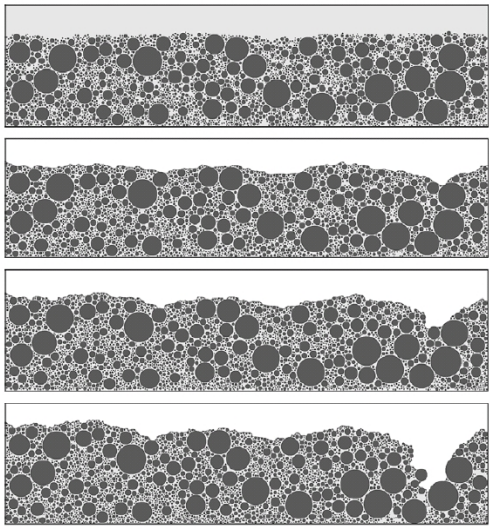

Figure 2.26. Results obtained by Slowik et al. (2009b) using a micro level modelling approach to model the cracking of an inert plastic material.

Meso level modelling differentiates between the cement paste and the aggregates as well as the physical processes that influence these phases. An example of such a model was introduced by Kwak et al. (2006), who developed an analytical model that can determine the drying time of a concrete slab by calculating and balancing the amount of bleed water with the amount of bleed water that has evaporated. The drying time can then be used to predict the occurrence of cracking by assuming that plastic shrinkage cracking is only possible once the drying time is reached. Although this is questionable, since the drying time only signifies the start of the capillary pressure development, the model itself remains useful. The model numerically calculated the bleeding which was considered to be described by the theory of consolidation while the evaporation was calculated with Equation 2.2 as proposed by Uno (1998). In addition, the increase in concrete temperature due to hydration was also taken into account when calculating the evaporation.

Marco level modelling homogenizes the behaviour of the structure by considering the entire structure or body as a whole. These models used average values for important material parameters which smear out any differences that might be present in the internal structure of the concrete

(Dolado et al., 2011). The model considers the material behaviour of the structure as well as external conditions such as loads and boundary conditions. All the constitutive laws that describe the behaviour of the structure are combined into governing equations (usually differential equations) which are solved for the entire structure normally by using finite element methods.

An example of a macro level model was introduced by Kwak et al. (2010), who used finite elements to model the stresses that develop due to differential settlement in plastic concrete. The settlement was analyses on the basis of small strain consolidation theory which considers the principles of both fluid and solid mechanics. The fluid mechanics principles included continuity and Darcy's law, while the solid mechanics principles included equilibrium, compatibility, stress-strain relationship and effective stress. These principles were combined into the two governing equations for Boit's consolidation theory and solved using finite element procedures. Finally, Kwak et al. (2010) used a finite element analysis to determine the stresses and strains that develop due to the differential settlement around a reinforcing steel bar. The model layout as well as the results obtained in terms of deformation and horizontal stresses are shown in Figure 2.27.

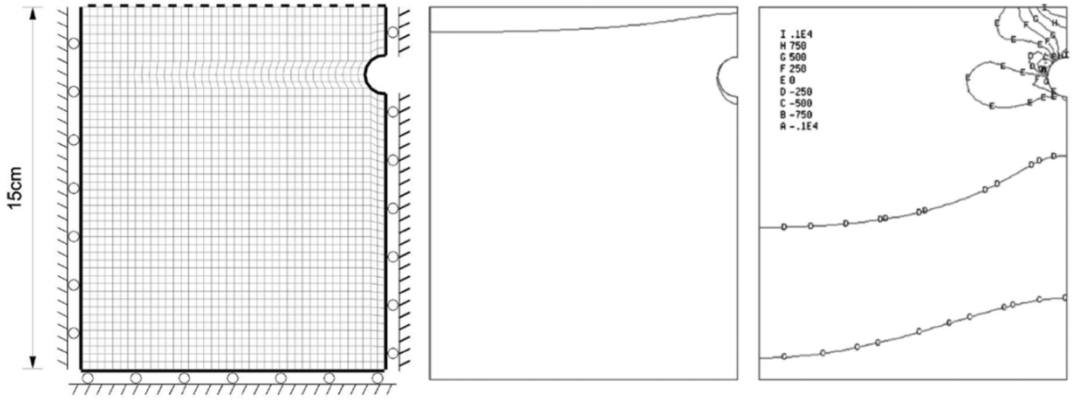

Figure 2.27. Finite element modelling of differential settlement around reinforcing steel bar as conducted by Kwak et al. (2010): a) Model layout. b) Deformed shape with scale factor of seven. c) Horizontal stresses.

2.11. Concluding summary

This chapter provides the needed background on the cracking of plastic concrete in slab-like elements. This includes discussions regarding the hydration and deformation of young concrete as well as durability issues related to cracking. The plastic settlement and shrinkage cracking are also described as well as the tensile material properties and modelling of plastic concrete. This background study is not only needed to understand the cracking of plastic concrete but also aided the planning of tests to be conducted in order to achieve the objectives of this study as discussed in Chapter 1. The details of the experimental framework are elaborated on in the next chapter.

Chapter 3. Experimental framework

This chapter contains the details of all the tests that were performed in this study. This includes tests on the actual cracking of plastic concrete as well as the direct tensile testing of plastic concrete. The test setups, moulds, measurement methods and test procedures followed for the cracking of plastic concrete tests are described first, followed by a description of the same aspects for the tensile tests. This is followed by a description regarding the mixes, materials and climatic conditions used during testing. Finally, a test program is provided that summarises all the tests that were conducted as well as the objectives of these tests.

3.1. Cracking of plastic concrete tests

To understand the cracking of plastic concrete, tests needed to be conducted on plastic settlement cracking, plastic shrinkage cracking and the combination of the two cracking types. These tests included the measurement and observation of cracks as well as the measurement of various influencing factors such as the evaporation, bleeding, settlement, shrinkage, setting times and capillary pressure build-up. Descriptions of the equipment used as well as the measurement methods and procedures followed are given in the following sections.

3.1.1. Climate chamber

Figure 3.1 shows four images of the climate chamber that was used for tests. The climate chamber was specifically designed to create extreme climatic conditions with high evaporation rates ideal for the plastic shrinkage cracking of concrete. The climate chamber contains a heating element, axial fans and dehumidifier as shown in the schematic drawing in Figure 3.1 a). The heating element controls the air temperature, while the dehumidifier controls the relative humidity. Air flow is created with two industrial axial fans which circulates air via an internal wind tunnel as shown in Figure 3.1 a) and b).

The climate chamber has a test compartment where concrete filled moulds can be placed for testing as shown in Figure 3.1 d). The temperature and relative humidity sensors that control the activation of the heating element and dehumidifier are situated at the start of the test compartment where air

exits the wind tunnel. This creates a closed-loop system able of creating and maintaining stable extreme climatic conditions with air temperatures as high as 50°C, relative humidity as low as 10 % and winds speeds up to 70 km/h. More details regarding the design of the climate chamber can be found elsewhere (Combrinck, 2011).

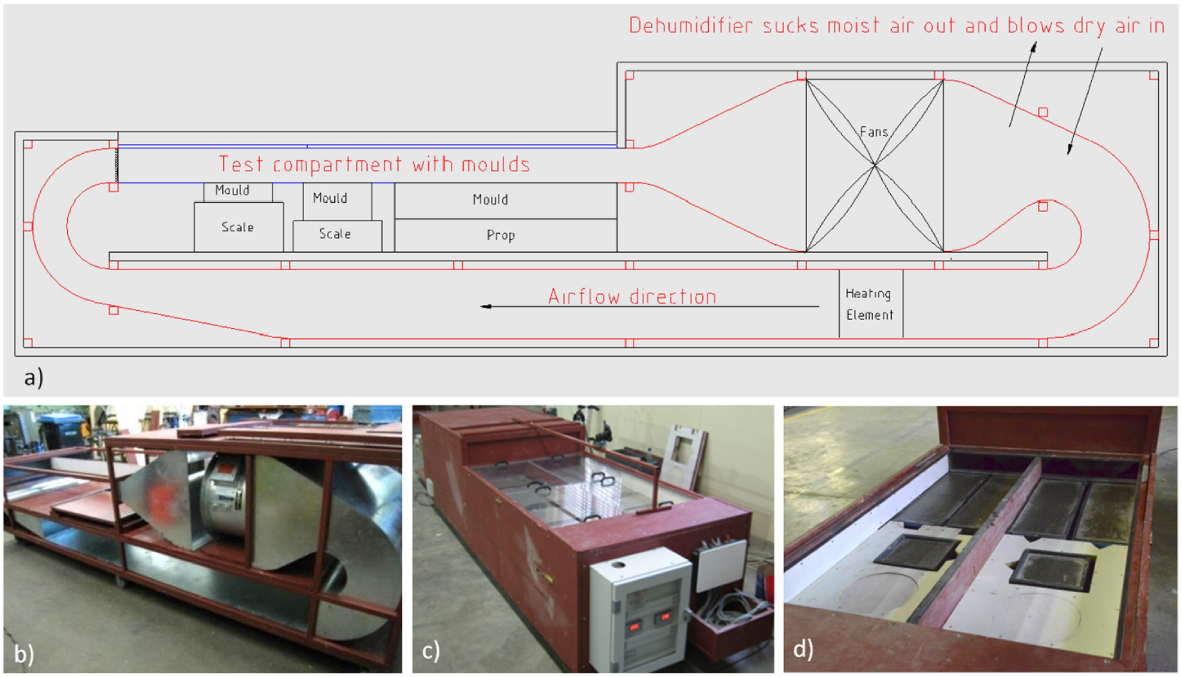

Figure 3.1. Images of climate chamber: a) Schematic drawing. b) Internal structure. c) Entire chamber during testing. d) Test compartment of chamber containing moulds during testing.

3.1.2. Moulds

Various moulds, each with a specific function, were used during testing and can be broadly divided into two groups. The first group of moulds are called cracking moulds since they were used to observe and measure cracks. This can be plastic settlement or plastic shrinkage cracks as well as a combination of the two. The layout of the cracking moulds generally restrains volume change or shrinkage to ensure the formation of cracks. These moulds also have transparent side panels to allow the observation of cracks beneath the surface of the concrete. The second group of moulds were used to measure factors that influence the cracking behaviour. These moulds generally have a regular layout that is free of any restraints. All moulds are made from plastic (PVC and Perspex) unless stated otherwise. This section only discusses the layout of each mould, while the measurements methods used together with each of these moulds are discussed in Section 3.1.3.

Shrinkage cracking mould

Figure 3.2 shows a rectangular mould with three triangular inserts. The layout and dimensions of the mould are based on the mould proposed for the testing of fresh concrete by ASTM C1579 (2006), except for an additional steel bar at each end of the mould. These steel bars were added to assist the

two smaller triangles in laterally restraining the concrete, since preliminary tests often showed insignificant to no cracking due to inadequate restraint against plastic shrinkage. In general, cracks form above the centre large triangle which acts as a stress raiser to force cracking within the central region of the mould. Cracking can start once the contraction of the concrete body due to plastic shrinkage is restrained by both the smaller triangle and steel bar at each end of the mould. This mould was mainly used to form and study plastic shrinkage cracks and is referred to as the shrinkage cracking mould.

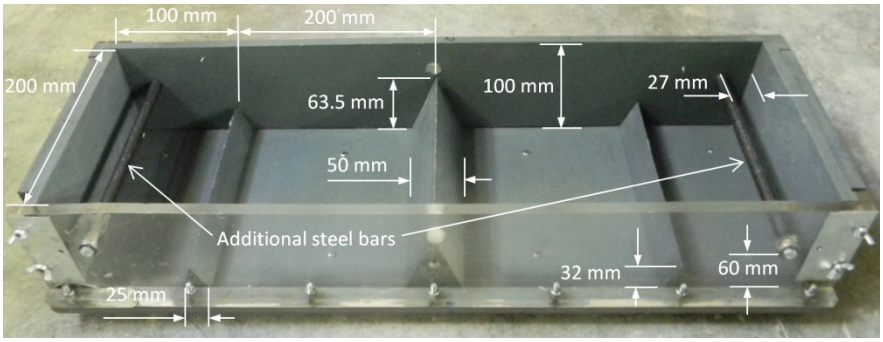

Figure 3.2. Shrinkage cracking mould.

L-box settlement cracking mould

Figure 3.3 shows an L-box shaped mould with a deep and shallow section. This shape results in the differential settlement of the concrete and therefore plastic settlement cracking. At the boundary between the deep and shallow sections there is a triangle to act as a stress raiser and ensure cracking by clearly distinguishing between the different settlement zones. The mould also has a small triangle at the end of the shallow section. This triangle provides the lateral restraint needed to form plastic shrinkage cracking in addition to the plastic settlement cracking. However, this mould mainly forms plastic settlement cracks and is referred to as the L-box settlement cracking mould.

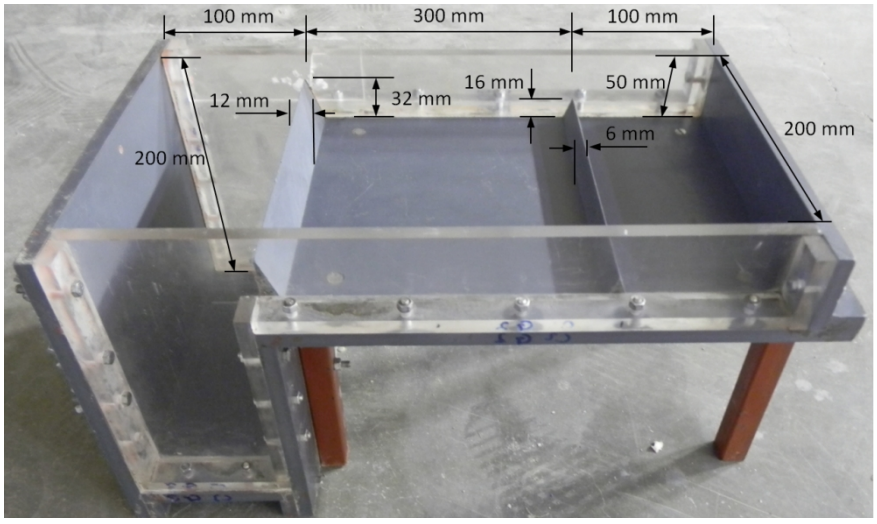

Figure 3.3. L-box settlement cracking mould.

Steel bar settlement cracking mould

Figure 3.4 shows a rectangular mould with steel bar inserts located near the top of the mould. This layout restrains the settlement of the concrete above the steel bars, resulting in differential settlement and therefore plastic settlement cracking. Furthermore, the cover of the steel bars can be varied (15, 30 or 45 mm) to investigate the influence of these variations on the cracking. This mould was mainly used to study plastic settlement cracking and is referred to as the steel bar settlement cracking mould.

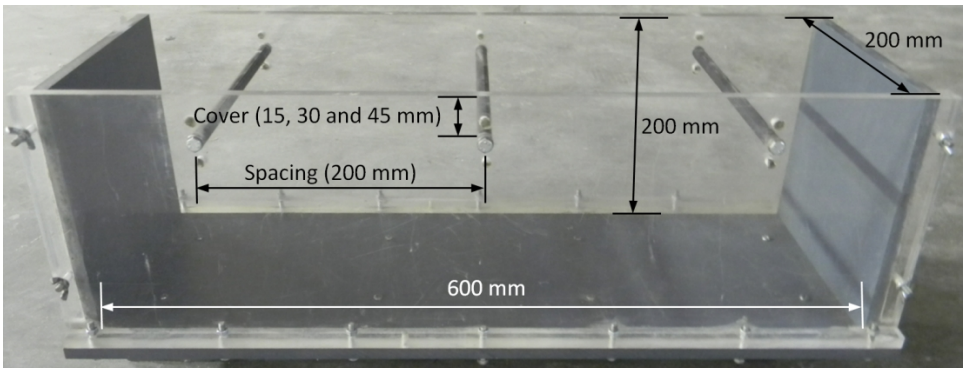

Figure 3.4. Steel bar settlement cracking mould.

Evaporation, settlement and shrinkage moulds

The evaporation of concrete surface water was measured using 200 x 200 x 100 mm moulds while the settlement and shrinkage was measure using 300 x 300 x 100 mm moulds. Figure 3.5 shows the settlement and shrinkage mould with a top mounted linear variable displacement transducer (LVDT). This LVDT was used to measure the unhindered settlement of the top surface of the concrete. Figure 3.6 shows the measurement of the shrinkage using two side mounted LVDTs. These LVDTs were used to measure the unrestrained horizontal shrinkage of the concrete. The methods followed to measure the settlement and the shrinkage are discussed in Section 3.1.3.

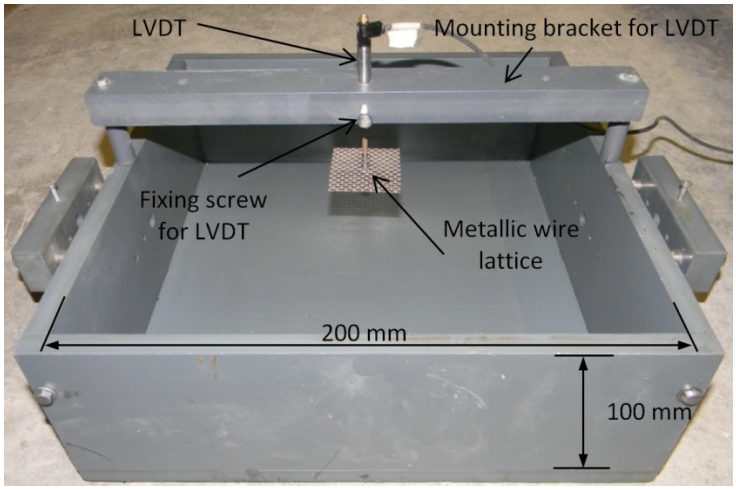

Figure 3.5. Settlement and shrinkage mould with LVDT for settlement measurement.

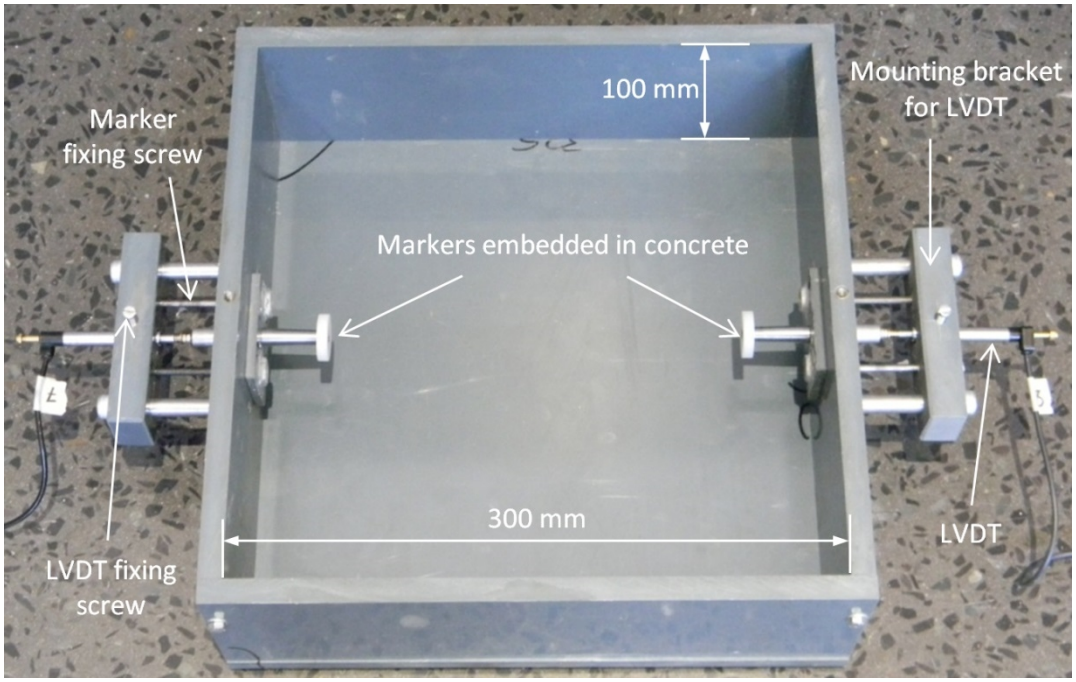

Figure 3.6. Settlement and shrinkage mould with LVDTs for shrinkage measurement.

Capillary pressure moulds

Figure 3.7 shows a 300 x 300 x100 mm mould with a capillary pressure sensor inserted from the side. The tip of the sensor is situated precisely in the middle of the mould in terms of vertical and lateral dimensions. A similar capillary sensor was also used to measure the pressure build-up in certain of the tests conducted with the shrinkage cracking and L-box settlement cracking moulds. The method followed to measure the capillary pressure is discussed in Section 3.1.3.

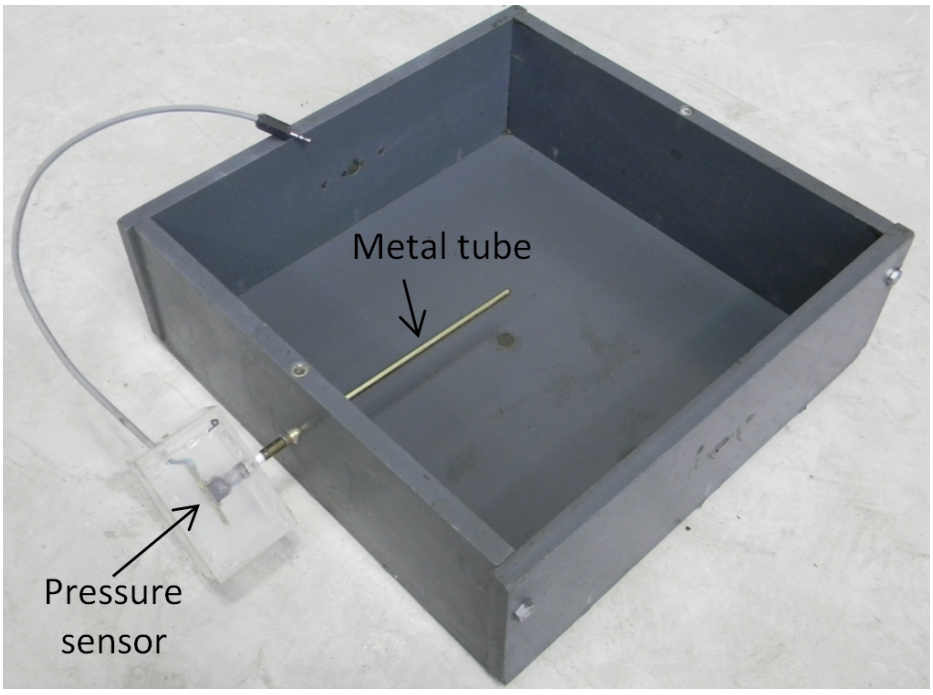

Figure 3.7. Capillary pressure mould with pressure sensor connected to a metal tube.

Setting time moulds

Figure 3.8 shows a small black cone shaped mould and a 150 mm steel cube as well as the several measuring apparatus. These moulds were used to measure the setting times of the concrete. The methods followed to measure the setting times as well as the apparatus needed are discussed in Section 3.1.3.

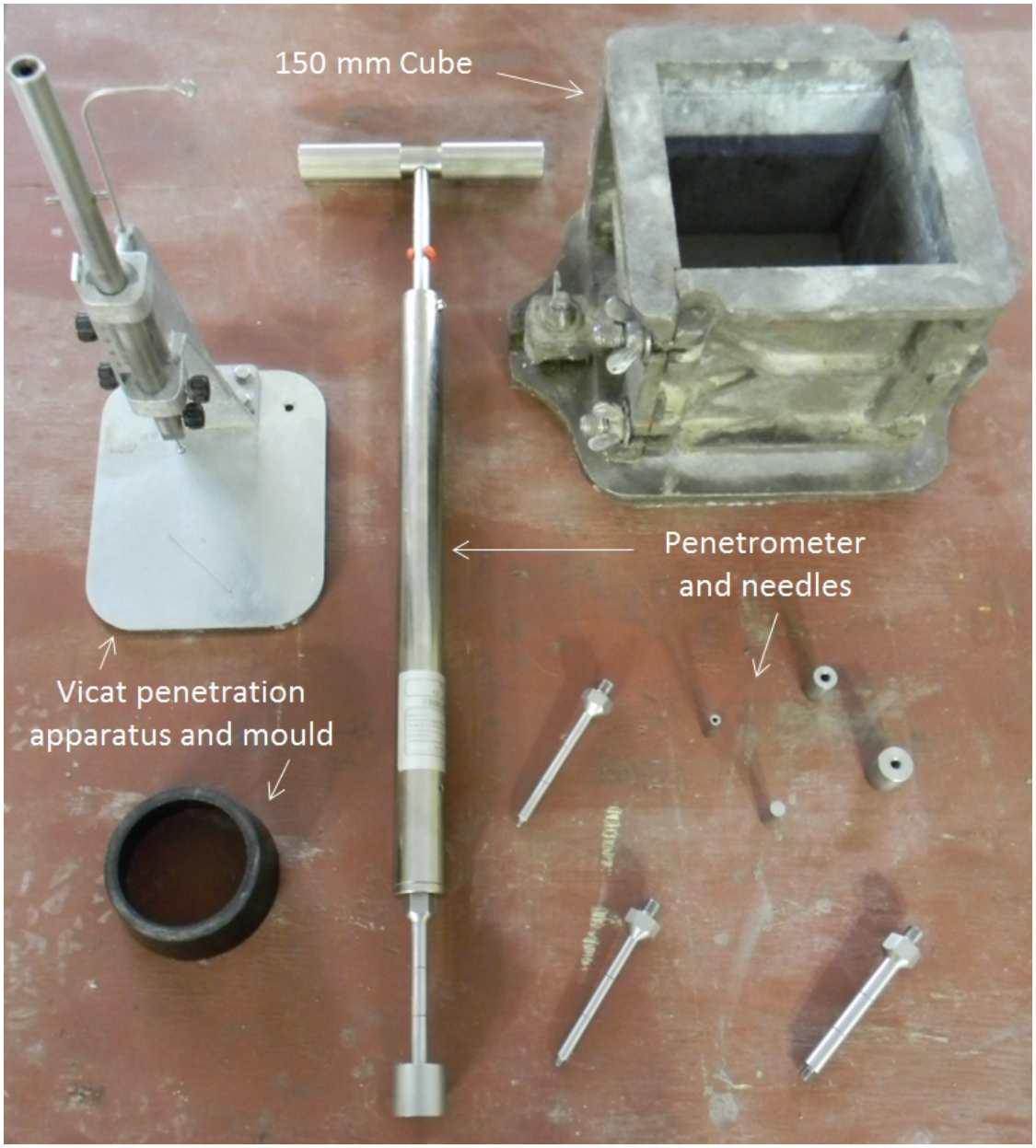

Figure 3.8. Setting time moulds and measuring apparatus.

Bleeding moulds

Figure 3.9 shows a PVC cylindrical mould as well as several other measuring apparatus and equipment. This mould was used to measure the bleeding of the concrete. The methods followed to measure the bleeding as well as the apparatus needed are discussed in Section 3.1.3.

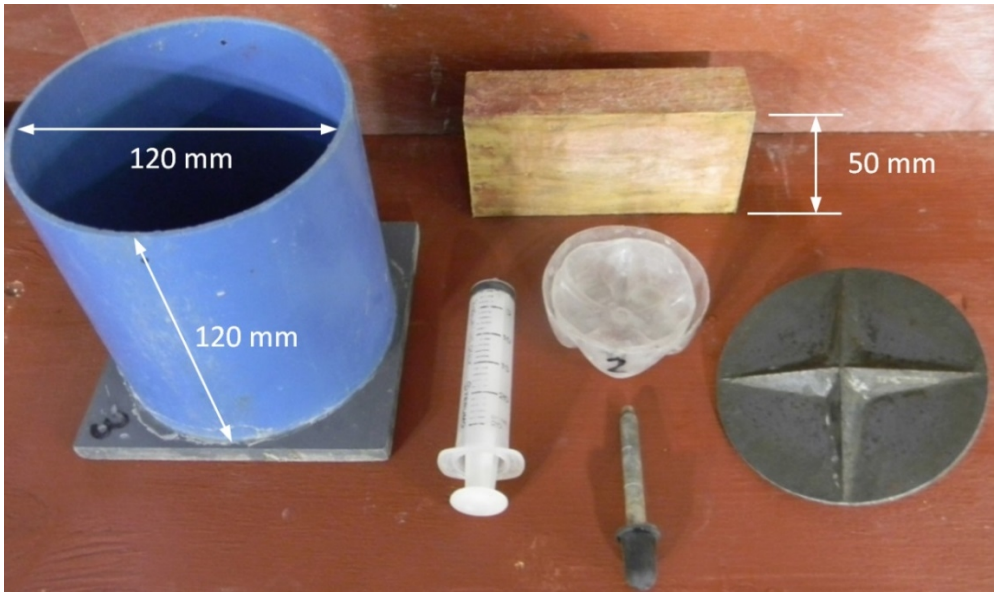

Figure 3.9. Bleeding mould and measuring apparatus

3.1.3. Measurement methods

Measurements were conducted during testing with each of the moulds described in the previous section. The measurement methods used are applied consistently throughout all the tests and are where possible based on standard codes of practice or methods used by other researchers. A discussion regarding each of the measurements and methods is given in the following sections.

Average crack width

The severity of cracks that occurred during tests with the cracking moulds can be quantified by calculating the average crack width of the surface crack as it develops with time. This was achieved by capturing high resolution images of the surface crack, as viewed from above, at 20 minute intervals. This resulted in a series of crack images for a specific specimen. An example of such an image is shown in Figure 3.10. To obtain the development of the crack or crack growth with time for a specific specimen the following procedure was used:

- All the images were scaled with CAD software using the length of a known object in the image, such as the ruler shown in Figure 3.10.
- A crack image close to the final setting time of the concrete was chosen as this is a normally a single, well-defined crack. This crack was divided into 10 mm line segments along its entire length (white lines in Figure 3.10). An additional centreline was drawn perpendicular to each line segment (green lines in Figure 3.10).
- The crack width of each line segment was measured using the direction and location of the centre lines as guidance. The exact crack pattern and measuring locations were then copied and fitted to all the other crack images of this specific specimen as captured at different times. This

allowed the measurement of the crack width for each line segment at different times at approximately the same location.

- The average crack width was calculated for each specimen at a specific time.

The reasons for using the average crack width and not total crack area, is because this allows the comparison of cracks in moulds with different widths and also since crack width is a more tangible measure of the crack severity compared to crack area. The equation used to calculate the average crack width is as follows:

$$Average\ crack\ width\ [mm] =$$

$$\sum\ (crack\ width\ of\ each\ 10\ mm\ line\ segment \times 10) \div mould\ width \qquad (Eq.\ 3.1)$$

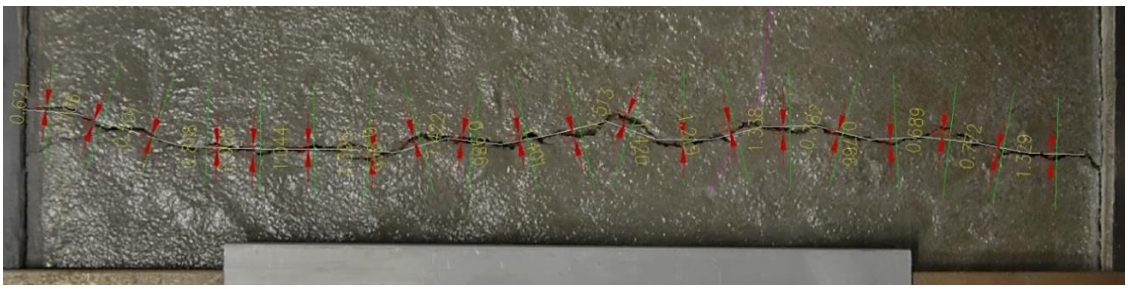

Figure 3.10. Crack measurement example.

Settlement and shrinkage

The methods used to measure the settlement and shrinkage of the concrete are similar to the methods used by Slowik et al. (2008). The settlement measurement involved the resting of a metallic wire lattice mesh on the concrete surface. The mesh is square with a length of 50 mm, a wire diameter of 0.6 mm, mesh opening of 2 mm and mass of 5 grams. A mesh was used to allow bleed water to pass which prevented the floating of the mesh and thereby ensured the mesh followed the settlement of the concrete surface. Once the mould was filled with concrete, the mesh was screwed to a top mounted non-spring loaded LVDT and lowered onto the concrete surface to measure the settlement. The mould, top mounted LVDT and wire lattice mesh are shown in Figure 3.5.

The shrinkage of the concrete refers in this case only to the horizontal or lateral shrinkage of the concrete which was measured by embedding two anchors in the concrete on opposite sides of the mould as shown in Figure 3.6. Each anchor has a round disk at the end to ensure the anchor remains embedded in the concrete as the concrete shrinks. The first step of the procedure followed to setup the anchors and LVDTs was to fix the anchors in position by two fixing screws as shown in Figure 3.6. This prevented the movement of the anchors during the placement and compaction of the concrete in the mould. Once the mould was filled with concrete, each anchor was connected to a side

mounted spring loaded LVDT. Finally, the fixing screws were removed allowing the anchors to move freely with the concrete.

It should be mentioned that for the shrinkage measurements, spring loaded LVDTs were preferred above non-spring loaded LVDTs which are screwed to the anchors. This was because preliminary test conducted using the non-spring loaded plunger type LVDTs showed significant resistance to movement due to friction between the plunger and the LVDT housing. The friction was caused by the difficulty in perfectly aligning the LVDT with the anchor as well as the slight downward movement of the anchor due to concrete settlement. In addition, the springs used for the spring-loaded LVDTs have a very low stiffness and cannot force or move the anchor deeper into the concrete.

Capillary pressure

The capillary pressure was measured with small electronic pressure sensors connected to long metal tubes as shown in Figure 3.7. This method is similar to that used by Slowik et al. (2008). The first step of the procedure followed to setup the sensor for measurement was to screw a long metal tube to the tip of the pressure sensor via a treaded connection. Once connected the tube was carefully filled with distilled water using a syringe and hypodermic needle. During filling the tube was tapped various times to remove trapped air bubbles. Once the tube was filled a small sponge was inserted into the tip of the metal tube to ensure that no solid particles from the concrete mix could enter the tube. The concrete mould was then filled to just below the sensor and tube insertion location. The tube was then inserted horizontally from the side of the mould, after which the mould was completely filled with concrete. Finally, the mould was moved to the climate chamber where the sensor was connected to a data acquisition system for measurement.

The depth of the capillary pressure sensor tip below the concrete surface for the mould shown in Figure 3.7 was 50 mm. This depth differs for the measurements conducted in the L-box settlement and shrinkage cracking moulds which were 15 and 35 mm below the concrete surface respectively. These depths are sufficient since according to Slowik et al. (2008), the capillary pressure within the interconnected pore system of a concrete paste is nearly uniform up to a depth of 100 mm below the concrete surface during the plastic phase. The sensor tips for the cracking moulds were located just above the triangle where cracking was expected to occur.

Evaporation

The evaporation of concrete surface water was measured by weighing the evaporation mould filled with concrete every 20 minutes. The amount of water evaporated during a 20 minute period was

then calculated as the difference in weight of the concrete filled mould at the start and end of each period.

Bleeding

The bleeding of the concrete was measured using two different methods. The methods differ mainly in the technique used to gather or collect the bleed water for extraction. The cylinder mould shown in Figure 3.8 was used for both methods. The first step of the procedure followed for both methods was to cover the top of each mould once filled with concrete to avoid excessive evaporation of bleed water. The bleed water was then extracted from the mould and weighed at 20 minute intervals. The water was extracted with a pipette for both methods, although a syringe was also used in this study for comparison. Finally, before each extraction of bleed water, the mould was weighed to account for the bleed water that evaporated during each measurement period.

As mentioned the technique used to gather or collect the bleed water differs for the two methods. The first method is based on the standard ASTM C232 (2004) test method for the measurement of concrete bleeding. Here, bleed water is gathered by tilting the concrete filled mould prior to extraction by placing a 50 mm block beneath one side of the mould. This allows all the bleed water to collect on the other side of the mould where it is extracted after the mould has been tilted for two minutes. The flaw in this method is the movement due to the tilting, which can influence the bleeding process.

The second method was developed by Josserand and De Larrard (2004) and involves the use of a star shaped stencil as shown in Figure 3.9 to create grooves on the concrete surface. As the concrete bleeds the water collects at the centre of the star shape grooves created on the surface, where it is extracted. This method was developed to minimise the movement of the mould. The flaw in this method is the difficulty of creating consistent grooves on the concrete surface, especially when using mixes with different stiffness's and workability's. This inconsistency can influence the amount of bleeding water that collects within the grooves. Both these techniques of gathering the bleed water were used in this study.

Setting times

Two different methods were used to determine the setting times of concrete. The first method is the standard ASTM C403 (2008) test method for the determination of setting times of concrete and mortars. The method involves the sieving of a freshly mixed concrete through a 4.75 mm sieve to obtain a concrete paste free of large aggregates and suitable for penetration resistance testing. It is important that the paste contains no large aggregate as this would greatly influence the measured

penetration resistance. The concrete paste is placed in a container with minimum lateral and vertical dimensions of 150 mm, such as the cube shown in Figure 3.9.

Different size needles are pressed into the concrete using a loading device, called a penetrometer which is also shown in Figure 3.9. The penetrometer is used to measure the force needed for the needle to penetrate the concrete paste to a depth of 25 mm. This force together with the size (area) of the needle is used to calculate the stress exerted on the concrete. The initial setting time is reached once a stress of 3.5 MPa is reached, while the final setting time is reached at a stress of 27.6 MPa. The drawback of the method is the time needed to sieve the concrete to obtain enough paste to fill the mould as well as the limited amount of penetrations that can be made on each specimen. In general, it takes about 20 to 25 minutes to fill a 150 mm cube which only has room for around nine penetration measurements.

The second method used is based on the standard EN 196-3 (2005) test method used to determine the setting times of cement paste with a standard consistency. This method uses a Vicat penetration apparatus and needles as shown in Figure 3.9. The concrete is also sieved through a 4.75 mm sieve to leave a concrete paste suitable for penetration resistance testing. The initial setting time is reached when a standard needle with 1.13 mm diameter penetrates the concrete to a depth of 6 ± 3 mm from the bottom of the mould. The final setting time is reached once the sharp circular edge of the final setting time needle no longer creates a mark when inserted onto the bottom surface of the concrete in the mould.

Strictly speaking this method is only applicable for the determination of setting times of cement paste (cement mixed with water) and not concrete paste and mortars. However, this method was used as an alternative to the first method since the black cone shaped mould used for this method, as shown in Figure 3.9, is much smaller and can be filled within 2 minutes. The time needed to fill these moulds could influence the results, especially for tests at high temperatures resulting in rapid setting times.

3.1.4. Test procedure

The same procedure was followed for all the tests conducted on the plastic cracking of concrete in this study. The first important step was to place the weighed quantities of the constituent materials in a climate controlled room with a temperature of 23°C at least the day before the test was to be conducted. This ensured that once mixed all fresh concrete had similar initial temperatures. This is important since the temperature of the concrete greatly influences the setting times and

evaporation rate as discussed in Section 2.5.3. The second step was to ensure the testing environment reached the desired climatic condition. This was only needed for tests conducted in the climate chamber, which needed to be switched on and set to the desired climate at least 2 hours before placing the concrete in the chamber.

The third step was to mix, place, consolidate and finish the concrete in the desired moulds. The dry constituents were firstly added and mixed for 30 seconds in a 50 litre pan type mixer before water was added. The wet mix was then mixed for a further 3 minutes. The moulds used for that specific test were then filled with concrete. The moulds were consolidated on a vibrating table until air bubbles were no longer visible on the surface. This consistently required a vibration time of between 2 and 3 minutes. After vibration the surface of the concrete was given a smooth finish with a steel trowel. Once finished, the moulds were moved to the testing environment where if needed connections with LVDTs or capillary pressure sensors were made as discussed in Section 3.1.3. These sensors were attached to a data acquisition system.

This entire process from adding the dry constituents into the mixer to placing the moulds in the testing environment (mostly the climate chamber) consistently took between 20 and 25 minutes to complete. The time zero for all tests in this study is defined as the time where the concrete filled moulds were placed in the testing environment. The reason for choosing this time zero is because the settlement and bleeding of concrete are influenced by movement and can therefore only be measured from the time the samples were left undisturbed in the testing environment. From the time zero all the measurements as described in Section 3.1.3 were commenced.

3.2. Tensile tests

A new test setup was designed and constructed for the determination of the tensile material properties of plastic concrete. This included a support beam, loading platforms, air bearing, actuator and mould as shown in Figure 3.11. The test setup as well as measurement methods and test procedures followed are discussed in the following sections.

3.2.1. Support beam and loading platforms

The support structure or base of the test setup is a steel H-beam (254 x 254 x 107 H-section) as shown in Figure 3.11. The beam is rigid and stable, providing more than adequate support for all the other components. Figure 3.11 also shows both the fixed and moving loading platforms consisting of stiffened steel end plates. The fixed loading platform is directly bolted to the support beam while the moving loading platform is bolted to the mechanical linear actuator, which in turn is bolted to the

support beam. The stationary mould halve is connected to the fixed loading platform while the moving mould halve is connected to the moving loading platform using bolts and treated rods as discussed further in Section 3.2.5.

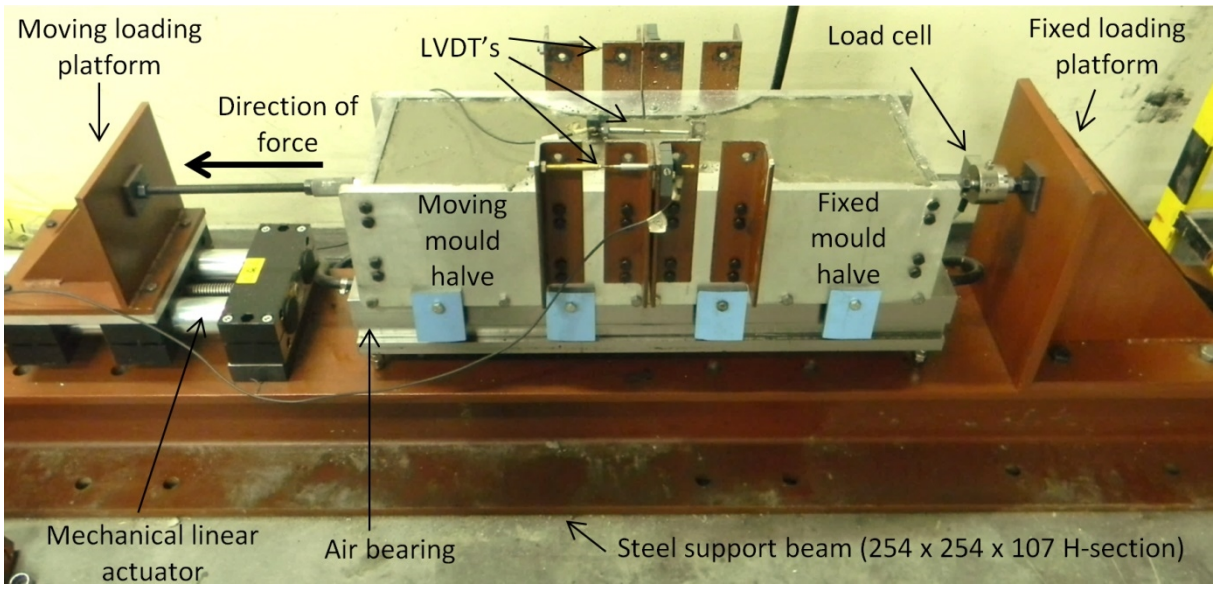

Figure 3.11. Tensile test setup showing the support beam, loading platforms, air bearing, mechanical linear actuator and mould.

3.2.2. Air bearing

At the heart of the setup is an air bearing which, as discussed in Section 2.7.1, is one of the essential components needed for the tensile testing of plastic concrete. An air bearing uses an ultrathin film of highly pressurised air to support a load, which in this case is a concrete filled mould. The ultrathin air film acts as a lubricant or bearing to enable frictionless lateral movement of the mould placed on it as shown in Figure 3.11.

The air bearing as shown in Figure 3.12 was machined from steel using computer numerical controlled (CNC) technology. The air bearing consists of an internal cavity connected to two rows of eight 1 mm diameter holes (called orifices) spaced 100 mm apart on a rectangular floating or bearing surface of 200 x 750 mm. The air bearing also has a treaded levelling system consisting of four dome nuts situated at the bottom of each corner of the air bearing. These nuts were used to perfectly level the air bearing.

Air is supplied to the air bearing via an industrial sized compressor with a working pressure of 750 kPa and large air reservoir of 1.35 m^3. Preliminary tests showed that the air bearing could easily and frictionlessly float the 80 kg concrete filled mould at a pressure of 120 kPa. Based on this, a conservative air pressure of 200 kPa was chosen and used for all the tests.

The flow of air in the system starts at the compressor at 750 kPa from where it enters a filter and regulator which both cleans the air and lowers the pressure to 200 kPa. The air then enters the inner cavity of the air bearing via inlets at both ends of the air bearing as shown in Figure 3.12. The air within the inner cavity then exits through the 1 mm diameter orifice outlets creating an ultrathin air film between the top surface of the air bearing and the bottom surface of the mould.

The 200 kPa air pressure proved to be an effective and sustainable operating pressure for floating the concrete filled mould without any friction and without depleting the air in the reservoir of the compressor.

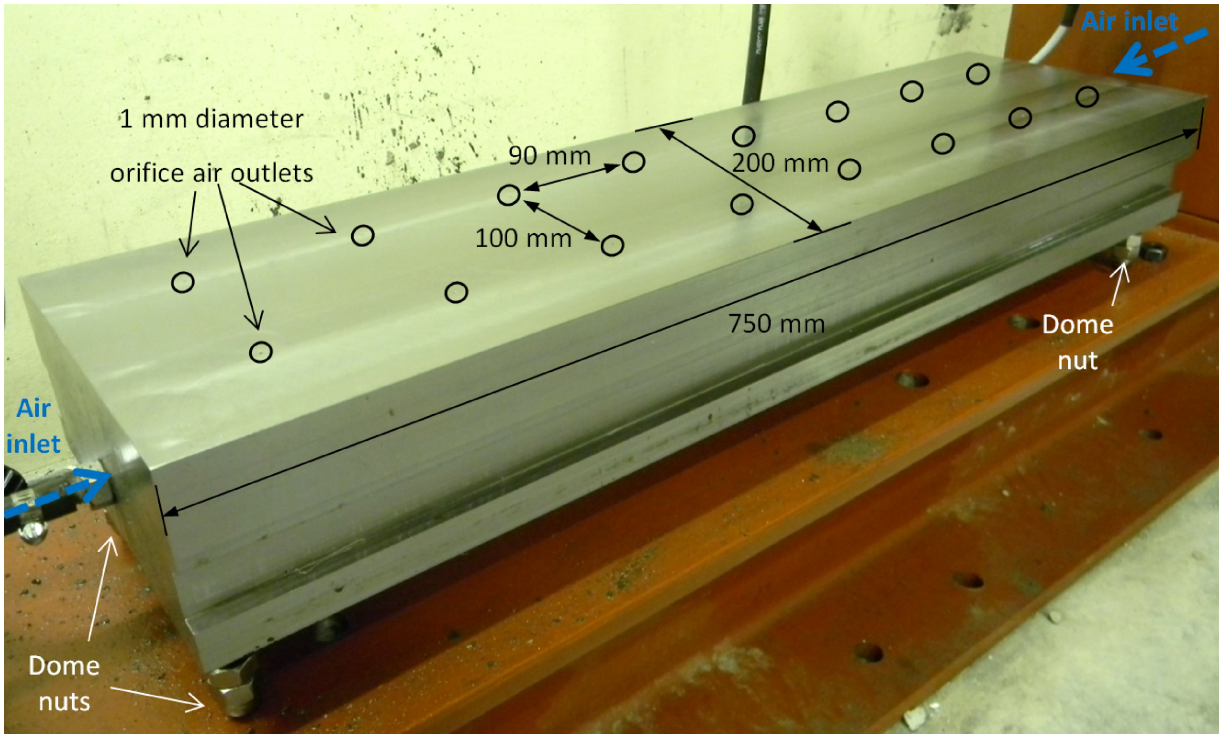

Figure 3.12. Air bearing.

3.2.3. Mechanical linear actuator

A mechanical linear actuator was bolted to the support beam as shown in Figure 3.13 and used to apply a horizontal displacement to the mould. The actuator is displacement controlled and capable of applying a maximum tensile force of 1.7 kN at a constant displacement rate as low as 0.05 mm/min. The actuator creates linear motion by rotating a centrally located treaded rod that is connected to a moving carriage via a ball bearing leadscrew. As the rod rotates the leadscrew moves the carriage, which slides over two rigid steel tubes. A brushless DC-servomotor with planetary gearhead is used to rotate the treaded rod. Bolted to the moving carriage is the steel loading platform which transfers the force to the mould.

The displacement rate of the actuator used during testing can significantly influence the results achieved. If the displacement rate is to slow it results in unpractical and questionable long testing periods, since the tensile properties of concrete can change considerably within a couple of hours due to continued hydration. The slow rate (0.05 mm/min) used by Dao et al. (2009) resulted in such undesirably long testing periods, where a total displacement of 7.5 mm took 150 minutes to achieve. On the other hand if the displacement rate is to fast it increases the difficulty of capturing the post-peak behaviour of the concrete as, for example, the results achieved by Hannant et al. (1999) for an ordinary concrete mix tested at a rate of 0.75 mm/min as shown in Figure 2.14. Based on this a displacement rate of 0.25 mm/min was chosen as appropriate for the tests. This rate results in a displacement of 7.5 mm in 30 minutes.

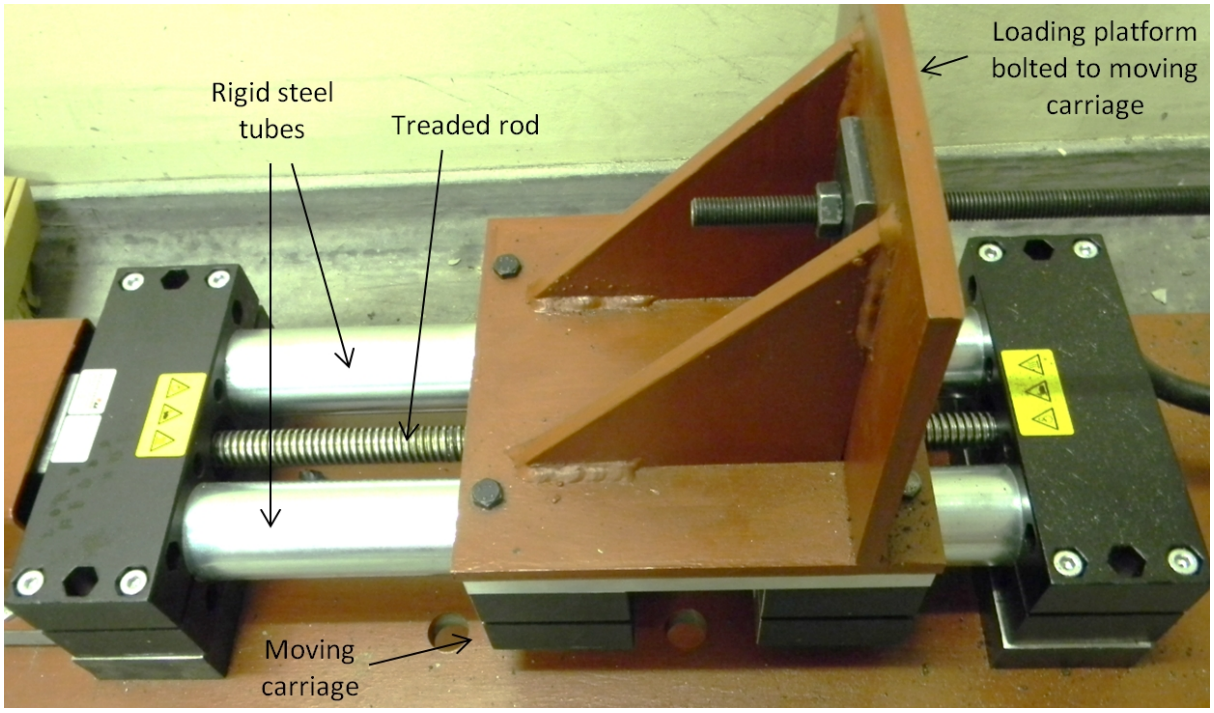

Figure 3.13. Mechanical linear actuator.

3.2.4. Moulds

Moulds in the shape of a dog-bone were used to conduct the tensile test. This shape was chosen as it minimises stress concentrations in the concrete sample. The precise shape of the curved sections of the mould is based on the mould used by Dao et al. (2009). However, the size of the mould was increased by a factor of 1.43 to allow for the testing of concrete mixes containing larger aggregates. The increase in size resulted in a neck section with cross sectional area of 100 x 140 mm, which is large enough for tests on concrete containing 19 mm aggregates according to SANS 10100-2 (1992). Two moulds were machined from aluminium using CNC technology and are referred to as the tensile

moulds as shown in Figure 3.14. Aluminium was chosen to keep the weight of the moulds as low as possible. This eased both the transportation and floatation of the mould.

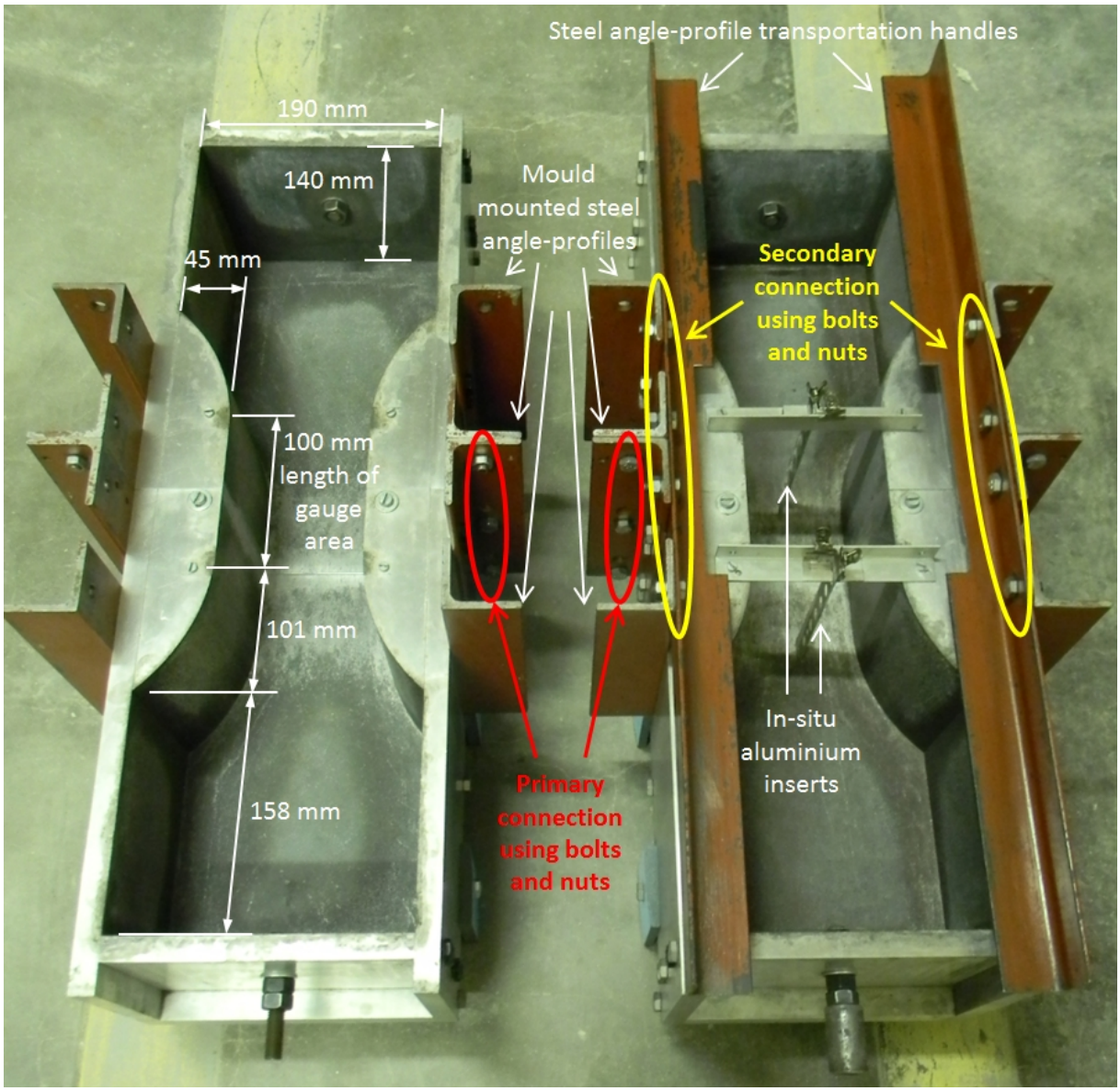

Figure 3.14. Tensile moulds.

Each mould consists of two halves that are connected with a series of bolts and steel angle-profiles. Each halve has four angle-profiles that are bolted vertically to the sides of the mould and are referred to as the mould mounted angle-profiles. The primary connection between the halves is made by bolting together the mould mounted angle-profiles at the junction between the halves as shown in Figure 3.14. Another set of angle-profiles is used as transportation handles and is bolted horizontally to the mould mounted angle-profiles and is referred to as the secondary connection as shown in Figure 3.14. The following procedure was used to prepare a mould for testing:

- The separate mould halves were floated on the air bearing. While floating the faces of the halves were bolted together via the primary connection. This created a flush and level connection between the vertical faces and bottom surfaces of the halves which ensured that the mould was perfectly aligned with the air bearing during testing. The mould on the left in Figure 3.14 illustrates the mould after the primary connection was made.
- The secondary connection was made between the angle-profile transportation handles and mould mounted angle-profiles.
- The in-situ aluminium inserts used to measure the concrete displacement over the 100 mm length of the gauge area were connected. The inserts, connection and measurement are discussed in more detail in Section 3.2.6. The mould on the right in Figure 3.14 shows the mould after the secondary connection was made as well as the connection of the aluminium inserts.
- Once the inside of the mould was lubricated it was ready to be filled with concrete. The lubrication involved a layer of grease at the junction between the mould halves to prevent any leakage of concrete as well as a thin-layer of mould-oil which was applied to all concrete-exposed regions to minimise friction and assist in the de-moulding process.

3.2.5. Boundary conditions

The boundary conditions were fixed on the stationary end and semi-fixed on the moving end of the mould. The treaded rod on the moving end was much longer than on the stationary end as shown in Figure 3.15. This allowed a certain amount of lateral movement at the moving end and therefore a semi-fixed boundary condition.

This configuration was chosen since the results of fixed boundary conditions are less scattered (Van Mier, 1997). In addition, the large lateral movement (due to excessive rotations) that can occur in completely freely rotating systems is believed to be a source of unreliable and inconsistent results. The connection between the mould at both ends and the loading platforms was made using a threaded coupling connector as shown in Figure 3.15. The following procedure was used to connect the mould to the loading platforms:

- The coupling connector on the stationary end was screwed to the treaded rod from both the loading platform and mould side. The tread at the platform side was from a 2 kN load cell as shown in Figure 3.15 b).
- The coupling connector was fixed with two lock nuts at both ends.
- The connection at the loading platform was fixed via nuts and perfectly flat steel washers.
- Steps 1 to 3 were repeated to connect the moving mould halve and loading platform.

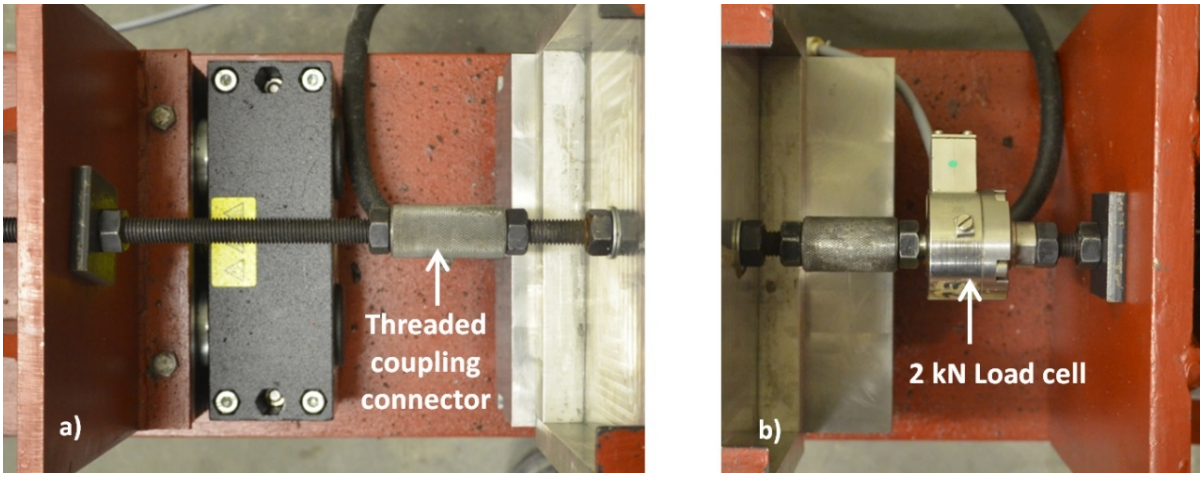

Figure 3.15. Boundary conditions between mould and loading platforms: a) Moving end. b) Stationary end.

3.2.6. Measurement methods

Both force and displacement need to be measured to obtain the tensile properties of plastic concrete. The force was measured with a HBM 2 kN load cell that was placed between the loading platform and stationary mould halve as shown in Figure 3.15 b). The displacement of the mould halves relative to each other as well as the displacement of the concrete inside the mould within the gauge area was measured as shown in Figure 3.16. The figure also shows a typical crack that formed during testing. The mould displacement was measured with two LVDTs, one placed on each side of the mould. The LVDTs were connected using a series of brackets and treaded extensions attached to the mould mounted steel angle-profiles.

The measurement of the concrete displacement is more complex, but still needed to obtain the actual deformation of the concrete. This is because the measurement of the mould displacement alone is not adequate due to the possible movement of the concrete within the mould as the load is transferred from the mould to the concrete as discussed in Section 2.7.1. To measure the deformation of the concrete two aluminium inserts were cast into the concrete, one at each end of the gauge area as shown in Figure 3.17. The inserts have a number of large holes along its length as shown in Figure 3.17 a) to improve the bond with the concrete. The aluminium inserts were connected to the moulds after the mould halves were connected via the primary and secondary connections. The following procedure was used to connect the inserts and LVDT:

- The aluminium inserts were held in positions before and during the filling of the mould with concrete by fixing the top of the inserts with clips to angle-profiles that spanned across the neck section of the mould as shown in Figure 3.17 b).

- The inserts were unclipped and the aluminium angle-profiles were removed after the mould has been filled with concrete. This left only the top section of the inserts extruding above the concrete surface as shown in Figure 3.17 c).
- The LVDT was attached to one of the inserts using a mounting bracket, while the spring-loaded point of the LVDT rested on the other insert as shown in Figure 3.17 d). It should be mentioned that the force exerted by the spring loaded LVDT was far less than 1 Newton and therefore regarded as insignificant.

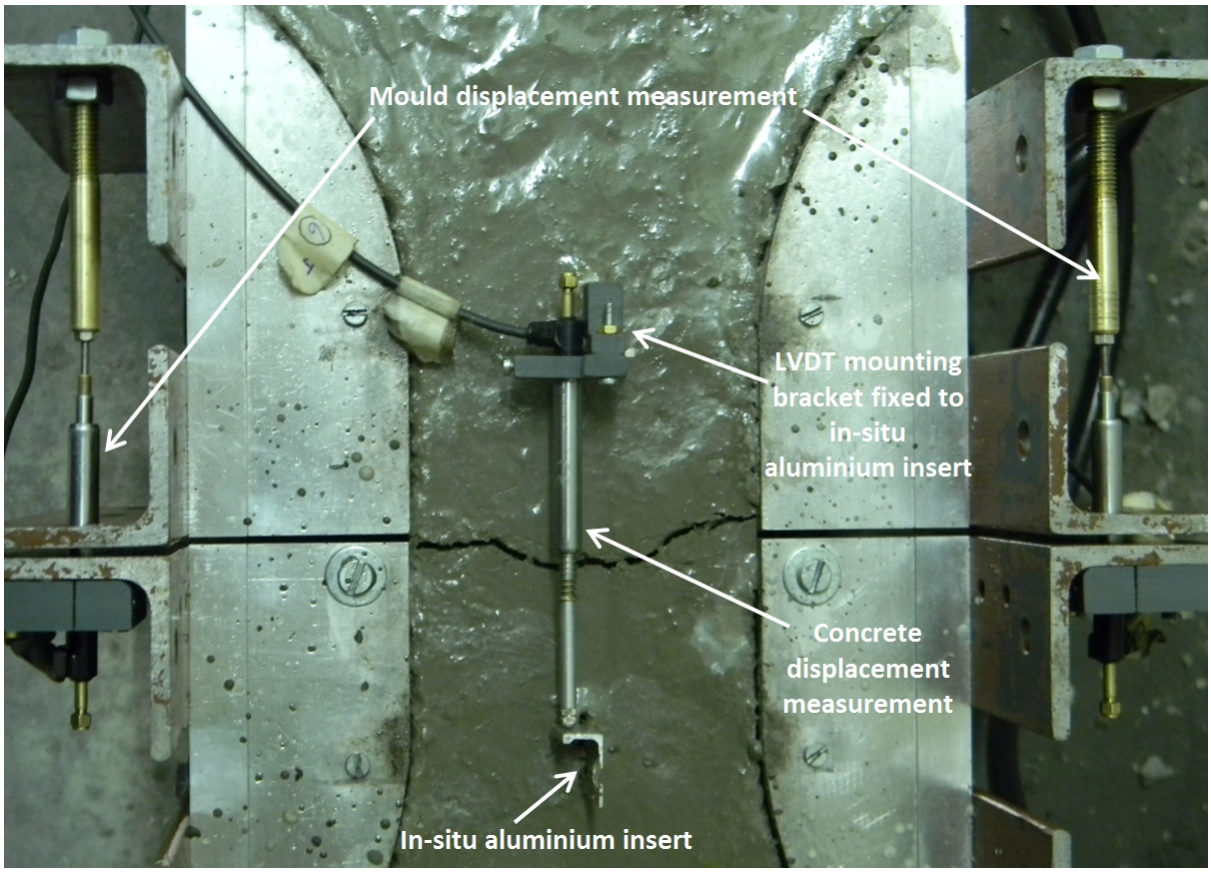

Figure 3.16. Measurement of mould and concrete displacement.

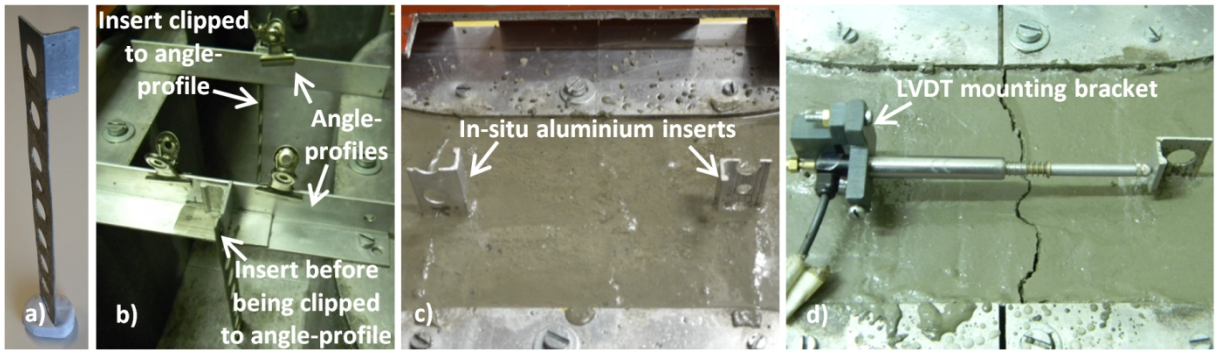

Figure 3.17. In-situ aluminium inserts used to measure concrete deformation: a) Loose standing aluminium insert. b) Inserts fixed to mould before adding concrete. c) Inserts embedded in concrete sample. d) LVDT attached to inserts during testing.

3.2.7. Test procedure

The same procedure was followed for all the tensile tests. The first two steps are identical to the steps followed for the cracking of plastic concrete tests as discussed in Section 3.1.4. In short, it involved the placement of weighed materials in a climatic controlled room the day before the test was conducted as well as ensuring the testing environment reached a constant and stable climatic condition once the test was to be started. The third step for the tensile tests was to assemble the tensile moulds as described in Section 3.2.4.

Once the moulds were assembled the concrete was mixed, followed by the filling, consolidation and finishing of the concrete in the tensile mould as described in Section 3.1.4. The mould was filled up to 5 mm below the top of the mould. In addition to a 2 to 3 minute consolidation on a vibration table, a poker vibrator was also inserted for 30 seconds at each end of the mould. This was needed to speed up the consolidation of the concrete which took longer than for the plastic cracking tests due to the larger depth of the concrete in the tensile mould. Next, the concrete filled mould was placed in an environment with the appropriate temperature (either 23 or 40°C) as needed for the specific test. The 23°C environment was in the same climate controlled room were the tensile tests were conducted, while the 40°C environment was in the climate chamber.

Once the mould was placed in the appropriate environment the aluminium angle-profiles and clips holding the aluminium inserts were removed leaving the mould as shown in Figure 3.17 c). The next important step was to ensure that no capillary pressure and therefore no plastic shrinkage could occur in the concrete sample, since this would influence the measured tensile strength of the concrete due to the build-up of residual stresses. This was done by ensuring that a thin layer of water continuously covered the entire surface of the concrete until testing. This was easily achieved in the 23°C environment where only a light fog spray was needed, while the 40°C environment was more challenging and required the ponding of a 2 to 3 mm layer of water on the concrete surface.

The concrete filled mould was left undisturbed at the appropriate temperature and only floated on the air-bearing 15 minutes before the test needed to be conducted. Once the mould was placed and floated on the air bearing, the coupling connectors were used to fix the moulds to the treaded rods from both the fixed and moving loading platforms. The final fixing of the treaded rods to the loading platforms was only made later as one of the last steps before the test started. Next, the primary connection bolts were loosened and fixed only by hand. This was done to ensure that the bolts could

easily and gently be removed without disturbing the fragile concrete just before starting the test. During this loosening of the primary bolts the secondary connection held the mould halves together.

Next, the transportation handles were removed through the secondary connection. This was followed by attaching of the LVTDs as discussed in Section 3.2.6. At this stage the load cell was set and locked to a zero value. After this, the final fixing of the treaded rods to the loading platforms was made as described in Section 3.2.5. The connection was made in such a way that the load cell measured a slight compression force. This ensured that no unintended tensile forces could develop in the concrete before the test began. Finally, the primary bolts were removed before the test was started. The entire process from moving the mould from the specific temperature to starting the test consistently took 15 minutes to complete.

3.3. Mixes and materials

Several different mixes were used during the duration of this study. The mixes can broadly be divided into two groups. The first group was used mainly for tests on setting times as well as the observation of pure plastic settlement cracking. Four such mixes were used and are referred to as the Mixes S1 to S4, where the S is short for setting and settlement. The mixes were chosen to represent three different types of mixes with different strength and workability. Mix S1 has a high strength as well as a low slump value and is suited for pre-fabricated slab elements or high strength workshop floors. Mix S2 has a medium strength as well as a medium slump value and is suited for industrial floor slabs. Finally, Mix S3 has a lower strength and high slump value and is suited for domestic driveways or slabs on ground where a high flowability is required. The material constituents and proportions as well as the properties of these four mixes are shown in Table 3.1.

Table 3.1. Material constituents and proportions as well as properties of Mixes S1 to S4.

Mix description	Mixes for Setting and plastic Settlement cracking tests 1 to 4			
Mix abbreviation	**Mix S1**	**Mix S2**	**Mix S3**	**Mix S4**
Material constituents [kg/m³]				
Water	200	200	200	205
Cement - CEM I 52.5N	571	444	364	331
13 mm Greywacke stone	834	889	924	993
Natural quarry sand - Batch 1	810	863	896	800
Mix properties				
Slump [mm]	20	75	140	90
28-day characteristic design strength [MPa]	60	45	35	30
Actual average 28-day strength [MPa]	60.3	41.8	38.2	-
w/c ratio	0.35	0.45	0.55	0.62

The second group of mixes was mainly used for tests where the actual crack sizes were measured at different climatic conditions. Four such mixes were used and are referred to as the Mixes C1 to C4, where the C is short for cracking. Mixes C1 and C3 were designed to have a lower bleeding than Mixes C2 and C4. The lower bleeding of Mix C1 and C3 was achieved by replacing part of the sand with a crusher dust that was sieved through a 2.36 mm sieve. The high fine content and angular particle shape of the crusher dust significantly lowered the bleeding as discussed in Section 2.4.2. In addition to the crack measurements conducted during the testing of these mixes several important influencing factors such settlement, shrinkage, bleeding, evaporation, setting times and capillary pressure were also measured. The material constituents and proportions as well as the properties of Mixes C1 to C4 are shown in Tables 3.2.

Table 3.2. Material constituents and proportions as well as properties of Mixes C1 to C4.

Mix description	Mixes for Cracking type tests 1 to 4			
Mix abbreviation	**Mix C1**	**Mix C2**	**Mix C3**	**Mix C4**
Material constituents [kg/m³]				
Water	250	205	205	205
Cement - CEM II 32.5N	510	370	-	-
Cement - CEM II 52.5N	-	-	342	342
13 mm Greywacke stone	800	900	1037	1037
Natural quarry sand - Batch 1	385	920	-	-
Natural quarry sand - Batch 2	-	-	569	799
Greywacke crusher dust - sieved through 2.36 mm sieve	400	-	244	-
Mix properties				
Slump [mm]	50	150	70	120
28-day characteristic design strength [MPa]	32	22	32	32
Actual average 28-day strength [MPa]	31.8	18.6	37.5	-
w/c ratio	0.49	0.55	0.6	0.6

The properties of the cement and aggregates used in the mixes are given in Table 3.3. Three different cements were used for the mixes. Cements A and C are both composite cements (CEM II), where between 6 and 20 % of the clinker content was replaced with limestone, while Cement B is an ordinary Portland cement (CEM I) containing more than 95 % clinker. Cement A has a 32.5 MPa strength class, while Cements B and C have a 52.5 MPa strength class. All the cement was supplied by PPC (Pretoria Portland Cement).

A stone with a nominal size of 13 mm as graded according to SANS 1083 (2002) was used for all mixes. This stone size was chosen as this is the maximum size that can be accommodated by the

L-box settlement cracking mould. The stone has a chunky angular shape since it was produced by the mechanical crushing of a metamorphic rock known as Greywacke.

Table 3.3. Cement and aggregates properties.

Material	Relative density	Fineness modulus	Particle shape
Cement A - CEM II 32.5N	3.00	-	-
Cement B - CEM I 52.5N	3.14	-	-
Cement C - CEM II 52.5N	3.14	-	-
13 mm Greywacke stone	2.74	-	Angular
Natural quarry sand - Batch 1	2.69	2.31	Round
Natural quarry sand - Batch 2	2.64	2.65	Round
Greywacke crusher dust - sieved through 2.36 mm sieve	2.60	2.43	Angular

Two different types of sand were used for the mixes. The first was a siliceous pit sand known locally as Malmesbury sand. This sand was formed by the natural disintegration and weathering of rock and therefore has a rounded particle shape. Two different batches of this sand were used for the mixes. The second type of sand used was a crusher dust that was sieved through a 2.36 mm sieve. This sand has an angular shape as it is formed as a by-product from the mechanical crushing of the Greywacke rock. The grading of the different sands is shown in Figure 3.18 as determined in accordance with SANS 1083 (2002). All the sands have a fairly continuous grading with a good distribution of particle sizes for all fractions smaller than 2.36 mm. The crusher dust used is further characterised by a high dust content which contains both fine and ultra-fine particles.

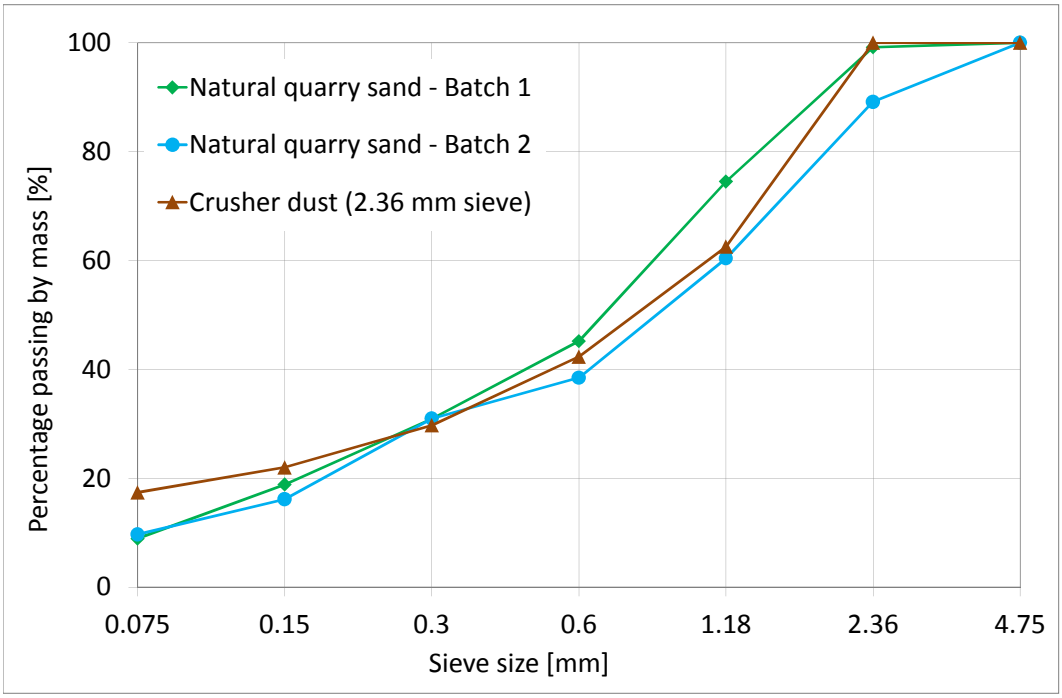

Figure 3.18. Grading of sands.

3.4. Climatic conditions

The five different climatic conditions that were used during testing are shown in Table 3.4. Two of these conditions have an ambient temperature of 23°C and relative humidity of 60 % and are referred to as normal climates (Climates N1 and N2). The only difference between the two normal climates is the wind speed, where Climate N1 has no significant wind and Climate N2 has a 21 km/h wind.

Table 3.4. Climatic conditions.

Climatic condition	Climate N1	Climate N2	Climate E1	Climate E2	Climate E3
Concrete temperature [°C]	23	23	23	23	23
Ambient temperature [°C]	23	23	40	40	40
Relative humidity [%]	60	60	20	10	-
Wind speed [km/h]	≈0	21	33	21	-
Evaporation rate based on Equation 2.2 [kg/m²/h]	< 0.1	0.54	1.04	1.03	-

The extreme climates (Climates E1 and E2) differ mainly from the normal climates by having a high ambient temperature of 40°C and low relative humidity. This together with the high wind speeds for both Climate E1 and Climate E2 results in evaporation rates of more than 1 kg/m²/h as calculated using Equation 2.1. These conditions were chosen since climates resulting in evaporation rates of more than 1 kg/m²/h are considered to be ideal for the formation of plastic shrinkage cracking (Uno, 1998). Climate E3 was only used for the tensile tests where the samples were coved with a 2 to 3 mm water layer to prevent evaporation as discussed in Section 3.2.7. The covering of the concrete samples at Climate E3 effectively meant that there was no influence of wind or relative humidity.

Only two locations were used to create these climatic conditions for the tests. The first was a large climate controlled room which is permanently set to Climate N1. The second was the climate chamber discussed in Section 3.1.1, which was used to simulate each of the five climate conditions (Climates N1, N2, E1, E2 and E3).

3.5. Test program

All the tests conducted in this study can be grouped into one of six different test sets (Tests 1 to 6), where each test set has a specific objective. The plastic nature of the concrete during these tests caused notable variation in results. This meant that a large number of tests needed to be performed

to allow the comparison of these results. This was achieved by conducting multiple tests (at least three, unless stated otherwise) on different samples to obtain average values for comparison purposes. This is especially important if the results are to be used as verification of a model as given and discussed in Chapter 6. Tests 1 to 5 involved the cracking of plastic concrete while the Tests 6 involved the tensile testing of plastic concrete.

Tests 1: Setting time

The objective of these tests was to choose an appropriate method for determining the setting times of concrete that is suited to the test procedures followed for all the other tests. This means the setting times must be easy to conduct in tandem and in synchronisation with any of the other tests. To achieve this, the results and procedures of both the ASTM C403 (2008) and EN 196-3 (2005) test methods were compared for three different mixes (Mixes S1-S3).

Tests 2: Bleeding versus settlement

The objective of these tests was to investigate the difference in results obtained between bleeding and settlement measurement methods. This is needed since settlement causes bleeding, as discussed in Section 2.4, and therefore bleeding and settlement are linked to one another but not necessarily identical, especially if measured using different methods.

The objective was achieved by using different methods of measuring the bleeding as discussed in Section 3.1.3 and comparing the results with settlement measurements. Two mixes were used for these tests, one with a low bleeding (Mix C3) and the other with a high bleeding (Mix C4).

Tests 3: Plastic settlement cracking

The objective of these tests was to observe and understand the behaviour or nature of pure plastic settlement cracking without the influence of plastic shrinkage cracking. This was achieved by conducting several tests using the L-box and steel bar settlement cracking moulds together with two standard mixes (Mix S2 and Mix S4) that are appropriate for use in slab-like elements. In addition, the surface of the test samples was covered with a thin layer of water during the tests to ensure that no capillary pressure and therefore no plastic shrinkage could develop.

Tests 4: Plastic shrinkage cracking

The objective of these tests was to observe and understand the pure plastic shrinkage cracking behaviour or nature of concrete without the influence of settlement. To achieve this, several tests were conducted on Mixes C1 to C4 at both normal and extreme climates.

Initially, the shrinkage cracking moulds were used and assumed to evaluated and observed pure plastic shrinkage cracking. This assumption was later questioned as signs of plastic settlement cracks were found, indicating the influence of differential settlement on the cracking behaviour observed in the shrinkage cracking mould. Finally, in an attempt to observe pure plastic shrinkage cracking, tests were conducted with modified shrinkage cracking moulds where the potential for differential settlement at the central restraint was removed.

Tests 5: Plastic settlement and shrinkage cracking combined

The objective of these tests was to observed and understand the cracking behaviour if both plastic settlement and shrinkage cracking occurs. This was achieved by conducting several tests where the potential for both cracking types were altered. The potential for settlement cracking was altered in two ways. Firstly, by using mixes with a low bleeding/settlement (Mixes C1 and C3) and a high bleeding/settlement (Mixes C2 and C4). Secondly, by using the L-box settlement cracking moulds as well as the shrinkage cracking moulds for tests, which both have different potentials for plastic settlement cracking.

In addition, the configuration of the central restraint of the shrinkage cracking mould was also altered to induce both a high and low potential for plastic settlement cracking. The potential for plastic shrinkage cracking was mainly altered by using climatic conditions with different evaporation rates (Climates N1 and E1), but also through the use of mixes with different bleeding potentials as discussed in Section 2.5.3.

Tests 6: Tensile material properties

The objectives of these tests were to determine the tensile material properties of plastic concrete as well as the influence of temperature/setting time on the development of these properties. The required material properties included: tensile strength, Young's modulus, strain capacity and fracture energy. These material properties were determined by conducting several direct tensile tests at 1 hour intervals using the tensile moulds and Mix C3 at both a low (23 °C) and a high (40 °C) ambient temperature as discussed in Section 3.2.7.

A summary of Tests 1 to 6 in terms of the mixes, climates and moulds used during testing is given in Table 3.5. The details regarding the mixes, materials and climates used can be found in Tables 3.1 to 3.4.

Table 3.5. Test program.

Test set	Mixes	Climates	Moulds
Tests 1. Setting time	S1, S2, S3	N1	Vicat penetration moulds, 150 mm steel cubes
Tests 2. Bleeding versus settlement	C3, C4	N1	Bleeding moulds, shrinkage moulds, settlement moulds
Tests 3. Plastic settlement cracking	S2, S4	N1	L-box settlement cracking moulds, steel bar settlement cracking moulds
Tests 4. Plastic shrinkage cracking	C1, C2	N1, E1	Shrinkage cracking moulds
	C3, C4	N2, E2	Shrinkage cracking moulds, shrinkage moulds, settlement moulds, capillary pressure moulds
Tests 5. Plastic settlement and shrinkage cracking	C1, C2	N1, E1	Shrinkage cracking moulds, L-box settlement cracking moulds
	C3, C4	N1, N2, E2	Shrinkage cracking moulds, shrinkage moulds, settlement moulds, capillary pressure moulds
Tests 6. Tensile material properties	C3	N1 (23°C), E3 (40°C)	Tensile moulds

3.6. Concluding summary

This chapter provides the framework and details of all the tests that were performed in this study. This includes descriptions of test setups, measurement methods, test procedures as well as materials and conditions used for the tests. In Chapter 4, the results of the tests conducted on the cracking of plastic concrete (Tests 1 to 5) are given and discussed while the results of the tensile tests (Tests 6) follow in Chapter 5.

Chapter 4. Cracking of plastic concrete test results and discussion

This chapter contains and discusses the results of the tests that were performed to observe and understand the cracking behaviour of plastic concrete. This includes tests on: setting times, bleeding versus settlement, plastic settlement and plastic shrinkage cracking as well as these two cracking types combined. For each of these tests the specific objective as discussed in Section 3.5 is briefly repeated, followed by the results and discussions as well as the main conclusions that can be drawn.

4.1. Setting times

The objective of these tests was to identify and choose an appropriate test method for determining the setting times of concrete that is suited to the test procedures followed for all the other tests. The average setting times for Mixes S1, S2 and S3 were determined using both a Vicat penetration apparatus and ASTM penetrometer respectively in accordance with EN 196-3 (2005) and ASTM C403 (2008) test methods as described in Section 3.1.3. It should be noted that the time zero for these tests was taken as the time when water was added to the mix and not the time when the moulds were placed in the testing environment as for all the other tests conducted in this study. This was done to simplify the comparison between the results of the two test methods used to determine the setting times in this section. Furthermore, only two samples were tested for each mix and each setting time test method, where each sample was obtained from a freshly mixed concrete batch. This is acceptable since the objective of these tests was only to identify an appropriate test method and not to compare mixes. It should be noted that all the other tests conducted in this study comprised of at least three samples (unless stated otherwise) as mentioned in Section 3.5.

Figure 4.1 shows the penetration resistance of one sample for each mix using the ASTM test method. Best-fit power curves (all with R^2-values of more than 0.98) were fitted to the data points as shown in the figure to obtain the setting times as recommended by ASTM C403 (2008). The figure shows the influence of the mix type on the setting or stiffening evolution of the concrete in terms of penetration resistance. The Mix S1 with the lowest slump and water-to-cement ratio, showed the

fastest setting times, while Mix S3 with the highest slump and water-to-cement ratio showed the longest setting time of the three mixes. The setting times achieved, slump and water-to-cement ratio of Mix S2 fitted as can be expected between the results of Mixes S1 and S3.

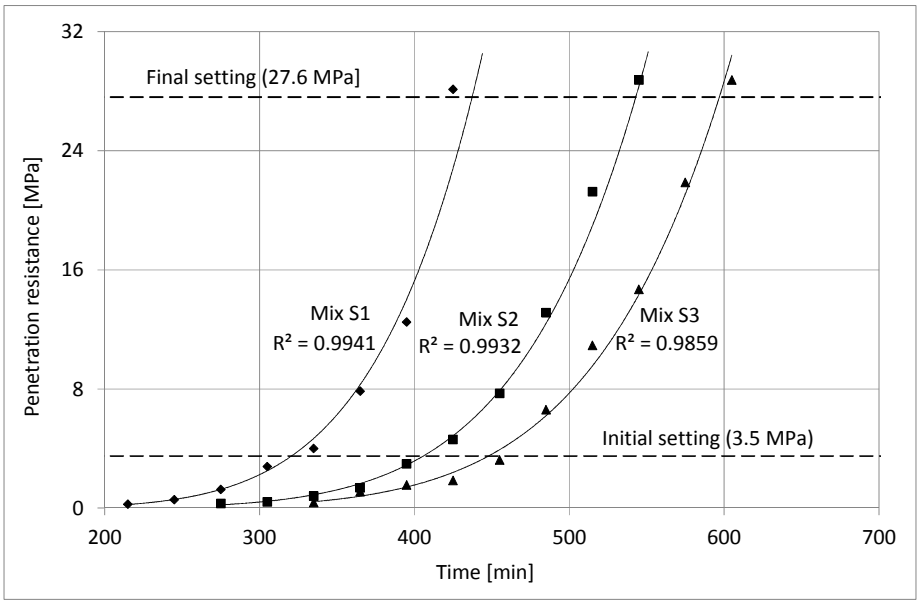

Figure 4.1. Evolution of penetration resistance as measured for one sample for Mixes S1, S2 and S3 in accordance with ASTM C403 (2008).

4.1.1. Practicality of test methods

In terms of practically performing the tests, it was found that the large ASTM mould (150 mm cube) took much longer to fill with the sieved paste than the small Vicat mould. The Vicat mould could easily be filled within 2 to 3 minutes, while it took between 20 to 25 minutes to fill a 150 mm cube depending on the workability of the mix. In general, the less workable the mix, the longer the sieving process. Furthermore, for mixes with extended setting times, a single 150 mm cube might not be large enough for all the needed penetration measurements. Practically, this means that the Vicat test method can easily be conducted in tandem with the other type of tests without causing a significant time delay between the tests, while this is troublesome with the ASTM test method.

4.1.2. Results of ASTM versus Vicat test method

Figure 4.2 shows the average setting times for Mixes S1, S2 and S3. The results show that the ASTM test method consistently estimated later or longer setting times than the Vicat test method for all three mixes.

The differences in measured setting times between the two test methods for all three mixes are shown in Figure 4.3. The figure shows that the type of mix did not significantly influence the difference in measured setting times between the Vicat and ASTM test methods. This means that the

difference between the results of the two methods is nearly consistent, irrespective of the type of concrete mix. On average for the three mixes, it took 62 and 92 minutes longer to reach the initial and final setting times respectively, when using the ASTM method compared to the Vicat method. These time differences also included a 20 minute difference in sample preparation time between the Vicat and ASTM methods.

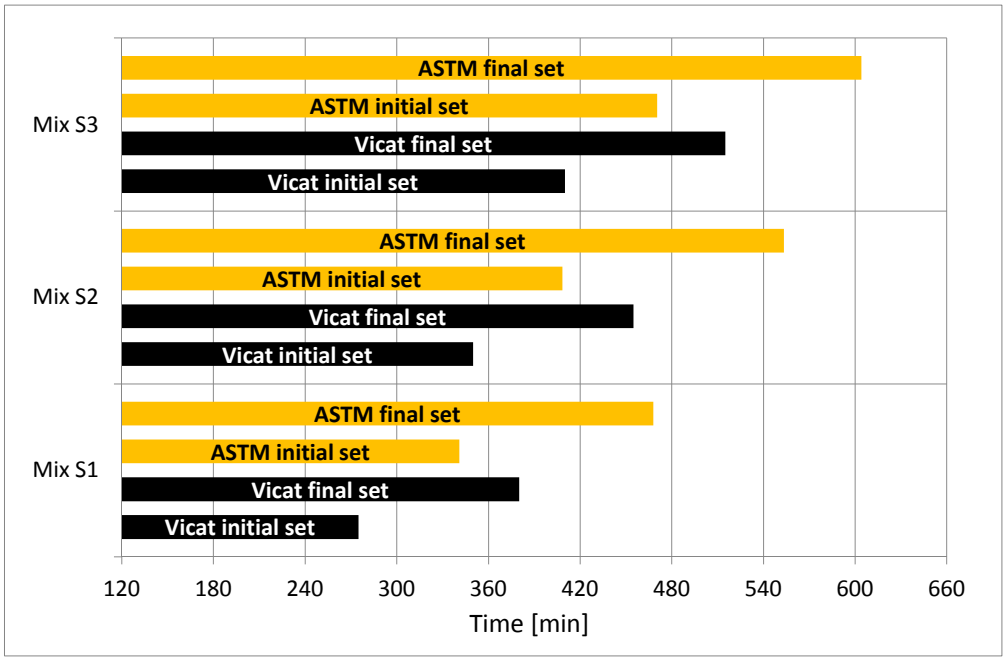

Figure 4.2. Average initial and final setting times for both the Vicat and ASTM test methods for Mixes S1, S2 and S3.

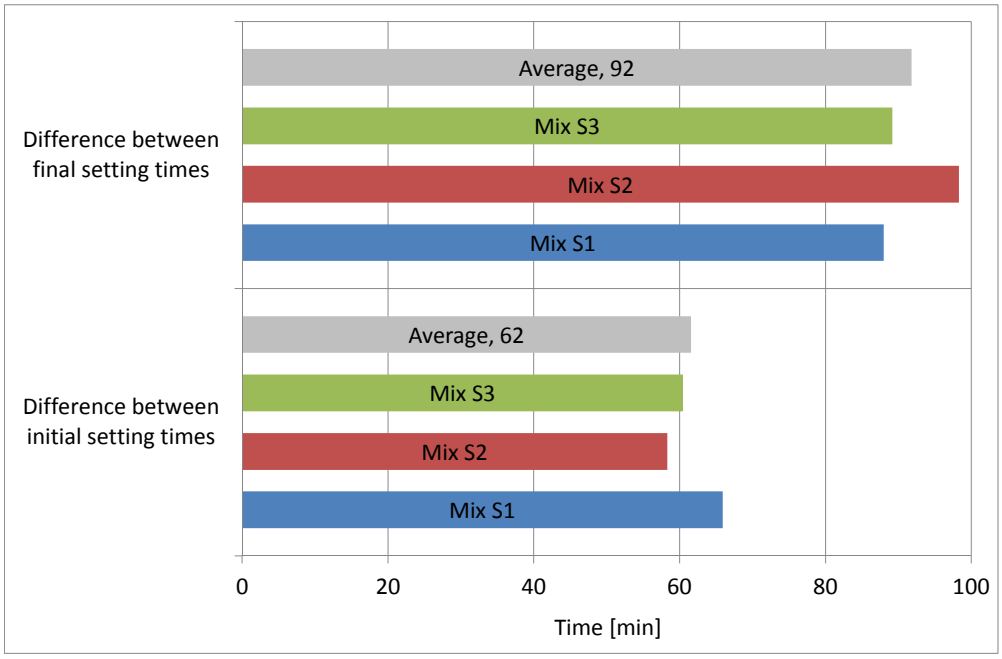

Figure 4.3. Difference in average setting times between the Vicat and ASTM test methods for Mixes S1, S2 and S3.

4.1.3. Conclusions

The ASTM test method is not practical to perform with the other tests in this study due its long sample preparation time. This together with the consistent difference between the results of the two test methods led to the decision that only the Vicat test method is suitable to be used in tandem with all of the other tests conducted in this study. This is acceptable since these setting times are not used as absolute or exact values, but rather as an indication of the setting or stiffening progress of a concrete mix, which is valuable information that was often used to decide when it is acceptable to terminate some of the other tests conducted. Furthermore, as long as the chosen test method is used consistently for all mixes it remains a valid method of distinguishing between the setting times of different mixes.

4.2. Bleeding versus settlement

The objective of these tests was to investigate and compare the results of the bleeding measurements methods with the settlement measurement methods used as described in Section 3.1.3. The bleeding was measured by extracting the bleed water from the concrete surface at various predetermined time intervals, while the settlement of the top surface of the concrete was measured with a linear variable displacement transducer (LVDT) connected to a wire mesh that rested on the concrete surface.

The results of the bleeding and settlement measurements for both Mixes C3 and C4 at Climate N1 are shown in Figures 4.4 and 4.5. Both figures show the cumulative amount of bleeding as measured with the tilting method (ASTM C1579, 2006) using five different measuring intervals namely: 20 minutes as well as 1, 2, 3 and 4 hours. The tilting method was preferred above the stencil method as discussed in Section 3.1.3 since it was difficult to create similar groove patterns on the concrete surface for Mixes C3 and C4. At each of these time intervals, bleed water was extracted and measured using two different concrete samples. These samples were left undisturbed and covered between time intervals. This means the result of cumulative bleeding for each time interval as shown in Figures 4.4 and 4.5 is the average of two concrete samples.

The results of the first measurement for each measuring interval are indicated by red markers in both Figures 4.4 and 4.5. The figures also show the average settlement results as calculated from measurements with LVDTs on four concrete filled moulds. The moulds used for these settlement measurements were the same as the mould used to measure the bleeding. This was done to ensure

that the results of bleeding and settlement are comparable, since the influence of the wall effect on the settlement and bleeding depend on the geometry of the mould as the discussed in Section 2.4.2.

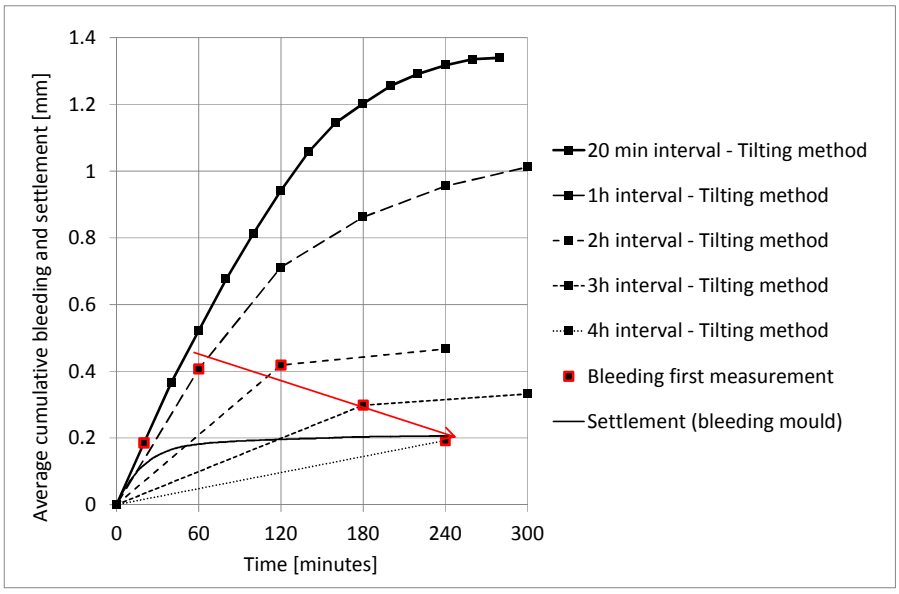

Figure 4.4. Average cumulative bleeding and settlement of Mix C3 at Climate N1.

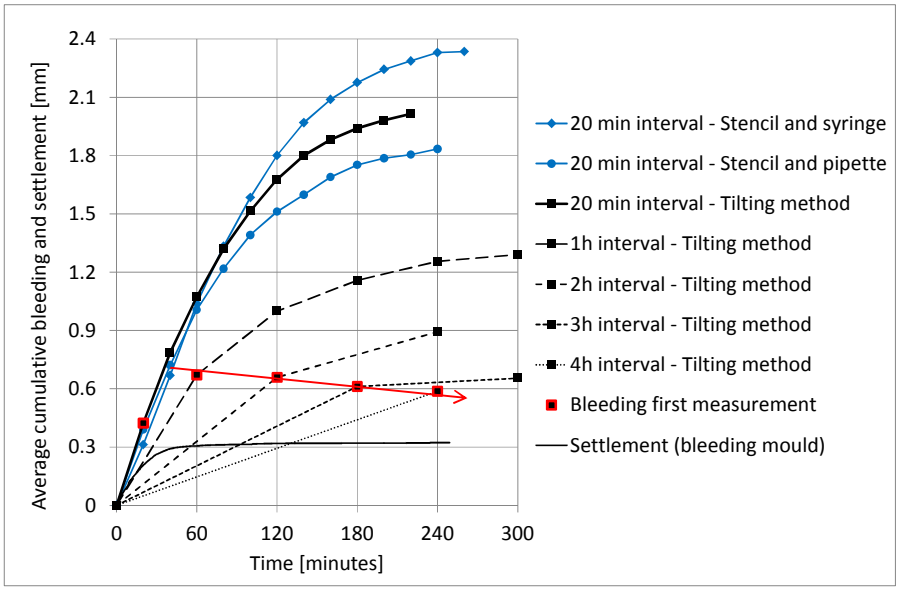

Figure 4.5. Average cumulative bleeding and settlement of Mix C4 at Climate N1 as measured using different methods and time intervals.

Figures 4.4 and 4.5 clearly show that the cumulative bleeding measured at 20 minute intervals is significantly more than the measured settlement for both mixes. The reasons for the difference are due to the extraction of bleed water from the concrete surface every twenty minutes for the bleeding test, whereas no bleed water is extracted for the settlement tests. This is confirmed by the significantly lower bleeding measured the longer the time interval between bleeding measurements as shown by the bleeding results in Figures 4.4 and 4.5.

These results suggest that the more frequently bleed water is removed from the concrete surface the more bleed water becomes available. The results of the first measurement of bleeding at each measuring interval also suggest that if left undisturbed the bleed water on the concrete surface gradually decreases. The underlying mechanisms for these results are the reabsorption of bleed water into the concrete as well as capillary pressure build-up. Both these mechanisms are discussed in the following sections.

Figure 4.5 also shows the results of bleeding measurements at 20 minute time intervals, where extraction was conducted with a stencil and syringe a well as a stencil and pipette as proposed by Josserand and De Larrard (2004). The results of these extraction methods are similar to the result achieved using the tilting method up to around 80 minutes, after which the method using a syringe for extraction resulted in more bleeding than the method using a pipette for extraction. This can be expected due to the greater suction force applied by the syringe compared to the pipette. The results suggest that the method of extraction does not significantly influence the results for the more critical initial part of the bleeding measurements and therefore it can be argued that any of these extraction methods can be used to give an adequate representation of the bleeding potential of a concrete mix as long as the same method is used when results are to be compared between mixes.

4.2.1. Reabsorption of bleed water

The red markers in both Figures 4.4 and 4.5 show the first measurement of bleeding after the moulds were left undisturbed for 20 minutes as well as 1, 2, 3 and 4 hours respectively. These results show an initial increase to a maximum amount of bleed water on the concrete surface at around 1 hour for both Mixes C3 and C4. This is followed by a decrease in the amount of bleed water on the concrete surface the later the bleeding was measured for the first time. This decrease is not due to evaporation of bleed water, since the evaporation is not only negligible at Climate N1 but mainly since the evaporation is taken into in account during the bleeding calculations as discussed in Section 3.1.3. The results suggest that the bleed water is drawn back or reabsorbed into the concrete specimen. This occurred at around 60 minutes after casting and finishing the concrete in the bleeding moulds. This is also the time where the measured settlement of the concrete started to stabilise to a maximum value.

The same observations were made by Kwak et al. (2010) who measured both the bleeding and the settlement simultaneously on a mortar specimen using a method that involved the covering of a sample with a layer of paraffin oil and monitoring the displacement of both the mortar and liquid surfaces. In contrast, the bleeding and settlement values presented in this study in Figures 4.4 and

4.5 were measured using completely different methods. However, the same conclusion can be drawn namely that if left undisturbed, bleed water is reabsorbed into the concrete, starting around the time when the maximum settlement is reached. Furthermore, the start of the reabsorption is believed to coincide with the start of hydration at the end of the dormant period as discussed in Section 2.2 (Sant et al., 2009 and Kwak et al., 2010). However, this requires further investigation and does not from part of the objectives of this study.

4.2.2. Capillary pressure

The results of Figures 4.4 and 4.5 suggest that the more frequently the bleed water is extracted the more bleeding becomes available. The reason for this is believed to be due to capillary pressure build-up. Each time the bleed water is extracted, the surface of the concrete is exposed, which causes a capillary pressure that draws more bleed water to the surface. In addition, the effect of the reabsorption of bleed water becomes negligible, since it can be is argued that the upward suction force due to capillary pressure overpowers the downward suction of the bleed water due to hydration.

Figure 4.6 and 4.7 show the results of settlement and capillary pressure build-up at three different climatic conditions for both Mixes C3 and C4. The figures clearly show that the settlement significantly increases once the capillary pressure starts to build-up as for Climates N2 and E2, whereas no additional settlement occurred without capillary pressure build-up as measured for Climate N1. The figures also show that if no capillary pressure is present, the settlement tends to stabilise at around 60 minutes which corresponds to the start of the reabsorption of bleed water.

It should be mentioned that the settlement at Climate N1 was measured in the bleeding mould, while the settlement for Climates N2 and E2 was measured in the much larger settlement and shrinkage mould. This difference in mould size influences the amount of settlement due to the wall effect as discussed in Section 2.4.2. The results also show that the settlement measured at Climate E2 is higher than at Climate N2, even though the same moulds were used for these measurements. This is due to the higher rate of bleed water evaporation for Climate E2 compared to Climate N2 which is even evident from the initial part of the capillary pressure build-up before the more obvious significant increase in capillary pressure.

The possible reasons for the difference in the measured settlement values between the two different moulds before the significant capillary pressure started to build-up are therefore the greater influence of the wall effect for the smaller mould used at Climate N1 as well as the lower rate of

bleed water evaporation for Climate N1. However, this requires further investigation and does not form part of the objectives of this study.

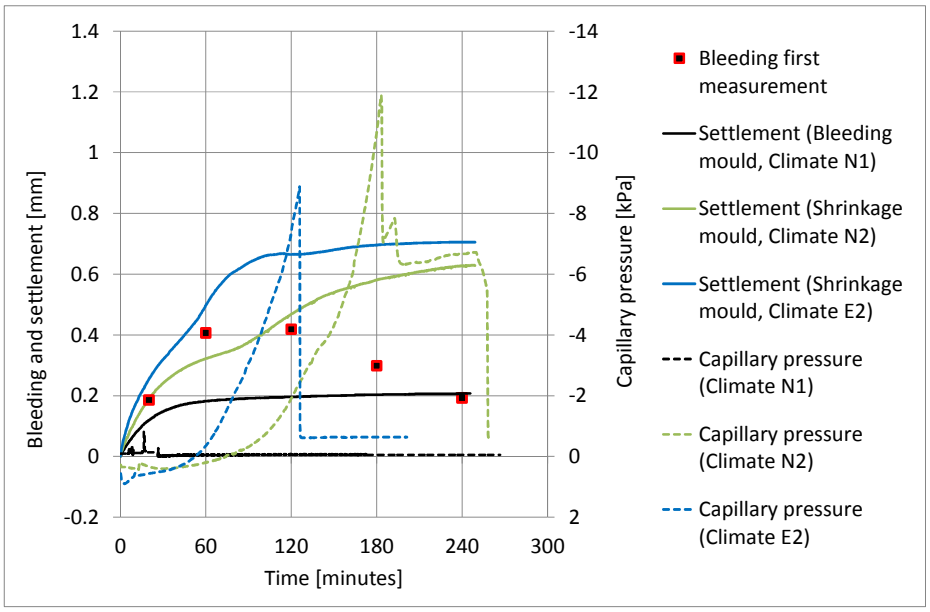

Figure 4.6. Settlement and capillary pressure build-up for Mix C3 at Climates N1, N2 and E2.

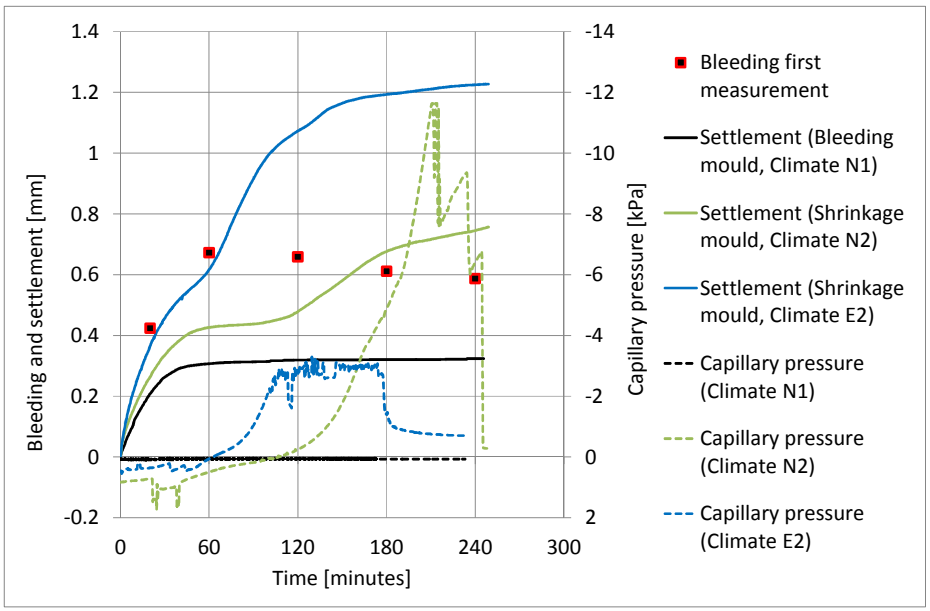

Figure 4.7. Settlement and capillary pressure build-up for Mix C4 at Climates N1, N2 and E2.

4.2.3. Conclusions

The following conclusions can be drawn regarding the bleeding and settlement of concrete:

- The measurement of bleed water at 20 minute intervals is not the same as the measured settlement of the concrete surface using a LVDT. This is due to reabsorption of bleed water into the concrete as well as capillary pressure build-up.

- Bleed water is reabsorbed into the concrete surface at approximately the time when the maximum settlement is reached, which is furthermore believed to be related to the start of hydration at the end of the dormant period (Sant et al., 2009 and Kwak et al., 2010).
- The settlement of concrete significantly increases as soon as capillary pressure starts building up in the concrete. The sooner the capillary pressure starts the more the settlement.

4.3. Plastic settlement cracking

The objective of these tests was to isolate and observe the behaviour of pure plastic settlement cracks without the influence of plastic shrinkage cracking. Both the L-box and steel bar settlement moulds were used for tests as these moulds represents the two most common causes of settlement restraint in slabs-like concrete elements namely: non-uniform slab depth and imbedded reinforcing steel. In addition, three different cover depths were used for the steel bar settlement cracking mould namely: 15, 30 and 45 mm. The tests were conducted with both Mixes S2 and S4 at Climate N1. Plastic shrinkage cracking was prevented by ensuring that no capillary pressure could develop in the concrete due to evaporation of concrete pore water. This was achieved by ensuring that the surfaces of the concrete test samples were continuously covered with a thin layer of water. The typical plan view of the crack patterns that were observed for the L-box and steel bar settlement cracking moulds as well as the shrinkage cracking mould are shown in Figure 4.8 a), b) and c) respectively.

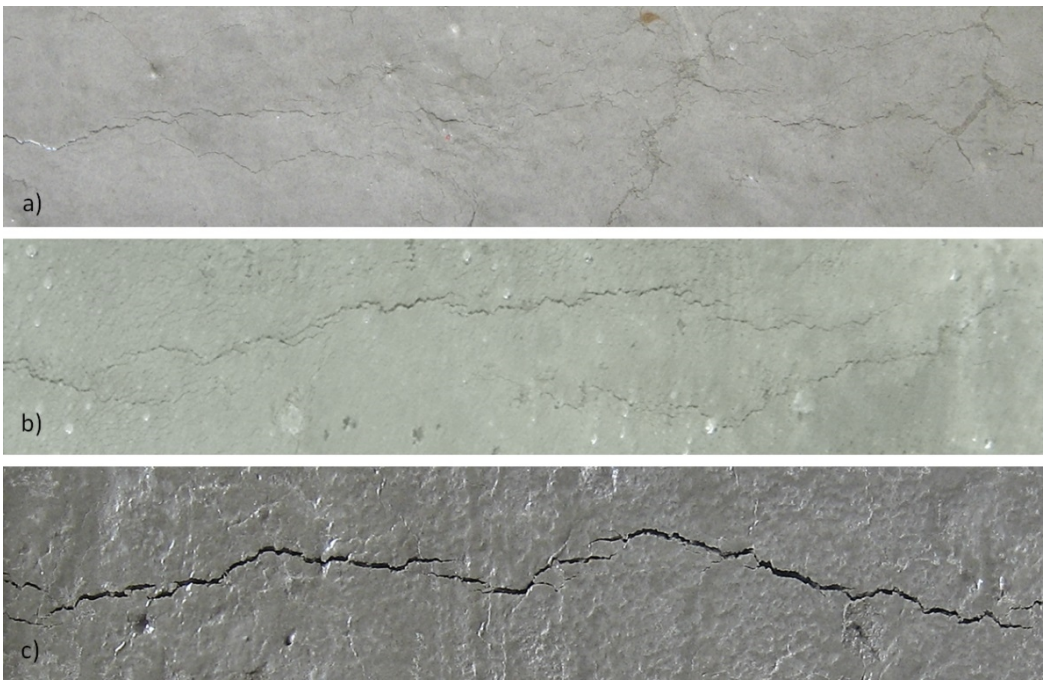

Figure 4.8. a) Typical plastic settlement crack pattern for L-box settlement cracking mould at Climate N1. b) Typical plastic settlement crack pattern for steel bar settlement cracking mould at Climate N1. c) Typical plastic shrinkage cracking pattern for shrinkage cracking mould at Climate E1.

Figure 4.8 shows that the plastic settlement cracks in Figure 4.8 a) and b) are relatively small and difficult to distinguish while in contrast the plastic shrinkage cracks in Figure 4.8 c) are large and clearly defined. Furthermore, it was difficult to capture clear and focused images of the plastic settlement cracks due to the thin layer of water on the concrete surface. It was therefore decided not to measure the cracks for these tests, but only observe the cracking behaviour. The cracks were observed from the surface as well as from the side through the Perspex side panels.

4.3.1. Tests with steel bar settlement cracking mould

Figure 4.9 shows the typical plastic settlement cracking that was observed from the side for Mix S4 in the steel bar settlement cracking mould. Figure 4.9 a) shows an image captured through the Perspex side panel of the cracks at the initial setting time, while Figure 4.9 b) shows an image of the same crack around the final setting time after the Perpex side panel was removed. The figure shows three distinctly different types of cracks or defects. A vertical crack was formed from the concrete surface downwards above the steel bar, while angled cracks formed upwards from the sides of the steel bar well below the concrete surface. Furthermore, a water pocket formed below the steel bar. Figure 4.9 c) and d) shows an illustration of the different settlement zones as well as the different types of cracks or defects. The three defects as well as the influence of cover depth and the observed crack pattern are discussed in the following sections.

Shear cracks

Angled cracks developed at the most left and most right points of the steel bar as can be seen in Figure 4.9 a) and b). The starting location of the cracks coincides with the boundary between the different settlement zones as shown in Figure 4.9 c). Figure 4.9 d) shows the shear stresses on a small block at the crack location as well as the rotation of the block to principal normal stresses. Although these cracks were ultimately formed by tensile stresses as illustrated by the principal stresses on the rotated block, the origin of these tensile stresses remain shear stresses caused by differential settlement. These cracks are therefore further referred to as shear cracks. In general, the shear cracks formed first from the bottom upwards and were not visible from the surface.

Tensile cracks

Vertical cracks developed at the concrete surface and propagated downward towards the steel bar as can be seen in Figure 4.9 a) and b). These cracks were formed due to the large difference in settlement between the concrete in the middle of the steel bars and the concrete above the steel bars. This differential settlement was also responsible for the shear cracks discussed previously, although in this case it resulted in a direct tensile stress situation as illustrated by the stresses on the small block just below the surface of the concrete in Figure 4.9 d). These cracks normally appeared

after the shear cracks and are further referred to as tensile cracks. These tensile cracks were visible on the concrete surface.

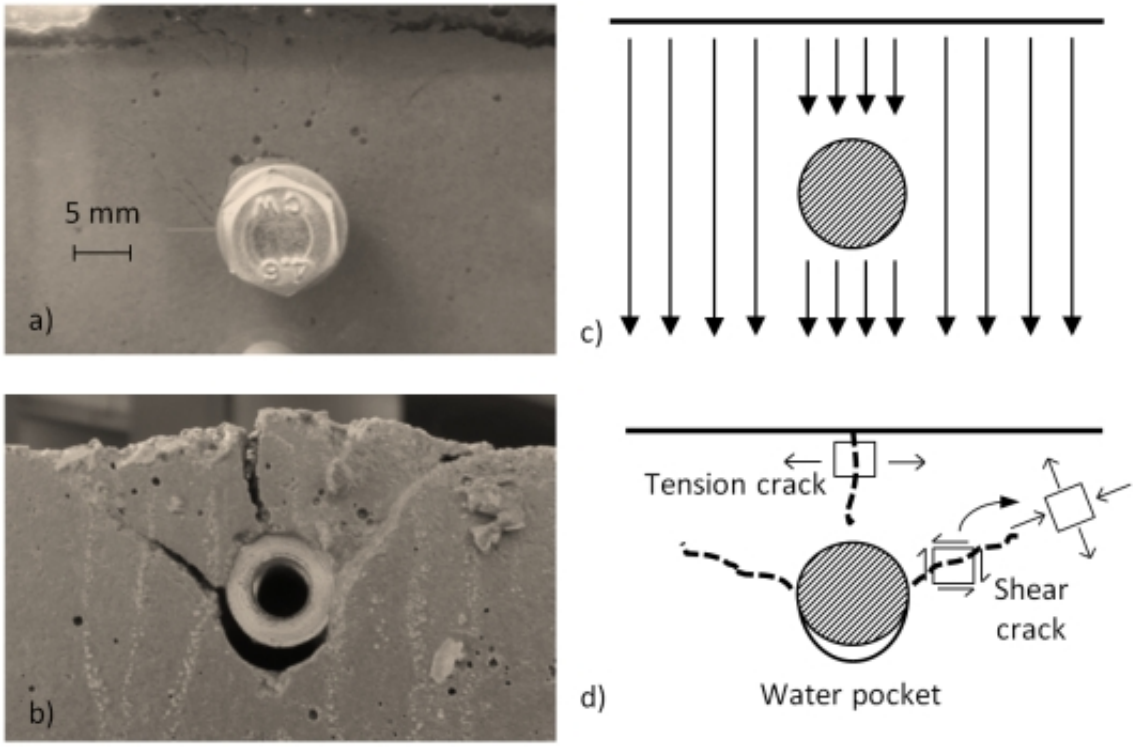

Figure 4.9. Plastic settlement cracking of Mix S4 in steel bar settlement cracking mould with 15 mm cover depth: a) Image of cracks around the steel bar captured at initial setting time through the Perspex side panel. b) Image of cracks around the steel bar captured just after final setting time with the Perspex side panel removed. c) Illustration of differential settlement around embedded steel bar. d) Illustration of local stress conditions at crack locations around the steel bar.

Water pocket

Bleed water was trapped just beneath the steel bars. This created water pockets which formed due to the settlement of the concrete below the steel bars. The water pocket is not clearly visible in Figure 4.9 a) as it was still filled with water at that stage. Figure 4.9 b) clearly shows the void left by the water pocket not filled with water after the Perspex side panel was removed. The voids left by these water pockets not only decrease the concrete strength and durability but also reduce the mechanical bond between the concrete and the reinforcing steel.

Influence of cover depth

The cover depth is the clear distance between the surface of the concrete and the top most point of the reinforcing steel embedded in the concrete. The cover depth is specified by the design engineer based on the durability and/or fire resistance requirements of the structure. For a normal density concrete structure exposed to a moderate exposure condition the concrete cover is often specified to be 30 mm (SANS 10100-2, 1992). However in practice, a uniform cover depth is hard to achieve and inadequate cover depths far less than 20 mm are often reality (Monteiro & Goncalves, 2011).

This can be due to imperfect construction or deflections of the reinforcing steel bars which causes sagging and hogging zones. This results in a reduced cover depth in the hogging zone. Figure 4.10 shows the results of tests conducted on cover depths of 15, 30 and 45 mm with 200 mm spacing between steel bars.

Figure 4.10 a), b) and c) shows a side view of the cracks over the entire mould with the Perspex covers removed just after the final setting time. From the figure it is clear that the smaller the cover depth the more severe the cracking. Figure 4.10 d), e) and f) show the angle of the shear cracks at the initial setting time with the Perspex covers not removed. The figure show that the angle of the shear cracks increases as the cover depth decreases. This means that the smaller the cover depth the more the shear cracks tend to behave like a tensile crack. It is also believed that the angle of these cracks coincide with the influence zone of the reinforcing steel on the settlement of the concrete above it as illustrated by the yellow shaded sections in Figure 4.10 a), b) and c). The figure also shows the wave-like shape of the surface of the concrete after settlement. The smaller the cover depth the more pointed or jagged the wave-like shape, which shows that the influence zone of the reinforcing steel on the settlement of the concrete above it reduces as the cover depth decreases.

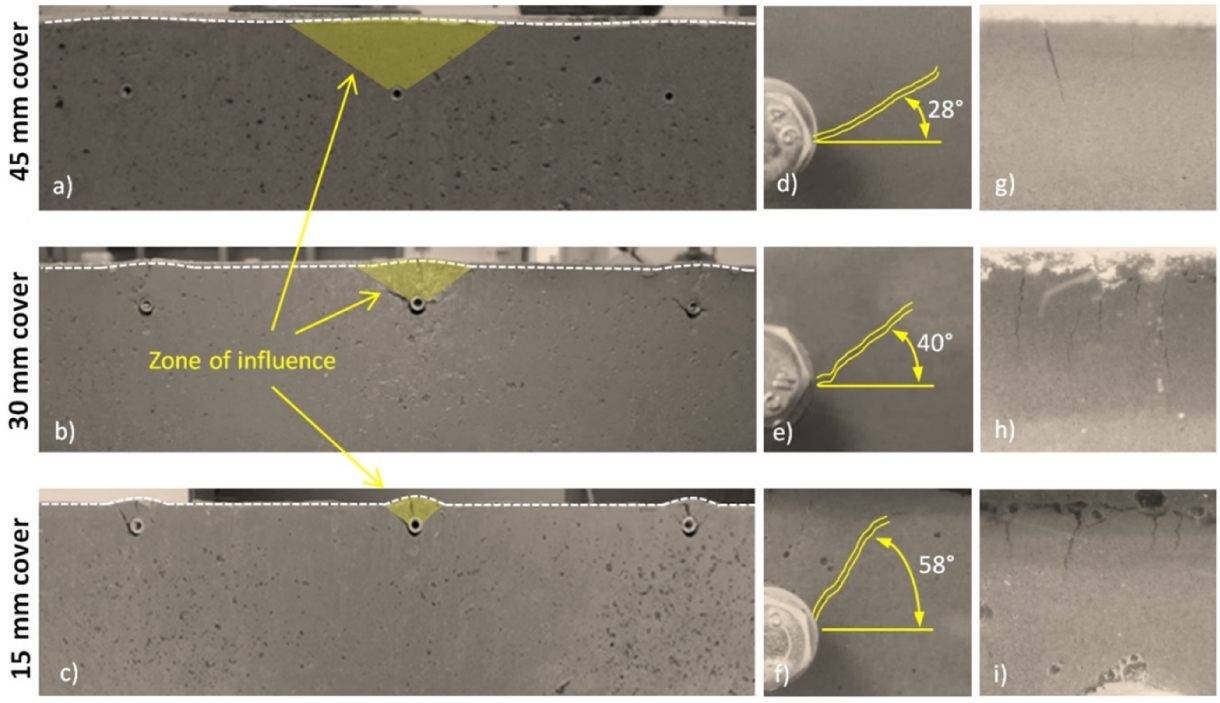

Figure 4.10. a, b, c) Image of cracks formed in mould containing embedded steel at a 200 mm spacing with cover depths of 45, 30 and 15 mm respectively captured just after the final setting time with the Perspex side panels removed. d, e, f) Images showing the angle of the interior shear cracks for a 45, 30 and 15 mm cover depths respectively captured through the Perspex side panels at the initial setting time. g, h, i) Images showing multiple tension surface cracks for a 45, 30 and 15 mm cover depths respectively captured through the Perspex side panels near initial setting time.

Multiple crack pattern

One of the most important observations made during these tests was the multiple surface tensile cracks that formed. This means that instead of forming a single isolated crack as would be expected, several smaller cracks were formed. This is shown in Figure 4.11 a) and b) which shows images of the multiple crack pattern as observed before the initial setting time in plan and from the side respectively. Figure 4.10 g), h) and i) also shows the multiple crack pattern as observed from the side for different cover depths of 45, 30 and 15 mm respectively. From the figure, it seems that the multiple cracking is more pronounced the smaller the cover depth and therefore the higher the potential for plastic settlement cracking. Finally, the multiple crack pattern that forms due to plastic settlement cracking has a distinct appearance that can greatly assist in the practical identification of these types of cracks.

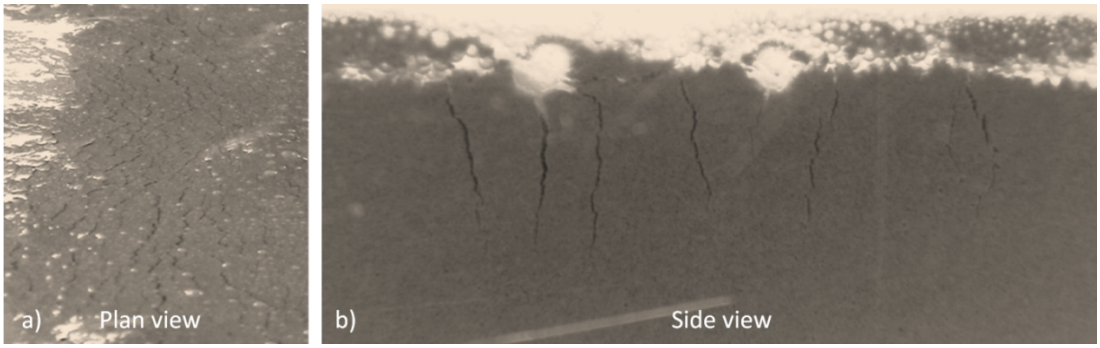

Figure 4.11. a) Plan view of the multiple crack pattern on the surface of the concrete captured before the initial setting time. b) Side view of the multiple cracks below the concrete surface as captured through the Perspex side panels before the initial setting time.

4.3.2. Tests with of L-box settlement cracking mould

Figure 4.12 shows the typical plastic settlement cracks that were observed from the side for Mix S2 in the L-box settlement cracking mould. Figure 4.12 a) shows an image captured through the Perspex side panel of the crack just after first appearance. This figure also shows the water layer that was present on the concrete surface to prevent evaporation of concrete pore water and therefore plastic shrinkage cracking. Figure 4.12 b) shows an image of the same crack around the initial setting time after the Perspex side panel was removed.

The cracks that formed are similar to cracks discussed previously for the steel bar settlement cracking mould. The interior crack at the tip of the triangle between the boundary of the deep and shallow sections of the mould can also be described as a shear crack, while the surface crack just below the surface of the concrete can be described as a tensile crack. Figure 4.12 d) illustrates the stresses on a small block at both these crack locations. The interior shear crack generally appeared first, followed closely by the surface crack at around 80 minutes after the concrete was cast. This was long before

the initial setting time of 330 minutes. In addition, it is important to note that the surface tensile crack was not visible when viewing the concrete surface from above, but only from the side.

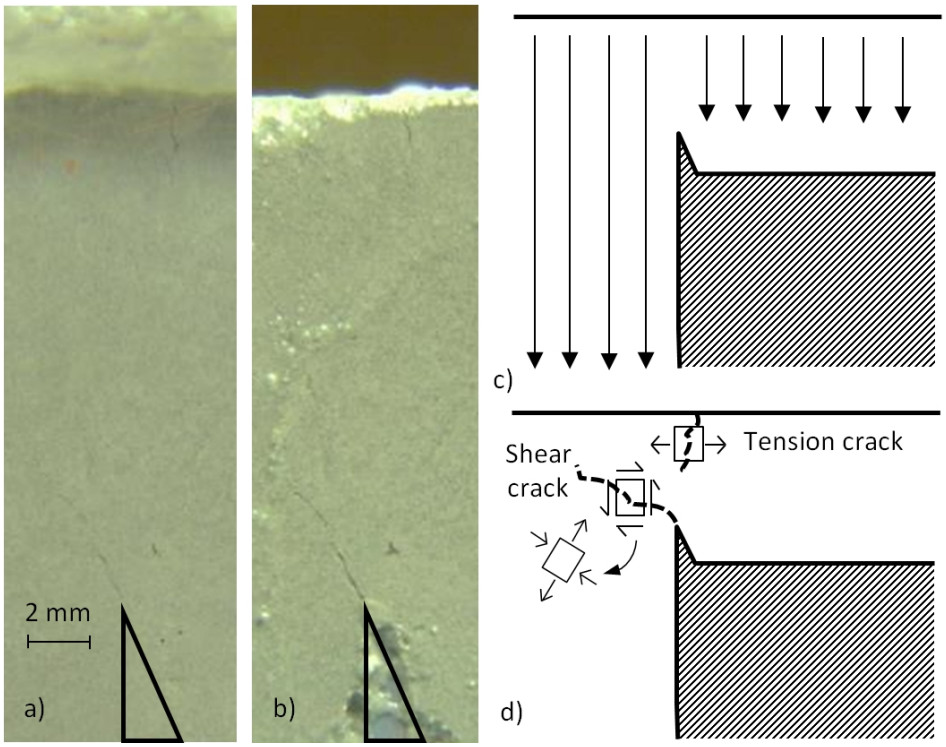

Figure 4.12. Plastic settlement cracking of Mix S2 in L-box settlement cracking mould: a) Image of cracks due to differential settlement captured through the Perspex side panel just after first appearance. b) Image of cracks due to differential settlement captured just after the initial setting time with the Perspex side panel removed. c) Illustration of differential settlement due to non-uniform mould depth. d) Illustration of local stress condition at crack locations.

4.3.3. Conclusions

The results and discussions regarding plastic settlement cracking revealed several fundamental insights that not only assist in the understanding of these cracks but also in the practical identification of these cracks. The insight gained can be summarised as follows:

- Two distinctly different types of cracks were observed due to differential settlement namely: pure tensile cracks at the surface as well as shear induced cracks beneath the concrete surface near the restraint.
- For both mould types the interior shear cracks appeared first followed by the surface tensile cracks. In addition, in several of the tests the tensile cracks were not visible in plan, but only from the side. This behaviour of plastic settlement cracks has important practical implications. It indicates that plastic settlement cracks may be present in concrete elements even if the cracks are not visible at the surface. In addition, these cracks may be present even if all evaporation was prevented through curing practices. If these cracks are not closed by techniques such as the re-

vibration of concrete just after the initial setting time, they from weak spots for future crack growth caused by for example plastic and/or drying shrinkage.

- The surface tensile crack pattern showed multiple cracks and not a single isolated crack. These multiple cracks provide insights into the plastic nature and strength of the concrete at such a young age. It is believed that the concrete acts as a ductile material with pseudo-strain hardening behaviour resulting in several cracks rather that a singular crack. This provides important information regarding the behaviour and appearance of plastic settlement cracks which can especially be helpful during the practical identification of these cracks.

4.4. Plastic shrinkage cracking

The objective of these tests was to observe and understand the behaviour of pure plastic shrinkage cracking without the influence of plastic settlement cracking. Tests were conducted using the shrinkage cracking moulds together with Mixes C1 to C4 at both normal and extreme climates (Climates N1, N2, E1 and E2). Initially, the shrinkage cracking moulds were used and assumed to evaluate and observe pure plastic shrinkage cracking. This assumption turned out to be incorrect as signs of plastic settlement cracks were found indicating cracking induced by differential settlement. Finally, in an attempt to observe pure plastic shrinkage cracking, tests were conducted with modified shrinkage cracking moulds, where the potential for differential settlement was removed.

4.4.1. Initial tests with shrinkage cracking mould

Figures 4.13 to 4.16 show the results of Mixes C1 and C2 at both Climates N1 and E1 as tested with the shrinkage cracking mould. The figures show the average cumulative amount of bleeding and evaporation as well as negative capillary pressure build-up on the left axis, while the average crack width is shown on the right axis, all as a function of time. The setting times are also indicated. All the results are average values of at least two samples, except for the capillary pressure build-up which shows the results of one of the shrinkage cracking mould samples as measured at the crack location just above the centre triangle. Unfortunately the shrinkage and settlement were not measured for these tests, since the equipment was not available at the time.

Mixes C1 and C2 showed no visible cracks up to the final setting time at Climate N1 as shown in Figures 4.13 and 4.14 respectively. This was expected as this climate has a very low potential for plastic shrinkage cracking due to the low evaporation rate of less than 0.1 kg/m²/h as calculated using Equation 2.2 (Uno, 1998). However, for Mix C1 a very fine crack was observed just after the final setting time. The origin of this crack is discussed in Section 4.5.1. For both these mixes the

surface was nearly completely covered with a thin film of water throughout the tests, which can also be confirmed by the lack of capillary pressure build-up.

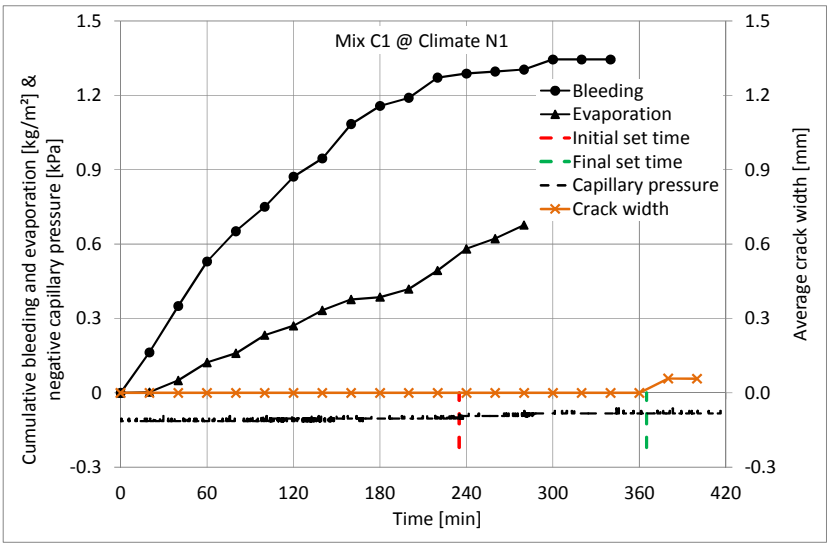

Figure 4.13. Results of Mix C1 at Climate N1.

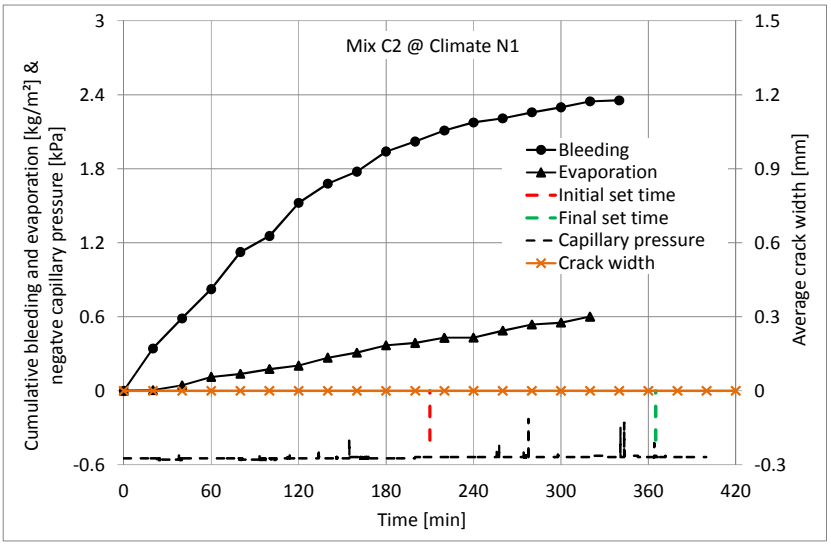

Figure 4.14. Results of Mix C2 at Climate N1.

Mixes C1 and C2 showed significant cracking at Climate E1 as shown in Figures 4.15 and 4.16 respectively. This was expected due the high potential for plastic shrinkage cracking due to the high evaporation rate of Climate E1 of more than 1 kg/m²/h as calculated using Equation 2.2 (Uno, 1998). For both mixes the first crack appeared just before the initial setting time, followed by a significant and rapid crack widening that stabilised before the final setting time. The term stabilised in this case refers to a significant reduction in the rate of crack widening. The capillary pressure started to increase around the drying time which indicates a point in time where all the bleed water on the concrete surface has evaporated. The capillary pressure continued to increase up to around the initial setting time where a significant drop in capillary pressure occurred, called air-entry. This

behaviour corresponds to the phenomological behaviour of plastic shrinkage cracking as described by Boshoff and Combrinck (2013) and discussed in Section 2.5.2.

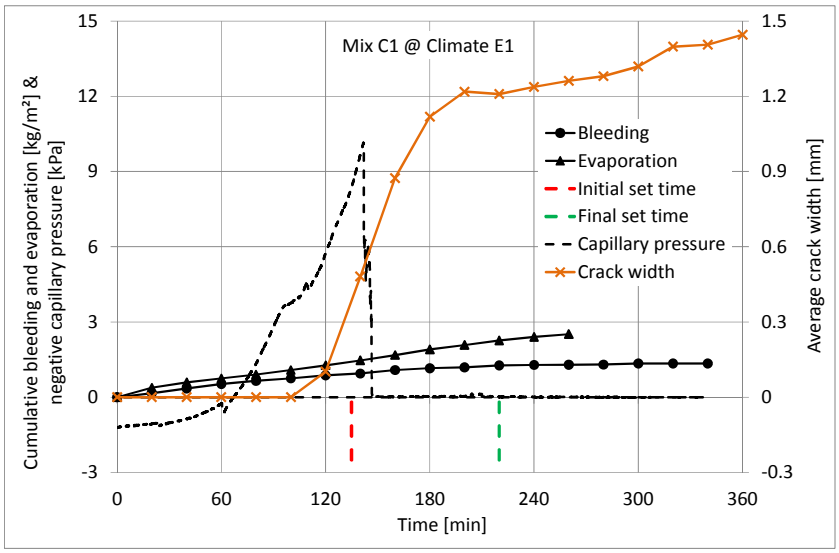

Figure 4.15. Results of Mix C1 at Climate E1.

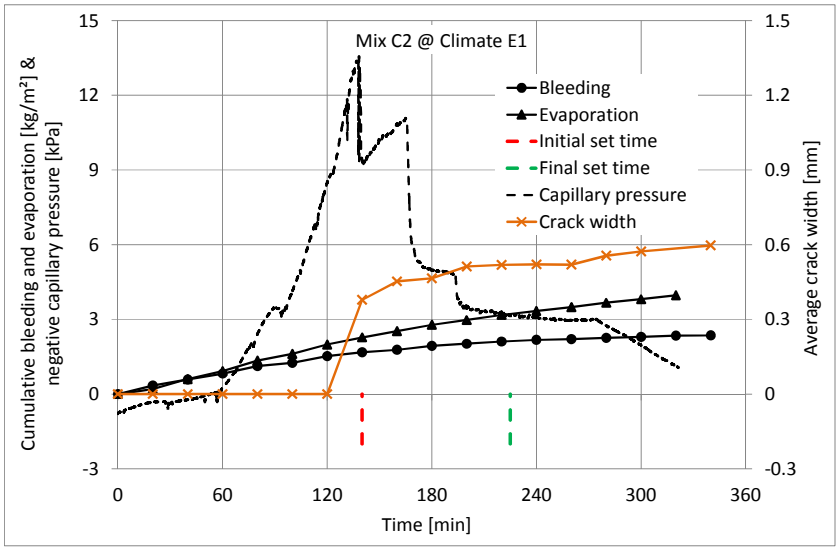

Figure 4.16. Results of Mix C2 at Climate E1.

4.4.2. Final tests with shrinkage cracking mould

Figures 4.17 to 4.20 show the results of Mixes C3 and C4 at both Climates N2 and E2 as tested with the shrinkage cracking mould. The figures show the average settlement strain and shrinkage strain as well as the negative capillary pressure build-up on the left axis, while the average crack width is shown on the right axis, all as a function of time. The setting times are also indicated. All the results are average values of at least three samples for these tests, except for the capillary pressure build-up which is a single result as measured in the capillary pressure mould and not the shrinkage cracking mould as for the initial tests in the previous section.

Mixes C3 and C4 cracked at Climate N2 as shown in Figures 4.17 and 4.18, whereas Mixes C1 and C2 at Climate N1 showed no cracks up to the final setting time. The only difference between Climates N1 and N2 is an added 21 km/h wind for Climate N2. This increased the evaporation rate from less than 0.1 kg/m²/h for Climate N1 to more than 0.5 kg/m²/h for Climate N2. This highlights the significant increase in cracking potential if wind is present. Furthermore, Figures 4.17 and 4.18 provide valuable insights into the interaction between vertical settlement, horizontal shrinkage and capillary pressure.

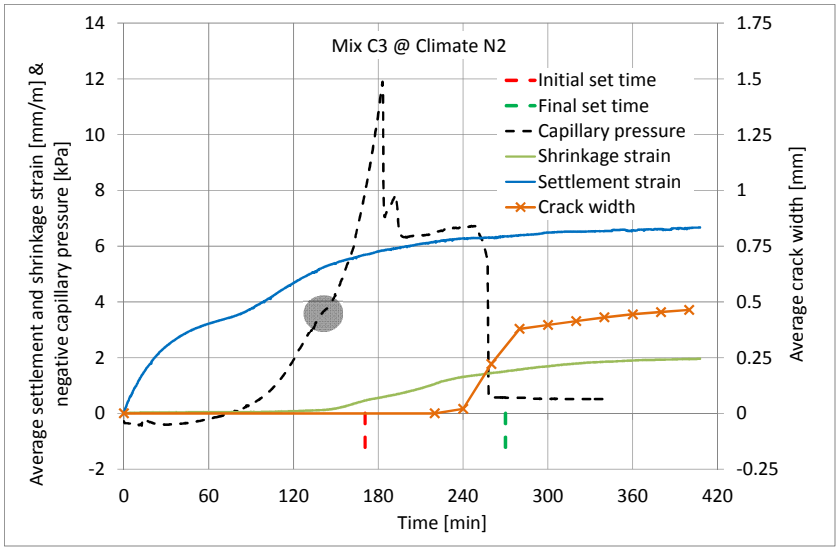

Figure 4.17. Results of Mix C3 at Climate N2.

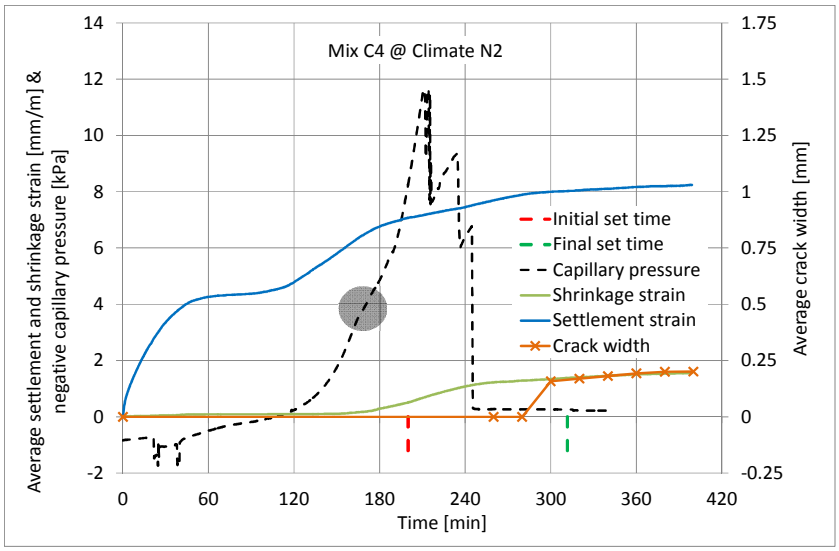

Figure 4.18. Results of Mix C4 at Climate N2.

The figures show that initially only the settlement is active with no significant capillary pressure build-up. The settlement tends to cease or stabilise around 60 minutes for both mixes which corresponds to the time when bleed water starts reabsorbing into the concrete as discussed in

Section 4.2.1. The settlement then increases once the capillary pressure starts to build-up. This is especially clear for Mix C4 in Figure 4.18, where the bleeding clearly ceases after 60 minutes and only starts increasing at around 120 minutes which corresponds to the start of the capillary pressure build-up. Interestingly, the horizontal shrinkage only starts long after the capillary pressure starts to build-up. Furthermore, as shown in Figure 4.18, the start of the horizontal shrinkage does not correspond to the observation of the first visible cracks at around 30 minutes before the final setting time. Once the first crack was formed the majority of the crack widened occurred between the initial and final setting times.

These observations provide significant insight into the capillary pressure build-up and cracking process of plastic concrete. To understand this it is important to grasp the concept that once the capillary pressure starts to build-up in plastic concrete, the concrete itself is searching for ways to relieve or reduce the pressure. The concrete can relieve the pressure in several ways including: vertical settlement/bleeding, horizontal shrinkage and/or cracking. The results indicate that the concrete firsts tends to relieve the capillary pressure by increasing only the vertical settlement even though the capillary pressure has a vertical and horizontal component as shown in Figure 2.7. This additional vertical settlement causes additional bleed water to rise to the concrete surface as discussed in Section 4.2.2, which increases the radii of the water menisci between the solid particles and therefore partly relieves the capillary pressure build-up.

At a certain stage the capillary pressure build-up can no longer be sufficiently relieved or controlled by vertical settlement. At this point the concrete starts to shrink horizontally to relieve the capillary pressure build-up. This point can be identified in the capillary pressure build-up curve by a slight kink more of less midway up the curve which corresponds to the start of the horizontal shrinkage. The kink indicates a slight relief in capillary pressure build-up which can only be explained by the start of the horizontal shrinkage which draws the particles closer together and thereby increases the radii of the menisci between particles and therefore reduces the capillary pressure. This kink is indicated with a small grey circle in both Figures 4.17 and 4.18. The results of Slowik et al. (2008) showed a similar kink although no reference was made to the start of the horizontal shrinkage.

Mixes C3 and C4 showed significant cracking at Climate E2 as shown in Figures 4.19 and 4.20 respectively. This was expected due the high potential for plastic shrinkage cracking due to the high evaporation rate of Climate E2 of more than 1 kg/m²/h. Due to the high evaporation, the capillary pressure started to build-up much earlier than at Climate N2 for both mixes. Once the capillary

pressure started at around 60 minutes, the settlement also increased significantly. The horizontal shrinkage also started much earlier, almost in unison with the capillary pressure and therefore also the additional settlement.

The early and rapid nature of the capillary pressure build-up resulted in a situation where the pressure is relieved or controlled almost simultaneously by both additional vertical settlement and horizontal shrinkage. This also meant no kink is present in the capillary pressure curve indicating the start of the horizontal shrinkage as for the tests with Mixes C3 and C4 at Climate N2. Furthermore, for both mixes the first crack appeared near the initial setting time, followed by the majority of crack widening between the initial and final setting times.

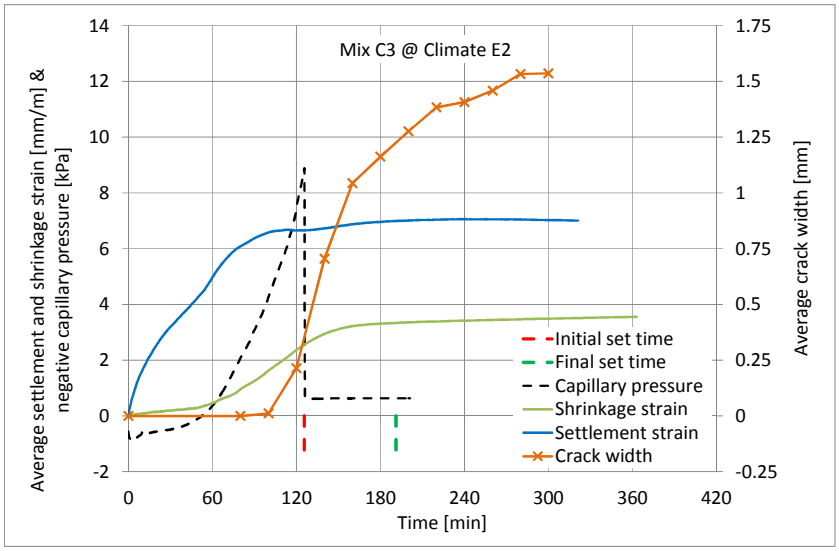

Figure 4.19. Results of Mix C3 at Climate E2.

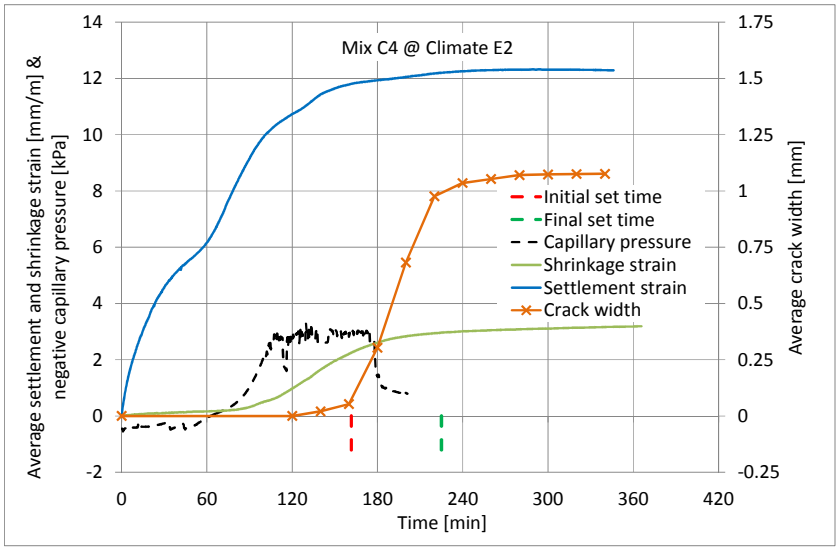

Figure 4.20. Results of Mix C4 at Climate E2.

4.4.3. Appearance of interior and surface cracks

During the final tests discussed in the previous section the cracks were also monitor from the side through Perspex side panels. Figure 4.21 shows the typical crack images that were captured from the side at around 90 minutes after the final setting time for Mixes C3 and C4 at both Climates N2 and E2. For Climate N2, as shown in Figure 4.21 a) and b), the observed crack near the surface of the concrete for both Mixes C3 and C4 was notably smaller than the actual interior crack below the concrete surface. The reason for this size discrepancy between the surface and interior crack is the high amount of bleed water on the concrete surface during tests at Climate N2.

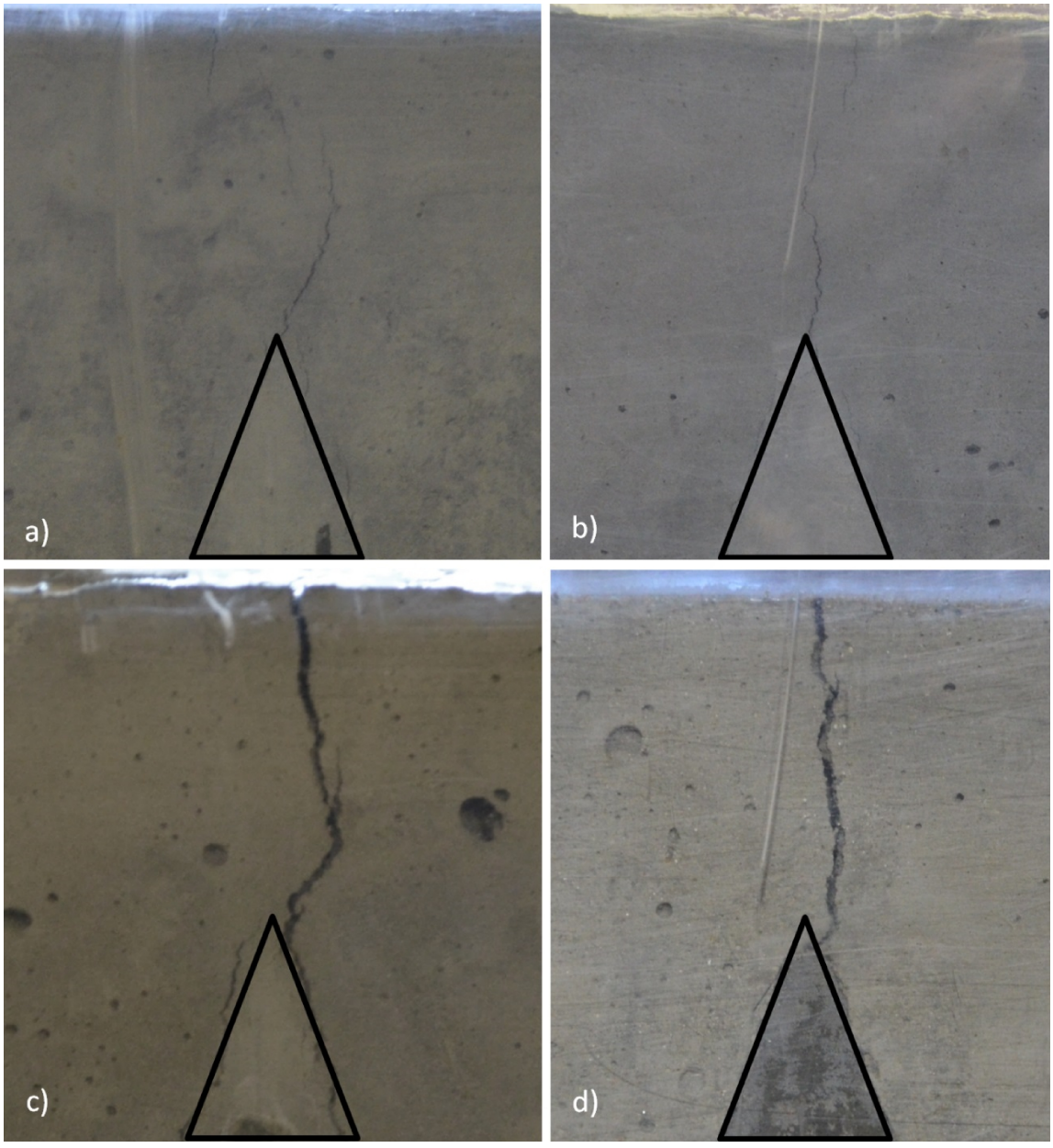

Figure 4.21. Images of cracking above the central triangular restraint captured from the side through a Perspex side panel at 90 minutes after the final setting time for: a) Mix C3 at Climate N2. b) Mix C4 at Climate N2. c) Mix C3 at Climate E2. d) Mix C3 at Climate E2.

Figure 4.22 shows an image of the concrete surface for Mix C3 at Climate N2 after 100 minutes from being placed. The figure shows that parts of the surface were covered with a clear film of bleed water, while other parts were covered by a thin crust layer that floated on the bleed water. This crust layer consisted of ultra-fine cement and dust particles that were kept in suspension by the surface tension of the water. As evaporation continued the film of bleed water was gradually removed, leaving the crust layer on the surface of the concrete. This crust layer often completely or partly obstructed the visibility of the crack at the surface. Furthermore, the bleed water also increased the water-to-cement ratio at the concrete surface as well as in any cracks near the surface. This higher water-to-cement ratio at the surface compared to the lower water-to-cement ratio for the interior concrete decreased the size of cracks at the surface due to a more dispersed formation of hydration products.

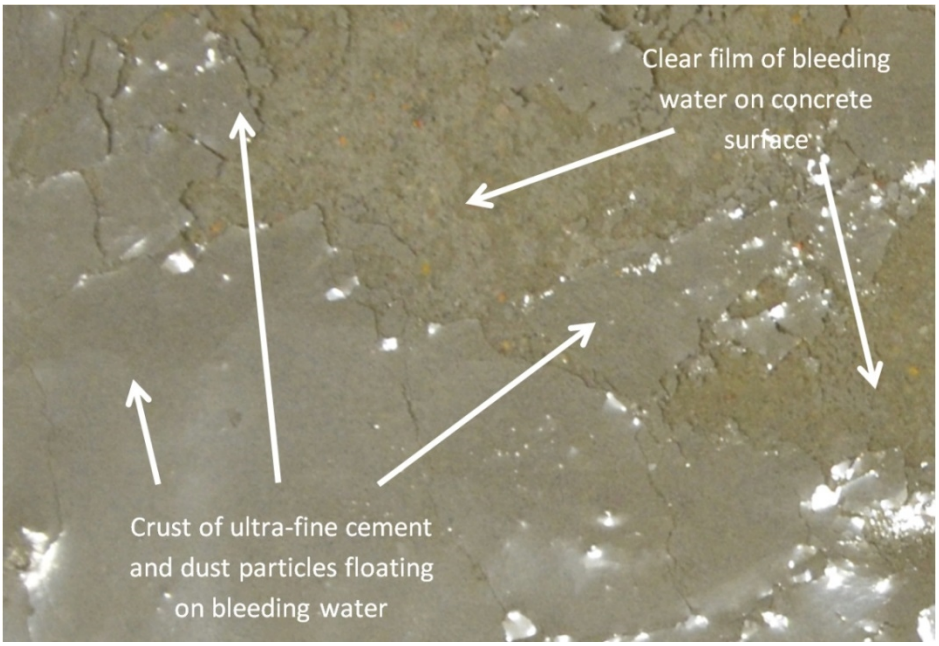

Figure 4.22. Plan view of the concrete surface covered partly by a clear film of bleed water and partly by a crust of ultra-fine cement and dust particles for Mix C3 at Climate N2 after 100 minutes from being placed.

Figure 4.21 c) and d) shows that this size discrepancy between the surface and interior crack was not significant for Mixes C3 and C4 at Climate E2. This is because the high rate of evaporation at Climate E2 resulted in the almost immediate removal of bleed water from the concrete surface. While in comparison, the bleed water for Mixes C3 and C4 at Climate N2 was ponded on the concrete surface and only gradually removed by evaporation. In conclusion, this ponded bleed water on the concrete surface at Climate N2 resulted in a size discrepancy between the interior and surface cracks during experiments, where the observed surface cracks were smaller than the actual interior crack below the concrete surface.

4.4.4. Influence of differential settlement

The results of the initial and final tests in Sections 4.4.1 and 4.4.2 on Mixes C1 to C4 at both extreme and normal climates using the shrinkage cracking mould coincide with the phenomological behaviour of plastic shrinkage cracking as described by Boshoff and Combrinck (2013) and discussed in Section 2.5.2. The shrinkage cracking mould, as shown in Figure 3.2, used for these test was also used by Boshoff and Combrinck (2013). Initially these moulds were believed and used to evaluate pure plastic shrinkage cracking of concrete without any influence of differential settlement. This was because the shape of the mould was developed by ASTM for the evaluation of the plastic shrinkage cracking of restrained fibre reinforced concrete as described in ASTM C1579 (2006). In this standard test method no reference is made to the influence of plastic settlement cracking.

In addition, it was incorrectly assumed that the gradual change in sectional height caused by the triangular shape of the restraining inserts results in near zero potential for differential settlement and therefore also plastic settlement cracking. An attempt was even made to verify this assumption by conducting a test on Mix C2 at Climate E2 where the centre triangle was removed and replaced with a thin plate as shown in Figure 4.23. The results of these tests were similar in size and behaviour as for the normal shrinkage cracking mould. This supported the incorrect assumption that the shrinkage cracking mould results in pure plastic shrinkage cracking, since it was believed that the plate insert gave no potential for plastic settlement cracking. This is indeed incorrect as large aggregates can easily be hindered by the rigid plate insert resulting in plastic settlement cracking.

Figure 4.23. Normal triangular insert and plate insert used in the centre of the shrinkage cracking mould.

After conducting the tests to observe the pure plastic settlement cracking behaviour as described in Section 4.3 a more fundamental understanding of these cracks was gained. This lead to the

questioning of the assumptions made earlier regarding the pure nature of plastic shrinkage cracks in the shrinkage cracking mould. The results and images given above were revisited and upon closer inspection signs of multiple cracking patterns that preceded the measured singular crack were found. The reason these cracks were not considered was because they were hardly visible and easily overlooked especially since the surface of the concrete was still highly plastic at that stage and often still covered with a thin layer of water. This means the cracks were also filled with water which greatly reduced its visibility.

Figures 4.24 and 4.25 show images of the cracking for one of the samples for Mix C3 at both Climates N2 and E2 respectively. Similar images can be shown for Mixes C1, C2 and C4. The figures show the growth or evolution of the cracks as time passes. The earliest image captured for both mixes show the presence of a multiple crack pattern. As mentioned, and as can be seen on the images, these multiple cracks are very fine and difficult to distinguish at such an early age due to the presence of bleed water. These multiple cracks are present before the measured crack (indicated by the white line) started to widen.

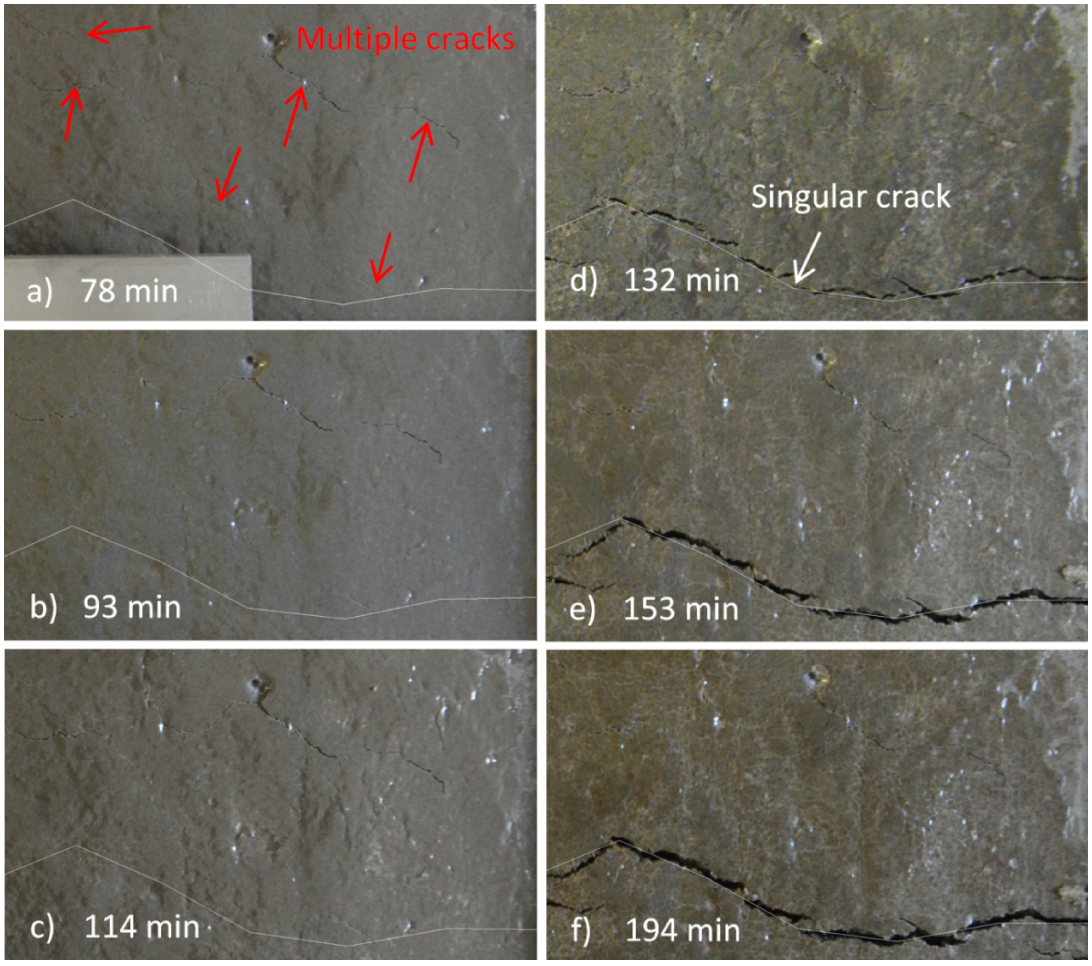

Figure 4.24. Crack evolution of Mix C3 at Climate E2 as a function of time.

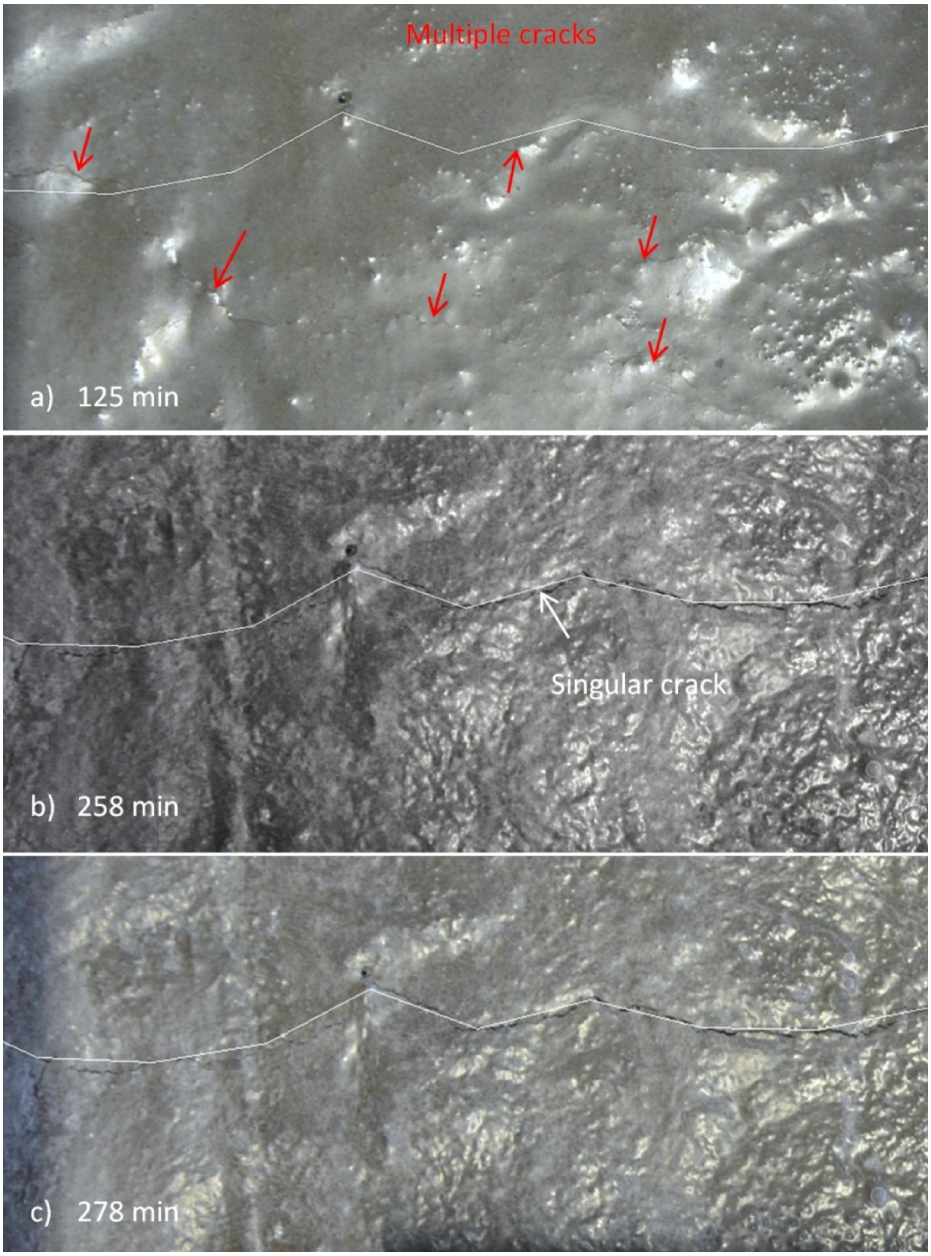

Figure 4.25. Crack evolution of Mix C4 at Climate N2 as a function of time.

Both Figures 4.24 and 4.25 shows that as time passed a singular, well defined crack started to widen, normally around the initial setting time. The location of this singular crack is indicated on all the images shown in Figures 4.24 and 4.25 by a white line, including the early images where the singular crack was yet to form. This singular crack is often linked to the location of one of the multiple cracks that were present long before this singular crack started to widen. During the measurements of the cracks in this study, only the singular and well defined crack pattern was measured as explained in Section 3.1.3. This means that most of the fine and sometimes near invisible multiple cracks were not included in the crack measurements, except in situations where the location of a multiple crack coincides with the singular crack. Another interesting observation is that the multiple cracks often reduced in size once the singular crack formed as can be seen in Figures 4.24 and 4.25.

The observed multiple cracks are similar to the multiple cracks observed for pure plastic settlement cracking in Section 4.3. It can be concluded that these multiple cracks are indeed plastic settlement cracks that are formed due to differential settlement, while the singular crack that formed is due to plastic shrinkage. The location of the final crack pattern is also influenced by the plastic settlement cracks, which can include both the multiple tensile cracks at the surface as well as the interior shear cracks as observed in Section 4.3. This is confirmed by the Figure 4.21 a) and c) which shows the crack for Mix C3 at both Climates N2 and E2 as captured from the side through the Perspex side panels. The figures show the angled shear crack at the tip of the triangle which links up with the surface tensile cracks. This means that if present plastic settlement cracks not only precedes the plastic shrinkage cracks but also influences where the plastic shrinkage crack forms. This is discussed further in Section 4.5.5.

The shrinkage cracking mould as used in this study with the triangle centre restraint therefore does not result in pure plastic shrinkage cracking, but rather in plastic shrinkage cracking induced by differential settlement. This also means that the phenomological behaviour of plastic shrinkage cracking as proposed by Boshoff and Combrinck (2013) should be described as plastic shrinkage cracking induced by differential settlement. However, it should be added that the degree of differential settlement due to centre triangle restraint used is relatively low as shown next in Section 4.4.5. This means that although plastic settlement cracks are present and help to induce and determine the crack location, the majority of the crack widening is still caused by plastic shrinkage cracking. Finally, a possible reason for the start of the plastic shrinkage cracks around the initial setting time is given in Section 5.2.4.

4.4.5. Tests with modified shrinkage cracking moulds

The previous section revealed that the shrinkage cracking mould does not result in pure plastic shrinkage cracking, but rather in plastic shrinkage cracking induced by differential settlement. In an attempt to understand pure plastic shrinkage cracking behaviour, tests were conducted with several modified shrinkage cracking moulds. The main modification was to remove the triangle restraint in the centre of the mould since this triangle results in gradual differential settlement by hindering the settlement of the concrete above it. The four modified moulds used for the tests are shown in Figure 4.26. The first mould contained no centre triangle, while the other three moulds contained triangles that were inserted on opposite inner sides of the mould. These inserts are as high as the mould and as a result do not hinder the settlement of the concrete causing differential settlement. These moulds therefore do not include plastic settlement cracking in the centre of the mould. The size of the side triangular inserts increases from 25, 50 to 64 mm as shown in Figure 4.25. The 64 mm

side triangle shrinkage mould has the same cross sectional crack area as the normal shrinkage cracking mould.

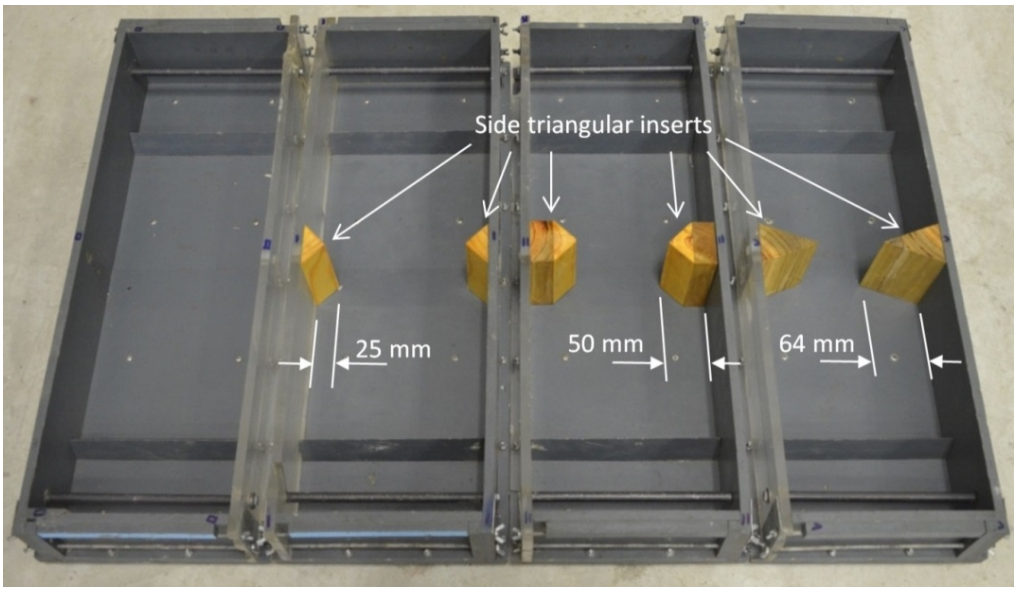

Figure 4.26. Layouts of modified shrinkage cracking moulds.

Figure 4.27 shows the crack width as well as the end and total deformation for Mix C3 at Climate E2 as tested in the normal and modified shrinkage cracking moulds. The crack width was determined for each mould as the total surface crack area divided by the width of the mould at the crack location as discussed in Section 3.1.3. This allows the comparison of cracks with different lengths due to the different layouts of the modified shrinkage cracking moulds. The end deformation was measured as the opening between the mould at opposing ends of the mould and the concrete itself. This opening was calculated as the sum of the average of six measurements at each end of the mould.

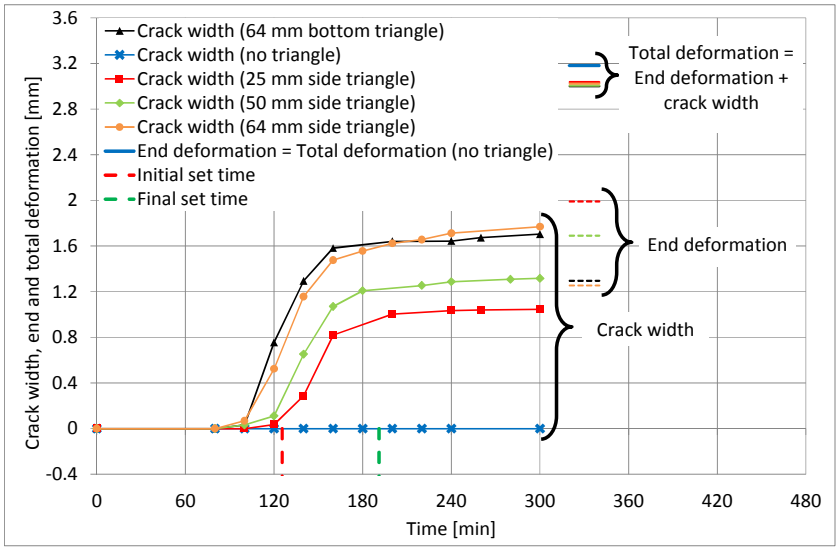

Figure 4.27. Crack width as well as end and total deformation for Mix C3 at Climate E2 as tested in the normal and modified shrinkage cracking moulds.

The total deformation can then be calculated as the sum of the end deformation and the crack width. Only one such test was conducted for each mould as the objective was only to observed pure plastic shrinkage cracking and compare this to the settlement induced plastic shrinkage cracking in the normal shrinkage cracking mould. The results show that the amount of end deformation and crack width as measured at the surface differ significantly between the different moulds, although the total deformation for all the moulds is similar. Furthermore, the majority of the cracking for all the moulds still occurred between the initial and final setting times of the concrete.

Figure 4.28 a) and b) shows the typical observed end deformation and cracking pattern for the normal shrinkage cracking mould as well as the modified shrinkage cracking mould. Figure 4.29 a) to d) shows images of the actual cracks and end deformation that were observed at the end restraints for the normal shrinkage cracking mould as well as the modified shrinkage cracking moulds. The restraints at both ends of the mould are a combination of a small triangular insert at the bottom of the mould as well as a steel bar in the top corner of the mould.

From these results two different cracking behaviours can be identified. The first is the behaviour of the normal shrinkage cracking mould as shown in Figure 4.28 a). The figure shows that for the normal shrinkage cracking mould the concrete is essentially split in two halves by the centre triangle, where each halve is restrained at the end of the mould by a combination of a smaller triangular insert and a steel bar. Once the concrete starts to shrink it results in cracking at the centre triangle which is a clearly defined weak spot due to the reduced cross sectional area of the concrete as well as possible plastic settlement cracks as discussed in Section 4.4.4. Figure 4.27 also shows that the majority of the total deformation for this mould is due to the cracking at the centre triangle, although there is still a reasonable amount of end deformation and even slight horizontal cracks at the steel bar as shown in Figure 4.29 a). However, the majority of the deformation is isolated at the central crack.

The second cracking behaviour is that of the modified shrinkage cracking mould with no centre triangular restraint as shown in Figures 4.28 b) and 4.29 b). The figures show that the majority of the cracking and deformation occurs at the ends of the mould, since there is no clear weak spot in the centre of the mould due to the absence of the centre triangular insert. Once shrinkage starts, the central portion of the concrete acts as one and shrinks towards the middle of the mould as shown in Figure 4.28 b). This causes vertical cracks to form at the smaller triangular inserts and steel bars as well as horizontal cracks at the steel bars at the ends of the mould as shown in Figures 4.28 b) and 4.29 b).

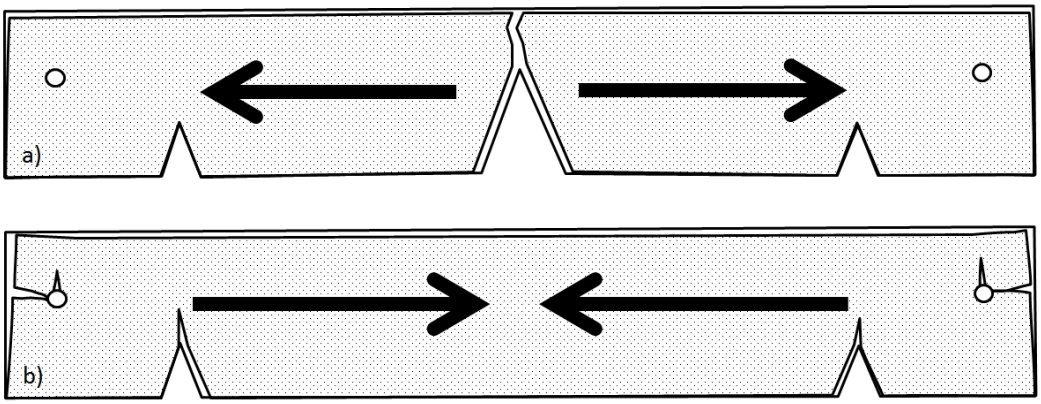

Figure 4.28. Illustration of cracking and shrinkage observed for: a) Normal shrinkage cracking mould with 64 mm bottom triangular insert at centre. b) Modified shrinkage cracking mould with no triangular insert at centre.

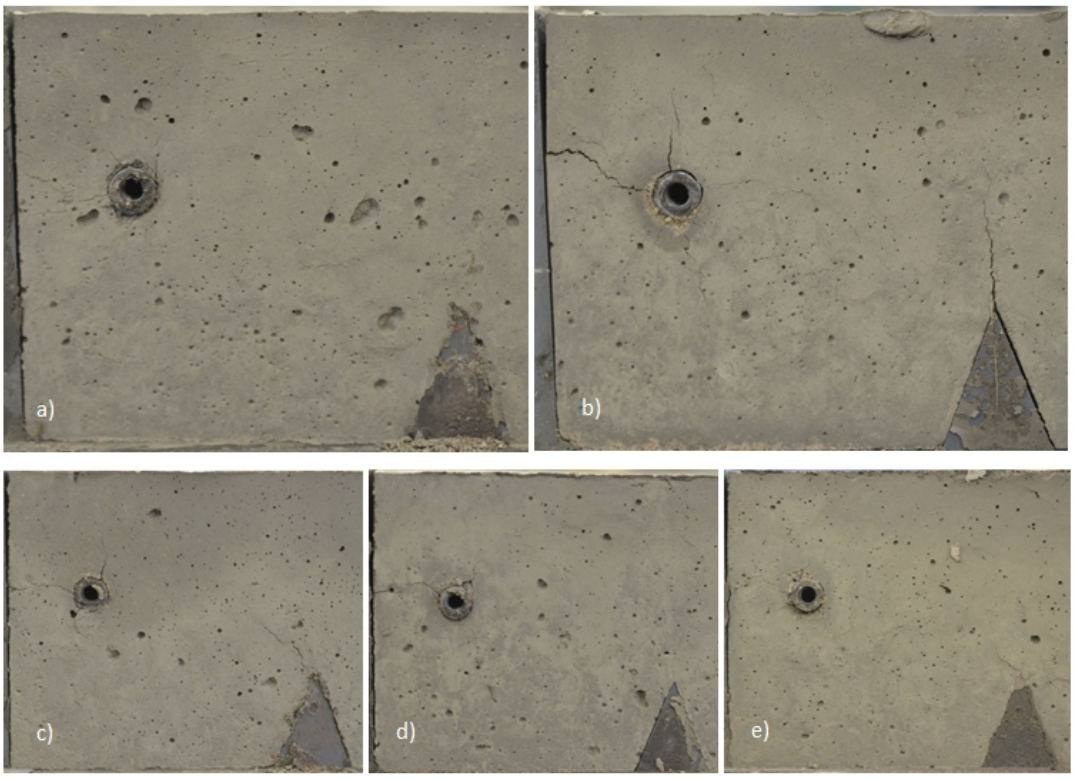

Figure 4.29. Images of the deformation and cracks at the end restraints as captured from the side with the Perspex side panels removed at 5 hours after casting for Mix C3 at Climate E2 for: a) Normal shrinkage cracking mould with 64 mm bottom triangular insert at centre. b) Modified shrinkage cracking mould with no triangular inserts at centre. c) Modified shrinkage cracking mould with 25mm side triangular inserts at centre. d) Modified shrinkage cracking mould with 50 mm side triangular inserts at centre. e) Modified shrinkage cracking mould with 64 mm side triangular inserts at centre.

The location of these cracks coincide with the locations of possible plastic settlement cracks at discussed in Section 4.3, although the majority of the crack widening is still due to plastic shrinkage cracking. Furthermore, these cracks are not visible at the surface of the concrete, which indicates that both plastic settlement cracking and plastic shrinkage cracks can be present beneath the surface

of the concrete. Figure 4.27 also shows that for this mould the total deformation is equal to the end deformation since no surface cracks occurred. In fact, the end deformation of this mould was more than double that of the other moulds.

These two moulds represent two extremes in terms of cracking behaviour, where for the normal shrinkage cracking mould the majority of the cracking and deformation are located at the centre of the mould and for the modified shrinkage cracking mould with no centre triangle the majority of the cracking and deformation are located at the ends of the mould. The other tests conducted with the modified shrinkage cracking mould containing the side triangular inserts fell between these two extremes. The results of Figure 4.29 c) to e) show that the cracking and deformation at the ends of the modified shrinkage cracking moulds containing the side triangular inserts were less severe than for the mould with no triangle as shown in Figure 4.29 a).

Furthermore, from Figure 4.29 c) to e) it can be seen that the cracking and end deformation becomes less severe the larger the side triangular inserts in the centre. The results of Figure 4.27 also show that the larger the side triangular inserts, the more pronounced the cracking in the centre and the less the end deformation. Figure 4.27 also shows that the smaller the side triangle, the later the start of the cracking at the centre. The cracks in the middle of these modified shrinkage cracking moulds containing the side triangular inserts are pure plastic shrinkage cracks with no influence of differential settlement.

The results indicate that for pure plastic shrinkage cracking a clear weak spot is required for crack formation and if this weak spot is not well defined the deformation and/or even cracking due to plastic shrinkage occurs at other locations, such as the end deformation of the concrete away from mould sides as well as internal cracks at the end restraints.

Furthermore, the behaviour and results of the modified shrinkage cracking mould containing the 64 mm side triangular inserts is similar to the normal shrinkage cracking mould as shown by Figure 4.29 a) and e) as well as Figure 4.27. These moulds have the same cross sectional crack area at the centre, although the normal shrinkage cracking mould can include plastic settlement cracking while the modified shrinkage cracking mould does not. This shows that the pure plastic shrinkage cracking in the modified mould behaves similar to the settlement induced plastic settlement cracking in the normal shrinkage cracking mould. This indicates that the potential or degree of differential settlement caused by the central triangular insert in the normal shrinkage cracking mould is low.

4.4.6. Conclusions

The results and discussions revealed several important insights into the behaviour of both plastic shrinkage cracking induced by differential settlement as well as pure plastic shrinkage cracking. These insights can be summarised as follows:

- During the capillary pressure build-up process in plastic concrete, the concrete is searching for ways to relieve or reduce the pressure. The concrete can relieve the pressure in several ways including: vertical settlement/bleeding, horizontal shrinkage and cracking. The concrete firsts tends to relieve the capillary pressure by increasing only the vertical settlement which relieves the capillary pressure by forcing additional bleed water to rise to the concrete surface. Once the capillary pressure can no longer be relieved or controlled by the additional vertical settlement, the concrete starts to shrink horizontally to relieve the capillary pressure build-up. This point can be identified in the capillary pressure build-up curve by a slight kink midway up the curve which corresponds to the start of the horizontal shrinkage. Only after both additional settlement and horizontal shrinkage has started, does plastic shrinkage cracking occur as a form of pressure relief. This can be pure plastic shrinkage cracking or plastic shrinkage cracking induced by differential settlement, where the severity of the differential settlement is low.
- The shrinkage cracking mould as used in this study with the centre triangular restraint does not result in pure plastic shrinkage cracking, but rather in plastic shrinkage cracking induced by differential settlement. This was confirmed by the presence of fine multiple cracks on the concrete surface before any significant capillary pressure build-up or horizontal shrinkage. These multiple cracks are similar to the multiple cracks observed for pure plastic settlement cracking. However, after the formation of the multiple cracks the final crack that forms is singular and well defined. It can be concluded that these fine multiple cracks are indeed plastic settlement cracks that precede the plastic shrinkage cracking which in turn can be identified by a much larger singular and well-defined crack pattern. This also means that although plastic settlement cracks are present and influence the crack location, the majority of the crack widening is still caused by plastic shrinkage cracking.
- Pure plastic shrinkage cracking revealed similar behaviour to settlement induced plastic shrinkage cracking where the degree of differential settlement is low as is the case for the normal shrinkage cracking mould. Furthermore, pure plastic shrinkage cracks require a clearly defined weak spot where they can form. These weak spots can be a reduced cross section due to the layout of the concrete mould as well as plastic settlement cracks. The more distinct the weak spot for cracking, the sooner cracking starts as well as the more of the total deformation results

in crack widening at this location. If this weak spot is not well defined, deformation occurs at other locations which include deformation away from mould sides or even cracking at restraints such as reinforcing steel or changes in the height of the element. These cracks are often internal and not visible at the surface, indicating that plastic shrinkage cracking, as for plastic settlement cracking, may be present beneath the surface of the concrete. These cracks form weak spots for further crack widening due to later shrinkage such as drying shrinkage.

- The shrinkage cracking mould used in this study is based on the layout proposed by ASTM C1579 (2006). This mould is not appropriate for testing where the influence of plastic settlement cracking is not wanted. This is since even the minor plastic settlement cracking, as for this mould, plays an important role in defining weak spots where plastic shrinkage cracks can form as discussed further in Section 4.5.5. Furthermore, the cracking behaviour with a high degree of differential settlement can differ significantly from the cracking behaviour with a low degree of differential settlement as discussed in Section 4.5.

4.5. Plastic settlement and shrinkage cracking combined

The objective of these tests was to observe and understand the cracking behaviour if both plastic settlement and plastic shrinkage cracking occur. This was achieved by conducting several tests where the potential for both cracking types was altered using various combinations of low and high severities for both cracking types. The results of these tests are discussed in the following sections.

4.5.1. Tests with low settlement and shrinkage cracking potential

To observe the cracking behaviour in conditions with a low potential for both plastic settlement and plastic shrinkage cracking, tests were conducted with Mixes C1 and C2 at Climate N1 in the shrinkage cracking moulds where the centre triangular restraint was replaced with a 10 mm steel bar at a cover depth of 40 mm. The 40 mm cover depth provided a relatively low potential for plastic settlement cracking compared to for example a 20 mm cover depth. This is confirmed by the results shown in Figure 4.10 of pure plastic settlement cracking as conducted with the steel bar settlement cracking mould with varying cover depths. Furthermore, the low evaporation rate of Climate N1 provided the low potential for plastic shrinkage cracking.

Figures 4.30 and 4.31 show the results of Mixes C1 and C2 respectively. The results of both mixes are similar to the results achieved for the normal shrinkage cracking mould as discussed in Section 4.4.1. The only difference was the time the crack was observed for Mix C1. For the normal shrinkage cracking mould the crack was only visible after the final setting time as shown in Figure 4.13, while

for the shrinkage cracking mould containing the steel bar at 40 mm cover depth the crack was visible after only 60 minutes as shown in Figure 4.30. For both mould types the crack was small and did not significantly increase in size after first observation. The origin of both cracks is believed to be plastic settlement cracks due to differential settlement caused by the centre restraints. This is confirmed by the lack of capillary pressure build-up and therefore plastic shrinkage cracking for these tests.

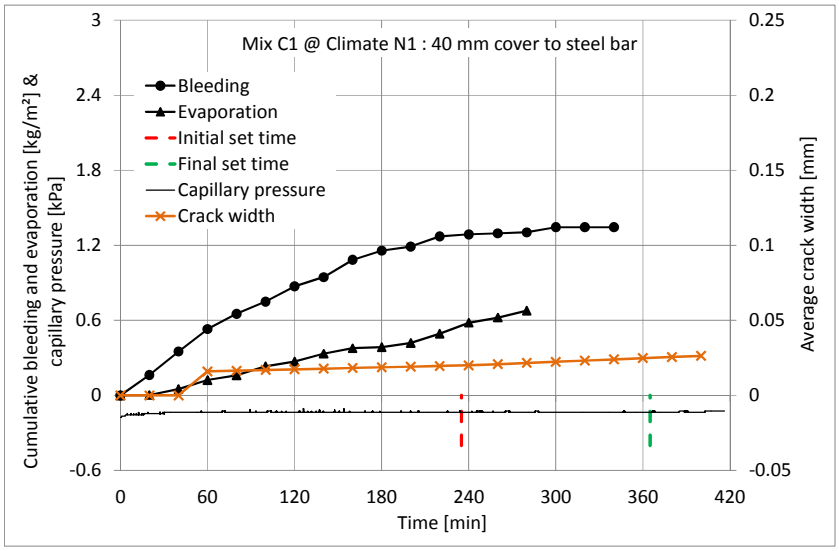

Figure 4.30. Results of Mix C1 at Climate N1 as tested in the shrinkage cracking mould with a steel bar restraint at the centre of the mould with a 40 mm concrete cover.

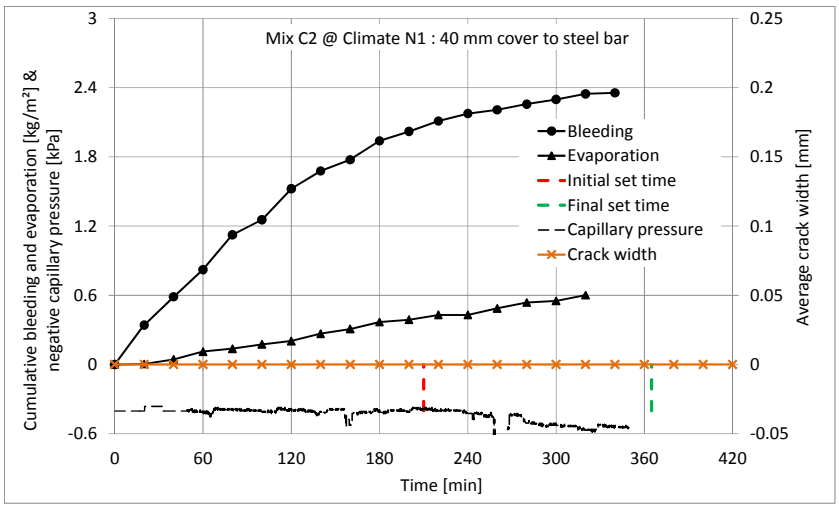

Figure 4.31. Results of Mix C2 at Climate N1 as tested in the shrinkage cracking mould with a steel bar restraint at the centre of the mould with a 40 mm concrete cover.

A possible reason why the crack was observed later for the normal shrinkage cracking mould is due to the more gradual nature of the differential settlement caused by the triangular centre restraint compared to the more abrupt nature of the differential settlement caused by the steel bar restraint. This resulted in a crack that was more visible for the mould containing the steel bar even at an age where the concrete surface was still covered with bleed water. While the crack in the normal

shrinkage cracking mould only became visible much later once most of the bleed water was removed.

4.5.2. Tests with low settlement and high shrinkage cracking potential

To observe the cracking behaviour in conditions with a low potential for plastic settlement cracking and a high potential for plastic shrinkage cracking, tests similar to the previous section were conducted on Mixes C1 and C2, except that Climate E1 was used to give a high potential for plastic shrinkage cracking. Figures 4.32 and 4.33 show the results of Mixes C1 and C2 respectively.

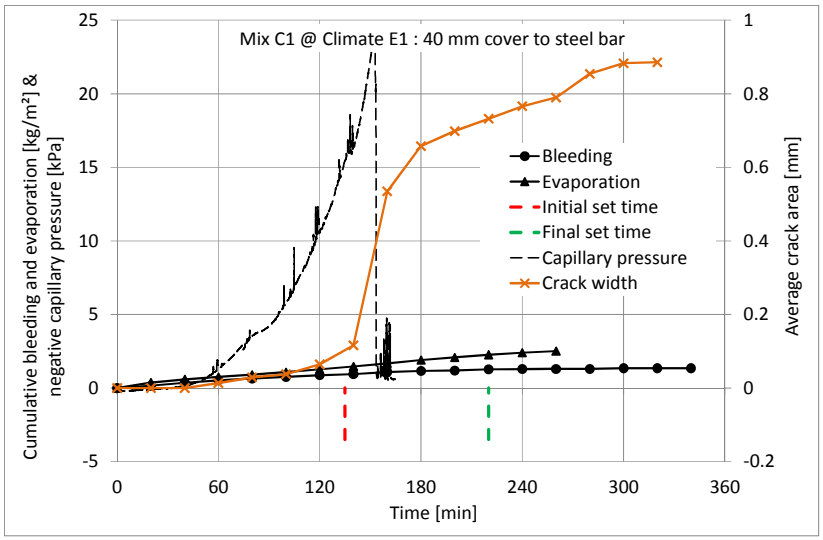

Figure 4.32. Results of Mix C1 at Climate E1 as tested in the shrinkage cracking mould with a steel bar restraint at the centre of the mould with a 40 mm concrete cover.

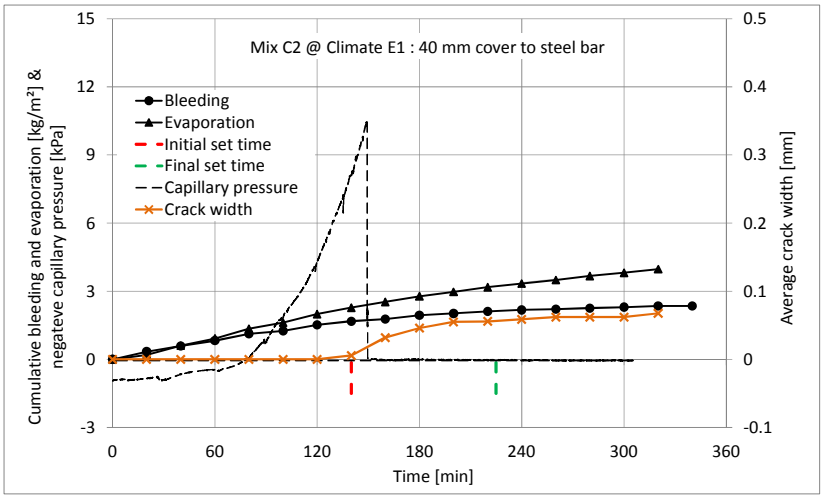

Figure 4.33. Results of Mix C2 at Climate E1 as tested in the shrinkage cracking mould with a steel bar restraint at the centre of the mould with a 40 mm concrete cover.

The results are similar to the results of the normal shrinkage cracking mould at Climate E1 as shown and discussed in Section 4.4.1, except that the cracks are significantly larger for the normal shrinkage cracking mould compared to the shrinkage cracking mould containing the steel bar with a concrete

cover of 40 mm. The reason for this is due to be the smaller cross sectional area of concrete that needed to crack for the normal shrinkage cracking mould compared to the mould containing the steel bar.

4.5.3. Tests with high settlement and low shrinkage cracking potential

Figures 4.34 and 4.35 show the results of Mix C1 and C2 at Climates N1 as tested in the shrinkage cracking mould where the triangular centre restraint was replaced by a 10 mm steel bar with a cover depth of 20 mm. This combines a high potential for plastic settlement cracking due to the 20 mm cover to the steel bar with a low potential for plastic shrinkage cracking due to the low evaporation rate of Climate N1.

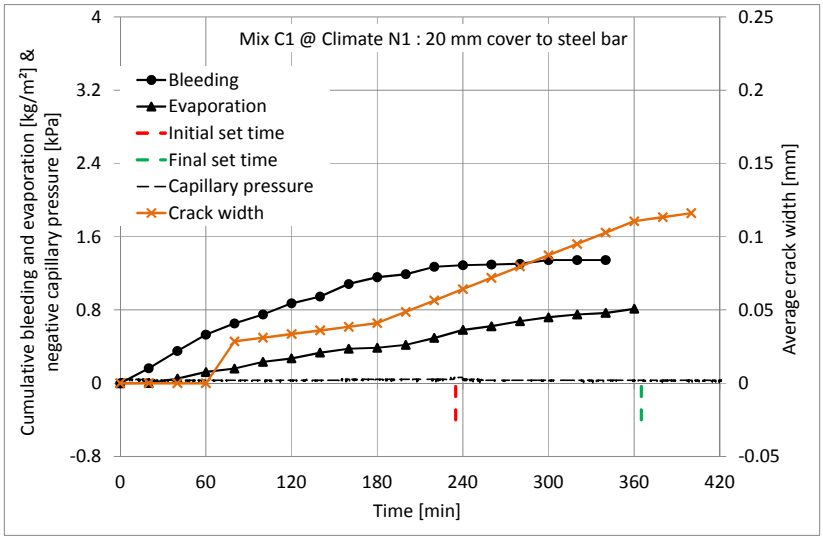

Figure 4.34. Results of Mix C1 at Climate N1 as tested in the shrinkage cracking mould with a steel bar restraint at the centre of the mould with a 20 mm concrete cover.

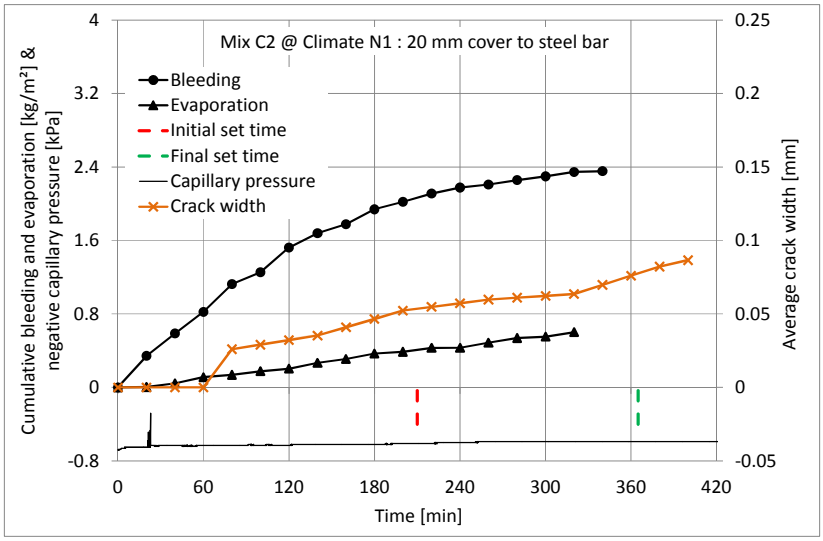

Figure 4.35. Results of Mix C2 at Climate N1 as tested in the shrinkage cracking mould with a steel bar restraint at the centre of the mould with a 20 mm concrete cover.

Figure 4.36 also shows images of part of the observed surface cracking as a function of time for both mixes. The results of Figures 4.34 to 4.36 show that for both mixes cracks were first observed 80 minutes after the concrete has been cast. This is more than 2 hours before the initial setting time, indicating plastic settlement cracking. This is also confirmed by the thin layer of bleed water on the surface of the concrete as well as no capillary pressure build-up. In addition, the image of the surface crack at 80 minutes in Figure 4.36 for both mixes show multiple cracks which is also an indication of plastic settlement cracking as discussed in Section 4.3.

Figures 4.34 and 4.35 also indicate that the crack continued to widen as time passed. This crack widening cannot be due to plastic shrinkage cracking due to the lack of capillary pressure build-up. It is believed that the crack only appears to widen as time passes due to the removal of bleed water, which increases the visibility of the crack. The bleed water can be removed by reabsorption into the concrete as well as evaporation. This means that the majority of the cracking occurred due to plastic settlement cracking only around 80 minutes after the concrete has been cast as can be seen in Figure 4.36. The figure also shows that several of the multiple cracks, that were present after 80 minutes, are not visible anymore at 380 minutes. This is believed to be due to the closing and reduced visibility of the cracks as hydration products are formed in the fine crack openings.

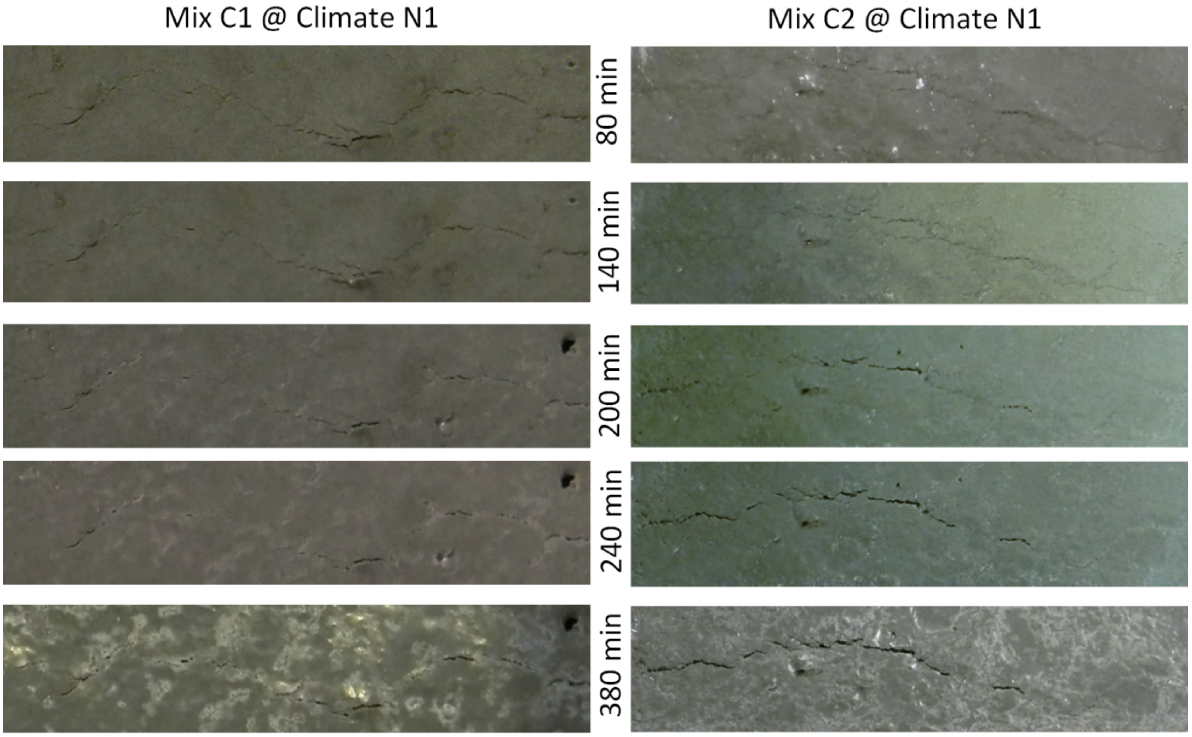

Figure 4.36. Images of part of the observed surface crack as a function of time for Mixes C1 and C2 at Climate N1 as tested in the shrinkage cracking mould with a steel bar restraint at the centre of the mould with a 20 mm concrete cover.

4.5.4. Tests with high settlement and shrinkage cracking potential

The cracking behaviour when a high potential for plastic settlement and plastic shrinkage cracking are combined was observed by conducting tests similar to the tests in the previous section, except that Climate E1 was used instead of Climate N1 to give a high potential for plastic shrinkage cracking. In addition, tests with the L-box settlement cracking mould on both Mixes C1 and C2 at Climate E1 were also conducted. The results of the shrinkage cracking moulds containing the centre steel bar restraint with 20 mm cover depth are shown in Figures 4.37 and 4.38 for Mixes C1 and C2 respectively, while Figure 4.39 shows images of part of the observed surface cracking during these tests as a function of time.

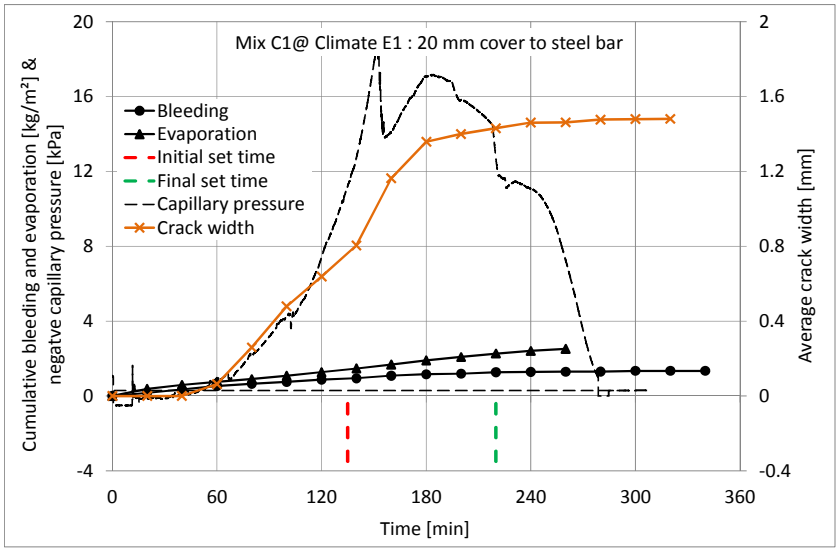

Figure 4.37. Results of Mix C1 at Climate E1 as tested in the shrinkage cracking mould with a steel bar restraint at the centre of the mould with a 20 mm concrete cover.

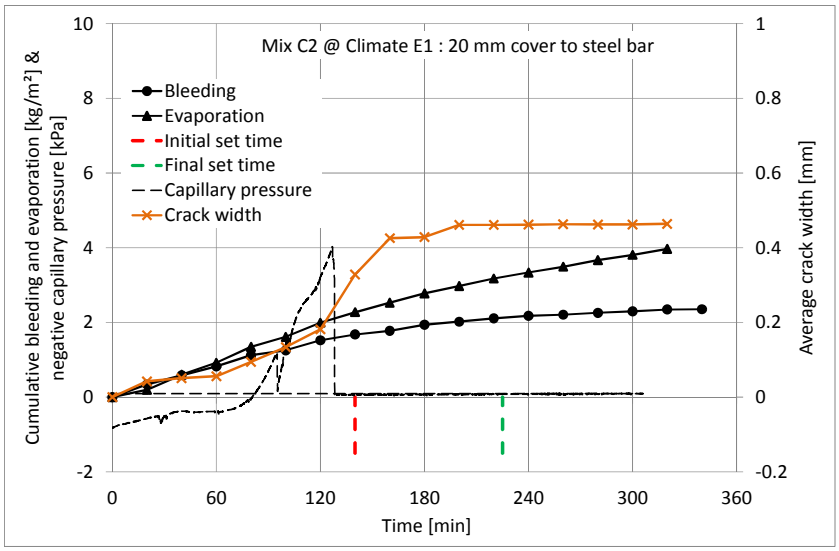

Figure 4.38. Results of Mix C2 at Climate E1 as tested in the shrinkage cracking mould with a steel bar restraint at the centre of the mould with a 20 mm concrete cover.

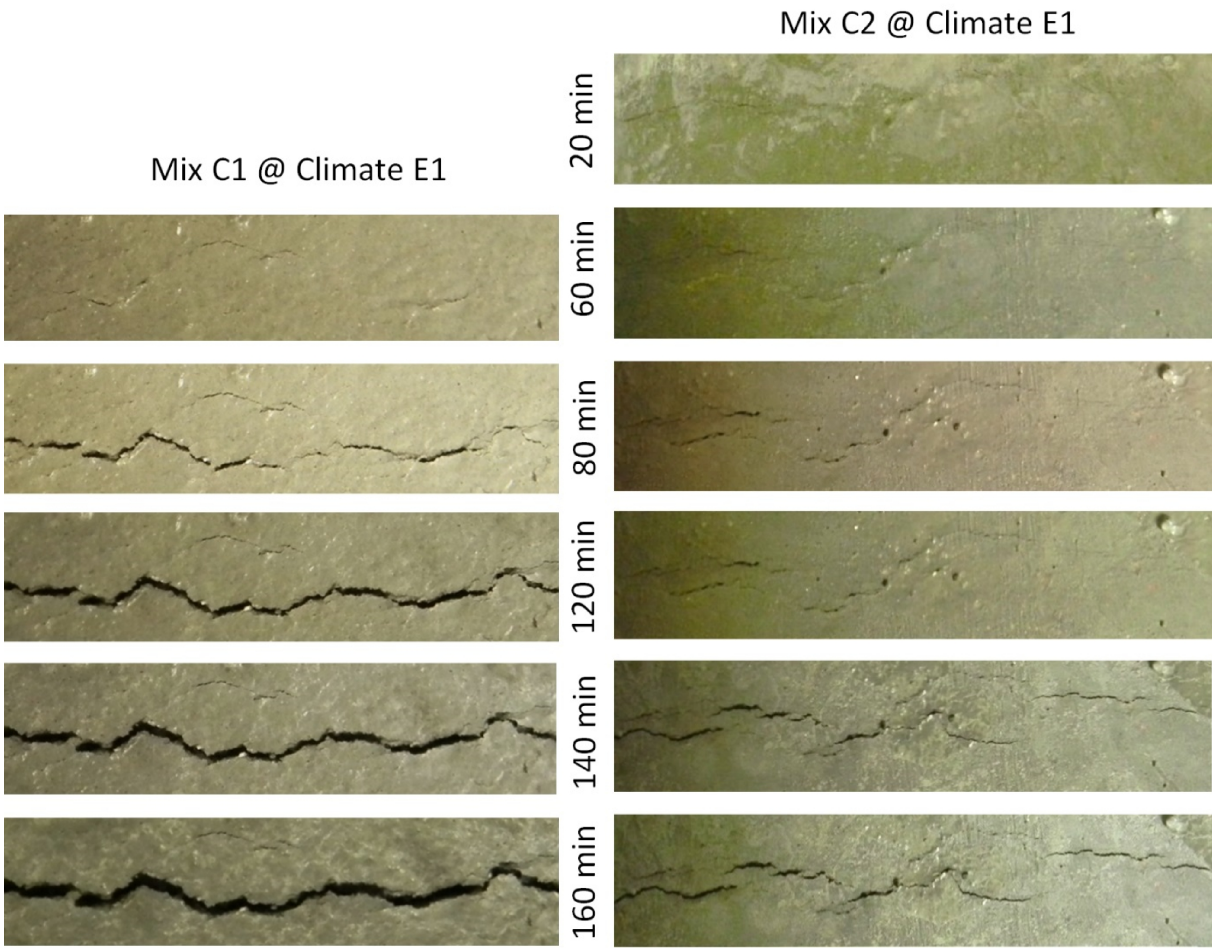

Figure 4.39. Images of part of the observed surface crack as a function of time for Mixes C1 and C2 at Climate E1 as tested in the shrinkage cracking mould with a steel bar restraint at the centre of the mould with a 20 mm concrete cover.

The results indicate that the initial crack formed 60 and 20 minutes after the concrete has been cast for Mixes C1 and C2 respectively. This suggests plastic settlement cracking, as confirmed by the lack of capillary pressure build-up as well as the multiple cracks visible at 60 minutes for both mixes as shown in Figure 4.39. After 60 minutes the capillary pressure started building up due to the high evaporation rate resulting in significant crack widening that stabilised around 40 and 20 minutes after the initial setting time for Mixes C1 and C2 respectively.

This crack widening after 60 minutes can be due to both additional vertical settlement and plastic shrinkage as shown and discussed in Section 4.4.2. This means that the crack widening can be due to both plastic settlement and plastic shrinkage cracking combined, although the majority of the crack widening is still believed to be due to plastic shrinkage since the settlement, including the additional settlement due to capillary pressure, normally ceases before the initial setting time as can be seen in Figures 4.19 and 4.20. The combination of an high potential for plastic settlement and plastic shrinkage cracking resulted in a situation where major cracking has already occurred by the initial

setting time where plastic shrinkage cracking is normally only expected to start. This means that the interaction between these two crack types can lead to significant cracking long before expected.

Figures 4.40 and 4.41 show the results of the Mixes C1 and C2 at Climate E1 as conducted in the L-box settlement cracking mould. The results show an extremely rapid crack widening just after the first crack was observed long before the initial setting time. The crack widening represents more than half of the total crack widening as measured two hours after the final setting times of both mixes. As for the shrinkage cracking mould containing the steel bar with 20 concrete cover the crack onset is due plastic settlement cracking. This is confirmed by the high degree of differential settlement as well as the early occurrence of the crack. The main difference between the mentioned moulds is the amount of capillary pressure that has build-up at the time of the crack onset.

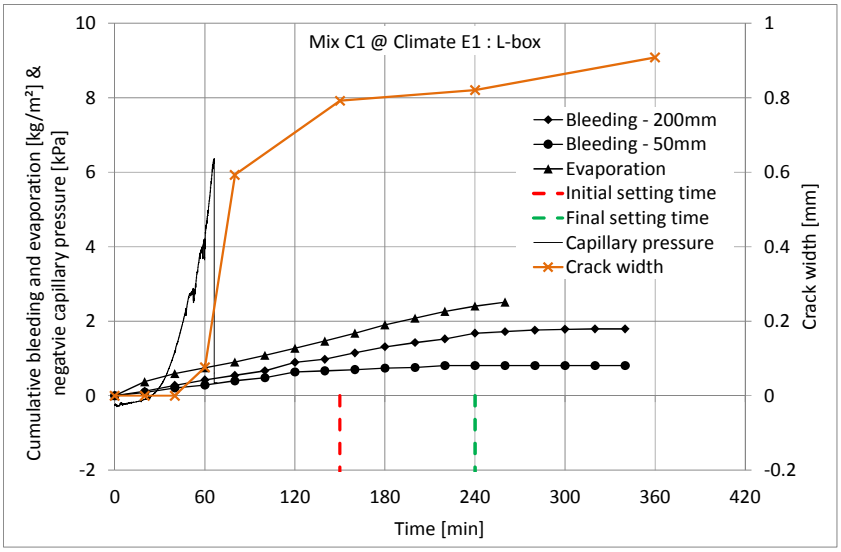

Figure 4.40. Results of Mix C1 at Climate E1 as tested in the L-box settlement cracking mould.

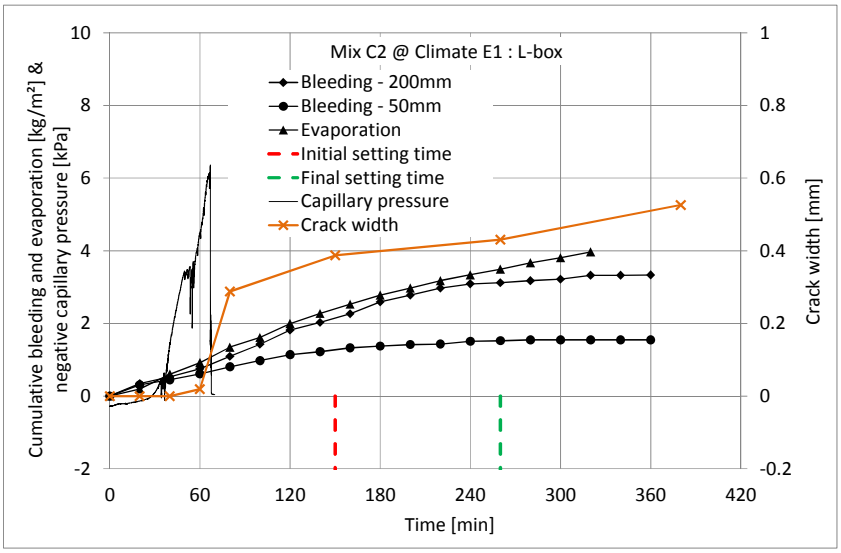

Figure 4.41. Results of Mix C2 at Climate E1 as tested in the L-box settlement cracking mould.

For the shrinkage cracking mould containing the steel bar with 20 mm concrete cover no significant capillary pressure is present at the time of crack onset which causes the crack to widen gradually as the pressure build-up increases as shown in Figures 4.37 and 4..38. In comparison, a significant amount of capillary pressure has already developed at the time of crack onset for the L-box settlement cracking mould. This means the concrete body is already under stress once the first crack or weak spot is formed due to differential settlement. This resulted in a global stress relief over the entire concrete body which localises all the deformation at the crack position. In addition to the global stress relief, the magnitude and the rate of the crack widening can also be explained by the plastic nature of the concrete which allowed crack widening due to both plastic settlement and plastic shrinkage cracking. This also occurred for the shrinkage cracking mould containing the steel bar at 20 mm cover depth in the centre. This type of sudden crack widening only occurs in situations where an extremely high potential for both plastic settlement and plastic shrinkage cracking are combined and is referred to as crack jump behaviour in this study.

In addition, it should also be mentioned that the potential for plastic shrinkage cracking in the L-box settlement cracking mould is even higher than for the shrinkage cracking mould. This is because of the difference in depth between the 50 mm shallow section of the L-box mould compared to the 100 mm depth of the shrinkage cracking mould and as discussed in Section 2.4.2, the shallower the concrete, the lower the settlement and therefore also the bleeding. This is confirmed by Figure 4.42 which shows the significant reduction in bleeding from a 100 to 50 mm depth as measured for both Mixes C1 and C2 at Climate N1. It is this reduction in bleeding that resulted in the earlier and more rapid increase in capillary pressure which also increases the plastic shrinkage cracking potential of the L-box settlement cracking mould compared to the normal shrinkage cracking mould.

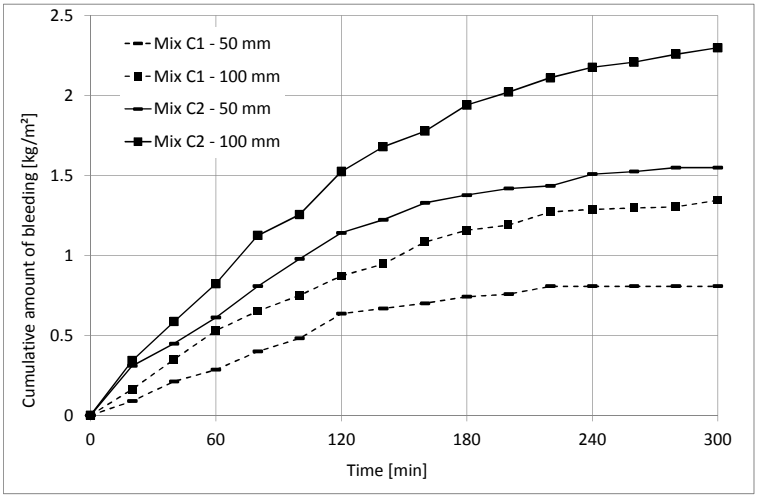

Figure 4.42. Cumulative amount of bleeding at 50 and 100 mm concrete depth for both Mixes C1 and C2 at Climate N1.

4.5.5. Influence of differential settlement on crack location and behaviour

Figure 4.43 a) and b) show illustrations of the typical observed end deformation and cracking for the shrinkage cracking mould containing a steel bar with a 20 and 40 mm concrete cover respectively. The actual cracking and deformation at the ends and centre of the mentioned moulds are shown in Figures 4.44 and 4.45 respectively.

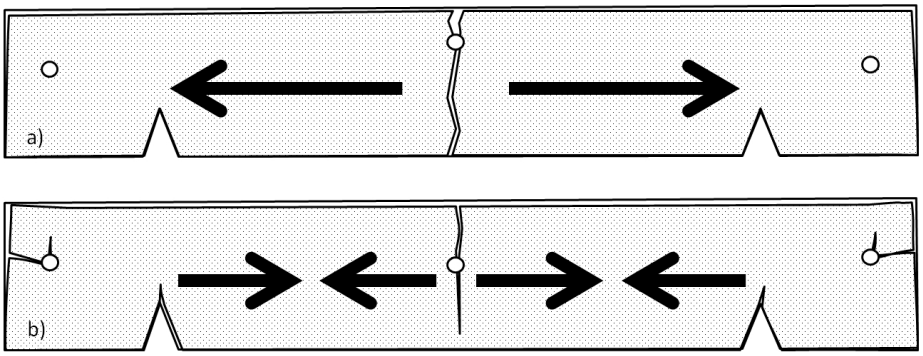

Figure 4.43. Illustration of cracking and shrinkage observed for: a) Shrinkage cracking mould with 10 mm steel bar at centre of mould with 20 mm concrete cover. b) Shrinkage cracking mould with 10 mm steel bar at centre of mould with 40 mm concrete cover.

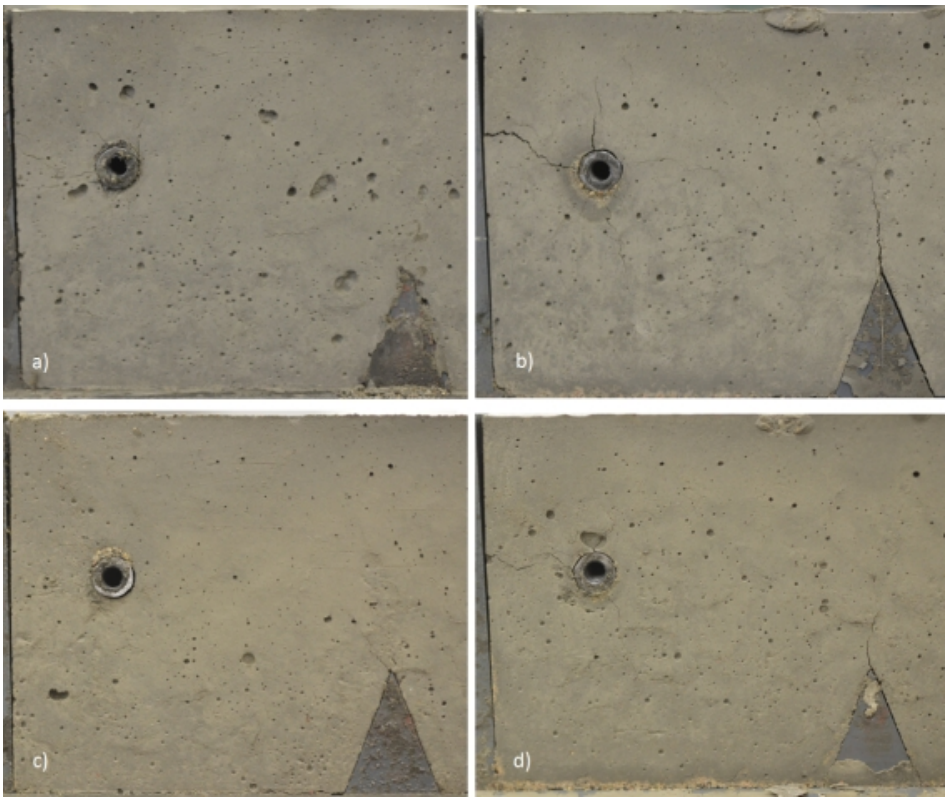

Figure 4.44. Images of the deformation and cracks at the left end restraints as captured from the side with the Perspex side panels removed at 5 hours after casting for Mix C3 at Climate E2 for: a) Shrinkage cracking mould with 64 mm bottom triangular insert at centre. b) Modified shrinkage cracking mould with no triangular inserts at centre. c) Modified shrinkage cracking mould with 10 mm steel bar with 20 mm concrete cover at centre. d) Modified shrinkage cracking mould with 10 mm steel bar with 40 mm concrete cover at centre.

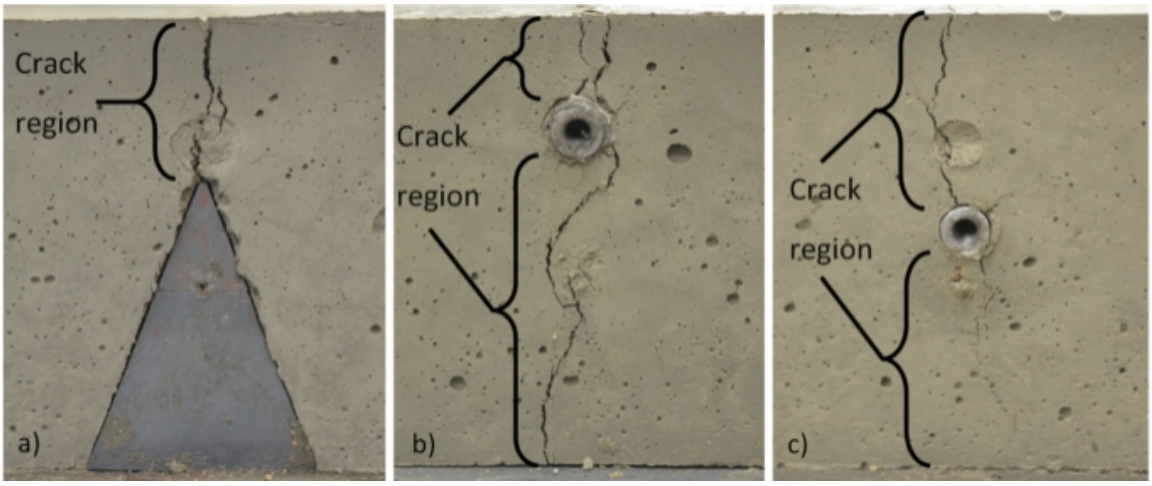

Figure 4.45. Images showing the centre cracks captured with the Perspex side panels removed at 5 hours after casting for Mix C1 at Climate E1 for: a) Shrinkage cracking mould with 64 mm bottom triangular insert at centre. b) Shrinkage cracking mould with 10 mm steel bar restraint at centre with 20 mm concrete cover. c) Shrinkage cracking mould with 10 mm steel bar restraint at centre with 40 mm concrete cover.

The results show that the cracking in the mould with a steel bar at 20 mm cover depth is significantly more severe than for the mould with a steel bar at 40 mm cover depth. The potential for plastic settlement cracking above a steel bar at 20 mm cover depth is much higher than at 40 mm cover depth. This caused an early and well defined weak spot (plastic settlement crack) to form above the steel bar with 20 mm cover depth, resulting in the majority of the plastic shrinkage cracking to occur at this weak spot.

For the mould containing the steel bar at 40 mm cover depth the plastic settlement cracking was not severe enough to result in a clear weak spot and hence cracking occurred at both the centre and the ends of the mould. The cracking at the centre was significantly smaller while the cracking and deformation at the ends were significantly higher than for the mould containing the steel bars at 20 mm cover depth as shown in Figures 4.44 and 4.45. These results confirms the effectiveness of plastic settlement cracking in forming a weak spot where plastic shrinkage cracking can form since the only difference between these mould was the cover depth to the steel bars and therefore the potential for plastic settlement cracking.

Section 4.4.5 identified two types of extreme cracking behaviours as illustrated in Figure 4.28. The first type occurs in the normal shrinkage cracking mould which has a clearly defend weak spot in the centre due to the triangular restraint, resulting in most of the cracking at the centre of the mould and not at the ends. The second occurs in the shrinkage cracking mould where the centre triangular restraint was removed, resulting in most of the cracking at the ends of the mould. The mould

containing the steel bar at 20 mm cover depth behaves similar to the first type of cracking behaviour where the majority of the cracking occurred at the centre of the mould. In comparison, the crack behaviour for the mould containing the steel bar at 40 mm cover depth is a combination of the two extreme types of cracking behaviours, where cracking occurred at both the centre and ends of the mould. This confirms the significant influence of plastic settlement cracking on the crack behaviour.

Another important aspect shown in Figure 4.45 a) to c) is the different sizes of the cross sectional crack area or crack region at the centre of the different moulds. The shrinkage cracking mould has the smallest crack region with only the concrete above the triangular insert requiring cracking for full penetration or separation of the concrete in the mould. The moulds containing steel bars have much larger crack regions where both the concrete above and below the steel bar requires cracking before the crack can reach full penetration. The larger the cross sectional crack area the stronger the concrete section. This is the reason why the measured cracking for the moulds containing steel bars are less severe than for the normal shrinkage cracking mould containing a triangular insert.

4.5.6. Conclusions

Section 4.5 reports on the cracking behaviour of plastic concrete where both plastic settlement and plastic shrinkage cracking are present at varying potentials. Six different types of cracking behaviours were identified, where two of these behaviours were also observed in Sections 4.3 and 4.4 as pure plastic settlement and pure plastic shrinkage cracking. The different behaviours are summarised in Figure 4.46 which shows the cracking behaviour that can be expected if plastic settlement and plastic shrinkage cracking are combined at potentials from low to high. It should be noted that this figure only illustrates the different cracking behaviour that can be expected, while the definition and assignment of more precise values and ranges to the figure requires further investigation and does not form part of the objectives of this study. The six cracking behaviour can be described as follows:

1. *No cracking*, for conditions with a low potential for both plastic settlement and plastic shrinkage cracking.
2. *Delayed cracking*, these are isolated, short and narrow cracks that are hardly visible on the surface of plastic concrete. These cracks often only become visible after all the bleed water has been removed long after the final setting time. The origin of these cracks is mostly plastic settlement cracking. These cracks occur in conditions where the potential for both plastic settlement and plastic shrinkage cracking is low, although not entirely insignificant.
3. *Pure plastic settlement cracking*, these are cracks that can be present at and/or below the surface of the concrete and forms near the source of differential settlement such as reinforcing

steel bars. These cracks include multiple tensile surface cracks as well as internal shear cracks and normally form well before the initial setting time of the concrete. These cracks may or may not be visible at the concrete surface during the plastic stage, but are visible as soon as soon as plastic and drying shrinkage of the concrete commences. These cracks occur in conditions with a moderate to high potential for plastic settlement cracking and can occur without any potential for plastic shrinkage cracking.

4. *Pure plastic shrinkage cracking,* these cracks can also be present at and or below the concrete surface, although surface cracking is most common. These cracks require a well defined weak spot where a crack can form and without plastic settlement cracking such weak spots can be due amongst others: positions of air-entry, large air voids or reduced cross sectional area caused by the geometry of the concrete element. These cracks are characterised by a singular, well defined crack pattern and normally starts around the initial setting time and stabilise before the final setting time. These cracks occur under conditions with moderate to high potential for plastic shrinkage cracking and can occur without any potential for plastic settlement cracking.
5. *Settlement induced plastic shrinkage cracking,* the majority of cracks in plastic concrete can be described as plastic shrinkage cracking that where induced by plastic settlement cracks (even if not that severe). As for pure plastic shrinkage cracking, a well-defined weak spot is needed where cracks can form. Plastic settlement cracks occur before plastic shrinkage and therefore form weak spots once plastic shrinkage cracking starts. The more severe the plastic settlement cracks, the earlier and more severe the plastic shrinkage cracking. These crack can even occur so early (long before initial setting time) that it can involve crack opening due to both vertical plastic settlement and horizontal plastic shrinkage, although the majority of the cracking is due to plastic shrinkage. As for pure plastic shrinkage cracking the crack pattern is also singular. These cracks can occur under conditions with moderate to extremely high potentials for both types of cracking.
6. *Crack jumping*, these are rapid forming and stabilising cracks that occur when extremely high potentials for both plastic settlement and plastic shrinkage cracking are present. Once the initial crack is induced by differential settlement, significant capillary pressure has already developed, resulting in a rapid crack growth where the majority of the crack widening occurs before the initial setting time. As for settlement induced plastic shrinkage cracking, the crack pattern is singular and can be opened due to both vertical plastic settlement and horizontal plastic shrinkage.

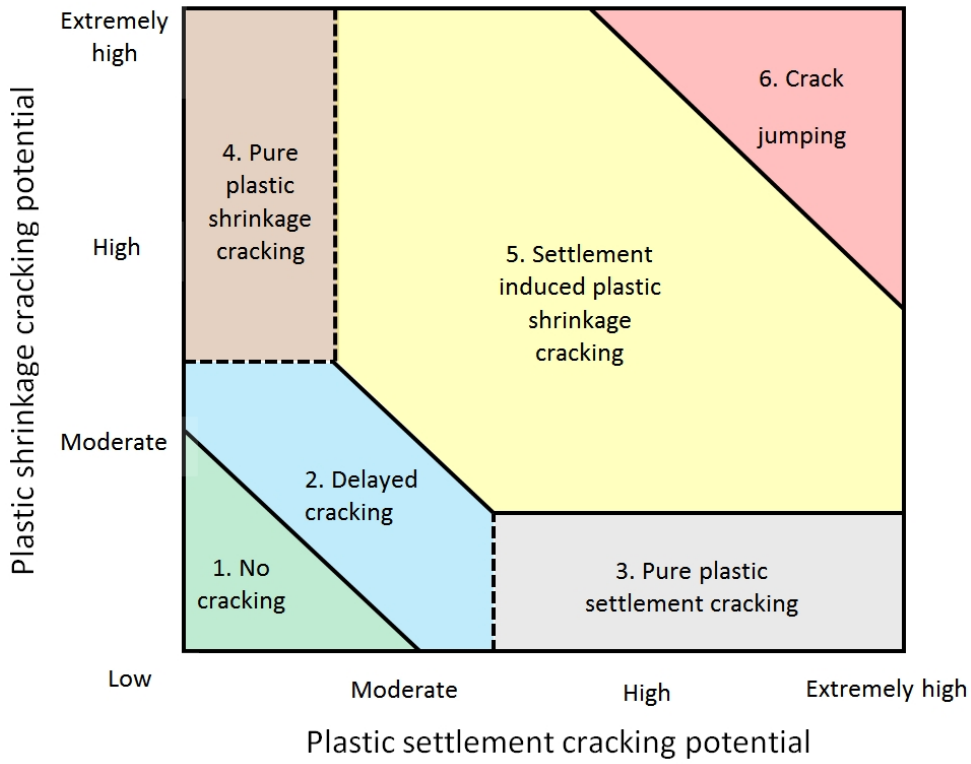

Figure 4.46. Summarising graph of six different cracking behaviours for plastic concrete if combined at different combinations of low and high potentials of both cracking types.

4.6. Concluding summary

This chapter provides the results of tests that were performed to understand the cracking behaviour of plastic concrete. This includes discussions of the results as well as the conclusions that could be drawn from tests regarding: setting times, bleeding versus settlement, plastic settlement and shrinkage cracking as well as these two cracking types combined. In the next chapter the results of the tests conducted to determine the tensile properties of plastic concrete are given and discussed.

Chapter 5. Tensile material properties test results and discussion

This chapter contains the results and discussions of the direct tensile tests performed on plastic concrete. These tests were conducted with a new test setup that was specifically designed and constructed to determine the tensile material properties of plastic concrete. The performance of this new test set up is firstly evaluated, followed by the tensile material properties that were achieved at two different temperatures. The variability of the results as well as the influence of cyclic loading are also discussed. Finally, possible links between the results of the tensile tests in this chapter with the results of the tests on the cracking of plastic concrete in the previous chapter are discussed.

5.1. Performance of test setup

The performance of the test setup is crucial in obtaining reliable and realistic results from which the tensile material properties can be determined. The discussion in Section 2.7.1 regarding the tensile testing of plastic concrete identified four key aspects that influence the performance of a direct tensile test setup. These aspects are the gripping of the fresh concrete, the friction caused by the vertical support, the measurement of concrete strain as well as the boundary conditions. The influence of each of these aspects on the performance of the test setup used in this study is discussed in the following sections.

5.1.1. Gripping method

A dog-bone shaped mould with curved transitions was used to grip the fresh concrete sample as discussed in Section 3.2.4. The curved transitions grip the fresh concrete sample through a combination of friction and normal stresses between the fresh concrete and the mould sides. The curved transitions also minimise stress concentrations outside of the gauge area, thereby promoting cracking somewhere within the gauge area over which the strain is measured. The performance of this gripping method can be deemed satisfactory if no cracks localised outside the gauge area. This means it is acceptable if small cracks occur outside the gauge area as long as the final and normally

single crack, that localises typically after the maximum tensile strength of the concrete has been reached, occurs within the gauge area.

Tables 5.1 and 5.2 show the number of tests conducted at a specific time as well as the number of these tests where cracking localised outside the gauge area for tests conducted at 23 and 40°C respectively. These tables were compiled by visually inspecting the cracking that occurred for each tensile test, where a localised crack was then identified as a singular, well defined crack that clearly formed outside of the gauge area as shown in Figure 5.1. From the results it can be seen that only the tests conducted at 23°C and 1 hour showed crack localisation outside the gauge area. Furthermore, for all the other tests the majority of the cracking, including the localised crack, occurred somewhere within the gauge area.

Table 5.1. Number of tensile tests conducted at 23°C with crack localisation outside the gauge area.

Time of testing after casting [minutes]	60	120	180	240	300	360
Number of tests conducted	3	3	3	3	3	3
Number of tests with crack localisation outside of the gauge area	3	none	none	none	none	none

Table 5.2. Number of tensile tests conducted at 40°C with crack localisation outside the gauge area.

Time of testing after casting [minutes]	60	120	180	240
Number of tests conducted	3	3	4	3
Number of tests with crack localisation outside the gauge area	none	none	none	None

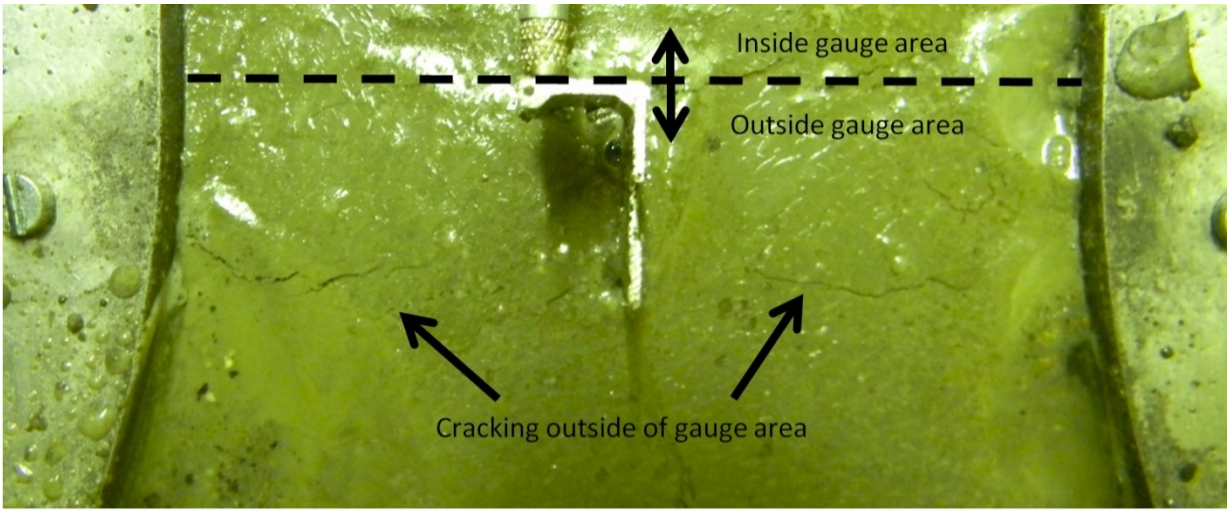

Figure 5.1. Example of crack localisation outside the gauge area for a tensile test at 1 hour on Mix C3 at 23°C.

It can be concluded that the gripping method is not well suited for concrete that has just been cast and is still highly plastic, but rather for concrete that has obtained a certain degree of firmness. For the test conducted in this study on Mix C3 it took more than an hour for the concrete to reach this firmness at 23°C and less than an hour at 40°C. However, after the concrete has reached this firmness the gripping method performed satisfactorily. Figures 5.2 and 5.3 show a number of concrete balls, where each ball was formed by hand directly after a tensile test was performed for each time interval at 23 and 40°C respectively. These figures provide an indication or sense of the degree of firmness that is needed for this griping method to work satisfactorily as well as how the stiffening and solidification of the plastic concrete progresses with time and temperature.

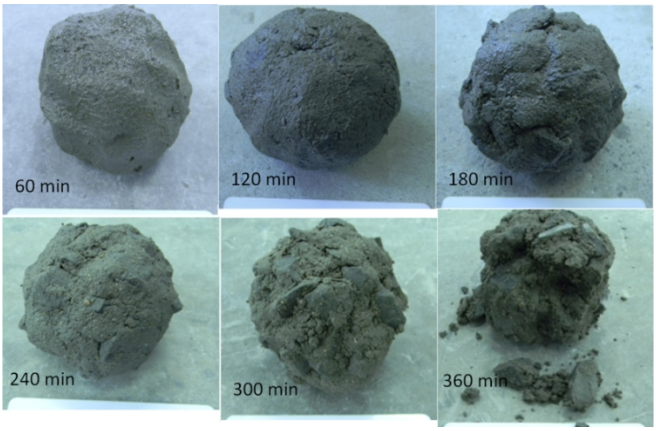

Figure 5.2. Images of the concrete balls that were formed by hand directly after a tensile test was performed for each time interval at 23°C.

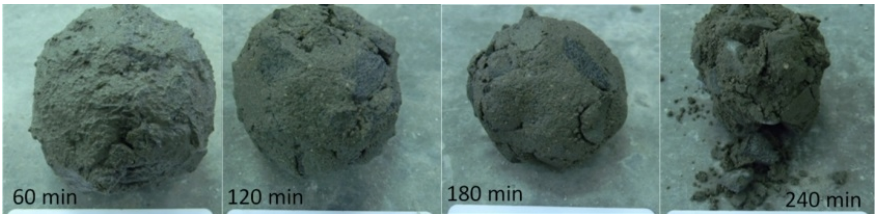

Figure 5.3. Images of the concrete balls that were formed by hand directly after a tensile test was performed for each time interval at 40°C.

5.1.2. Friction caused by vertical support

An air bearing was used as the vertical support structure beneath the dog-bone shaped mould. The function of the air bearing is to provide frictionless horizontal motion of the mould, since even a small amount of friction could significantly influence the results, especially for plastic concrete where the strength of the concrete is low. The amount of friction between the mould and the air bearing is difficult to evaluate due to the location of the load cell at the fixed end of the mould. In an attempt to evaluate the effectiveness of the air bearing, a dry run tensile test was performed where the mould was not filled with concrete. Instead several weights were placed on the mould to simulate the precise mass of the concrete as shown in Figure 5.4. During the dry run test the normal test

procedures were followed as explained in Section 3.2.7, except that no concrete was added to the mould. This meant that only the displacement of the mould at both sides could be measured and not the displacement of the concrete.

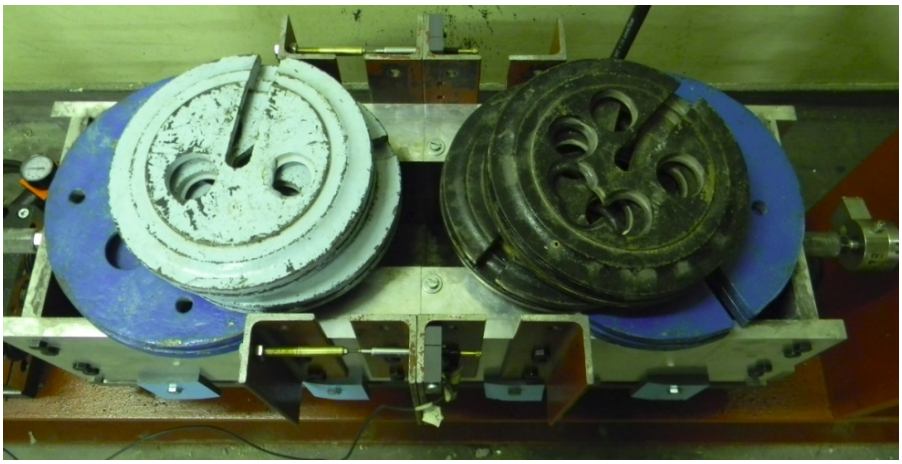

Figure 5.4. Dry run tensile tests with weights to simulate the mass of the concrete.

Figure 5.5 shows the results of the dry run test in terms of the measured displacements of the mould at both sides and the average of these displacements as well as the force measured by the load cell, all as a function of time. Initially, the load cell measured a compression force of around 30 Newton which was applied to ensure no unintended tensile forces on the specimen before testing. Once the actuator was started the compression force decreased as the mould halves were pulled apart. At first, the mould mainly displaced at one side, although the other side also showed a slight displacement. This caused a slight rotation or skewing of the mould halves to the side with the larger displacement.

If this rotation is severe enough it can cause contact between the faces of the mould halves on the side with the lesser displacement, which can increase the measured compression force. However, the rotation was not severe enough to cause this as confirmed by the steady decrease in compression force as the mould halves were pulled apart as well as the slight increase in displacement between the mould halve faces on the side with the lesser displacement. The reason for the rotating/skewing of the mould halves is still unclear and can be due to factors such as: slight non-flush line-up of mould halve faces and/or eccentric connection and line-up of the treaded connecting rods during the setup of the mould on the air bearing.

As the test continued the force reached zero at around 135 seconds indicating the start of tensile forces between the mould halves. The tensile force continued to increase for about 50 seconds, where after it stabilised at a constant value of around 1.8 Newton. This time of stabilising

corresponds to the time the rotation/skewing of the mould halves ceased as indicated on Figure 5.5. Finally, at the end of the test the treaded connections of the linear variable displacement transducers (LVDTs) between the mould halves were disconnected, which caused the constant tensile force to drop to near zero. This means that the tensile force that was measured, was due to the friction between the plunger and the sleeves of the LVDTs. This is confirmed by the slight increase in measured tensile force up to the stable 1.8 Newton where the skewing of the mould ceased, resulting in a constant LVDT friction and measured tensile force.

The fact that the load cell was able to pick up this slight friction between the plunger and the sleeves of the LVDTs due to the skewing of the mould, can only be possible if there is near zero friction between the air bearing and the bottom of the mould halves. This confirms the effectiveness of the air bearing in providing virtually frictionless horizontal motion for the mould halves, because if the air bearing resulted in the slightest amount of friction the load cell would not have been able to pick up the slight friction between plunger and sleeves of the LVDTs.

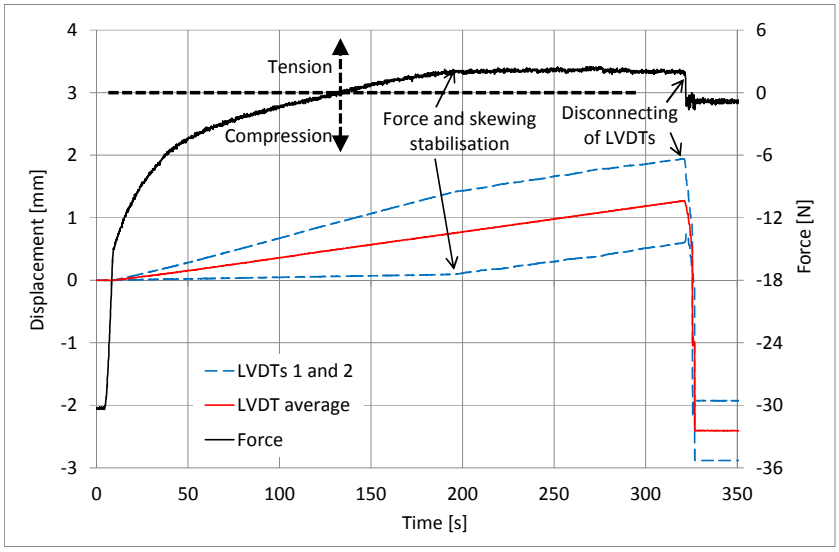

Figure 5.5. Dry run tensile test result.

5.1.3. Strain measurement

The actual strain of the concrete over the gauge area with a length of 100 mm was measured using a single LVDT that was attached to aluminium inserts that were embedded into the concrete during casting as explained in Section 3.2.6. This is needed since the measurement of only the mould displacement is not adequate for the determination of the tensile material properties of plastic concrete due to the possible movement between the plastic concrete and the mould halves. Figures 5.6 to 5.7 show the typical results that were achieved for tensile tests on Mix C3 at 23°C after 1, 2 and 3 hours after casting respectively.

The results show that for the 1 hour tests, the concrete displacement did not equal the mould displacement in the critical ascending and initial descending part of the force curve. In fact, after an initial slight increase in concrete displacement measurement, the displacement showed a decrease and only started to increase once the concrete has reached the maximum tensile force at around 250 seconds. This indicates that there was movement of the aluminium inserts relative to the concrete. At around 350 seconds (indicated by the red circle in Figure 5.6) the measurement of the concrete and mould displacements started to increase at the same rate. By this time cracks have already started to localise outside the gauge area as shown in Figure 5.1. The main reason for the difficult measurement of concrete displacement at 1 hour after casting is the plastic nature of the concrete which resulted in both movement of the aluminium inserts relative to the concrete as well as localised cracking outside the gauge area.

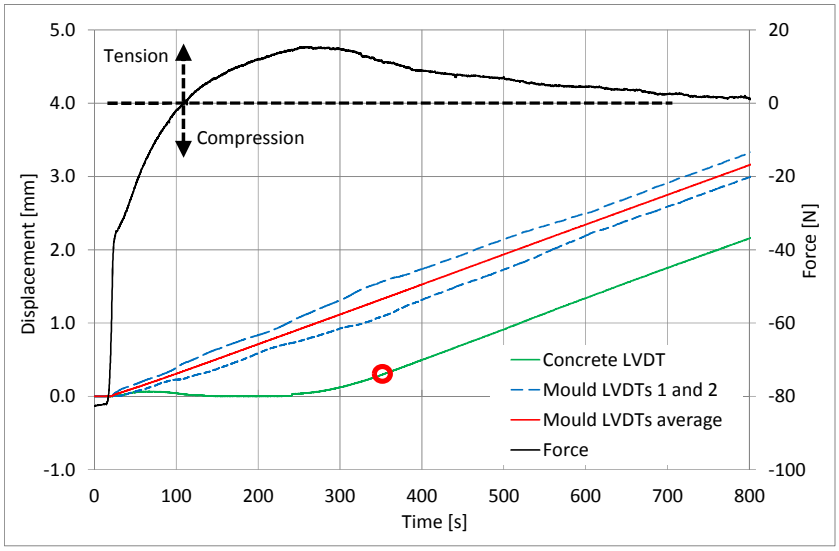

Figure 5.6. Results of tensile test on Mix C3 at 23°C only 1 hour after casting.

The results of the tests after 2 and 3 hours after casting are more promising as shown in Figures 5.7 and 5.8. For the 2 hour tests the concrete displacement immediately increased with the mould displacement during the ascending part of the force curve, although at a slightly lower rate than the mould displacement, indicating that there was some relative movement between the concrete and the mould. At around 160 seconds at the start of the descending part of the force curve the concrete and mould displacements started to increase at the same rate indicating crack localisation within the gauge area. For the 3 hour test and onwards, the concrete and mould displacement were identical throughout the entire test as shown in Figure 5.8.

These results indicate that the concrete strain measurement using a LVDT attached to aluminium inserts embedded in the concrete was successful for all tensile tests, except for the 1 hour tests at

23°C where the displacement of the concrete within the gauge area could not successfully be measured over the ascending and initial descending parts of the force curve. It should be mentioned that the 1 hour tests at 40°C gave similar behaviour as the for the 2 hour tests at 23°C, while the tests from 2 hours and onwards at 40°C gave similar behaviour as for the 3 hour tests at 23°C and onwards.

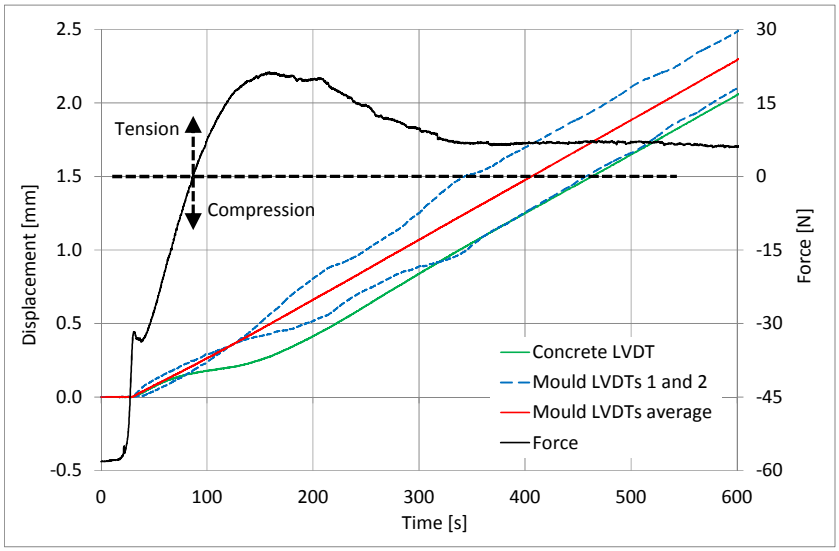

Figure 5.7. Results of tensile test on Mix C3 at 23°C only 2 hours after casting.

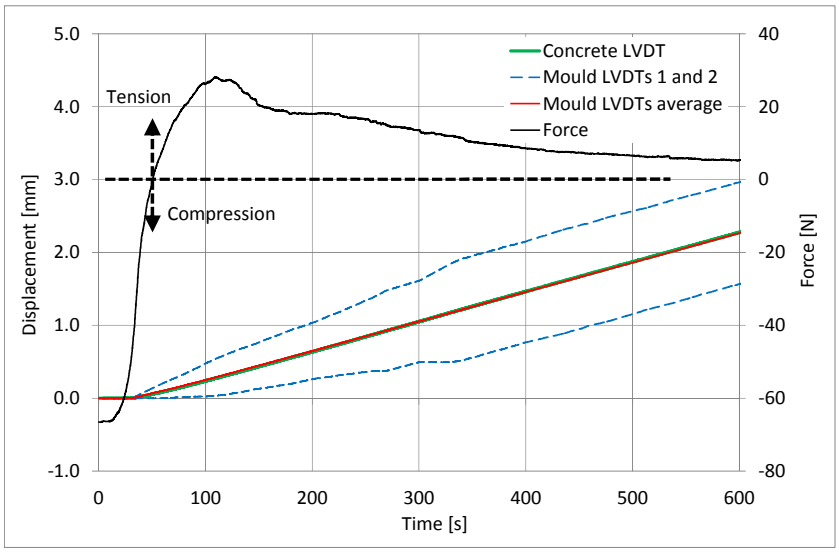

Figure 5.8. Results of tensile test on Mix C3 at 23°C only 3 hours after casting.

5.1.4. Boundary conditions

The boundary conditions used were fixed on the stationary mould halve end and semi-fixed on the moving end. This is a compromise between fully fixed and freely rotating, although it leans more towards a fully fixed situation. This configuration was chosen since the results of direct tensile test on hardened concrete with fixed boundary conditions are less scattered (Van Mier, 1997).

Figure 5.9 shows the stress-strain curves obtained from tensile tests on Mix C3 at 2, 4 and 6 hours after casting at 23°C. The results show that the initial ascending part of the curve is adequately captured and suitable for the determination of the pre-peak material properties. The initial part of the post-peak descending or softening branch of the curve is also adequately captured. However, the latter part of the softening branch shows a second unexpected increase in stress that gradually decreases as the strain increases. This is especially evident for the 2 and 6 hour tests. The reason for this second increase in stress is believed to be due to friction between the moulds sides and the concrete as shown in Figure 5.10. This friction is caused by the chosen boundary conditions that allow a certain degree of rotation on the moving side, but not on the fixed side. As the strain increases the contact area of this friction decreases causing the stress to gradually decrease. The older the concrete the higher this friction and therefore the higher this second increase in stress.

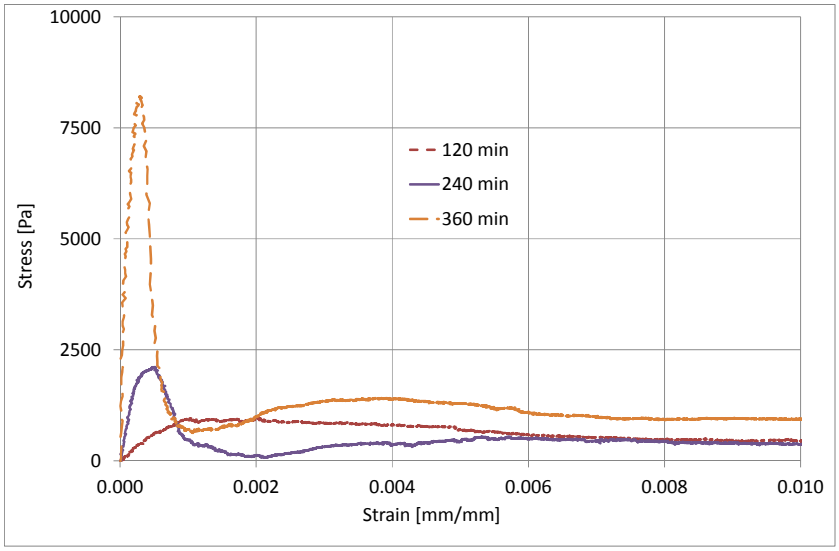

Figure 5.9. Stress-strain curves of Mix C3 at 2, 4 and 6 hours after casting as tested at 23°C.

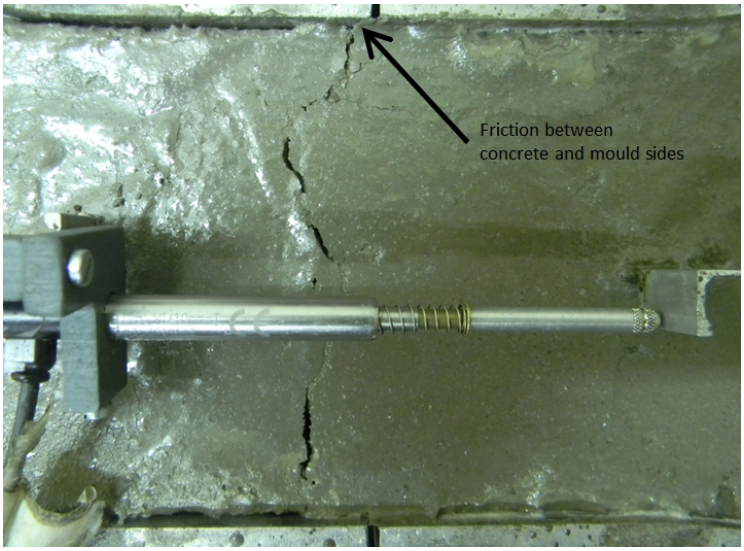

Figure 5.10. Friction between concrete and mould side at crack location.

The results suggest that the chosen boundary conditions for this particular mould are suitable for determination of the ascending as well as initial softening parts of the stress-strain curve, but not for the latter part of the softening branch.

5.1.5. Conclusions

Section 5.1 evaluates the performance of the direct tensile test setup in terms of four key aspects. The following conclusions can be drawn for each of these aspects:

- The dog bone shape of the mould acts as the gripping method of the fresh concrete. This method proved to be well suited for all tests, except the 1 hour tests at 23°C where the concrete is still highly plastic.
- The friction caused between the air-bearing surface and the bottom of the mould is near zero and can be seen as insignificant.
- The strain measurement on the concrete using aluminium inserts imbedded in the concrete is effective and suitable, except for the 1 hour tests at 23°C where the concrete is still highly plastic.
- The chosen boundary conditions for this particular mould proved to be suitable for determination of the ascending as well as initial softening parts of the stress-strain curve, but not for the latter part of the softening curve.

5.2. Tensile material properties

Figure 5.11 show the typical stress-strain curves that were obtained from the direct tensile tests on Mix C3 at 1 hour time intervals as tested at 23°C.

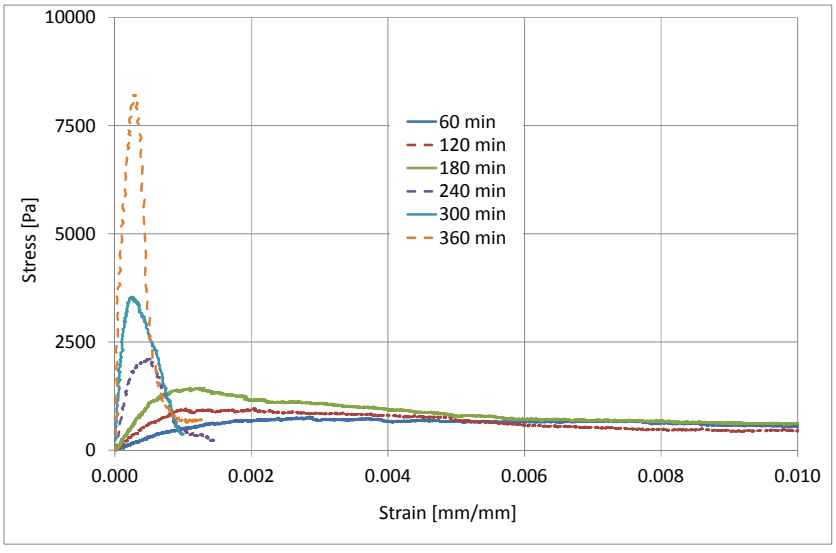

Figure 5.11. Typical stress-strain curves of Mix C3 at 60, 120, 180, 240, 300 and 360 minutes after casting as tested at 23°C.

The objectives of these tests were to determine the tensile material properties of plastic concrete and to investigate the influence of temperature on the development of these properties. Figure 5.11 only show the result of a typical specimen at each time interval, although at least three specimens were tested at each interval. The stress-strain curves of all the tests conducted were used to determine the pre-peak material properties, which are properties that can be determined up to where the maximum tensile strength (also called peak stress) is reached and includes the tensile strength, Young's modulus and strain capacity. The curves were also used to determine some of the post-peak material properties such as initial fracture energy.

5.2.1. Data processing methodology

Stress-strain curves as shown in Figure 5.11 are needed to determine the tensile material properties of fresh concrete. These graphs are compiled by calculating the stress in the concrete as the forces recorded with the load cell at the stationary mould halve end divided by the cross sectional area of the concrete over the gauge area. This stress is plotted against the strain in the concrete, which is calculated as the displacement measured with a single LVDT connected to aluminium inserts that are embedded in the concrete divided by the 100 mm length of the gauge area. This was done for all tensile tests conducted, with the exception of the 1 hour tests on Mix C3 at 23°C. For these early tests the strain measurement on the concrete only gave useable results after the tensile strength was reached due to the highly plastic nature of the concrete as discussed in Section 5.1.3.

As alternative for these 1 hour tests, the displacements measured between the mould halves were used to calculate the strains up to the time where the measured mould displacements become equal to the concrete displacements (this time is illustrated by the red circles in Figure 5.6), where after the actual measured concrete displacements were used to calculate the strains. Furthermore, since there is a possible relative movement between the mould and concrete during testing, the mould displacements cannot be taken as the displacement of the concrete itself. To account for this the same assumption made by Dao et al. (2009) was used, where the displacement of the concrete was taken as 50 % and 90 % of the mould displacement before and after the maximum tensile strength is reached respectively. However, as stated this was only needed for the 1 hour tests at 23°C, compared to all the other tests that used the actual measured concrete displacements over the gauge area to calculate the strain, which is significantly better than assuming the amount of concrete displacement.

Figure 5.12 graphically shows all the definitions of the pre-peak material properties on the ascending part of the stress-strain curve. The tensile strength (f_t) was determined as the maximum tensile

stress that the specimen can withstand before failure and gives an indication of the strength of a material. The strain capacity (ε_{cap}) was determined as the strain at maximum tensile strength and gives an indication of the amount of strain the material can undergo before failure. Materials with a large strain capacity are generally considered to be ductile materials, while materials with a small strain capacity are brittle materials.

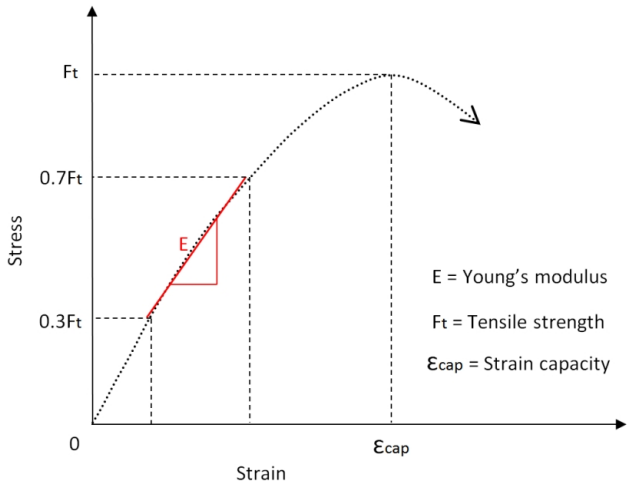

Figure 5.12. Ascending part of stress-strain curve showing the definitions of the Young's modulus, tensile strength and strain capacity.

The Young's modulus (E) was determined by fitting a straight line to the ascending section of the stress-strain curve between 30 % and 70 % of the ultimate tensile strength as illustrated in Figure 5.12. The gradient of this line was then taken as the Young's modulus. This method differs from tradition methods used for hardened concrete in compression where for example, the initial tangent modulus can be determined by fitting a tangent straight line to the initial linear or elastic part of the ascending curve or the secant modulus can be determined by fitting a straight line between two points (normally between 30 % and 50 % of the ultimate stress) on the ascending part of the stress-strain curve (Owens, 2009).

The reason the chosen method was preferred above the more traditional approaches is mainly since the Young's modulus was ultimately used as an input value for a model which is discussed later in Chapter 6. The model assumes a linear elastic material behaviour for the entire ascending part of the stress-strain curve up to the tensile strength and uses the input value of Young's modulus as the gradient for this ascending part. The results obtained with the model are finally compared to the cracking results obtained in Chapter 4. For the model to give a realistic simulation of the cracking results, the input value for Young's modulus should give an representation of the ascending part of stress-strain curve that is not dominated by either the initially steep linear part or the final non-linear part of the curve.

For this reason the part between 30 and 70 % of the tensile strength on the stress-strain curve was chosen since this gives a Young's modulus that overall, better represents the entire ascending part of the curve without being significantly influenced by the initial or final part of the curve. In addition, this approach also better accounts for the significant differences in the shape of the stress-strain curves at different ages due to the rather rapid change of concrete from a semi-plastic weak material that can withstand large deformations before failure to a much stronger solid material that fails at much lower deformations as can be seen in Figure 5.11.

Fracture energy is the amount of external energy needed to create and fully separate a unit crack surface area and can be calculated as the area under the stress-displacement curve as shown in Figure 2.12. The fracture energy does not include the unshaded area as shown in Figures 2.12 as this represents irreversible strains outside of the fracture process zone (Dao et al., 2009). The calculation of the fracture energy therefore requires the entire softening branch of the stress-displacement curve.

However, as discussed in Section 5.1.4, the tensile test setup used does not provide suitable results for the latter part of the softening branch, but rather for the ascending and initial descending part of the curve. For this reason it was decided to rather use the initial fracture energy (G_f) which, as shown in Figure 2.12, only considers the ascending and initial descending parts of the stress-displacement curve. The area under the stress-strain curve that represents the initial fracture energy is shown in Figure 5.13 and can be explained as an ascending straight line with the gradient of Young's modulus (determined earlier in this section) up to the maximum tensile strength, followed by a descending straight line that is fitted graphically to the initial gradient of the softening branch.

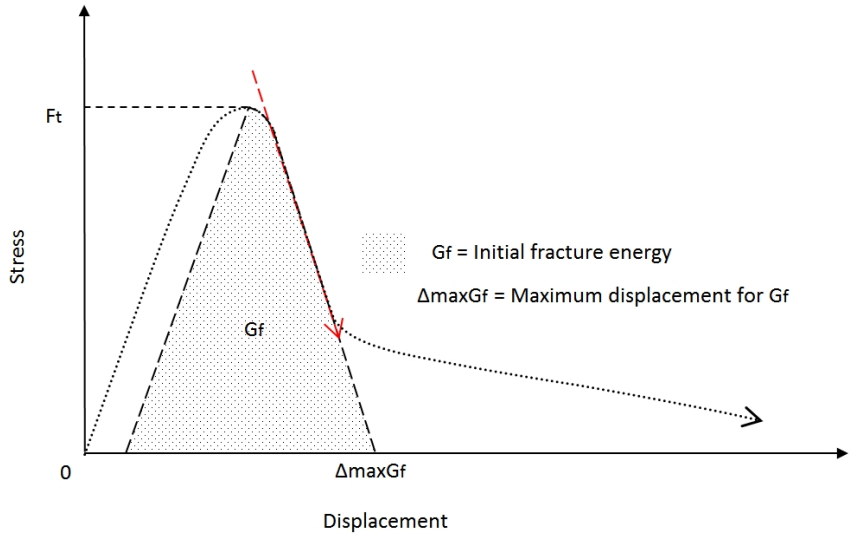

Figure 5.13. Stress-strain curve showing the definitions of the initial fracture energy.

The intersection of this graphically fitted descending line with the x-axis gives the maximum displacement (ΔmaxGf) corresponding with the initial fracture energy. This value gives an indication of the ultimate displacement that the concrete can withstand before the crack has completely opened. This means that there are no longer any stresses transferred across the crack and the material has failed completely. It should be mentioned that this only applies if the initial fracture energy definition is used and that there might still be small stresses present across the crack if the total fracture energy is considered. However, since the stresses are very small the initial fracture energy definition is believed to be adequate in describing the post-peak behaviour of plastic concrete.

5.2.2. Tensile strength (Ft)

Figure 5.14 shows the results of the tensile strength as it develops with time as well as the setting times for Mix C3 at 23°C. The figure also shows the error bar linked to one standard deviation as well as the coefficient of variation (COV) for the tests conducted at each time interval. The figure indicates that the strength initially develops slowly for the first four hours up to just before the final setting time where after the strength dramatically increases more than threefold within the next two hours to around 9 kPa.

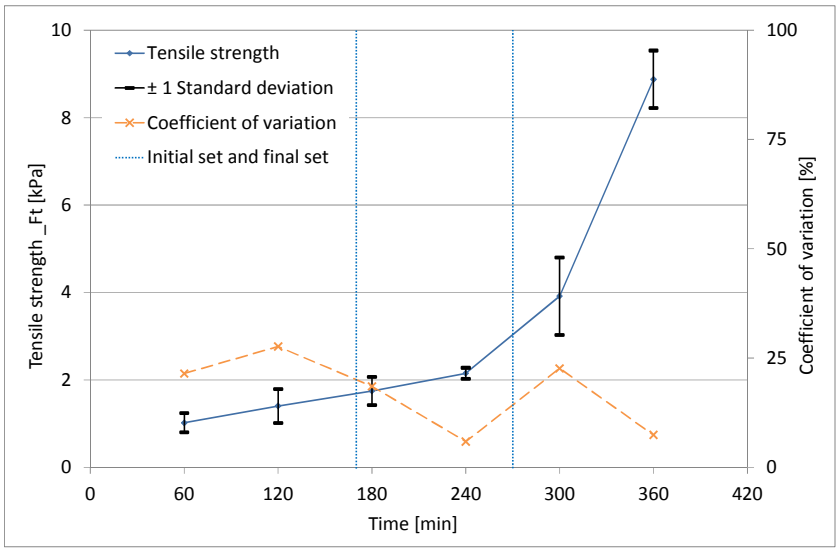

Figure 5.14. Tensile strength at different ages of Mix C3 at 23°C.

The tensile strength and its development with time is slightly lower and develops slower if compared to results at similar temperatures found in literature, where the tensile strengths varied between 10 and 100 kPa at 5 hours (Hannant et al., 1999; Branch et al., 2002 and Dao et al., 2009). The reason for this is mainly due to the difference in mixes, where the mixes in literature are generally much stiffer, stronger and faster setting mixes than the mix used in this study. However, the general shape of the curve with the sharp increase in strength agrees well with results from literature. The variability of

the results as well as the influence of temperature is discussed in Sections 5.2.7 and 5.2.8 respectively.

5.2.3. Young's modulus (E)

Figure 5.15 show the results of the Young's modulus as it develops with time for Mix C3 at 23°C. The development of the Young's modulus with time is similar to the tensile strength, although it does seem that the Young's modulus tends to develop a bit earlier, around the initial setting time, where the tensile strength mainly starts developing around the final setting time. This can be explained by the stages of hydration for concrete which first goes through stiffening and solidification stages before it starts to harden and gain strength from the final setting time onwards as explained in Section 2.2.1.

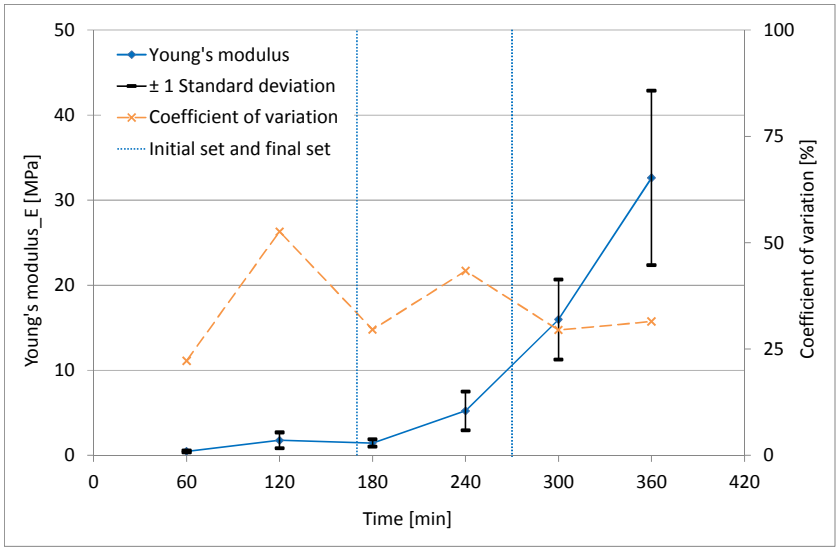

Figure 5.15. Young's modulus at different ages of Mix C3 at 23°C.

The magnitude and development with time of the Young's modulus is, as observed for the tensile strength, lower and develops slower than found in literature (Hannant et al., 1999; Branch et al., 2002 and Dao et al., 2009). This is partly due to the difference in the mixes used, but also due to the method of determining the Young's modulus, where in literature the tangent straight line through the origin of the stress-strain curve is used to determine the Young's modulus compared to the fitted straight line between 30 % and 70 % of the tensile strength method used in this study as explained in Section 5.2.1. Furthermore, there exists a near linear relationship between Young's modulus and tensile strength as shown in Figure 5.16, which is similar to the results of Dao et al. (2009).

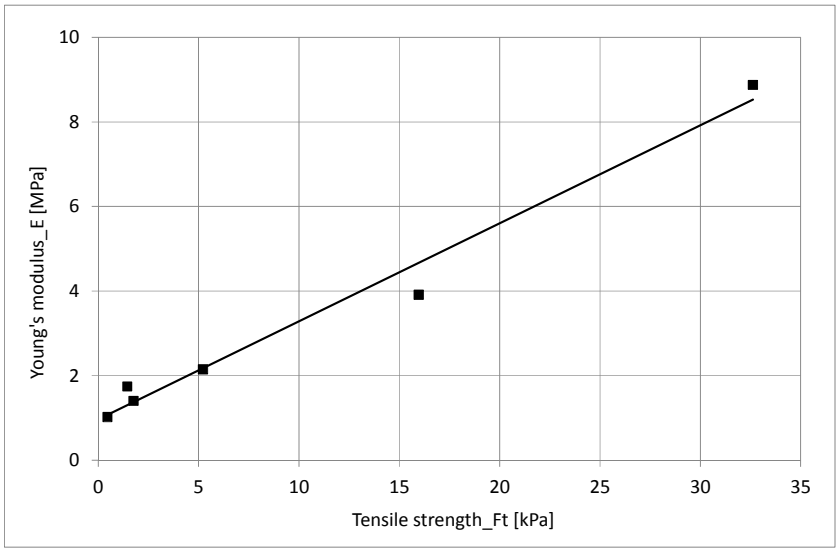

Figure 5.16. Young's modulus versus tensile strength of Mix C3 at 23°C.

5.2.4. Strain capacity (εcap)

Figure 5.17 show the results of the strain capacity (εcap) as it develops with time for Mix C3 at 23°C. The strain capacity is calculated as the measured displacement at maximum tensile strength divided by the 100 mm length of the gauge area. For the first three hours the strain capacity is high at between 0.2 to 0.3 % elongation, then between the initial and final setting times it decreases significantly to around 0.067 % elongation within one hour. After this dramatic decrease it continues to drop to around 0.027 % elongation at 5 hours, after which it increases slightly to 0.035 % at 6 hours.

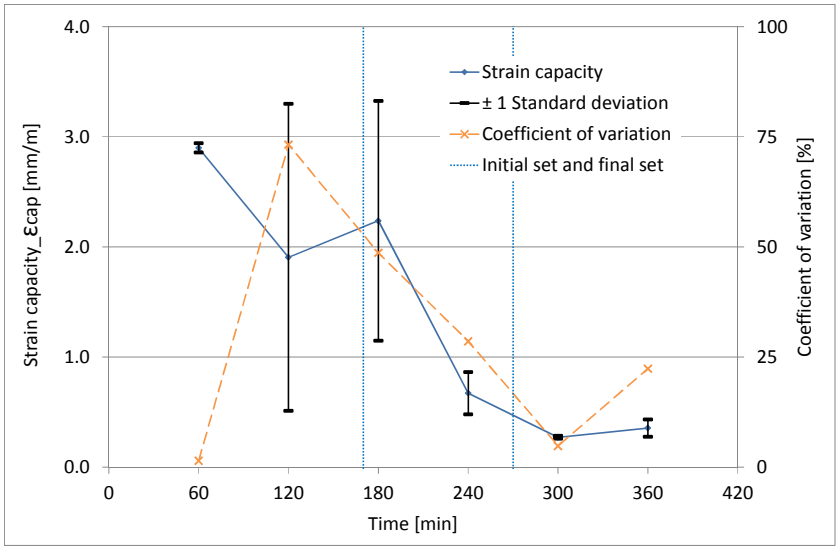

Figure 5.17. Strain capacity at different ages of Mix C3 at 23°C.

This sudden and significant decrease in strain capacity between the initial and final setting times, means that the concrete suddenly changes from a ductile material that can undergo large

deformations before failure/cracking to a brittle material that fails/cracks at much lower deformations. This observation corresponds to hydration or setting process of the concrete, where the concrete is in transition from a plastic to a solid material between the initial and final setting times as discussed in Section 2.2.1.

The sudden decrease in strain capacity is believed to be one of the main reasons why the majority of plastic shrinkage cracking occurs between the initial and final setting times as described by Boshoff and Combrinck (2013) and observed in Section 4.4. Interestingly, the magnitude and development with time of the strain capacity is still lower and develops slower than the results found in literature but much less so than the results of tensile strength and Young's modulus as discussed in the previous two sections (Hannant et al., 1999; Branch et al., 2002 and Dao et al., 2009). This suggests that the strain capacity is less depended or influenced by differences in the stiffness and strength of the specific mix.

5.2.5. Initial fracture energy (G_f)

Figure 5.18 shows the results of the initial fracture energy as it develops with time for Mix C3 at 23°C. The results indicate that the initial fracture energy is high for the first three hours, where after it decreased significantly between the initial and final setting times, followed by a slight increase after the final setting time. No literature could be found on the initial fracture energy values of plastic concrete, but only on the total fracture energies of plastic concrete between 2 and 7 hours after casting as reported by Dao et al. (2009).

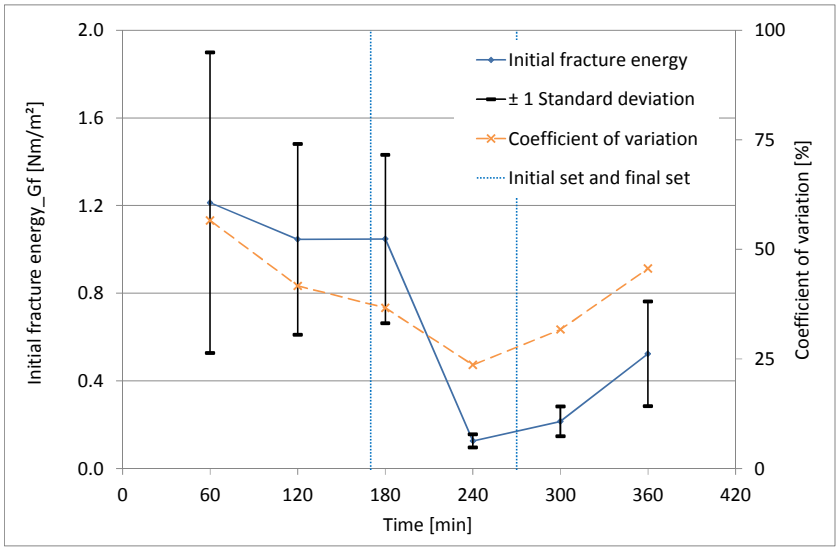

Figure 5.18. Initial fracture energy at different ages of Mix C3 at 23°C.

The initial values of total fracture energy reported by Doa et al. (2009) compare well with the initial fracture energy values, although after 3 hours the values and behaviour differs significantly. The

results of Dao et al. (2009) show a significant increase in total fracture energy after 3 hours, while the initial fracture energy values show a significant decrease. This is due to the difference in calculation, where the total fracture energy considers the total area under the stress-displacement curve and the initial fracture energy only considers up to the initial descending part of the softening branch as shown in Figure 2.12. Furthermore, the reason for the sudden dip in the initial fracture energy results between the initial and final setting times is due to, as discussed for the strain capacity in Section 5.2.4, the transition of the concrete from a ductile to a brittle material within this setting stage.

5.2.6. Maximum displacement linked to initial fracture energy (ΔmaxGf)

Figure 5.19 shows the results of the maximum displacement linked to the determination of the initial fracture energy (as defined in Figure 5.13) as it develops with time for Mix C3 at 23°C. The maximum displacement gives an indication of the amount of displacement that needs to occur over the gauge area before a fully separated crack forms. The results are similar to the results of strain capacity in Section 5.2.4 where the values are initially high between 1.4 and 2.4 mm up to around 3 hours after which the capacity decreases significantly to around 0.2 mm. This again illustrates the fast transition from a plastic material that can undergo large deformations to a more brittle material that cannot withstand large deformations. No literature could be found as comparison for these results.

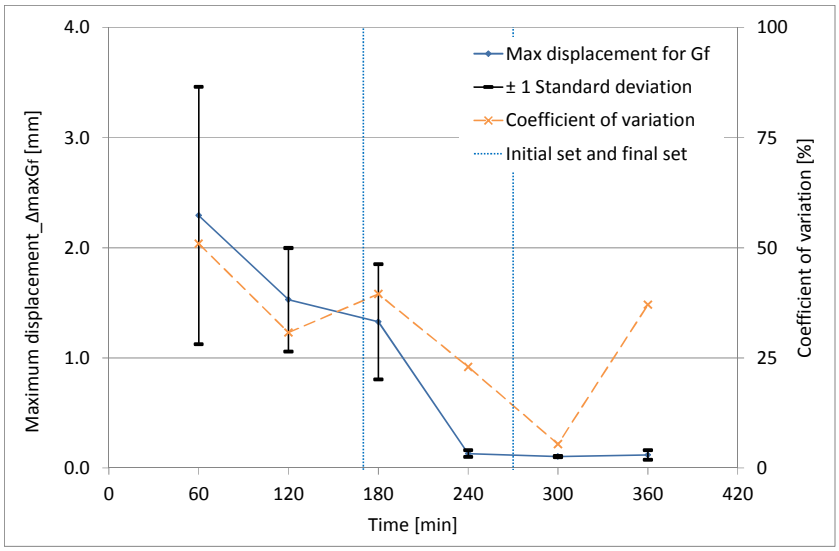

Figure 5.19. Maximum displacement linked to initial fracture energy at different ages of Mix C3 at 23°C.

5.2.7. Variability of results

The variability of the results of the tensile tests conducted on Mix C3 at 23°C differs between the various material properties. The COVs for the tensile strength results as shown in Figure 5.14 are generally well below 25 %, while the COVs for the results of Young's modulus, strain capacity and initial fracture energy are generally between 25 % and 50 % as shown in Figures 5.15, 5.17 and 5.18

respectively. The tensile strength showed the least amount of variability of all the different material properties. Furthermore, it seems that the COV tends to decrease the later the test is conducted, indicating that the results are less variable the less plastic the material. This is especially true for the pre-peak material properties. The variability of the results is similar to the variability reported by Branch et al. (2002). Figure 2.19 shows a graph produced by Branch et al. (2002) where the COVs generally varied between 10 % and 40 % for tensile strength and between 20 % and 50 % for strain capacity.

The high variability in the test results can be expected and be deemed acceptable due to both the type of test that is conducted as well as the type of material used for the tests. In general, for tensile type tests it is reported that the COV may be twice that of compression testing on cubes (Sheriff et al., 1972). Furthermore, the COV for the tensile strength of hardened concrete is around 18 % as calculated using the values given in Table 3.1 of EN 1992-1-1 (2004), which is similar to the COV achieved for tensile strength as shown in Figure 5.14. However, since the COV of tensile strength on hardened concrete is this high, it is not unreasonable to expect an even higher COV for tensile tests on plastic concrete. However, as mentioned only three samples were used to determine the mean, standard deviation and COV. This is acceptable for a good indication of the mean values, but not for other statistical parameters such as standard deviation and COV. It requires additional tests or other statistical techniques such as the t-student distribution to obtain statistically valid results for such parameters (Montgomery and Runger, 2006).

The seemingly small sample size of the results presented is, however, statistically improved by the hourly nature of the tests that were conducted on each mix and temperature, since this provides a trend of the development of the material property with time. This means that if a material property at a specific time is significantly different from the mean of that material property as determined an hour before or after, it clearly indicates a time where a possible error may have occurred. This also increases the confidence level of the results since the hourly tests are not entirely independent from each other, since they were conducted in 1 hour intervals on the same concrete mix and at the same temperature. This could possibly increase the sample size of the results which could increase the confidence level of the results. This, however, requires statistical verification that is not within the scope of this study, especially since this would not significantly influence the findings or conclusions drawn. In conclusion, the variability of tensile test on plastic concrete is inevitable and is mainly due to the nature of the test as well as the plastic nature of the concrete tested and for the purposes of this study the presented data can be deemed acceptable.

5.2.8. Influence of temperature

Figures 5.20 to 5.24 show the results of materials properties of Mix C3 at 40°C in terms of the tensile strength, Young's modulus, strain capacity, initial fracture energy and maximum displacement linked to initial fracture energy respectively. The figures show the development of these material properties with time as well as the error bar linked to one standard deviation as well as the COV for the tests conducted at each time interval at 40°C. In addition, for comparison purposes, the figures also show the development with time of these material properties at 23°C as well as the initial and final setting times at both 23 and 40°C. However, the error bars and COVs for the material properties at 23°C are not shown on these figures to prevent a cluttered presentation. The error bars and COVs at 23°C can be seen in the figures presented in Sections 5.2.2 to 5.2.6.

As discussed in Section 2.4.2 the higher the ambient temperature the faster the concrete sets to form a stiff and strong solid. This is confirmed by the results shown in the Figures 5.20 and 5.21, where the tensile strength and Young's modulus develop significantly faster and with higher values at 40°C compared to 23°C. Similar observations can be made for the strain capacity, initial fracture energy and maximum displacement linked to initial fracture energy as shown Figures 5.22 to 5.24, although here the significant decrease in these values occurred much earlier at 40°C compared to 23°C as discussed in Sections 5.2.4 to 5.2.6.

Furthermore, the development with time for all of these material properties, whether it is the start of the increase of the tensile strength and Young's modulus or whether it is the significant drop in strain capacity and fracture energy, seems to occur at similar times relative to the initial and final setting times at both 23 and 40°C. This highlights the significance of the initial and final setting times which can act at varying temperatures not only as time markers for the development of tensile material properties, but also for the understanding of cracking behaviour in plastic concrete. For example, as discussed in Section 5.2.4, the significant decrease in the strain capacity around the initial setting time explains the tendency for plastic shrinkage cracking to start near the initial setting time.

In addition, the COVs of the results at 40°C as shown in Figures 5.20 to 5.24 are much lower than the COVs at 23°C as shown in the figures presented in Sections 5.2.2 to 5.2.6. This means that the variability of the results at 40°C is less than at 23°C. This reason is believed to be the faster stiffening and setting of the mix at 40°C, which results in a less plastic material that, as discussed in Section 5.2.7, results in less variability.

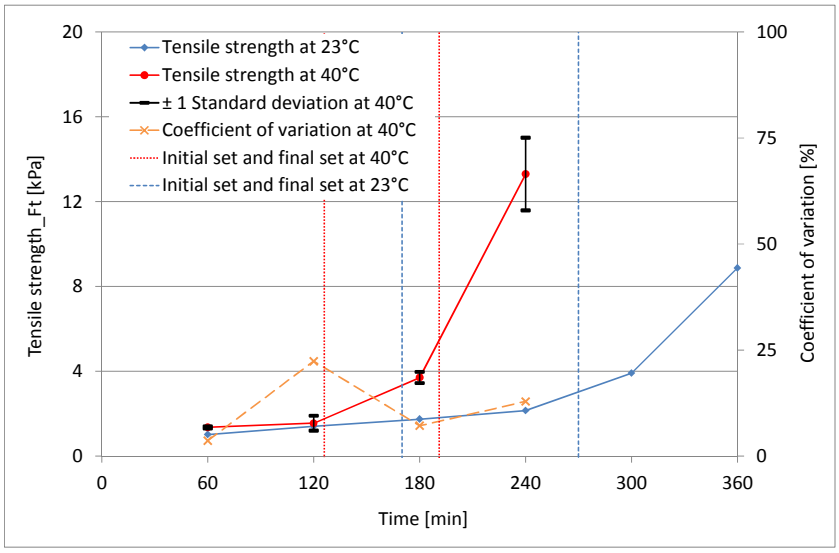

Figure 5.20. Tensile strength at different ages of Mix C3 at 23 and 40°C.

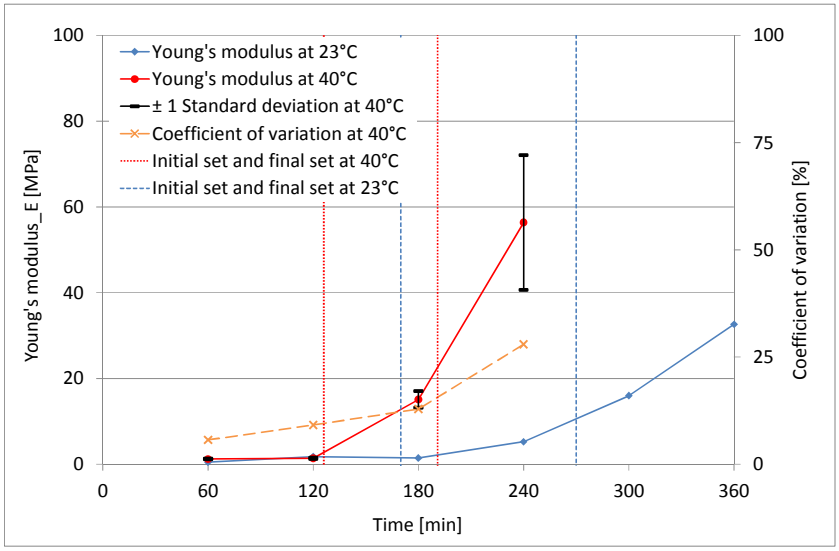

Figure 5.21. Young's modulus at different ages of Mix C3 at 23 and 40°C.

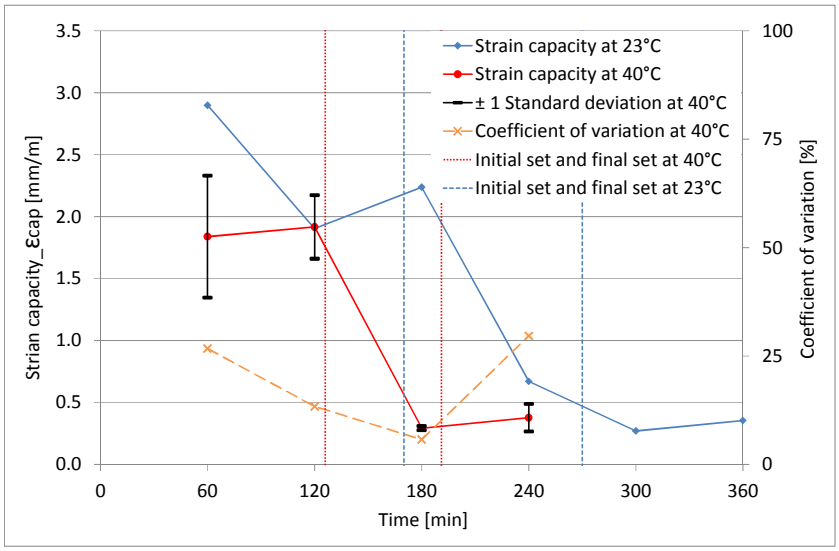

Figure 5.22. Strain capacity at different ages of Mix C3 at 23 and 40°C.

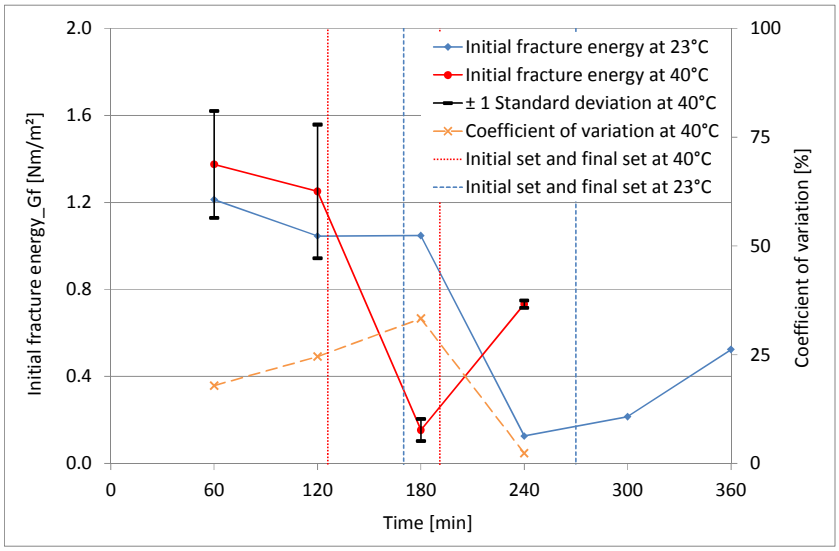

Figure 5.23. Initial fracture energy at different ages of Mix C3 at 23 and 40°C.

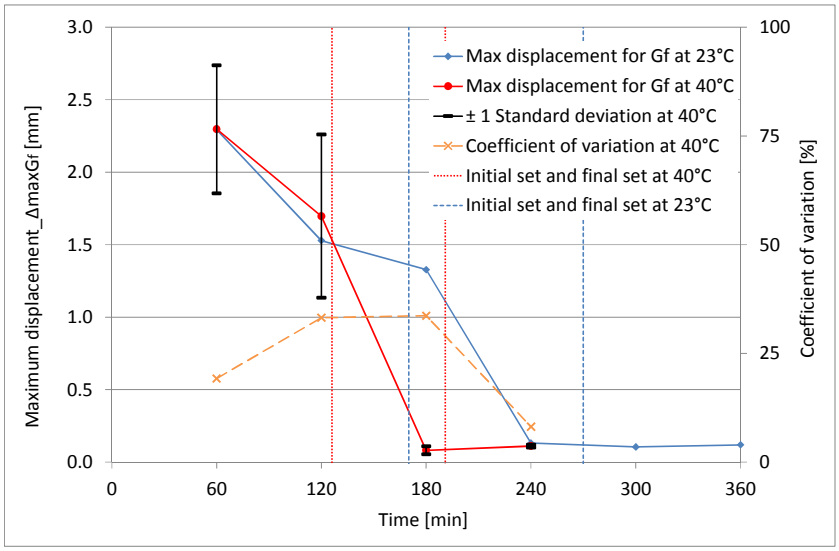

Figure 5.24. Maximum displacement linked to Initial fracture energy at different ages of Mix C3 at 23 and 40°C.

5.2.9. Influence of cyclic loading

The cyclic loading of a plastic concrete slab can occur in practice if a slab is for example exposed to alternating wetting and drying cycles. The drying cycle is caused by capillary pressure build-up due to evaporation while the wetting cycle is due to, for example, curing with a fog spray which relieves the capillary pressure. This results in the loading or deformation of the concrete during the drying cycle followed by a no deformation or loading during the wetting cycle. To simulate this, a tensile test was conducted on both a 3 and 6 hour concrete samples where the load was applied using the actuator up to 50 % of the average maximum tensile strength of the concrete at each specific age, followed by an abrupt stop of the loading by ceasing the displacement of the actuator.

The results of these cyclic tests on 3 and 6 hour concrete samples are shown in Figures 5.25 and 5.26 respectively. The figures show the mould and concrete displacement as measured with LVDTs on the left axis as well as the force measured by the load cell on the right axis. The figures show that both test samples were first loaded to 50 % of their tensile capacity after which the displacement of the actuator was ceased for around 200 seconds. Once the actuator ceased, both test samples showed a significant decrease in load up to a point where the load cell registered a compression force. The reason for the compression force is still uncertain, but is believed to be partly due to hydrostatic forces applied by the still plastic to semi-plastic concrete. After this 200 second constant deformation or ceased loading period, the load was once again applied to 50 % of the loading capacity of the samples via the actuator. However, only the 3 hour sample could once again reach 50 % of its loading capacity, while the 6 hour sample could only reach around 13 % of its loading capacity before failure.

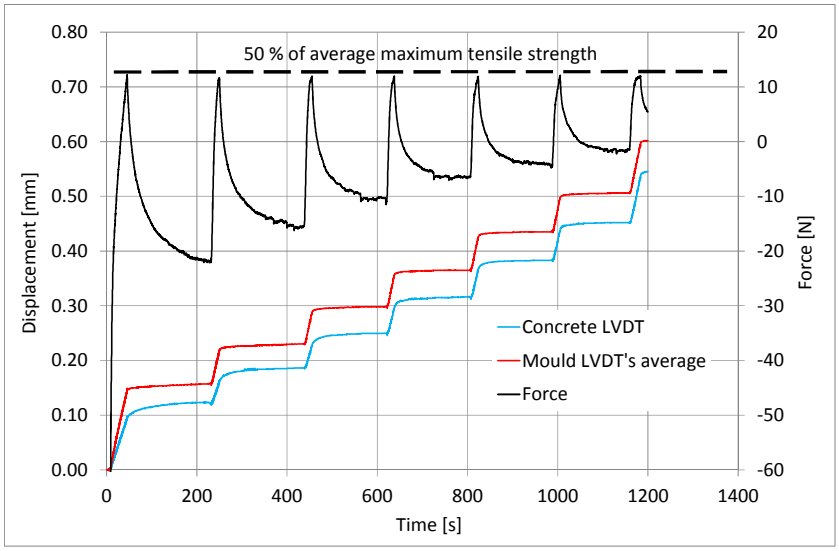

Figure 5.25. Cyclic tensile loading test on a 3 hours sample of Mix C3 at 23°C.

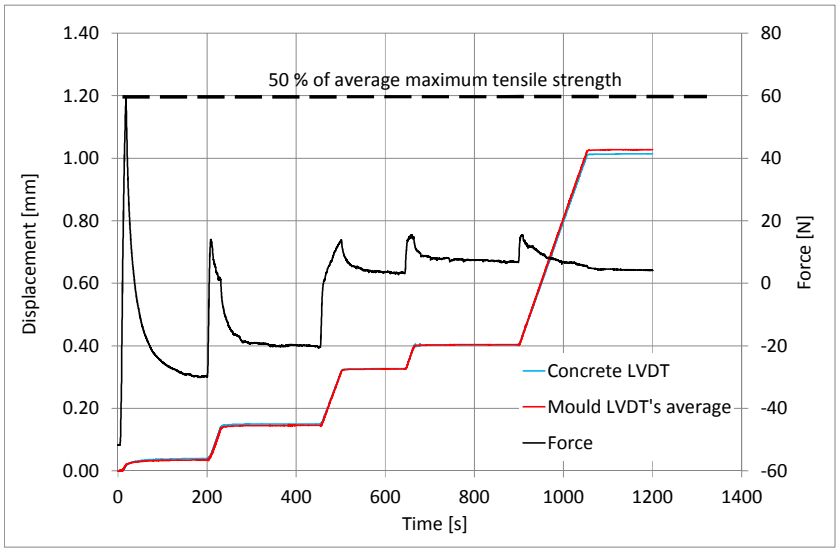

Figure 5.26. Cyclic tensile loading test on a 6 hours sample of Mix C3 at 23°C.

This cycle of loading followed by around a 200 second ceased loading period was applied several times for both samples. However, the unexpected failure of the 6 hour sample before reaching 50 % of its tensile capacity at only the second loading cycle disrupted the planned timing of following loading cycles as well as the length of the ceased loading periods for the 6 hour test. This is the reason why the load and ceased loading cycles were not perfectly executed for the 6 hour test compared to the 3 hour test where the concrete sample managed to reach its 50 % tensile capacity for each loading cycle. For both tests, the stiffness of the samples also decreased during each loading cycle, while the significant drop in force continued to occur during each ceased loading cycle, although at a lesser amount as the cycles progressed.

The results give an indication of the ability of the material to withstand repetitive or cyclic loadings. At 3 hours the concrete is still resilient and can withstand repetitive loading without failure, while at 6 hours the material could not withstand repetitive loading and failed after the second applied loading cycle. Furthermore, the nature of the test and the results achieved suggest that there is time-dependent relaxation of stresses in plastic concrete due to an applied strain. This means the stress applied to a concrete through for example plastic shrinkage can reduce or relax with time. Related to the relaxation of stresses due to an applied strain is the creep or increase in deformation due to a sustained load. However, no literature could found on the either the relaxation or creep of plastic concrete and is a subject that requires further investigation.

5.2.10. Conclusions

This section provides the tensile material properties of plastic concrete as well as discusses aspects such as the variability of results, influence of temperature and cyclic loading. The following significant conclusions can be drawn:

- Both the tensile strength and the Young's modulus initially develop slowly, followed by an exponential increase. This increase occurs near the final setting time for the tensile strength, while the Young's modulus starts to increase around the initial setting time.
- The strain capacity of plastic concrete is initially high, followed by a significant decrease between the initial and final setting times, indicating that in a short period of time the concrete changes from a material that can undergo large deformations before failure to a material that fails at relatively small deformations. This is believed to be one of the main reasons why the majority of plastic shrinkage cracking occurs between the initial and final setting times as described by Boshoff and Combrinck (2013). The initial fracture energy and maximum displacement linked to initial fracture energy behave similar to the strain capacity.

- The high variability of the test results is due to the tensile nature of the test as well as the plastic nature of the concrete tested. The results indicate that the tensile strength showed the least amount of variability of all the material properties tested. In addition, the variability tends to decrease the later the test is conducted, indicating that results are less variable the less plastic the concrete. However, only three samples were used to determine these statistical parameters for the mix at a specific time and temperature. This is acceptable with regards to the mean values, but not for the standard deviation and COV, which requires additional tests or other statistical techniques to improve the confidence level. The confidence level of the data is however improved by the hourly nature of the testing, which provides a trend of the development of the material property with time. The variability and conference level of the tensile test results is a subject that requires further investigation and for the purposes of this study the presented data can be deemed adequate.
- The tensile material properties develop significantly faster and reach more significant values the greater the ambient temperature surrounding the concrete. In addition, the development with time of the material properties, whether it is the start of the exponential increase of the tensile strength or the significant drop in strain capacity, occurs at similar times relative to the initial and final setting times at varying temperatures. This highlights the significance of setting times which not only act as time markers for the development of tensile material properties at varying temperatures, but also assist the understanding of the cracking behaviour of plastic concrete.
- Plastic to semi-plastic concrete (at 3 hours after casting in this study) revealed to be resilient and capable of withstanding cyclic loading without failure, while a solid but still weak concrete (at 6 hours after casting in this study) cannot withstand cyclic loading. In addition, the cyclic tests also suggest that there is time-dependent relaxation of stresses in plastic concrete due to an applied strain and is a subject that requires further investigation.

5.3. Link with cracking of plastic concrete tests

The tensile material properties of plastic concrete add great value to the understanding of not only the material behaviour, but also in terms of the cracking behaviour of plastic concrete. With this in mind the following links in terms of cracking behaviour can be drawn between the results of tensile material properties presented in this chapter and the results of the cracking of plastic concrete discussed in Chapter 4.

5.3.1. Observed cracking behaviour

Figure 5.27 shows the typical cracking that was observed in the gauge area during testing on Mix C3 at 23°C as tested at hourly intervals. As shown in the figure, multiple cracking occurred randomly in the gauge area for the 1, 2 and 3 hour tests. For the 1 hour test, the multiple cracks were generally finer and more difficult to see than for the 2 and 3 hour tests and as mentioned in Section 5.1.1 the 1 hour test also showed several cracks outside of the gauge area. In addition, the multiple cracks became less the later the test was conducted up to a point where from 4 hours onwards (even for some of the 3 hour tests) only singular, well defined cracks were observed during the tests.

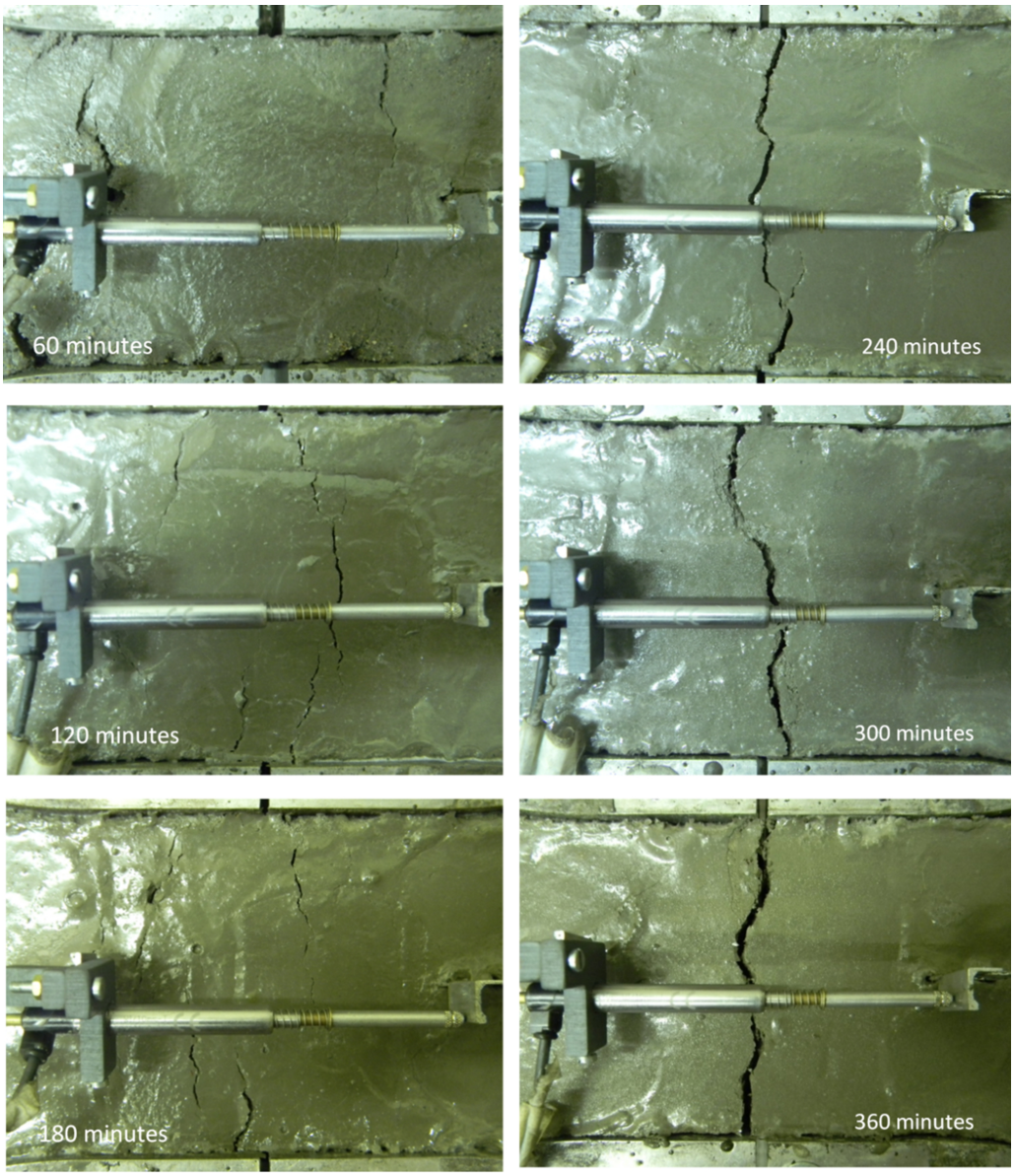

Figure 5.27. Typical observed cracking during tensile testing on Mix C3 at 23°C as tested at 1 hour (image captured at around 5 mm displacement) and at 2, 3, 4, 5 and 6 hours (images captured at around 2.5 mm displacement) after casting.

Similar observations were made by Branch et al. (2002) who stated that for their 1 and 2 hour tensile tests the failure was fairly random within the gauge area, while after 3 hours the failure became a single crack. These observations support the cracking behaviour of plastic concrete as discussed and observed in Sections 4.4 and 4.5, where the plastic settlement cracks that occur before the initial setting time have a multiple crack pattern, while the plastic shrinkage cracking that normally start around the initial setting time has a singular, well defined cracking pattern.

5.3.2. Analytical cracking behaviour of plastic concrete

The tensile material properties of plastic concrete as determined with the tensile tests can be combined with the settlement and shrinkage measurements conducted as part of the cracking of plastic concrete tests to calculate an analytical prediction of the cracking behaviour of plastic concrete. The analytical cracking behaviour can be determined in terms the onset or starting time of cracking as well as the size of the cracks.

For the onset of cracking the analytical cracking behaviour uses the two principles of crack formation as discussed in Section 2.9, where the first principle states that cracking can only occur if the tensile stress that develops in a concrete body is higher than the tensile strength of concrete. The second principle of cracking states that cracks can only occur if the tensile strain that develops in a concrete body is higher than the tensile strain capacity of the concrete. The application of these crack principles to plastic cracking requires the tensile strength and strain capacity of the plastic concrete as well as the actual tensile stress and strain responsible for the cracking. The results of the tensile tests provide the tensile strength and stain capacity of the plastic concrete, while the cracking tests provide the actual measured settlement and shrinkage strains.

However, the strains were measured in the settlement and shrinkage moulds as explained in Section 3.1.2 and represent the total free settlement and shrinkage values without any restraint. Once the concrete is placed in the shrinkage cracking mould a certain amount of the settlement and shrinkage is restrained and it is this restrained settlement and shrinkage that is responsible for the cracking of the concrete. However, the restrained settlement and shrinkage strains were not measure directly and as alternative certain crude assumptions regarding the magnitude of these strains in the shrinkage cracking mould need to be made.

The first assumption is that only 14 % of the total free settlement strain is restrained. This assumption is based on the results of Mix C1 at Climate N1 which showed a final crack width of

0.05 mm as shown in Figure 4.13. As discussed in Section 4.5.1, this crack widened mainly due to plastic settlement cracking due to the lack of capillary pressure build-up and therefore also plastic shrinkage cracking. Furthermore, since the settlement of this particular mix was not measured, it is assumed to have similar settlement than Mix C3, since the bleeding measurements of these two mixes are reasonably similar as can be seen in Figures 4.4 and 4.13. The total amount of free settlement without the influence of capillary pressure for Mix C3 at Climate N2 was 0.35 mm after around 80 minutes as shown in Figure 4.17. The same amount of free settlement is assumed to have occurred for Mix C1 at Climate N1 where no capillary pressure was present. The percentage of the final crack width of Mix C1 at Climate N1 with regards to the total amount of free settlement is 14 % (0.05 ÷ 0.35) as used for the first assumption.

The second assumption is that 62 % of the total free shrinkage strain is restrained. This assumption is based on the results of Mix C3 at Climate E2 which showed a crack width at 240 minutes of 1.4 mm as shown in Figure 4.19. However, this crack includes both the effect of plastic settlement and shrinkage cracking. The magnitude of the settlement crack for this case is calculated to be 0.1 mm. This calculation is based on the first assumption where 14 % of the free settlement (0.7 mm in this case for Mix C3 at Climate E2) results in plastic settlement cracking. This calculation also applies the 14 % assuming a linear relationship between settlement values of different mixes and conditions. Taking the plastic settlement crack into account, the width of the plastic shrinkage crack is only 1.3 mm (1.4 - 0.1). Furthermore, the free shrinkage strain of 0.0035 for Mix C3 at Climate E2 multiplied by the 600 mm length of the shrinkage cracking mould gives a free shrinkage of 2.1 mm. The percentage of the crack width due to plastic shrinkage cracking with regards to the free shrinkage is 62 % (1.3 ÷ 2.1) as used for the second assumption.

Finally, using these two assumptions, the total restrained strain (ε_{res}) that results in cracking in the centre of the shrinkage cracking mould can be calculated as 14 % of the measured free settlement (Se) strain plus 62 % of the measured free shrinkage (Shr) strain. The correctness of this calculated restrained strain using these two assumptions remains highly questionable, but it is believed to give an adequate approximation of reality for the purposes of this discussion. The restrained strain can now be used together with the strain capacity from the tensile tests to determine the onset of cracking according to the second principle of crack formation. For the first principle of crack formation the tensile stress is required together with the tensile strength to determine the onset of cracking. The tensile stress can be calculated as the restrained strain multiplied by the Young's modulus as determined with the tensile tests (Tensile stress = ε_{res} x E).

The analytical prediction of crack onset using these assumptions are shown in Figures 5.28 and 5.29 for Mix C3 at Climate E2 and in Figures 5.30 and 5.31 for Mix C3 at Climate N2 in terms of both the first and second principles of crack formation. These figures also indicate the predicted onset of cracking with a red circle according to the first principle of crack formation (stress exceeding capacity) in Figures 5.28 and 5.30 as well as according to the second principle (strain exceeding capacity) in Figures 5.29 and 5.31.

Furthermore, it should be noted that the values of Young's modulus and tensile strength at 0 hours were assumed to be the same as at 1 hour, while there was further linearly interpolated between hourly values to obtain estimates of values at 20 minute intervals. These figures also present an analytical crack width envelope and experimental crack widths on the right axis.

These envelopes represent the possible sizes of cracks as predicted by the analytical cracking behaviour. The determination of the upper and lower boundaries of this crack width envelope is based on two extremes, with the actual crack falling somewhere in between. The first extreme forms the upper boundary and assumes that the failure occurs in a brittle manner, i.e. there is no post-cracking strength or ductility after the crack has formed. The second extreme forms the lower boundary and assumes that once the crack has formed it retains a post-cracking strength and ductility equal to the measured tensile strength (first principle of crack formation) and tensile strain capacity (second principle of crack formation). The calculations of the crack width for the upper and lower boundaries for both principles of crack formation are as follows:

- Upper boundary for both the first and second principles of crack formation:

$$Crack\ width\ (time) = \varepsilon_{res}\ (time) \times\ length\ of\ shrinkage\ cracking\ mould \qquad (Eq.\ 5.1)$$

- Lower boundary for first principle of crack formation:

$$Crack\ width\ (time) = \frac{Tensile\ stress\ (time) - Ft\ (time)}{E\ (time)} \times length\ of\ shrinkage\ cracking\ mould \qquad (Eq.\ 5.2)$$

- Lower boundary for second principle of crack formation:

$$Crack\ width\ (time) = [(\varepsilon_{res}\ (time) - \varepsilon_{cap}\ (time)] \times\ length\ of\ shrinkage\ cracking\ mould \qquad (Eq.\ 5.3)$$

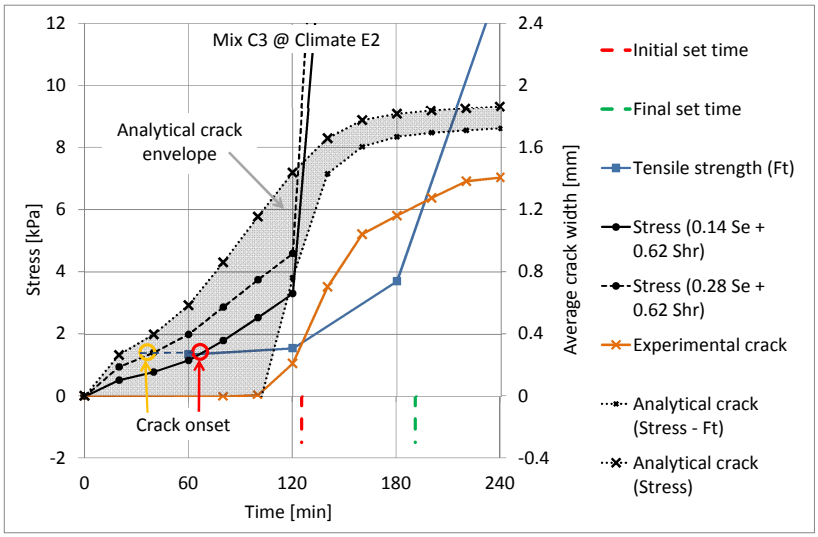

Figure 5.28. Results of Mix C3 at Climate E2 illustrating the first principle of crack formation.

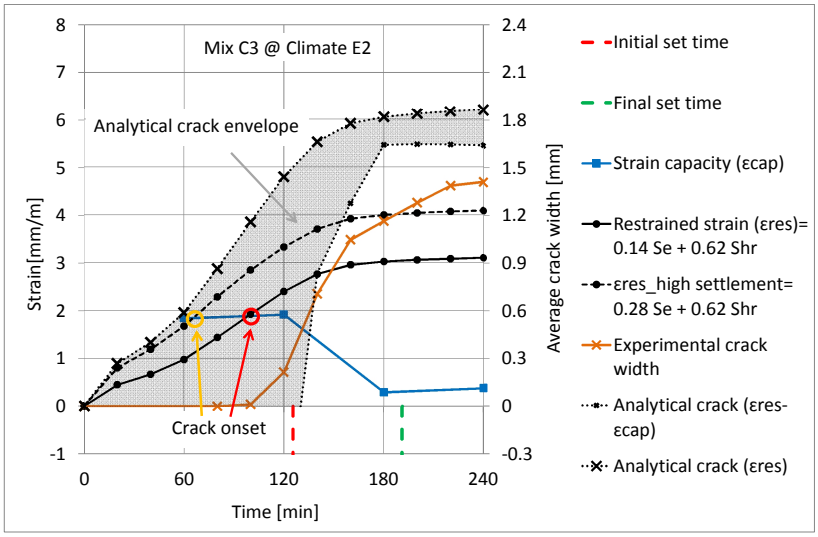

Figure 5.29. Results of Mix C3 at Climate E2 illustrating the second principle of crack formation.

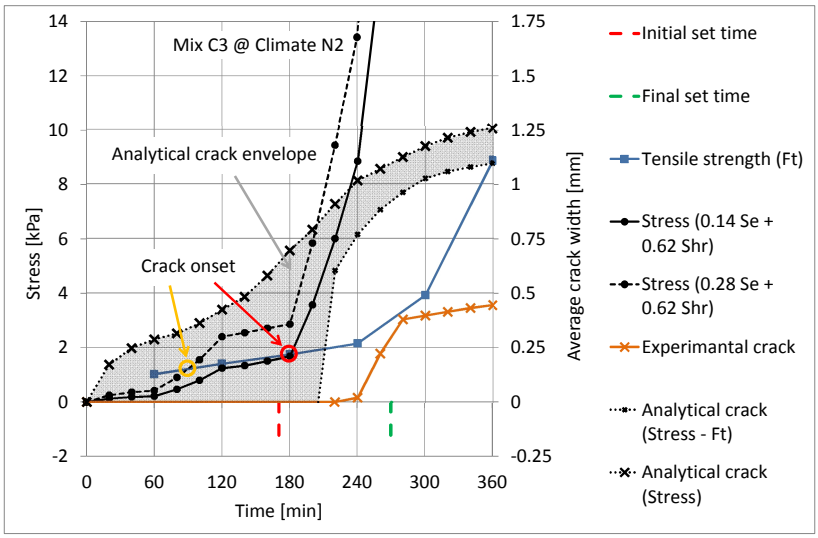

Figure 5.30. Results of Mix C3 at Climate N2 illustrating the first principle of crack formation.

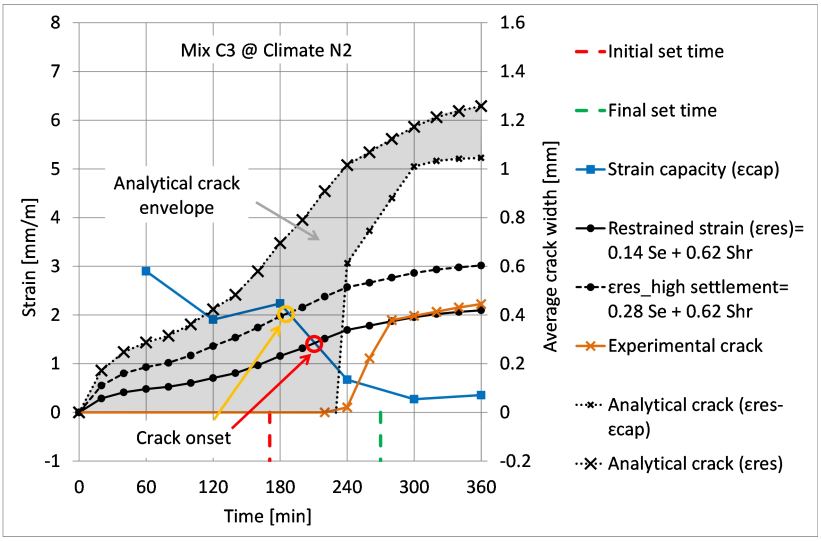

Figure 5.31. Results of Mix C3 at Climate N2 illustrating the second principle of crack formation.

The results of the analytical cracking behaviour in terms of the onset of cracking and size of crack can be compared to the measured experimental cracks at both Climates E2 and N2. For both Climates E2 and N2 the second principle of crack formation provides a good estimation of crack onset, since the experimental crack started close to where the tensile strain in the concrete body exceeded the tensile stain capacity as shown by the red circles in Figures 5.29 and 5.31. This is especially notable at Climate E2 where the crack onset is nearly exactly where the tensile strain exceeded the tensile stain capacity. In comparison, the first principle of crack formation estimates a much earlier onset of cracking compared to the experiments for both Climates N2 and E2 as shown by the red circles in Figure 5.28 and 5.30.

In terms of the size of the crack widths, the experimental cracks at Climate E2 are slightly smaller (around 20 %) than predicted by the analytical crack envelope for both principles of crack formation. While at Climate N2 the predicted analytical crack envelope is more than double the experimental crack widths for both principles of crack formation. Furthermore, for both climates it seems that the lower boundary of the analytical crack envelope of the second principle gives a slightly better estimation of the experimental crack compared to the lower boundary of the first principle.

The results suggests that the predicted analytical cracking behaviour provides an adequate approximation of the experimental cracking behaviour at Climate E2, especially in terms of the onset of cracking using the second principle of crack formation as well as only slightly larger crack widths. The results for both climates also suggest the strain capacity (related to the second principal of crack formation) of plastic concrete gives a better approximation of the onset and size of cracking in plastic concrete compared to the tensile strength (first principal of crack formation) of plastic concrete.

However, at Climate N2 the analytical results do not compare that well to the experimental results especially in term of the crack size. The reason for this is the size discrepancy between the surface and interior cracks during experiments at Climate N2 as shown in Figure 4.21. This means the experimental results at Climate N2 are misleading, since the measured surface crack is much smaller than the actual interior crack due to the abundance of bleed water as discussed in Section 4.4.3. Therefore the actual crack widths for Climate N2 are believed to develop much faster and possess higher values than what is presented in Figures 5.30 and 5.31. If this is taken into account, the analytical prediction of the cracking potentially shows more favourable agreement with the actual cracking behaviour at Climate N2 than what is perceived by the current experimental results. However, this requires further investigation and improvement, especially in terms of the observation and measurement of interior cracking beneath the concrete surface.

Finally, Figures 5.28 to 5.31 also show a light orange circle which indicates the predicted crack onset if the restrained strain is composed of double the percentage of settlement (28 % settlement compared to the previous 14 %). This simulates a situation where the layout of a mould gives a greater potential for plastic settlement cracking. The results in the figures illustrate that crack onset occurs much earlier with this higher potential for plastic settlement cracking. This behaviour is similar to the experimental results in Sections 4.5.3 and 4.5.4, where crack onset occurred much earlier due to a high potential for plastic settlement cracking. This suggests that analytical crack behaviour combined with the principles of crack formation can also be applied to the cracking of plastic concrete if both plastic settlement and plastic shrinkage cracking are present. However, further refinement and investigation regarding the amount of restrained strain that is responsible of the cracking at a certain location is required.

5.3.3. Conclusions

This section investigates possible links between the results obtained with the tensile and cracking of plastic concrete tests. The following links could be found.

- The cracking patterns observed during the tensile tests are similar to the cracking patterns observed during the cracking of plastic concrete tests, where generally up to around the initial setting time multiple cracking occurs while after initial setting time singular, well defined cracking occurs.
- The results of tensile strength, Young's modulus and strain capacity from the tensile tests can be combined with the results of measured settlement and shrinkage strains to obtain an analytical

estimation of the cracking behaviour of plastic concrete. The analytical cracking behaviour gives an adequate approximation of the experimental cracking behaviour for extreme climates with a high evaporation rate. At normal climates the analytical cracking behaviour does not give a good representation of the experimental results, mainly due to the size discrepancy between surface and interior cracks during experiments at normal climates.

- The strain capacity of plastic concrete gives a better approximation of the onset and size of cracking in plastic concrete compared to the tensile strength of plastic concrete.
- The analytical cracking behaviour as presented in this section follows a rather pragmatic approach to represent to complex cracking behaviour of plastic concrete. The approach requires rather crude assumptions and does not correctly account for the complexities involved such as the layout of the mould, interaction between settlement and shrinkage as well as the pre- and post-cracking behaviour of the plastic concrete. A better approach or method to simulate the cracking behaviour of plastic concrete is to combine these measured material properties, strains and behaviours into a numerical model that is able to account for all the complexities involved. The following chapter gives and discusses such a model.

5.4. Concluding summary

This chapter provides the results of the tensile tests that were performed on plastic concrete to determine the tensile material properties of plastic concrete as a function of time. This includes discussions regarding the performance of the test setup as well as the results obtained and conclusions that can be drawn on the tensile materials properties of plastic concrete such as: tensile strength, Young's modulus, strain capacity and initial fracture energy. Finally, possible links are drawn between the results obtained with the tensile testing in this chapter with the results of cracking in plastic concrete as obtained in the previous chapter. The next chapter gives and discusses a model that can be used to simulate the cracking of plastic concrete.

Chapter 6. Modelling the cracking of plastic concrete

This chapter describes a finite element model that can be used to simulate the cracking behaviour of plastic concrete. This includes discussions regarding the challenges involved with such a model, the constitutive material law needed for the model as well as the general layout, input parameters and solution procedures needed to analyse the model. This is followed by a mesh sensitivity analysis as well as the validation of results achieved with the model using experimental results. Finally, a parameter study is conducted which is followed by an application of the model to a large scale example as illustration of its applicability to a real-world situation.

6.1. Time dependency and anisotropic volume change

One of the biggest challenges associated with the modelling of the cracking of plastic concrete is the significant and rapid change of the concrete from a plastic or semi-plastic material to a weak-solid within a couple of hours. This means that the behaviour of the concrete also changes from a ductile type to a brittle type material, while the material properties such as strength, stiffness and deformability also change dramatically with time as the concrete sets and strengthens.

Furthermore, the volume change associated with plastic concrete is also time dependent and includes settlement which starts once the concrete has been cast as well as plastic shrinkage which starts once concrete pore water is removed by evaporation. In addition, the settlement and shrinkage do not start or end at the same time, while the rate and magnitude of both also change with time. The complexity is further increased by the anisotropic nature of the settlement and shrinkage in terms of direction, where settlement is mainly in the vertical direction while plastic shrinkage is mainly in the horizontal direction.

Any model aiming to realistically simulate the cracking of plastic concrete needs to account for the time dependency of material properties and volume change as well as the anisotropic nature of the volume change.

6.2. Constitutive model

A model requires a constitutive law that governs the behaviour of the material under applied action such as loads. The constitutive model applicable to the cracking behaviour of plastic concrete is not well researched or defined in literature. Some of the available models in literature, as discussed in Section 2.10, simulated the cracking by searching for equilibrium of numerous forces acting on and between individual solid particles in a cement paste (Slowik et al., 2009b), while others used theories such as the consolidation of soils to model the settlement of concrete (Kwak et al., 2010). As an alternative to these approaches it was decided to adopt one of the several existing constitutive crack models that are already well establish and used for mature concrete.

These cracking models of concrete can broadly be defined as either discontinuous or continuous. Discontinuous cracking, also called discrete cracking, assumes cracking or fracture along surfaces or lines of displacement discontinuities according to the fictitious crack concept introduced by Hillerborg et al. (1976) as discussed in Section 2.8.2. In finite element analysis (FEA) these cracks are often modelled using interface elements that are placed along element boundaries to act as crack openings which are described by a stress-crack opening relationship (Alfaiate et al., 1997). The drawback of this approach is that the location of the crack/s needs to be known beforehand to allow the manual placement of the interface elements. If the placement of interface elements is to be automated it requires continuous remeshing and topological redefining in FEA, which leads to a more complex solution procedure as well as computer implementation.

Continuous cracking on the other hand, also referred to as smeared cracking, smears or distributes the cracking over a band or region in the continuum according to the crack band theory introduced by Bazant et al. (1983) and discussed in Section 2.8.2. This approach describes the cracking behaviour in FEA in terms of a stress-strain relationship that exhibits strain softening and where the cracked solid is assumed to be a continuum in which the concepts of stress and strain are still valid. The advantage of this approach is that the crack location does not need to be known beforehand and it can easily be implemented and integrated with FEA since the original topology of the mesh remains preserved (Li and Zimmerman, 1998). For these reasons, the smeared cracking approach is believed to be better suited to model the cracking behaviour of plastic concrete.

The smeared cracking approach can further be distinguished as either a fixed or rotating crack model. For the fixed crack model the orientation of the crack is fixed upon crack initiation. Any further crack propagation occurs in this fixed orientation which is perpendicular to the initial maximum tensile

strain upon crack initiation. The drawback of this model is that as cracking proceeds the orientation of the principal strains may change causing a shear stress over the crack plane, resulting in a situation where the residual normal stress may exceed the tensile strength in a direction other than the original fixed crack orientation. In addition, the fixed crack model also requires the delicate choice of a shear retention factor to account for the shear stiffness over the crack plane (Li et al., 1998).

For the rotating crack model the orientation of the crack continuously rotates to align perpendicular to the maximum principal tensile strain direction. As the crack propagates, the crack plane rotates to ensure the crack orientation remains perpendicular to the principal strain direction and therefore also parallel to the maximum principal tensile stress. This ensures that no shear stress develops over the crack plane, removing the possibility of a normal stress exceeding the tensile stress in another direction as well as the need for a shear retention factor as with the fixed crack model (Li et al., 1998). For these reasons the rotating crack model is reasoned to be better suited for the modelling of the cracking behaviour of plastic concrete.

Cracks are initiated in the smeared rotating crack model once the maximum principal tensile stress exceeds the tensile strength of the material in the orientation of the crack perpendicular to the maximum principal tensile strain. Once the crack is initiated the post-cracking behaviour or softening branch of the stress-strain curve of the concrete needs to be described. Early attempts to model this softening behaviour made use of a reduction factor that gradually reduced the tensile strength of the concrete upon further crack opening (De Borst, 2002). This however lead to results that were highly dependent on the size of the mesh, since the same amount of energy was released after cracking for different element sizes.

As solution to this problem, the material property of fracture energy was introduced, where the fracture energy can be defined as the amount of external energy needed to create and fully separate an unit area of a continuous crack as discussed in Section 2.7.2. The fictitious crack model introduced by Hillerborg et al. (1976) was developed to prevent mesh dependent release of fracture energy during cracking. Bazant et al. (1983) applied this concept to their crack band model, assuming that the fracture energy is smeared out over a crack band width which is linked to the FEA mesh where cracking is initiated. The crack band width is furthermore a function of the element or mesh size where the cracking occurs, which greatly reduces the mentioned problem regarding the mesh dependent release of energy (De Borst, 2002). For these reasons a tension softening stress-strain

relationship that is based on fracture energy to govern crack propagation and related to a crack band width is believed to be appropriate for modelling the cracking behaviour of plastic concrete.

In conclusion, the appropriate constitutive model for the plastic cracking behaviour of concrete as identified above is a smeared rotating crack model that uses fracture energy and a crack band width for crack propagation. Furthermore, this type of model can easily be implemented in a finite element analysis as discussed in the following section.

6.3. Finite element model description

Literature regarding the finite element modelling of cracking in plastic concrete is rare. The model developed by Kwak et al. (2010) to investigate the plastic settlement cracking of concrete using the theory of consolidation as discussed in Section 2.10 was the only meaningful finite element model that could be found. This is mostly due to the challenges involved with the modelling of plastic concrete such as the time dependency of material properties as well as the anisotropic nature of volume change.

This section provides details on the finite element model for the cracking of plastic concrete that is implemented in this study using the Diana Software Package Version 9.6 (2014). The implementation of such a model requires parameter experiments to characterise the material properties as well as verification experiments for comparison and validation of the results achieved with the model. The model uses the results of the tensile tests in the previous chapter as well as the results of shrinkage and settlement measurements in Chapter 4 to serve as input values for material properties and volume change of plastic concrete respectively. The experiments used to verify the results achieved with the model are the results obtained in Section 4.4.2 on the cracking of plastic concrete using the shrinkage cracking mould. A detailed description of the model is given in the following sections.

6.3.1. Geometry, elements and boundary conditions

Figure 6.1 shows the finite element mesh as well as boundary conditions that were used to model the experiments with the shrinkage cracking mould. The geometry of the mesh was similar to the dimensions of the shrinkage cracking mould as shown in Figure 3.2. The mesh size was also consistent, with the dimensions of all the elements at 5 x 5 mm. The model further used linearly interpolated four node quadrilateral isoparametric plane stress elements. The thickness of the elements was 200 mm which corresponds to the width of the shrinkage cracking mould. The shape of the three triangular restraints were not modelled perfectly, instead a stepped of zagged

approximation of the triangular shape was used. The same is true for the shape of the steel bar at each end of the mould which was modelled as a square instead of a circle.

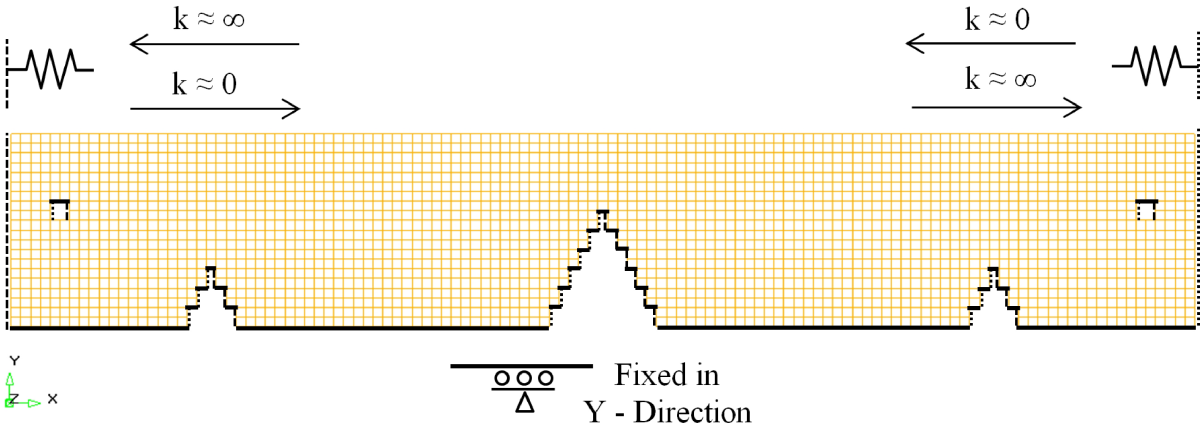

Figure 6.1. Finite element mesh including the boundary conditions used to model the cracking in the shrinkage cracking mould.

To verify that the stepped shape of the restraints provided similar results than for a smooth shape, an experiment was conducted with two shrinkage cracking moulds, where the normal smooth centre triangular restraint was replaced with a stepped triangle identical to the shape of the triangle in the model. Figure 6.2 shows the results of this test for Mix C3 at Climate E2 in terms of average crack width compared to the results achieved with the shrinkage cracking mould. The figure shows that the results achieved with the stepped triangular restraint are similar to the results achieved with the normal smooth triangular restraint. This confirms that the use of a stepped triangle in the model is acceptable.

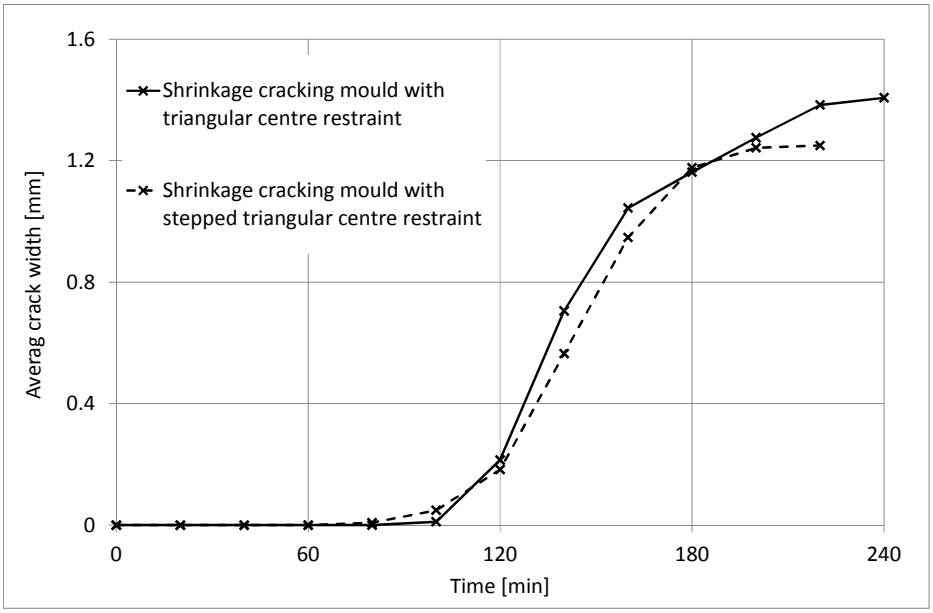

Figure 6.2. Average crack width measured for Mix C3 at Climate E2 in the shrinkage cracking mould with a smooth centre triangular restraint as well as a stepped central triangular restraint.

Figure 6.1 also shows the boundary conditions used for the model. All the elements in contact with the bottom of the mould or other fixed horizontal surfaces (restraining inserts), indicated with solid black lines in the figure, were fixed in the y-direction but free to move in the x-direction. The vertical boundary conditions at the ends of the mould and other fixed vertical surfaces are more complex as these boundary conditions should allow movement of the elements away from the fixed surface but not towards it. To achieve this, one-node axial translational spring elements were placed at all nodes that exists between the vertical surfaces of the mould and the four node plane stress elements.

The spring elements placed at the left vertical boundaries surfaces, indicated by the dashed lines in Figure 6.1, were given an overly high stiffness in the negative x-direction and a near zero stiffness in the positive x-direction. The springs at the right vertical boundaries of the mould, indicated by the dotted lines in Figure 6.1, were assigned stiffness's opposite to the springs at left vertical boundaries. These springs allow the plastic concrete to move away from the vertical mould surfaces due to settlement and shrinkage, but also support and prevent movement in the opposite direction past or into mould vertical surfaces. These boundary conditions therefore assume that there is no adhesion or friction between the mould and the concrete.

6.3.2. Constitutive law

The appropriate constitutive law to govern the cracking behaviour of plastic concrete was identified in Section 6.2 as a smeared rotating crack model that uses fracture energy and a crack band width for crack propagation. The rotating total strain cracking model available in the DIANA Software Package Version 9.6 (2014) was chosen to achieve this. The total strain based crack model uses a coaxial stress-strain concept where the stress-strain relationship is the same in both tension and compression in the elastic region, together with a smeared approach for the tension softening part of the stress-strain curve using fracture energy and a crack band width.

The total strain concept further assumes an injective (one to one) relationship between stress and strain, where the total strain field is taken as a combination of the concrete strain and the cracking strain (De Borst, 2002). This allows the constitutive behaviour of the concrete to be modelled separately from the cracking behaviour at the crack location. This means the strain due to crack opening is added to the total strains at a material point. Total strain models have been shown to work for various applications and are especially suited for serviceability and ultimate limit state analyses that are dominated by the cracking of concrete in the tensile regime (DIANA, 2014). The drawback of total strain models is that they cannot be combined with other constitutive models within the same material, although they can be combined with ambient influences (DIANA, 2014).

6.3.3. Material properties

One the main reasons for the lack of finite element models in literature for the cracking in plastic concrete is the difficulty in obtaining the material parameters needed as input values for a model. The parameters needed for a total strain crack model are the tensile strength (F_t), Young's modulus (E) and fracture energy (G_F), all as a function of time. For hardened concrete these parameters are normally determined by conducting tensile tests on several concrete samples. However, these type of tests present a much bigger challenge if conducted on fresh concrete samples, which is not as easy to grip and load as hardened concrete. This problem was overcome in this study by the development of a new tensile test setup suitable for the testing of plastic concrete. The details of the test setup are given in Section 3.2, while the results achieved are shown and discussed in Chapter 5.

Figures 5.20, 5.21 and 5.23 show the results at hourly intervals achieved at both 23 and 40°C for tensile strength (F_t), Young's modulus (E) and initial fracture energy (G_f) respectively. These material properties were tested at hourly intervals while the model was analysed at smaller time steps or intervals (mainly 20 minute time steps, although smaller time steps were also used). To obtain the material properties at these smaller time intervals as needed and used for model input values, there was linearly interpolated between the mentioned experimentally determined hourly material properties. Furthermore, since no tensile tests were conducted on plastic concrete at 0 hours, it was assumed that the values of the material properties at 0 hours were the same as determined at 1 hour.

It should further be mentioned that DIANA (2014) requires a choice of the several predefined tension softening curves for the total strain crack constitutive model. Figure 6.3 shows the tension softening curves available in DIANA (2014) that can be combined with ambient influences which is an important aspect exploited and discussed later for time dependency purposes. The linear tension softening curve (Figure 6.3.e) based on fracture energy which is smeared over a crack band width was chosen as this best represents the initial fracture energy values obtained during the experiments as shown in Figure 5.13 and discussed in the latter part of Section 5.2.1.

The crack band width was further chosen as a constant value of 5 mm, which is the width of the four node plane stress elements used in the model. This is acceptable for the release of the correct amount of fracture energy after cracking as long as the crack remains perfectly vertical or horizontal and does not skew. For skew cracks, it is better to use a crack band width equal to the square root of twice the area of the element (DIANA, 2014). Finally, the Poisson's ratio was chosen as nearly zero,

since no information is available on the Poisson's ratio of plastic concrete. This is acceptable since the measured vertical settlement and horizontal shrinkage strains as used in the model include the possible effect of Poisson's ratio.

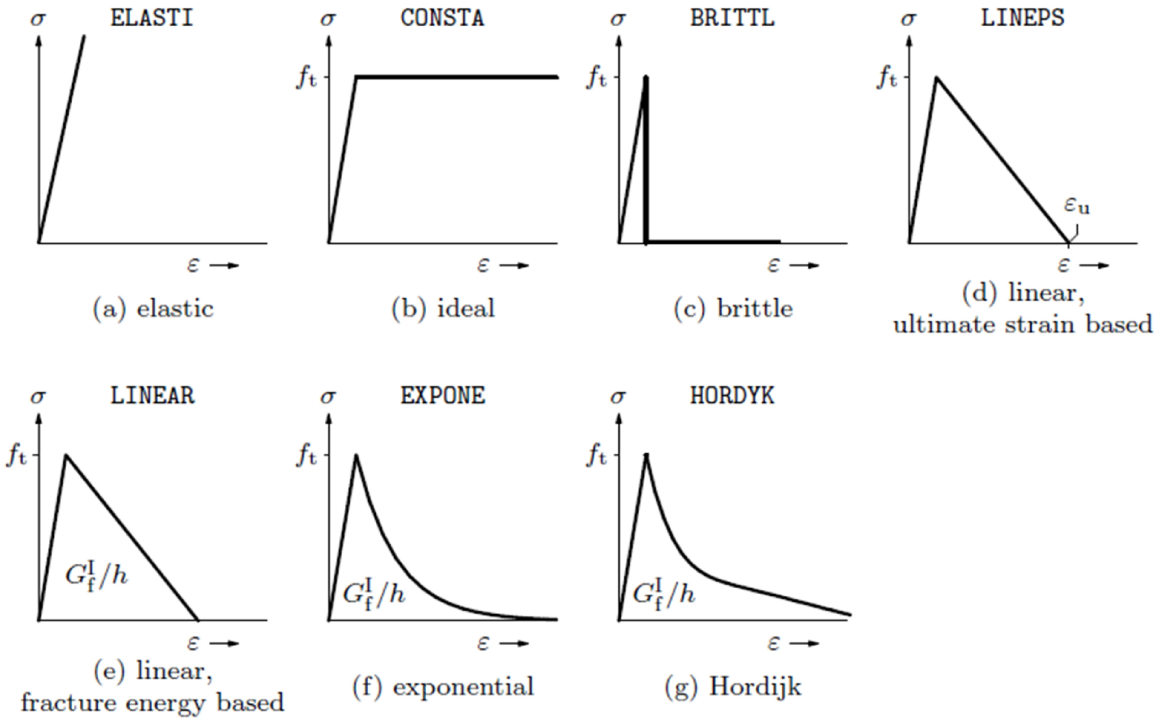

Figure 6.3. Predefined tension softening curves for the total strain crack model that are available in DIANA (2014) which can be combined with ambient influences.

6.3.4. Crack element layout

Figure 6.4 shows three different crack element layouts that were used for analyses. The first crack element layout is referred to as the full crack layout, since all plane stress elements were given cracking behaviour as shown in Figure 6.4 a). The second crack element layout is referred to as the singular crack layout since only the column of elements above the central triangular restraint were given crack behaviour as shown in Figure 6.4 b).

The third crack element layout is referred to as the selective crack layout, since only certain elements were given cracking behaviour as shown in Figure 6.4 c). The decision of which elements were allowed to crack was based on the typical cracks that were observed from the side during experiments with the shrinkage cracking mould on Mix C3 at Climate E2 as shown in Figure 6.5. The figure shows that aside from the obvious crack above the central restraint, smaller cracks also occurred just above the smaller triangular restraints as well as the region above the steel bar restraints. The location of the elements with cracking behaviour for the selective crack layout corresponds to these observed experimental cracks.

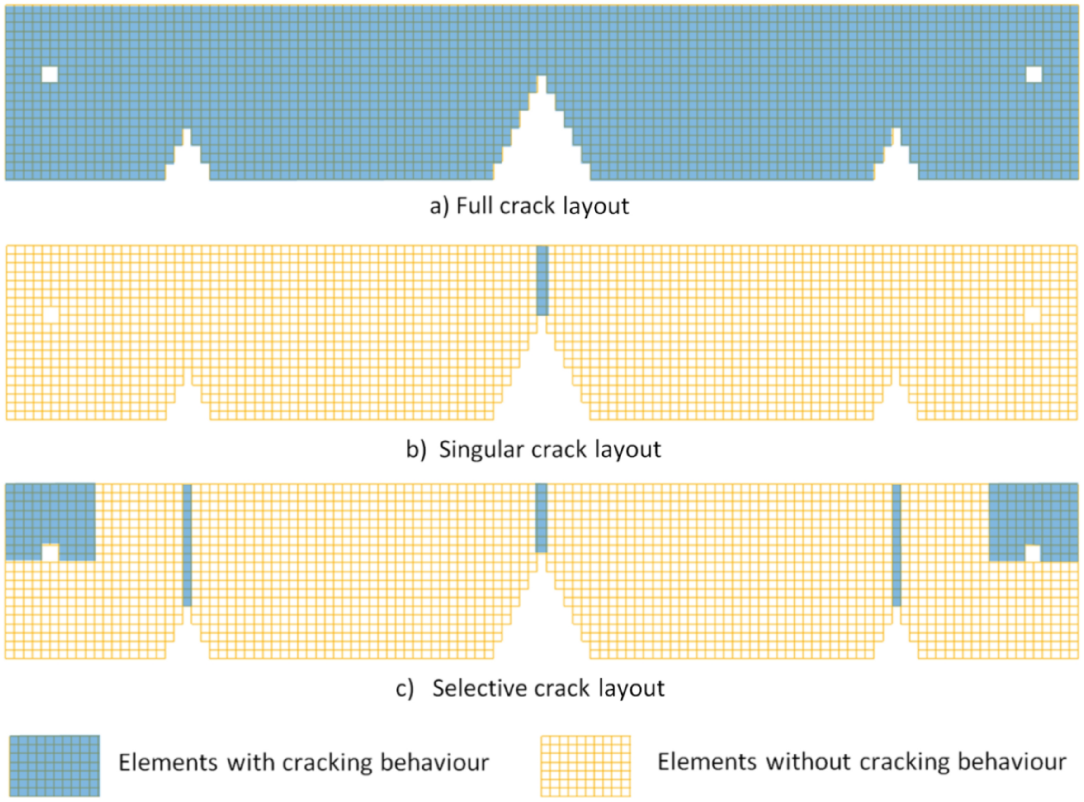

Figure 6.4. Finite element mesh layout showing the elements with crack material properties for: a) Full crack layout. b) Singular crack layout. c) Selective crack layout.

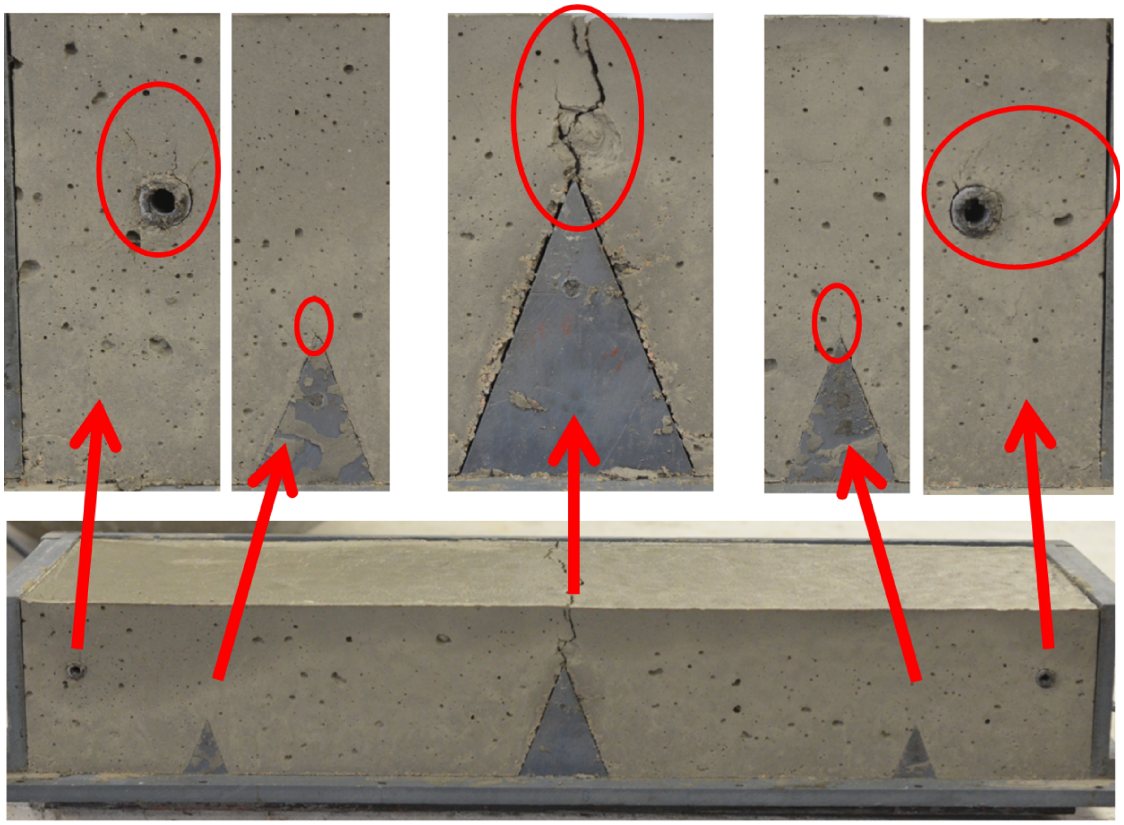

Figure 6.5. Images of typical cracks observed from the side during experiments with the shrinkage cracking mould for Mix C3 at Climate E2 around 2 hours after the final setting time.

6.3.5. Settlement and shrinkage

The settlement and shrinkage of plastic concrete act as the applied loads on a structure as for a traditional model. As mentioned in Section 6.1, the volume change of plastic concrete is anisotropic, meaning different magnitudes and rates of strain in both the vertical and horizontal directions. The shrinkage was modelled as a function of time using the discrete shrinkage function available in DIANA (2014). This shrinkage strain as specified at each specific time is added to the concrete strain which allows this discrete shrinkage function it to be used in conjunction with the total strain crack model (De Borst, 2002). The discrete shrinkage function also assumes isotropic shrinkage, meaning that shrinkage strains are the same in both the vertical and horizontal directions. However, the measured shrinkage in the experiments was only in the horizontal direction and hence the vertical shrinkage imposed by the discrete shrinkage function in the model is incorrect.

This is accounted for the by the method used to model the vertical settlement of the concrete. The settlement was modelled by gradually increasing the own weight of the elements with time to such an extent as to result in a deformation due to own weight that is equal to the experimentally measured vertical settlement. In DIANA (2014) this was achieved by changing the load factor applied to the gravitational acceleration used to calculated the own weight of the elements for each time interval. To account for the incorrect vertical shrinkage caused by the discrete shrinkage function as discussed in the previous paragraph the load factor responsible for the settlement due to own weight was calculated using the measured settlement strains minus the shrinkage stains as shown in Figures 6.6 and 6.7. These figures also show the measured settlement and shrinkage strains as well as the strain values at 20 minute intervals for the settlement and shrinkage as used for the model.

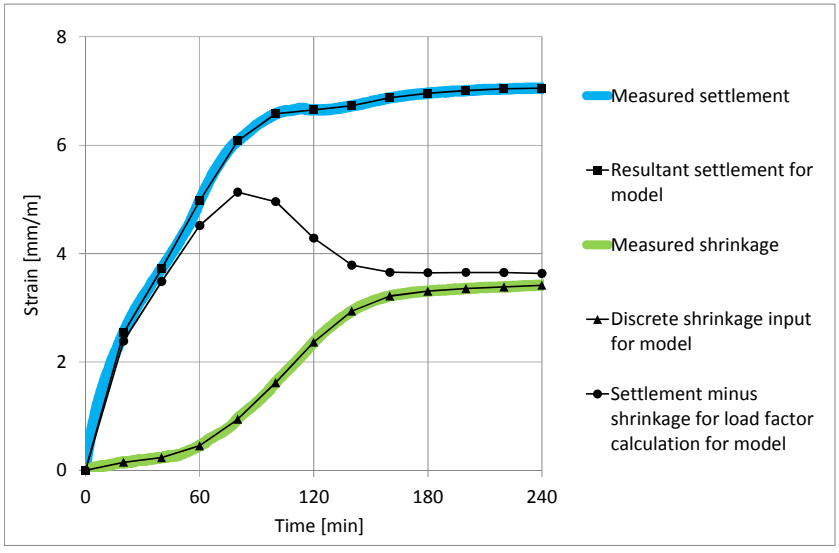

Figure 6.6. Settlement and shrinkage strains of Mix C3 at Climate E2 as measured and as used for the model.

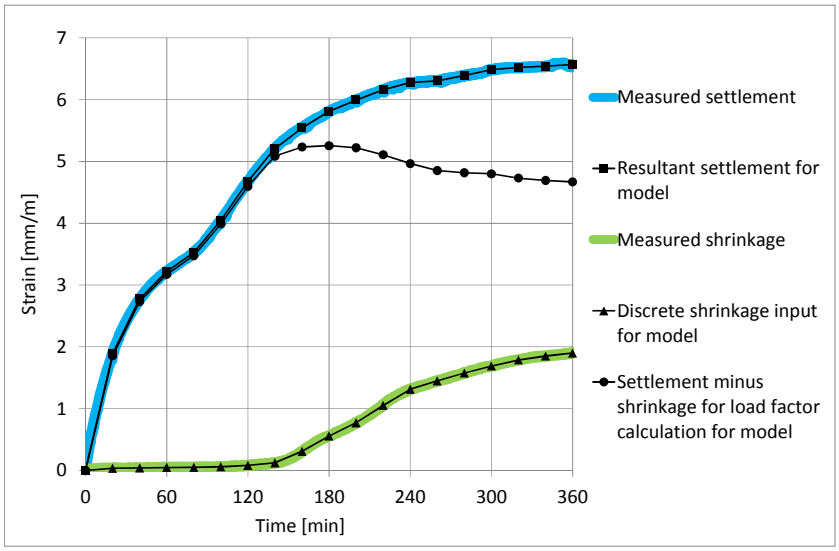

Figure 6.7. Settlement and shrinkage strains of Mix C3 at Climate N2 as measured and as used for the model.

The calculation of the load factor applied to the gravitational acceleration of the elements to give the needed settlement is illustrated in Figure 6.8. As shown in the figure the load factor is dependent on the magnitude of the settlement and shrinkage strains as well as on the Young's modulus of the concrete. It is therefore necessary to recalculate the load factor for each specific analysis where settlement strains, shrinkage strains or Young's modulus were varied to ensure that the correct settlement and shrinkage strains were applied during each analysis.

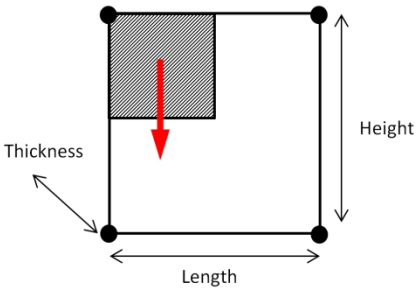

$$Force\ to\ node = density \times \frac{length}{2} \times \frac{thickness}{2} \times \frac{height}{2} \times gravity_{set-shr} \quad \text{(Eq. 6.1)}$$

$$Force\ to\ node = Strain_{set-shr} \times Young's\ Modulus \times \frac{length}{2} \times \frac{thickness}{2} \quad \text{(Eq. 6.2)}$$

$$Set\ (\text{Eq. 6.1}) = (\text{Eq. 6.2})$$

$$gravity_{set-shr} = \frac{Strain_{set-shr}\,(time) \times Young's\ Modulus(time)}{density \times height/2} \quad \text{(Eq. 6.3)}$$

$$Load\ factor\ (time) = \frac{gravity_{set-shr}\,(time)}{gravity_{normal}} \quad \text{(Eq. 6.4)}$$

Figure 6.8. Calculation of load factor applied to the gravitational acceleration to model the settlement of the concrete.

6.3.6. Time dependency

The material properties and volume change of plastic concrete is time dependent and needs to be accounted for in the model. The volume change is taken into account by directly specifying the shrinkage (discreet shrinkage function) and settlement (load factor applied to gravity/own weight of elements) as a function of time as explained in the previous section. The material properties needed for the total strain crack model can however not be directly changed with time in the current implementation of the model.

The implementation does however allow these material properties to change with variations in ambient (temperature) conditions (DIANA, 2014). This was exploited to also change the material properties with time by specifying the material properties needed for the total strain crack model (tensile strength, Young's modulus and fracture energy) at temperatures that corresponds to the time steps used in the analyses. A temperature load was then applied to all the elements, followed by changing the temperature load with time, which also changed the material properties to the appropriate values needed at each specific time step. With this method the needed material properties were changed with time to the values measured during tensile tests.

6.3.7. Analyses description

The model was executed using a physical non-linear time dependent analysis that employed an incremental-iterative procedure in a series of time steps. The time steps were increased in 20 minute increments up to 4 and 6 hours for the analyses at Climates E2 and N2 respectively. The material properties as well as settlement and shrinkage strain input values, as discussed in Sections 6.3.3 and 6.3.5, were also specified at 20 minute intervals.

It should be noted that for the analyses where either the full crack or selective crack layout, as shown in Figure 6.4, was implemented smaller time steps were required to prevent divergence of the iteration method used for the analysis. In these cases the material properties as well as settlement and shrinkage strains were specified at each of these smaller time steps.

The regular Newton-Raphson incremental-iteration procedure was used together with a tangent stiffness matrix, since this approached proved to be robust and stable for analyses with crack localisation and propagation (DIANA, 2014). Furthermore, an energy convergence criterion was used where convergence is reached in an iteration of a specific time step once the resultant energy variation relative to an equilibrium state is less than 0.00001.

6.4. Mesh sensitivity

The influence of mesh and therefore also element size on the results obtained with the finite element model was investigated by conducting three different analyses using element sizes of 5 x 5, 10 x 10 and 20 x 20 mm respectively as shown in Figure 6.9. For these analyses the singular crack layout as shown in Figure 6.4 was used, as this layout requires much less implementation and computational time compared to the full and selective crack layouts, while still providing appropriate results for investigating the sensitivity of the model to element size.

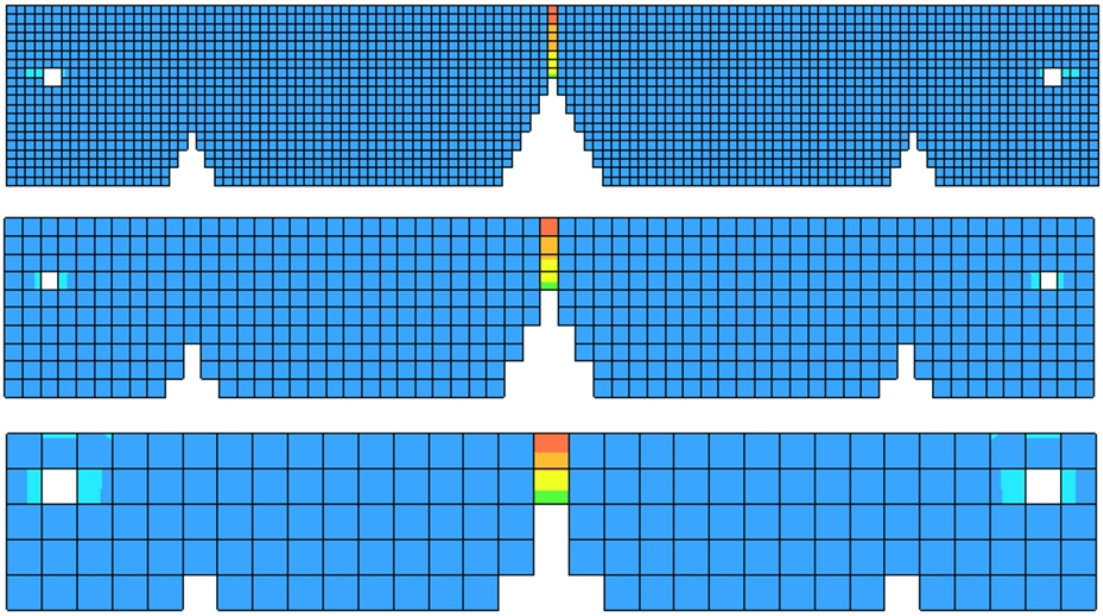

Figure 6.9. Finite element mesh layouts including indication of cracks above central restraint using three different element sizes of 5 x 5, 10 x 10 and 20 x 20 mm respectively.

The crack width results of the analyses using three different elements sizes for Mix C3 at both Climate N2 and E2 are shown in Figure 6.10. The crack width was calculated for each analysis as the maximum principal tensile strain of the top most element (at the concrete surface) above the central triangular restraint multiplied by the crack band width which was taken as the length of the element. The figure shows that as the elements become smaller, the results of crack width start to converge. This can be seen from the similar crack widths for the 5 x 5 and 10 x 10 mm elements while the crack width of the 20 x 20 mm elements are noticeably smaller at both climates. The results confirm that the size of the chosen 5 x 5 mm elements, as used for the majority of analyses, is small enough to give reliable results that are independent of element size.

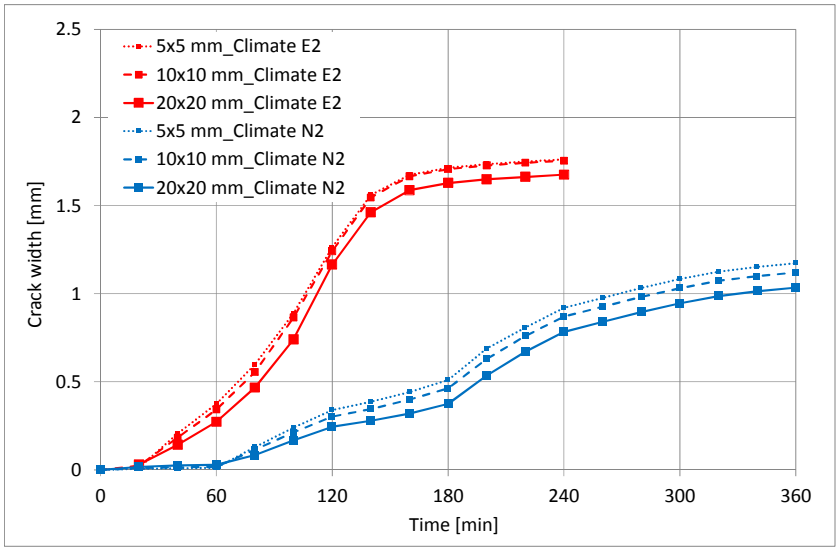

Figure 6.10. Influence of element size on the FEA results of Mix C3 at both Climates N2 and E2.

6.5. Model validation at extreme climate

The results of the FEA of Mix C3 at Climate E2, where the full crack layout was implemented, are shown in Figure 6.11. The figure shows the resultant displacements of the mesh in undeformed and deformed shape as well as the maximum principle tensile strain in the elements at progressive time steps in the analysis.

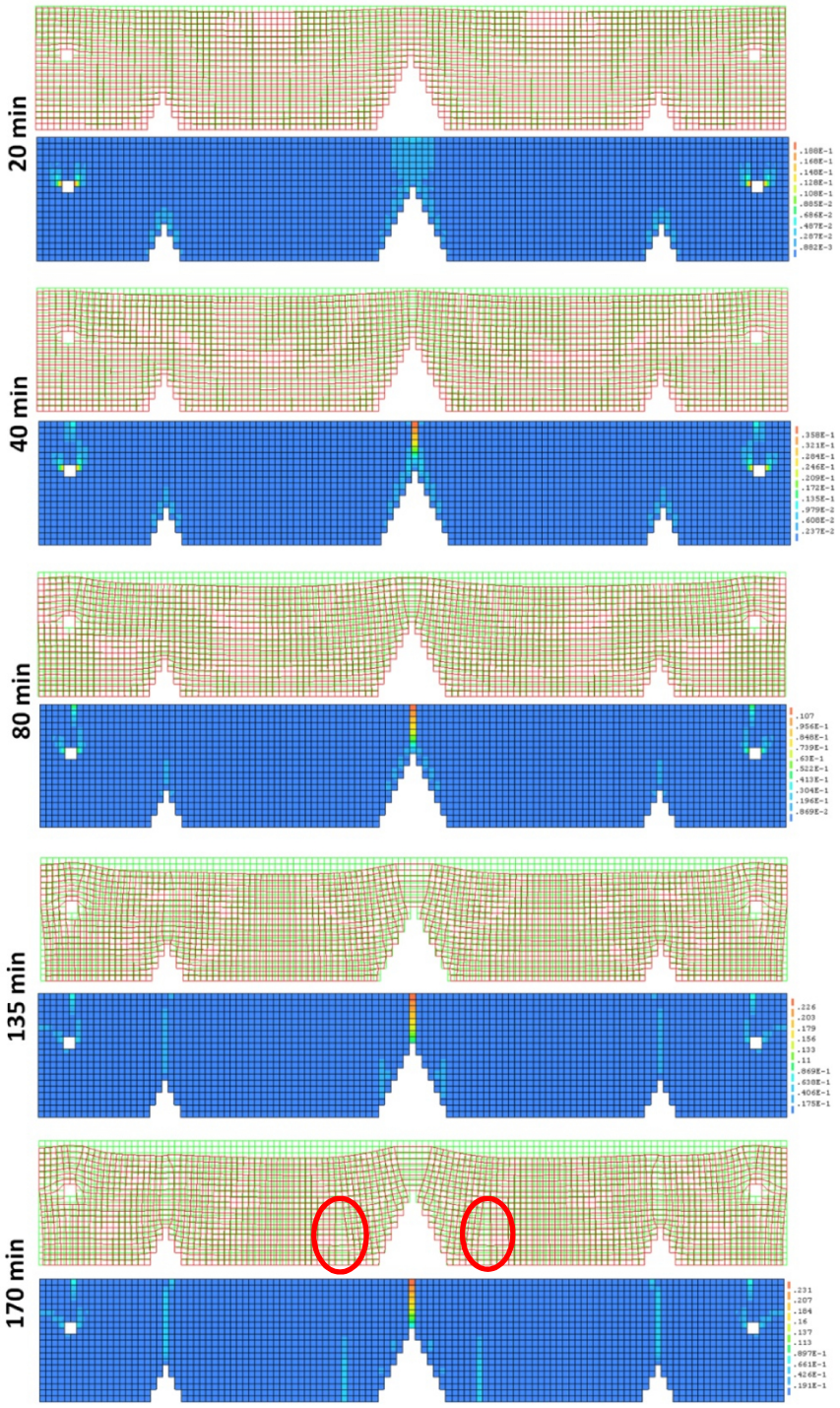

Figure 6.11. FEA results for full crack layout where all elements can crack for Mix C3 at Climate E2 showing the resultant displacement and maximum principal tensile strain at different times.

Figure 6.11 also shows various cracks, with the most notable and severe crack located above the central triangular restraint. Smaller cracks also occurred from the tip of the smaller triangular restraints upwards as well as around the steel bar restraint at both ends of the mould. This included two shear cracks starting from the sides of the steel bar as well as a tensile crack at the surface above the steel bar, similar to the plastic settlement cracks observed during experiments as discussed in Section 4.3.

Similar cracks were also observed during experiments with the shrinkage cracking mould on Mix C3 at Climate E2 as shown in Figure 6.5. The figure shows the typical cracks that were visible from the side of the mould with the Perspex cover removed at around 2 hours after the final setting time. The figure clearly shows the major crack above the central triangular restraint as well as the smaller cracks around the steel bars and smaller triangular restraints. Furthermore, the analysis also shows additional cracking next to the central triangular restraint which was not visible during experiments. These cracks next to the central triangular restraint became more severe as time progressed in the analysis as can be seen in Figure 6.11.

Figure 6.12 shows the results of crack width as obtained with FEA of Mix C3 at Climate E2. The figure also shows the experimental crack widths for each of the Mix C3 samples tested at Climate E2. The crack widths were determined as explained in Section 3.1.3. For the model to be validated as an accurate and appropriate representation of the cracking of plastic concrete, it needs to closely resemble the experimental results. The results can be evaluated and compared in terms of the final crack size, time of crack onset as well as the rate at which the cracking occurs.

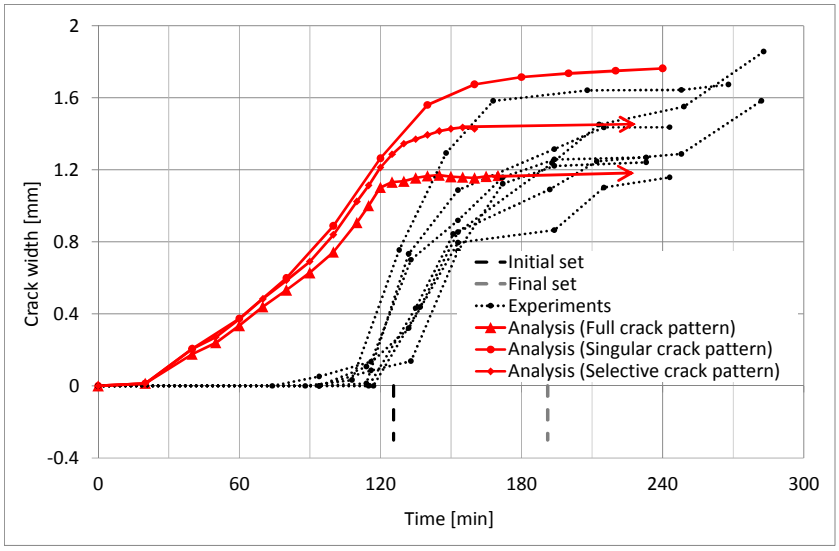

Figure 6.12. Crack width results obtained with FEA compared to crack width obtained during experiments with Mix C3 at Climate E2.

6.5.1. Final crack size

The final crack size is the most important of the three evaluation criteria as it gives an indication of the final cracking severity. Figure 6.12 shows that the final crack width obtained during the full crack layout analysis (solid red line with triangular markers) is similar to the cracks observed during experiments, although more towards the lower end or less severe cracks of the experiments. The reason the analysis results are more toward the lower end of the experimental results is because of the severity of cracks that formed at locations other than the main crack above the central restraint. Several of these cracks are more pronounced in the analysis (Figure 6.11) than what was observed during the experiments (Figure 6.5). This especially applies to the cracks that formed next to the central restraint during the analysis as indicated with the red circles in Figure 6.11.

The reason the cracks next to the central restraint are present in the analysis and not observed in the experiments is due to the assumption made that for the finite element model there is no adhesion and/or friction between the concrete and the mould sides. The incorporation of friction into the model would decrease the severity of these cracks. Especially since these cracks occurred rather late in the model long after the central main crack has formed and since the concrete has obtained some strength and therefore also increased friction at this stage. However, it was decided not to add friction to the model, as there is currently no information available regarding appropriate friction values and since these friction values are also time dependent which would over complicate an already complex time-dependent model.

As alternative to the incorporation of friction to the model, two additional crack layouts were used for analyses to account for cracks that formed at inappropriate locations such as next to the central restraint. For the first of these analysis, referred to as the singular crack layout analysis, only the column of elements above the central restraint were allowed to crack while for the second analysis, referred to as the selective crack layout analysis, only the elements around the steel bars and the smaller triangular restraints were allowed to crack as shown in Figure 6.5. The results of both these analyses are also shown in Figure 6.12. For the singular crack layout analysis the crack width results are towards the higher end of the experimental results. This is since all of the crack growth due to shrinkage and settlement is isolated at this single crack location. Furthermore, the results of the selective crack layout analysis give the best representation of the experiments and fit as can be expected between the results of the full and singular crack layout analyses.

From Figure 6.12 it can also be seen that the three different crack layout analyses are initially reasonably similar and only start to diverge at around 120 minutes, which is also the time in the analysis where, if allowed, significant crack growth started to occur at locations other that the crack above the central restraint. It should also be mentioned that for the full and selective crack layout analyses more time steps were needed to avoid divergence during the analysis. Furthermore, even with more time steps these analyses started to diverge once the crack growth above the central restraint started to stabilise, partly due to the widening of crack at other locations as well as the low amount of settlement and shrinkage active at that stage. For these reasons, it was decided to rather use the more stable singular crack layout for the majority of analyses to follow in this study.

6.5.2. Time of crack onset and rate of crack growth

In terms of the time of crack onset and rate of crack growth the analyses and the experiments do not compare as well as for the final crack size. The cracking during analyses occurred much earlier than during experiments, while once formed, the cracks widened at a much faster rate in the experiments than in the analyses. There are two reasons for the earlier and slower rate of cracking in the analyses compared to the experiments.

The first reason is the smaller strain capacity of the concrete in the analyses compared to the much higher strain capacity measured during experiments. This is especially noticeable for the first few hours while the concrete is still highly plastic as can be seen in Figure 6.13. The figure shows the measured strain capacity during experiments as well as the strain capacity used as input values for the analyses at both 23 and 40°C.

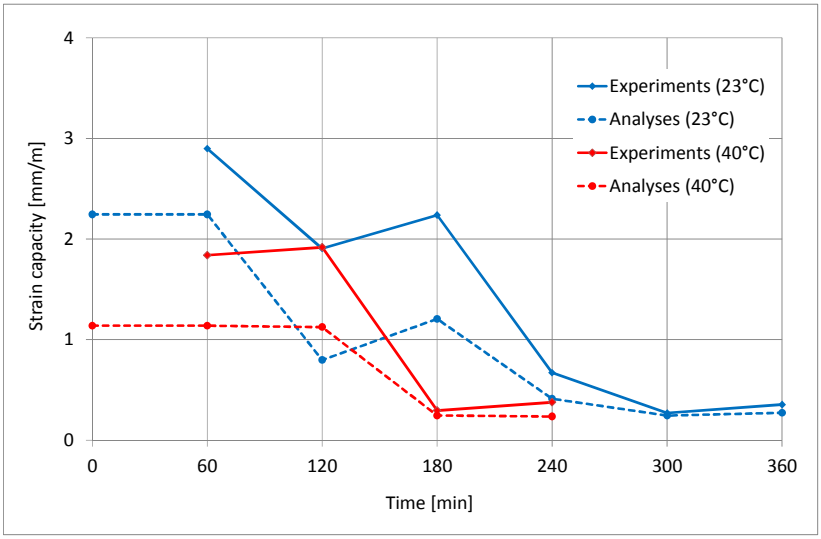

Figure 6.13. Strain capacity obtained with experiments compared to strain capacity used for analysis for Mix C3 at both extreme and normal climates.

The reason for the smaller strain capacity for the analyses is because of the 30 - 70 % method used to determine the Young's modulus of the plastic concrete during the tensile testing as illustrated in Figure 6.14. The figure illustrates the determination of the strain capacity as used for the analysis and linked to the 30 - 70 % method to determine the Young's modulus (indicated in red) as well as the actual strain capacity of the concrete from experiments (indicated in black).

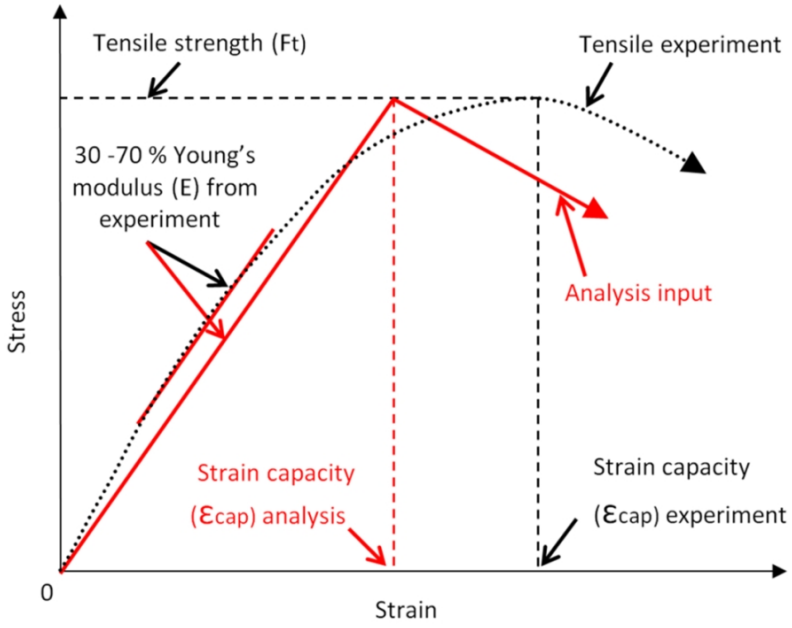

Figure 6.14. Illustration of the determination of the strain capacity as used for analyses (indicated in red) as well as the actual strain capacity of the concrete from experiments (indicated in black).

The Young's modulus is used together with the results of tensile strength, also obtained during tensile testing, as input values for the analyses. The analyses use these input values to calculate the strain capacity by assuming a linear elastic material behaviour in the ascending part of the stress-strain curve. This assumption of linear elastic material behaviour does not account for the significant non-linear strain or strain capacity that especially the still highly plastic concrete exhibits before failure or cracking at maximum tensile strength. This resulted in the analyses predicting earlier cracks than what was observed during experiments. This was confirmed by conducting an analysis where the input values of Young's modulus were halved as shown in Figure 6.15. The figure shows that the cracking started later in terms of time with a lower Young's modulus which in this case represents a lower strain capacity.

It should be noted that any traditional method for determining the Young's modulus as discussed in Section 5.2.1 would underestimate the strain capacity. A more appropriate method to determine the Young's modulus, that will give the same strain capacity for both analyses and experiments, is a secant modulus method that fits a straight line between 0 and 100 % of the ultimate strength.

However, this method does not capture the initial near linear elastic part or the final non-linear part of the ascending stress-strain curve. In this regard, the most appropriate method to ensure that the correct strain capacity is modelled is to use a bi-linear or even multi-linear approximation of the ascending portion of the stress-strain curve as illustrated in Figure 6.16. However, in the current implementation of the model any multi-linear stress-strain curve, especially with regards to the ascending portion, cannot be combined with the method used to model the time-dependency of the material properties as discussed in Section 6.3.6. For these reasons the 30 - 70 % method was chosen as a compromise and used to determine the Young's modulus for the analyses.

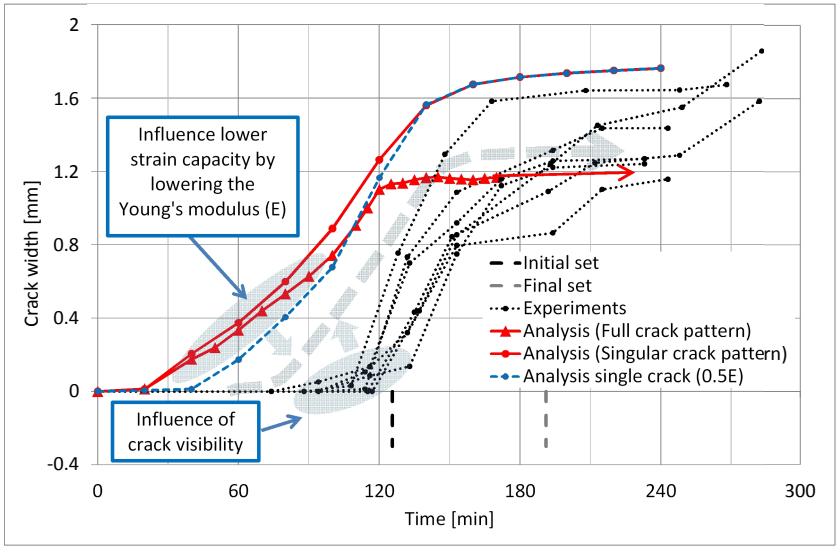

Figure 6.15. Influence of strain capacity and crack visibility on the crack width results obtained with FEA compared to crack width obtained during experiments with Mix C3 at Climate E2.

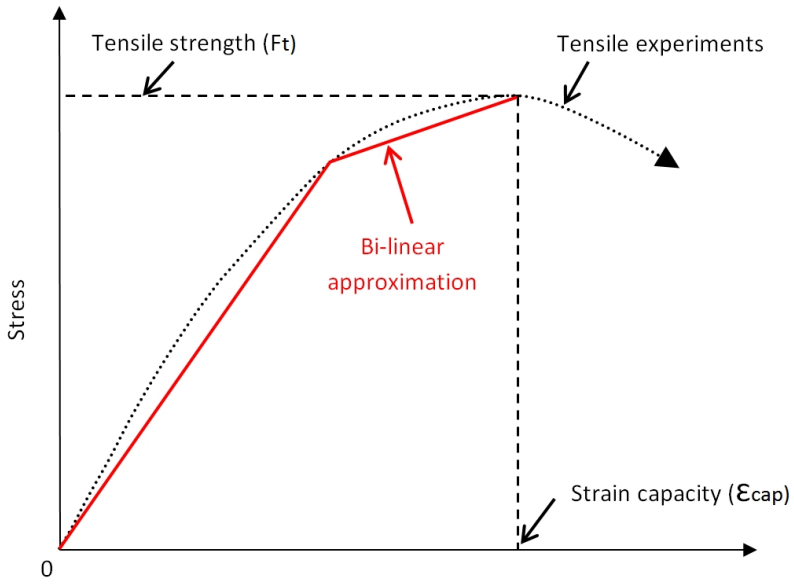

Figure 6.16. Illustration of a bi-linear approximation (indicated in red) of the ascending portion of the experimental stress-strain curve (indicated in black).

The second reason for the earlier and slower rate of cracking in the model compared to the experiments is the difficulty in observing and measuring cracks on the surface of plastic concrete during experiments. The earlier the cracks occur and the smaller the crack, the less visible the crack and the more difficult to measure, especially within the first few hours where the cracks are often still filled with bleed water. Furthermore, as discussed in Section 4.3, these cracks can even be present beneath the concrete surface and therefore not be visible if viewed from above. This means that the experimental results presented only show the onset of cracking once the cracks were clearly visible with the naked eye and therefore do not include any possible preceding micro cracking. The analysis can however capture the most insignificant crack. This resulted in the experimental results showing slightly delayed and less severe onset of cracking compared to the analyses.

If both these reasons of strain capacity and crack visibility are taken into account, the difference between the time of crack onset and rate of cracking between the analyses and the experiments become much less as illustrated in Figure 6.15.

6.6. Model validation at normal climate

Figure 6.17 shows the experimental crack width results as well as the crack width as obtained with a full and singular crack layout analyses for Mix C3 at Climate N2. Furthermore, although the size and crack onset of the modelled cracks at Climate N2 are much smaller and start later with time than for the full crack layout analysis at Climate E2, the general location and cracking behaviour at Climate N2 is similar to that observed and shown for Climate E2 in Figure 6.11.

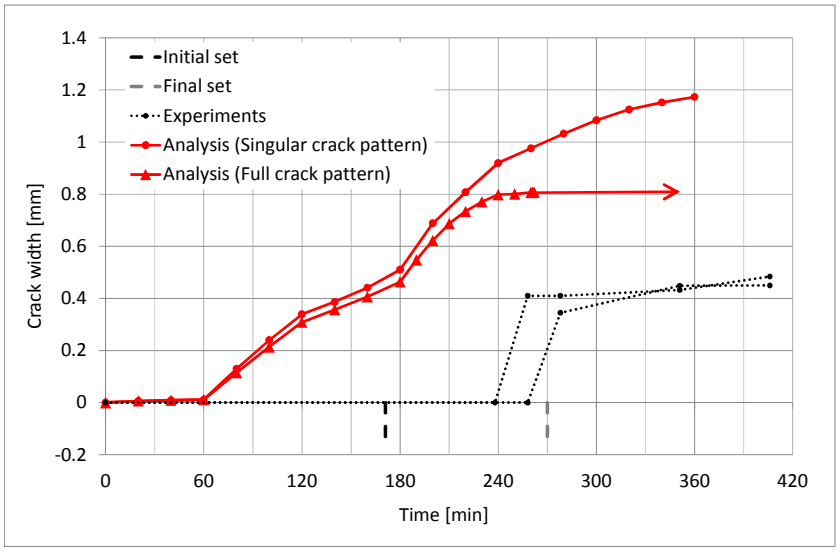

Figure 6.17. Crack width results obtained with FEA compared to crack width results obtained during experiments with Mix C3 at Climate N2.

6.6.1. Final crack size

Figure 6.17 shows that the final sizes of the cracks in the analyses at Climate N2 are more than twice the sizes of the cracks observed during experiments. The main reason for this significant difference between the experimental and analyses results is the size discrepancy between interior and surface cracks as observed during experiments and discussed in Section 4.4.3. This is the same reason for the poor correlation between the analytical cracking behaviour and the experimental cracking as discussed in Section 5.3.2. In short, the abundance of bleed water on the concrete surface at Climate N2 resulted in much smaller observed (also measured) surface cracks than the size of the actual interior crack below the concrete surface.

Another reason for the poor correlation between the analyses and experiments at Climate N2 is the relaxation of stresses in the plastic concrete as identified in Section 5.2.9 during the cyclic tensile testing of plastic concrete. This means that as stresses are induced in the plastic concrete, part of the stress can be reduced or relaxed with time. No literature could be found on the relaxation of plastic concrete and the cyclic tests conducted are not enough to properly quantify the relaxation effect of plastic concrete. The only clear conclusion that can be drawn from the cyclic tests in terms of relaxation is that the more plastic the concrete the more pronounced the effect of relaxation. This is then also the reason why relaxation is only considered to be significant for Climate N2 and not Climate E2, since at Climate E2 the stresses developing in the concrete as well as the setting and hardening of the concrete are too rapid to allow ample time for relaxation to take effect.

The appropriate approach to account for this relaxation of stresses in the finite element model is to include a time-dependent constitutive material model that lowers the Young's modulus of the material with time such as visco-elasticity. This also requires tensile relaxation testing of plastic concrete where the effect of relaxation is quantified. Since no such tests were conducted and since the addition of more time-dependency in an already complex time-dependent model is problematic, a more pragmatic approach to model the possible effect of relaxation was followed.

The approach consisted of lowering the settlement and shrinkage strains used as input values during the analysis. This is not unrealistic since relaxation lowers the stresses induced by the settlement and shrinkage strains, and if relaxation cannot be directly accounted for in the model an indirect method to lower the stresses is to lower the settlement and shrinkage strains.

With this in mind, analyses were performed where the input values for settlement and shrinkage strains were halved to act as a rather extreme simulation of the possible effect of relaxation on the cracking behaviour of plastic concrete. The results of these analyses (full and singular crack layout analyses), together with the results of the original unchanged analyses and experiments are shown in Figure 6.18. The figure shows that if relaxation is taken into account by lowering the settlement and shrinkage strains the results of the analyses are closer to the experimental results. However, these analyses were only performed to provide an indication of the possible exaggerated effect of relaxation on the cracking of plastic concrete and more work needs to be done to firstly quantify and secondly to model the effect of relaxation on the cracking behaviour of plastic concrete.

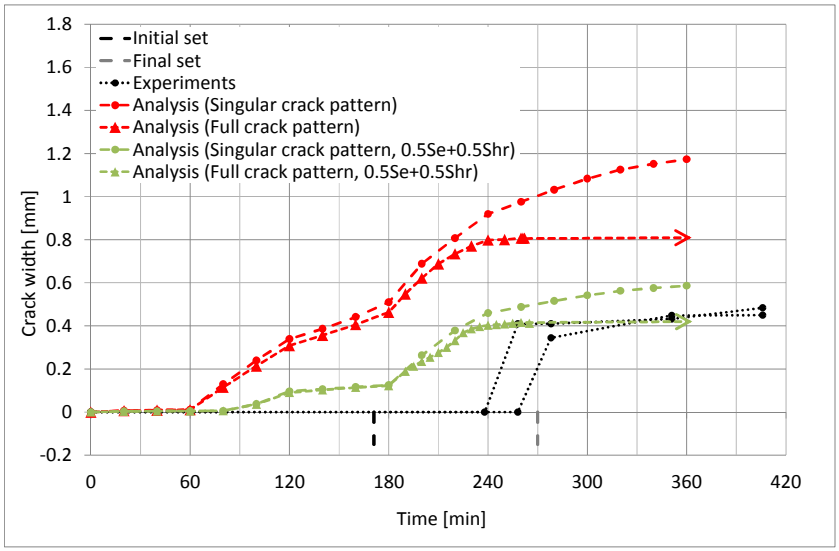

Figure 6.18. Influence of possible relaxation of stresses in plastic concrete (by halving the settlement and shrinkage strains) on the crack width results obtained with FEA compared to crack width obtained during experiments with Mix C3 at Climate N2.

6.6.2. Time of crack onset and rate of crack growth

The results of Figure 6.17 also show the crack onset much earlier in the analyses compared to the experiments, while the rate of crack growth is much faster in the experiments. The reasons for this can be due to the size discrepancy between interior and surface cracks during experiments as well as the effect of relaxation as discussed in the previous section.

In addition, the smaller strain capacity used in the analyses compared to the experiments as well as the poor visibility of cracks while the concrete is still highly plastic as discussed in Section 6.5.1 can also be reasons for the difference between the analyses and experimental results. If all of these factors are taken into account the difference between experimental and analyses results become much less as illustrated in Figure 6.19.

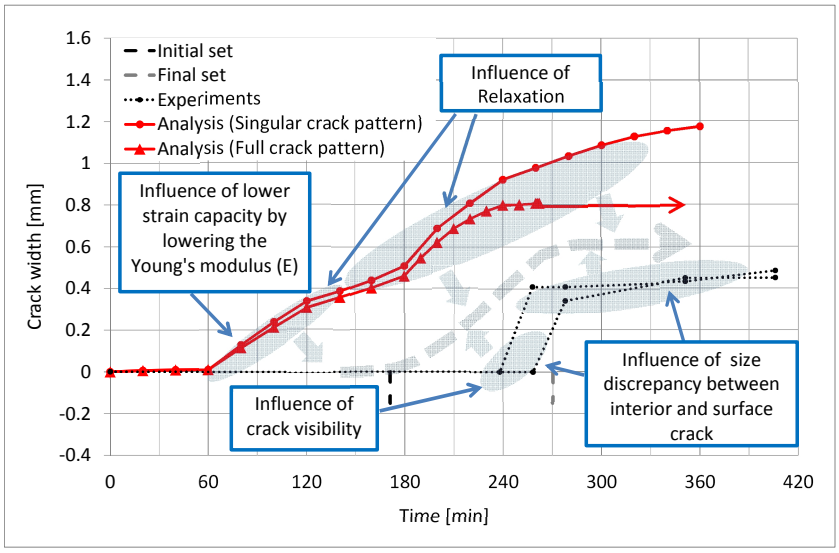

Figure 6.19. Influence of relaxation, size discrepancy between interior and surface cracks during experiments, strain capacity and crack visibility on the crack width results obtained with FEA compared to crack width obtained during experiments with Mix C3 at Climate N2.

6.7. Parameter study

A parameter study was conducted to investigate the influence of variable input values on the results obtained with the model. The input parameters investigated consist of both material properties as well as settlement and shrinkage strains. The material properties are tensile strength, Young's modulus and initial fracture energy. During each of the analyses conducted for the parameter study, only the applicable parameter (material property, settlement strain or shrinkage strain) was varied while all the other parameters were not changed from the original input values. This allows the influence of a specific parameter to be investigated. Furthermore, only the results of the parameter study at Climate N2 and not Climate E2 are presented since it is easier to distinguish between the influence of settlement and shrinkage strain at Climate N2. This is acceptable, especially since the parameter study at Climate E2 showed similar trends compared to the parameter study at Climate N2.

6.7.1. Material properties

Figures 6.20 to 6.22 show how the crack width results obtained with FEA of Mix C3 at Climate N2 are influenced by varying the tensile strength, Young's modulus and fracture energy respectively. Each of these material properties were varied by respectively using 25 %, 50 %, 200 % and 400 % of the original input values as determined with the tensile experiments. For tensile strength and Young's modulus, as shown in Figures 6.20 and 6.21 respectively, the variation of input values mainly influences the time of crack onset and rate of cracking. The larger the tensile strength and the lower the Young's modulus, the later the onset of cracking, but also the greater the rate of

cracking once initiated. The opposite is also true, where the smaller the tensile strength and the greater the Young's modulus, the earlier the onset of cracking and the lower the rate of cracking once initiated. The results also suggest that decreasing the Young's modulus and increasing the tensile strength has a more significant influence on the results than increasing the Young's modulus and decreasing the tensile strength respectively.

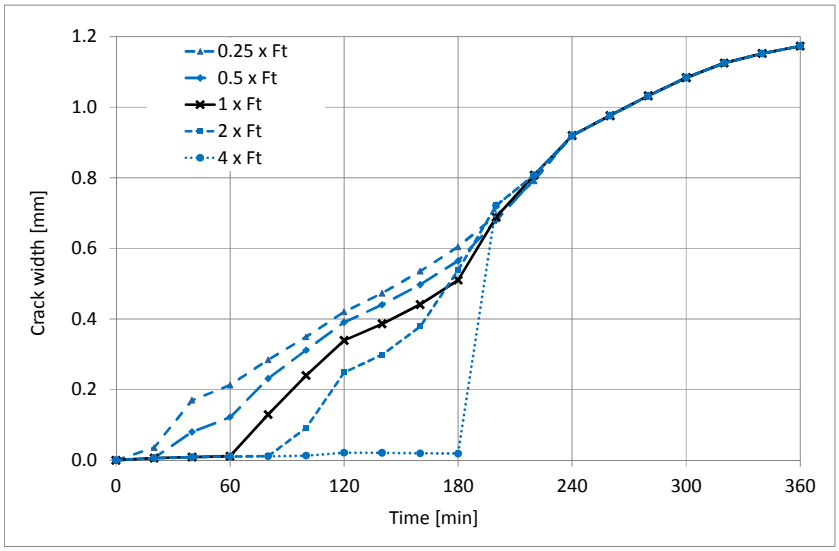

Figure 6.20. Influence of varying the tensile strength (Ft) on the crack width results obtained with FEA of Mix C3 at Climate N2.

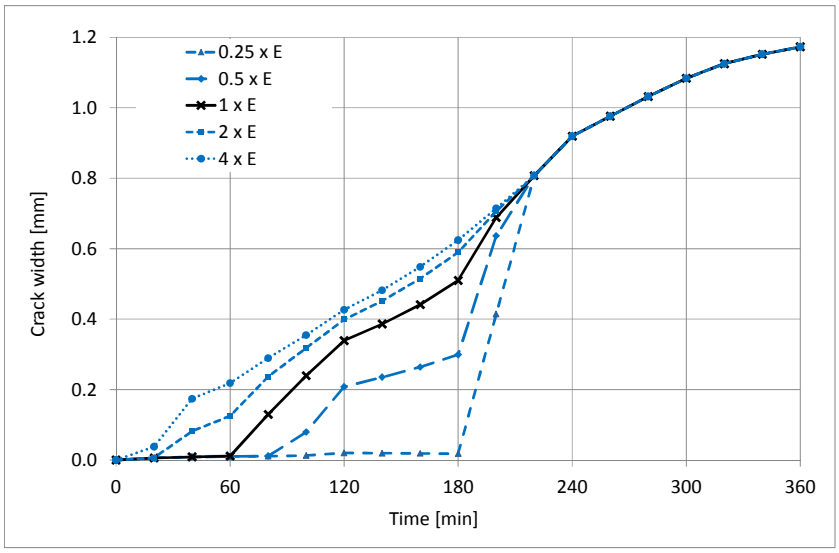

Figure 6.21. Influence of varying the Young's modulus (E) on the crack width results obtained with FEA of Mix C3 at Climate N2.

It should also be mentioned that changing the input values of Young's modulus and tensile strength for the analyses has some physical meaning as this represents a change in the strain capacity of the concrete, which as shown in Figure 6.13 has lower values in the analyses compared to experimental measurements. This is one of main reasons why the onset of cracking as predicted by the analyses

does not correspond to experiments. This means the larger the tensile strength and the lower the Young's modulus, the higher the strain capacity of the concrete in the analyses and therefore the later the onset of cracking, which improves the correlation between the experimental and analyses results as illustrated in Figures 6.15 and 6.19.

The reasons for the lower strain capacity in the analyses compared to the experiments are the method used to determine the Young's modulus as discussed in Section 6.5.2 as well as possibly the displacement rate at which the tensile tests were conducted. The latter would influence the magnitude of both the Young's modulus and tensile strength. However, this requires further investigation and does not form part of this study.

For fracture energy, as shown in Figure 6.22, the variation of input values mainly influences the rate of cracking and not the time of crack onset. The lower the fracture energy the greater the initial rate of cracking but also the lower the later rate of cracking and vice versa. However, the time at which cracking starts is not influenced by the fracture energy, which can be expected since fracture energy is essentially a post-cracking material property.

The results also suggest that a decrease in fracture energy has a more significant influence than an increase in the fracture energy. In fact, an increase in fracture energy has a negligible influence on the results. This indicates that the use of the initial fracture energy instead of the total fracture energy in the model as discussed in Sections 5.2.1 and 6.3.3 does not significantly influence the results obtained with the model.

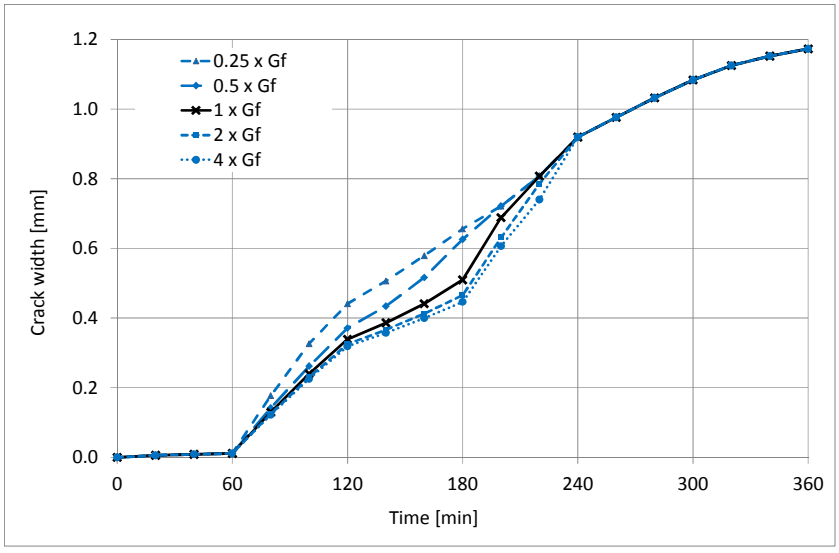

Figure 6.22. Influence of varying the fracture energy (Gf) on the crack width results obtained with FEA of Mix C3 at Climate N2.

Finally, the results of the parameter study for all three material properties show that the final size and behaviour of the crack from 240 to 360 minutes are not influenced by variations in material properties. The input parameters that govern the final size and behaviour of the cracks in the model are discussed in the next section.

6.7.2. Settlement and shrinkage

Figures 6.23 and 6.24 shows the influence of varying the settlement and shrinkage strains respectively on the crack width results obtained with the FEA of Mix C3 at Climate N2. Each of these strains was varied by respectively using 50 %, 75 %, 150 % and 200 % of the original input strain as determined by the experiments.

For settlement strain, as shown in Figure 6.23, the variation of input values influences the time of crack onset, rate of cracking as well as the final crack size. The influence of varying the settlement strain is only up to around 240 minutes, after which the increase of settlement strain becomes negligible. The greater the settlement, the earlier the cracking starts as well as the greater the initial rate of the cracking. More importantly, the greater the settlement, the larger the final crack size at 360 minutes. This shows the important role of plastic settlement cracking in not only inducing cracking but also aggravating the severity of the cracking as discussed in Section 4.5.5.

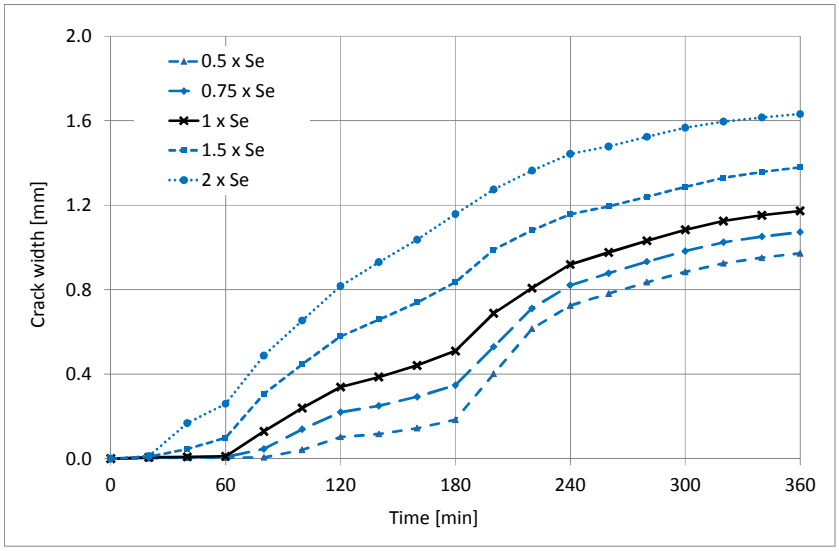

Figure 6.23. Influence of varying the settlement (Se) strain on the crack width results obtained with FEA of Mix C3 at Climate N2.

For shrinkage strain, as shown in Figure 6.24, the variation of input values influences mainly the rate of the cracking once shrinkage becomes significant at around 140 minutes as well as the size of the final crack at 360 minutes. The time of crack onset is not influenced by the variation of the shrinkage strain, which can be expected since the shrinkage only becomes significant long after the crack has

been induced by plastic settlement cracking. The greater the shrinkage the greater the rate of cracking once significant shrinkage starts at around 120 minutes as well as the size of the final crack at 360 minutes.

Finally, the parameter study on both settlement and shrinkage strains indicate that, the size of the final crack is determined by the amount of settlement and shrinkage, while the material properties discussed in the previous section have no effect on the final crack size.

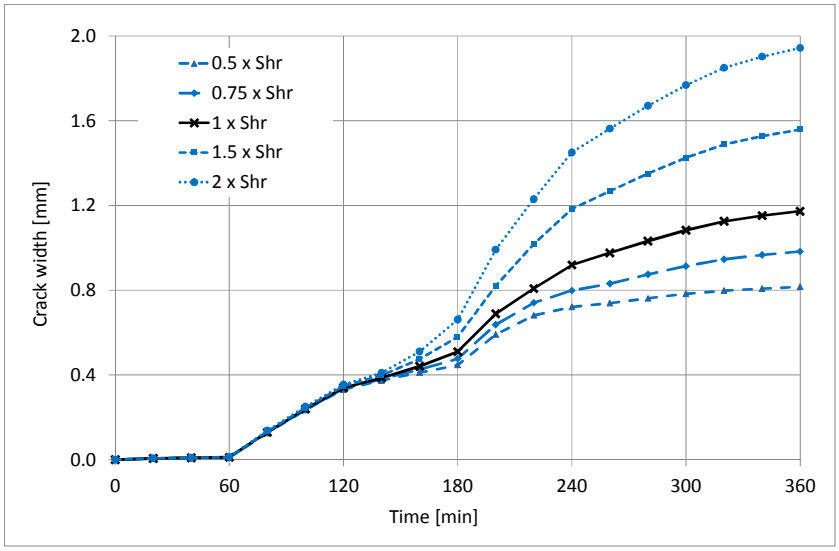

Figure 6.24. Influence of varying the shrinkage strain (Shr) on the crack width results obtained with FEA of Mix C3 at Climate N2.

6.8. Application of model to large scale example

The finite element model discussed in this chapter can also be used to evaluate the severity and potential for the cracking of plastic concrete in large scale concrete elements more commonly found in practice. As example of a possible application of the model, an analysis was conducted of a 100 mm thick concrete slab on ground that contains a single layer of steel reinforcing at a spacing of 200 mm and cover depth of 15 mm.

Only a unit width (1 meter) of the slab was modelled as this is representative of the entire slab. The boundary conditions at both ends were fixed against translation in the x-direction to simulate a slab with much greater width using symmetry. Furthermore, to investigate the influence of cover depth, two additional analyses were also conducted where the cover depth to the steel bars was increased to 30 and 45 mm respectively.

Only the elements above and below the steel bars were given crack material properties. These crack elements were 5 x 5 mm in size while the size of the rests of the elements gradually increased in size towards the middle region between steel bars. All the other aspects such as input values of material properties, shrinkage and settlement as well as the boundary conditions and the use of spring elements were applied similarly to the model discussed in Section 6.3 for Mix C3 at Climate E2.

Figure 6.25 shows a typical output of maximum tensile strain from the analysis of the concrete floor slab at 240 minutes. The figure also shows the layout of the mesh as well as the location of the reinforcing steel bars and the typical cracks that formed above and below the steel bars.

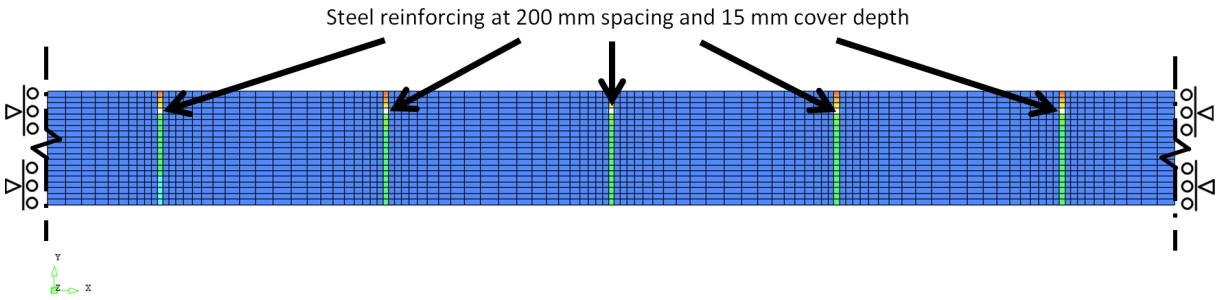

Figure 6.25. Layout of finite element mesh of large scale concrete floor slab, showing the location of steel bars as well as the typical cracks that occurred above and below the steel bars during an analysis.

Figure 6.26 shows the results of crack width at the top most surface elements above the steel bars as well as the bottom most elements below the steel bars for the analyses at the three chosen cover depths. It should be noted that the crack behaviour at all five steel bars locations was similar. The results indicate that the cracks above the steel bars are more severe and also occur almost immediately, mainly due to plastic settlement, compared to the cracks below the steel bars which are much smaller and only start after 100 minutes. The results also show that the smaller the cover depth the more severe the cracking and also the earlier cracking starts, which once again highlights the significant influence of plastic settlement cracking on plastic shrinkage cracking.

Finally, the results also indicate that the model can be a helpful tool not only to determine the severity of plastic cracking, but also to investigate the influence of various influencing factors on the severity of cracking without the need to perform timely experimental tests. These influencing factors can include aspects such as: cover depth, spacing of steel, different reinforcing steel layouts, depth of concrete elements, different climates etc.

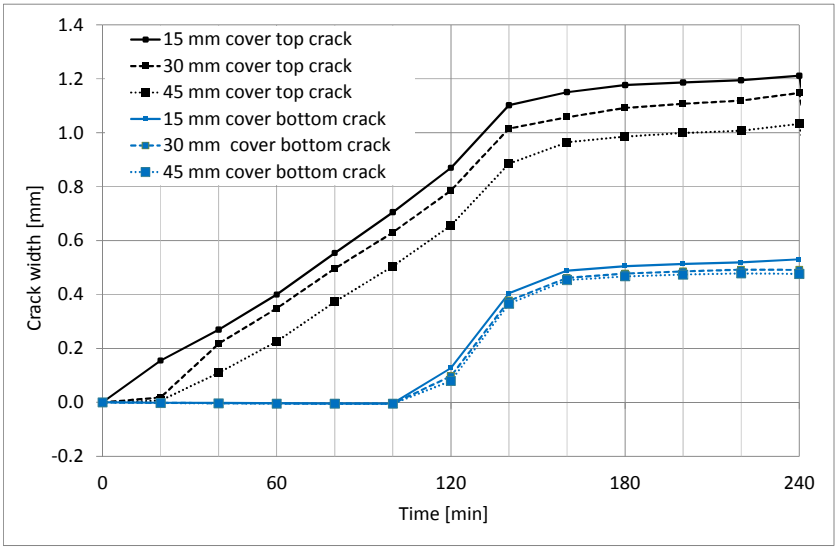

Figure 6.26. FEA results of crack width at the top most surface element above steel bars as well as the bottom most element below steel bars at a 15, 30 and 45 mm cover depth respectively.

6.9. Conclusions

This chapter introduces a finite element model that can simulate the cracking behaviour of plastic concrete. The model utilises a smeared rotating crack constitutive material model that uses fracture energy and a crack band width for crack propagation. All the material properties and volume change of the plastic concrete were changed with time while the model was solved using a physical non-linear time dependent analysis that employed an incremental-iterative solution procedure in a series of time steps. The following significant conclusions can be drawn from this chapter:

- The model gives an adequate representation of the cracking behaviour of plastic concrete for extreme climates with high evaporation rates where especially the size of the final crack is in good agreement with experimental results. However, the crack results of the model at less severe (normal) climates are significantly larger compared to the experimental results. The reasons for this are the size discrepancy between the interior and surface cracks during experiments as well as the relaxation of stresses in plastic concrete that were not accounted for in the model. Similar conclusions were drawn in Section 5.3.2 where the analytical cracking behaviour was compared to the experimental results.

- The parameter study showed that the tensile strength and Young's modulus mainly influences the time of crack onset and rate of cracking, where a greater tensile strength and a lower Young's modulus delays the onset of cracking, but increases the rate of cracking once initiated and vice versa. This is also one of the reasons for the predicted onset of cracking in the model to

be earlier than observed during experiments, since the method of determining the Young's modulus resulted in a lower strain capacity in the analysis than for the experiments which resulted in the earlier onset of cracking for the model. The second reason for the early prediction of crack onset for the model is the difficulty in observing and measuring cracks on plastic concrete during the experiments. The parameter study also showed that the fracture energy only slightly influences the rate of cracking and does not influence the time of crack onset. Finally, none of these three material properties influences the final size of the crack.

- The parameter study showed that a decrease in settlement strain decreases the size and rate of cracking as well as delays the onset of cracking and vice versa, while a decrease in shrinkage strain decreases the size and rate of cracking and vice versa, but does not influence the onset of cracking. This highlights the important role of plastic settlement cracking in not only inducing cracking but also aggravating the severity of the cracking. Finally, both the settlement and shrinkage strains significantly influence and therefore govern the size of the final crack.

- The model was successfully applied to a large scale example of a concrete slab containing steel bars, indicating that the model can be a helpful tool not only to determine the severity of plastic cracking, but also investigate the influence of various influencing factors on the severity of plastic cracking without the need to perform timely experimental tests.

Chapter 7. Conclusions

This study investigates the cracking of plastic concrete in slab-like elements and consists of a thorough background study, experiments on the cracking and tensile behaviour of plastic concrete as well as the modelling of plastic concrete. The main objectives of this study were to fundamentally understand both plastic settlement and plastic shrinkage cracking of concrete individually and combined as well as determine the tensile material properties of plastic concrete. In addition, the final objective was to develop a model that can simulate the cracking of plastic concrete. The significant conclusions that can be drawn from this study are given in bullet form in the following sections.

7.1. Plastic settlement cracking

- Pure plastic settlement cracking forms three distinctly different types of defects. The first two are classified as plastic settlement cracks and includes tensile cracks at the surface and shear induced cracks beneath the concrete surface near the restraint (reinforcing steel and/or non-uniform slab depth). The third defect is a water pocket that forms beneath the restraint (only for reinforcing steel).
- Plastic settlement cracks are not always visible at the concrete surface, indicating that these cracks may be present in concrete elements even if not initially visible at the surface. In addition, these cracks may be present even if all evaporation is prevented through curing practices. If these cracks are not closed by techniques such as the re-vibration of concrete, they form weak spots for future crack growth.
- The surface plastic settlement cracks have a multiple crack pattern and not a single, isolated crack. This provides important information regarding the behaviour and appearance of plastic settlement cracks which is helpful during the practical identification of these cracks.

7.2. Plastic shrinkage cracking

- Plastic concrete can relieve the capillary pressure build-up through vertical settlement/bleeding, horizontal shrinkage and/or cracking. The concrete first tends to relieve the pressure by increasing only the vertical settlement which relieves the pressure by forcing additional bleed water to the surface. Once the pressure can no longer be sufficiently relieved by additional vertical settlement, the concrete starts to shrink horizontally to relieve the pressure. Plastic

shrinkage cracking only occur as a form of pressure relief after both additional vertical settlement and horizontal shrinkage have started.

- The shrinkage cracking mould as used in this study and based on the layout proposed by ASTM C1579 (2006) does not result in pure plastic shrinkage cracking, but rather in plastic shrinkage cracking induced by differential settlement or plastic settlement cracking. This mould is not appropriate for testing where the influence of plastic settlement cracking is not wanted.
- Pure plastic shrinkage cracking was observed in modified shrinkage cracking moulds with no potential for plastic settlement cracking near the centre and can be described as a singular, well defined crack that normally starts around the initial setting time and stabilises before the final setting time.
- Plastic shrinkage cracks requires a weak spot (reduced cross section or plastic settlement cracks) where it can form and the more distinct the weak spot, the sooner cracking commences and the more crack widening occurs at this weak spot. If this weak spot is not well defined, increased deformations occurs at other locations often in the form of additional plastic shrinkage cracking at less well defined weak spots. These additional cracks are often internal and not visible at the surface indicating that plastic shrinkage cracking, as for plastic settlement cracking, may be present beneath the surface of the concrete to act as locations for further cracking widening.

7.3. Plastic settlement and plastic shrinkage cracking combined

- Plastic settlement cracking due to differential settlement plays an important role in defining weak spots for plastic shrinkage crack formation. The crack behaviour, if both plastic settlement and plastic shrinkage cracking are present, can differ significantly from the individual behaviours of pure plastic settlement and pure plastic shrinkage cracking.
- For conditions with a low potential for both plastic settlement and plastic shrinkage cracking, there are either no cracks or delayed cracks. Delayed cracks are isolated, short, narrow and hardly visible cracks that often only become visible after the bleed water has been removed. The origin of these cracks is mostly plastic settlement cracking.
- For conditions with moderate to very high potentials for plastic settlement and plastic shrinkage cracking, settlement induced plastic shrinkage cracking occurs. These cracks commence as plastic settlement cracks that are further widened soon after formation by plastic shrinkage cracking. The more severe the plastic settlement cracking the earlier and more severe the plastic shrinkage cracking. These cracks can occur long before the initial setting time and is dominated by a singular crack.

- For conditions with extremely high potentials for plastic settlement and plastic shrinkage cracking, crack jumping behaviour occurs which is a rapid forming and stabilising crack due to early plastic settlement crack initiation in combination with the presence of a significant capillary pressure build-up. This results in the majority of the crack widening of a singular crack to occur before the initial setting time.

7.4. Tensile material properties of plastic concrete

- A new direct tensile test setup was built for determining the tensile material properties of plastic concrete. The test setup performed satisfactorily and succeeded in providing stress-strain curves that could be used to determine the pre-peak and post-peak tensile material properties of plastic concrete.
- The tensile strength and the Young's modulus of plastic concrete initially develop slowly, followed by an exponential increase. This increase occurs near the final setting time for the tensile strength, while the Young's modulus starts to increase around the initial setting time.
- The strain capacity of plastic concrete is initially high, followed by a significant decrease between the initial and final setting times, indicating a change in a short period from a material that can undergo large deformations before failure to a material that fails at minor deformations. This is one of the main reasons why the majority of pure plastic shrinkage cracking occurs between the initial and final setting times.
- The variability of the tensile test on plastic concrete is high due to the tensile nature of the test as well as the plastic nature of the concrete tested. The tensile strength showed the least amount of variability of all the determined material properties. The variability also tends to decrease the less plastic the concrete. However, the variability and conference level of the tensile test results is a subject that requires further investigation.
- The tensile material properties develop significantly faster and reach more significant values the greater the ambient temperature surrounding the concrete.
- Plastic to semi-plastic concrete revealed to be resilient and capable of withstanding cyclic loading without failure, while a solid but still weak concrete cannot withstand cyclic loading. The cyclic tests also revealed that there is time-dependent relaxation of stresses in plastic concrete due to an applied strain.
- The results of tensile material properties and shrinkage and settlement strains of plastic concrete can be combined to provide an analytical estimation of the cracking behaviour of plastic concrete. The analytical cracking behaviour is similar to the experimental cracks at extreme

climates, but not at normal climates due to the size discrepancy between surface and interior cracks during experiments at normal climates.

- The strain capacity of plastic concrete gives a better approximation of the onset and size of cracking in plastic concrete compared to the tensile strength of plastic concrete.

7.5. Modelling the cracking of plastic concrete

- The finite element model presented in this study uses a total strain smeared cracking approach to model the cracking and accounts for both the time dependency of material properties and the anisotropic volume change of plastic concrete.
- The model gives an adequate representation of the cracking behaviour of plastic concrete for extreme climates with high evaporation rates but not for normal climates. The reasons for the poor correlation with experimental results at normal climates are the size discrepancy between the interior and surface cracks during experiments as well as the relaxation of stresses in plastic concrete that were not accounted for in the model.
- The model also predicts an earlier onset of cracking compared to the experiments. The reasons for this are the lower strain capacity used in the analyses as while as the difficulty in observing and measuring cracks on plastic concrete during experiments.
- The parameter study showed that both the settlement and shrinkage strains significantly influence and therefore govern the size of the final crack, while the material properties only influence the time of crack onset and rate of crack widening.
- The model was successfully applied to a large scale example of a concrete slab, indicating that the model can be a helpful tool to simulate the cracking of plastic concrete without the need to perform timely experimental tests.

Chapter 8. Recommendations

This study revealed several aspects that holds potential for future research and include the following:

- The layout of a suitable mould for the testing of plastic settlement cracking should be investigated and standardised.
- The layout and shape of moulds used to test the pure plastic shrinkage cracking of concrete can be improved by illuminating any sources of differential settlement and therefore plastic settlement cracking. This will result in less variability of results, since as shown in this study plastic settlement cracking can significantly influence the observed cracking behaviour.
- The influence of slab depth on the behaviour of plastic settlement and plastic shrinkage cracking individually as well as combined should be investigated, since this study mainly considered one slab depth.
- The influence of curing and finishing techniques, including the timing thereof, on the cracking of plastic concrete should be investigated. In addition, the influence of UV-light on the severity of plastic shrinkage cracking also requires investigation.
- An improved method of observing and measuring cracks beneath the surface of the concrete is required. This will shed light on the size discrepancy between the interior and surface cracks at normal climates.
- An investigation is needed to determine the amount of restrained settlement and shrinkage that is responsible for the cracking at a specific location.
- The boundary conditions of the tensile test setup should be improved to allow the determination of the entire stress-strain curve, including the entire softening branch.
- The appropriate displacement rate for the direct tensile testing of plastic concrete requires investigation.
- The variability and conference level of the tensile test results requires further investigation.
- The tensile material properties of different concrete mixes should be tested to obtain an indication of how the tensile material properties of plastic concrete differ between mixes. The mixes must have different stiffness's, workability's, setting times, material constituents and well as rheology properties. The plastic cracking behaviour of these mixes should also be tested in an

attempt to draw a link between the tensile material properties and observed cracking behaviour. This is especially needed for concrete mixes which often displays uncommon behaviour such as mixed containing certain admixtures.

- The time-dependent relaxation of stresses in plastic concrete due to an applied strain should be firstly experimentally investigated and once characterised it should be incorporated into the modelling of plastic concrete.
- The finite element model created in this study should be used to conduct numerous simulations of random plastic cracking scenarios where influencing factors such as shrinkage, settlement, boundary conditions, layout as well as material properties are altered to obtain a numerical database that can be used to create a design guideline for engineers and contractor for the prevention of cracking in plastic concrete.

References

Abel, J. & Hover, K. 1998. Effect of Water/Cement Ratio on the Early Age Tensile Strength of Concrete. *Transportation Research Record,* 1610:33-38.

ACI 308R. 2001. *Guide to Curing Concrete.* Farmington Hills: American Concrete Institute.

ACI 201.1R. 2008. *Guide for Conducting a Visual Inspection of Concrete in Service*. Farmington Hills: American Concrete Institute.

ACI 231R. 2010. *Report on Early-Age Cracking: Causes, Measurement, and Mitigation*. Farmington Hills: American Concrete Institute.

Alfaiate, J., Pires, E.B. & Martins, J.A.C. 1997. A Finite Elements Analysis of Nonb-Prescribed Crack Propagation in Concrete. *Computers and Structures,* 63(1):17-26.

ASTM C 232. 2004. *Standard Test Method for Bleeding of Concrete*. West Conshohocken: ASTM International.

ASTM C 1579. 2006. *Standard Test Method for Evaluating Plastic Shrinkage Cracking of Restrained Fiber Reinforced Concrete*. West Conshohocken: ASTM International.

ASTM C 403/C 403M. 2008. *Standard Test Method for Time of Setting of Concrete Mixtures by Penetration Resistance*. West Conshohocken: ASTM International.

Bazant, Z.P. & Oh, B.H. 1983. Crack band theory for fracture of concrete. *Materials and Structures,* 16(93):155-177.

Bazant, Z. P., 2002. Concrete fracture models:testing and practice. *Engineering Fracture Mechanics,* 69:165-205.

Boshoff, W.P. & Combrinck, R. 2013. Modelling the severity of plastic shrinkage cracking in concrete. *Cement and Concrete Research*, 48:34-39.

Branch, J., Hannant, D.J. & Mulheron, M. 2002. Factors affecting the plastic shrinkage cracking of high-strength concrete. *Magazine of Concrete Research,* 54(5): 347-354.

CCIP-048. 2010. *Technical Report No.22: Non-structural cracks in concrete.* (4th ed). Surrey: The Concrete Society: A Cement and Concrete Industry Publication.

Cohen, M.D., Olek, J. & Dolch, W.L. 1990. Mechanisms of Plastic Shrinkage Cracking in Portland Cement and Portland Cement-Silica Fume Paste and Mortar. *Cement and Concrete Research*, 20:103-119.

Combrinck, R. 2011. *Plastic shrinkage cracking in conventional and low volume fibre reinforced concrete*. Stellenbosch: The University of Stellenbosch. (MSc thesis).

Dao, V. T., Dux, P. F. & Morris, P. H. 2009. Tensile Properties of Early-Age Concrete. *ACI Materials Journal,* 106(6):483-492.

De Borst, R. 2002. Fracture in quasi-brittle materials: a review of continuum damge-based approaches. *Engineering Fracture Mechanics, 69*:95-112.

Deif, A., Martín-Pérez, B., & Cousin, B. 2009. Experimental study of chloride penetration in an RC slab sustaining in-service loads. *Proceedings of the Eighth International Conference on Creep, Shrinkage and Durability of Concrete and Concrete Structures*, Ise-Shima, 30 September - 2 October 2008, 1107 -1113. London: CRC Press/Balkema.

Diana Software Package Version 9.6. 2010*. User's manual*. TNO Building Construction, Delft, The Netherlands.

Dolado, J.S. & Van Breugel, K. 2011. Recent advances in modelling for cementitious materials. *Cement and Concrete Research,* 41:711-726.

Domone, P.L.J. & Illstone, J.M. 2010. *Construction Materials: their nature and behaviour*. 4th ed. New York: Spon Press.

EN 1992-1-1. 2004. *Design of concrete structures - Part 1-1: General rules and rule for buildings.* Brussels: European Committee for Standardization.

EN 196-3. 2005. *Methods for testing cement - Part 3: Determination of setting times and soundness.* Brussels: European Committee for Standardization.

Ghoddousi, P. & Javid, A.A.S. 2011. Effect of reinforcement on plastic shrinkage and settlement of self-consolidating concrete as repair material. *Materials and Structures*.

Griffith, A. A. 1920. The phenomena of rupture and flow in solds. *Philosophical Transactions of the Royal Society of London,* A221:162-198.

Hannant, D.J., Branch, J. & Mulheron, M. 1999. Equipment for Tensile Testing of Fresh Concrete. *Magazine of Concrete Research,* 51(4):263-267.

Hillerborg, A., Modeer, M. & Petersson, P.E. 1976. Analysis of crack formation and crack growth in concrete by means of fracture mechanics and finite elements. *Cement and Concrete Research,* 6(6): 773-781.

Holt, E. & Leivo, M. 2004. Cracking risks associated with early age shrinkage, *Cement and Concrete Composites,* 26:521-520.

Josserand, L. & De Larrard, F. 2004. A method for concrete bleeding measurement. *Materials and Structures*, 37:666-670.

Kronlöf, A., Markku, L., & Sipari, P. 1995. Experimental study on the basic phenomena of shrinkage and cracking of fresh mortar. *Cement and Concrete Research*, 25:1747-1754.

Kwak, H.-G. & Ha, S.-J. 2006. Plastic shrinkage cracking in concrete slabs. Part II: numerical experiment and prediction of occurrence. *Magazine of Concrete Research*, 58(8):517-532.

Kwak, H.-G. & Ha, S.-J. 2008. Bleeding and evaporation in concrete slabs with sequential placement. *Magazine of Concrete Research*, 60(10):769-783.

Kwak, H.-G., Ha, S. & Weiss, W.J. 2010. Experimental and Numerical Quantification of Plastic Settlement in Fresh Cementitious Systems. *Journal of Materials in Civil Engineering*, 22(10):951-966, October.

Lerch, W., 1957. Plastic Shrinkage. *ACI Journal*, 53: 797-802.

Li, Y.-J. & Zimmerman, Th. 1998. Numerical evaluation of the rotating crack model. *Computers & Structures*, 69: 487-497.

Lura, P., Pease, B., Mazzotta, G.B., Rajabipour, F. & Weiss, J. 2007. Influence of shrinkage-reducing admixtures on development of plastic shrinkage cracks. *ACI Materials Journal,* 104(2).

Maritz, J. 2012. *An investigation on the use of low volume-fibre reinforced concrete for controlling plastic shrinkage cracking*. Stellenbosch: The University of Stellenbosch. (MSc thesis).

Mehta, P.K. & Monteiro, P.J.M. 2006. *Concrete: microstructure, properties, and materials*. 3rd ed. New York: McGraw-Hill.

Monteiro, A. V. & Goncalves, A. F. 2011. Assessment of concrete cover in structures Part 1 - Statistical tolerance analysis approach. *Proceedings of the workshop on Performance based spesifications for Concrete,* Leipzig, June 2011, 220-230. Leipzig: MFPA Leipzig GmbH.

Montgomery, D.C. & Runger, G.C. 2006. Applied Statistics and Probability for Engineers. 4th ed. New York: John Wiley & Sons, Inc.

Neville, A.M. 2011. *Properties of Concrete*. 5th ed. London: Pearson.

Ostergaard, L., Lange, D. & Stang, H., 2004. Early-age stress-crack opening relationships. *Cement and Concrete Composites,* 5(26), pp. 563-572.

Otieno, M.B., Alexander, M.G. & Beushausen, H.-D. 2010. Corrosion in cracked and uncracked concrete - influence of crack width, concrete quality and crack reopening, *Magazine of Concrete Research,* 62(6):393-404.

Owens, G. 2009. *Fulton's Concrete Technology.* 9th ed. Midrand: Cement and Concrete Institute.

Powers, T.C. 1968. *The Properties of Fresh Concrete*. New York: John Wiley & Sons, Inc.

Qi, C. 2003. *Quantitative assessment of plastic shrinkage cracking and its effect on the corrosion of steel reinforcement*. Indiana: Purdue University. (PhD thesis).

Ravina, D. & Shalon, R. 1968. Plastic Shrinkage Cracking. *ACI Journal*, 65: 282-291.

SANS 10100-2. 1992. *The structural use of concrete. Part 2: Materials and execution of work.* Edition 2. Pretoria: Standards South Africa.

SANS 1083. 2002. *Aggregates from natural sources - Aggregates for concrete.* Edition 2.1. Pretoria: Standards South Africa.

Sant, G., Dehadrai, M., Bentz, D., Lura, P., Ferraris, C.F., Bullard, J.W. & Weiss, J. 2009. Detecting the Fluid-to-Solid Transition in Cement Pastes. *Concrete International*, June.

Shaeles, C.A., Hover, K.C., 1988, "Influence of Mix Proportions and Construction Operations on Plastic Shrinkage Cracking in Thin Slabs," ACI Materials Journal, Vol 48, pp 495-504.

Sheriff, T. 1972. The control of ready-mixed concrete using the indirect tensile test – an appreciation of the DoE requirements. Institute of Concrete Technology, advanced concrete technology project.

Shi, Z. 2009. Crack Analysis in Structural Concrete - Theory and Application. 1st ed. Oxford: Elsevier Ltd.

Slowik, V., Schmidt, M. & Fritzsch, R. 2008. Capillary pressure in fresh cement-based materials and identification of the air entry value. *Cement & Concrete Composites*, 30:557-565.

Slowik, V., Neumann, A., Dorow, J. & Schmidt, M. 2009a. Early age cracking and its influence on the durability of concrete structures. *Proceedings of the Eighth International Conference on Creep, Shrinkage and Durability of Concrete and Concrete Structures*, Ise-Shima, 30 September - 2 October 2008, 471-477 . London: CRC Press/Balkema.

Slowik, V., Schmidt, M., Hubner, T. & Villmann, B. 2009b. Simulation of capillary shrinkage cracking in cement-like materials. *Cement & Concrete Composites*, 31:461-469.

Swaddiwudhipong, S., Lu, H.-R. & Wee, T.-H. 2003. Direct tension test and tensile strain capacity of concrete at early age. *Cement and Concrete Research,* 33:2077–2084.

Uno, P.J. 1998. Plastic Shrinkage Cracking and Evaporation Formulas. *ACI Materials Journal*, 95(4):365-375, July-August.

Van Mier, J.G.M. 1997. *Fracture Processes of Concrete: Assessment of Material Parameters for Fracture Models*. Boca Raton: CRC Press, Inc.

Van Mier, J. & van Vliet, M. 2002. Uniaxial tension test for the determination of freacture parameters of concrete: state of the art. *Engineering Fracture Mechanics,* 69:235-247.

Weyers, R.E., Conway, J.C. & Cady, P.D. 1982. Photoelastic analysis of rigid inclusions in fresh concrete. *Cement and Concrete Research*, 12:475-484.

Wittmann, F.H. 1976. On the Action of Capillary Pressure in Fresh Concrete. *Cement and Concrete Research*, 6(1):49-56.

Wongtanakitcharoen, T. 2005. *Effect of Randomly Distributed Fibres on Plastic Shrinkage Cracking of Cement Composites*. Michigan: The University of Michigan. (PHD-thesis).